



The
University
Of
Sheffield.

**Development and evaluation of a one-pot self-assembly route
to switchable adhesives**

By:

William David Seddon

A thesis submitted in partial fulfilment of the requirements for the degree of
Doctor of Philosophy

The University of Sheffield
Faculty of Science
Department of Chemistry

March 2019

Abstract

The lack of reversibility in traditional adhesives has led to the development of a range of switchable adhesives. However, most switchable adhesives cannot be applied to a substrate, and must be created on the surface using stringent laboratory conditions. In this thesis, a new type of pH switchable adhesive which could be applied directly to a surface was developed and tested for adhesive strength. This material was compared to the ‘grafted-from’ pH switchable adhesives in the literature, and found to have a similar adhesive strength.

A series of synthetic transformations were used to mono-functionalise a calix[4]resorcinarene, which can modify surfaces, with either poly(2-(dimethylamino)ethyl methacrylate) or poly(methacrylic acid) using atom transfer radical polymerisation. This new material was then deposited onto hydrophobic silicon wafers using Langmuir-Schaefer deposition to give densely grafted monolayers of adhesive. Adhesion studies using hydrogels of oppositely charged polyelectrolytes showed that the measured adhesion was due to adhesive failure at the gel-monolayer interface, rather than the monolayer-wafer interface. This deposited material was shown to have a similar adhesive strength to material grafted from the surface, demonstrating that the calixarenes are sufficiently anchoring the polyelectrolytes to the substrate. When the calixarene brush layer was replaced with a polyelectrolyte multilayer deposited by layer-by-layer deposition for comparison, it could be concluded that the strength of the calix[4]resorcinarene binding compensates for any reduction in surface coverage in this system. Variation of the load applied showed that there is a dependency on the observed adhesion due to the onset of plastic deformation of the hydrogel.

Overall, these experiments provide a first step towards creating a reversible adhesive that would be practicable in commercial applications. Although further work needs to be done to improve the quality of this adhesion, this thesis demonstrates that a one-pot route to reversible and repeatable adhesion is viable.

Acknowledgements

I would like to express my gratitude to the Engineering and Physical Sciences Research Council (EPSRC) for funding my research, and to the Centre for Doctoral Training (CDT) in Molecular Scale Engineering for organising the research programme and providing the additional courses for the MSc in Molecular Scale Engineering. I would also like to thank the universities of Sheffield and Leeds; and the departments of Chemistry, Physics and Astronomy, and Chemical and Biological Engineering at Sheffield for the use of their facilities.

I would like to thank both of my supervisors, Prof. Nick H. Williams and Prof. Mark Geoghegan, for their tireless support and attention to detail. I would like to thank Prof. Nick H. Williams for his weekly meetings and ensuring I maintained a healthy dose of scepticism towards any results, good or bad. He made sure I endeavoured for well-supported proof and a reasoned explanation for the sometimes surprising results obtained from these new materials. I would like to thank Prof. Mark Geoghegan for his helpful suggestions and interpretation of physical data. His suggestion to resurrect the Langmuir trough to improve the deposition of material proved more than fortuitous. I would like to thank Dr. Alan Dunbar for his help in setting up the Langmuir trough and showing me how to use it. I would like to thank Prof. Graham Leggett for his support as my tutor, and for his role in the CDT, his advice when the synthesis of the polyacid proved challenging was most helpful in steering the synthesis back to success. I would also like to thank the other directors of the CDT: Prof. Giles Davies, Prof. Christoph Wälti, and Prof. Jamie Hobbs.

I am also indebted to all the support staff in the department of Chemistry, without whom nothing would be possible. I would like to thank Pete Farran and Nick Smith for running stores as a friendly and efficient service, without their hard work, patience, and good humour there would be no chemicals, and therefore no chemistry. I would like to thank Denise Richards and Louise Brown-Leng for all their work processing orders, and helping us resolve any problems when they occurred. I would like to thank Keith Owen and Stephen Atkin for their hard work as lab technicians and for running the Grubbs solvent service. As someone who has fixed pumps and manually operated a Grubbs system before, I have a small appreciation of what they can accomplish. I would like to thank Robert Hanson for running the GPC service and for taking the time to show me how to use the equipment.

I would like to thank Dr. Craig C. Robertson and Dr. Sandra van Meurs for running an outstanding NMR service which has continued to improve with new ideas and functionality. I would also like to thank Kath Tattersall and Rose Nightingale, whose constant efforts have helped all of us on the CDT navigate the labyrinthine tracks of the administrative systems of not one, but two universities.

I would like to express my gratitude to my fellow students who have helped me throughout the course of my studies. First and foremost is Dr. Latifah Alfahid, who has helped show me how to use both the ellipsometer and mechanical tester, and how to prepare polyelectrolyte hydrogels. She has helped me with questions about the pH switchable adhesives and in return I have helped her with her questions on chemistry. I would also like to thank Thomas Kennelly for all his help using the atomic force microscope, even if the work did not quite make it into this thesis.

Thanks are also due to the other students and people I have shared laboratory and office space with. First among them is Emeritus Prof Charles J.M. Stirling, FRS, who I had the privilege of sharing a fume cupboard with for many years. The very pinnacle of a chemist, I always enjoyed our conversations. My favourite phrase, though, has to be: "I blame the *project students!*". Of my student colleagues, special thanks go to PJ 'Peej' Taylor and Adel 'skin you alive' O Al Hussain, who went through the trenches with me, and gave birth to the wall of Thornberry. Thanks go to Oscar Siles Brüggés and Ellen Bradley, for sharing a house with me and making it a home, and for one day which brought fresh madness to the word *typeface*. I would like to thank Zeyed Abdulkarim for all our late-night chemistry sessions, otherwise known as 'date night'. Thanks are also due to my 'protégé' Matt 'Matastrophe' Watson, from fresh-faced 3rd year summer student to seasoned PhD student I have watched him grow in fine young chemist. However, I will *always* remember being the responsible adult when he cut his finger open with a volumetric flask, and I had to apply a first field dressing and take him to A&E. I would also like to thank our newest and coolest post-doc Jim Scotson, and all the other members of the Nick Williams group past and present.

I would like to thank Thomas Andrews for his understanding and friendship. I would also like to thank the other members of my year from the CDT: Chris Taylor, Stephen Jackson, Rebecca Smith, Adam Churchman, and Alban Smith. I would like to thank Nick 'Rage-quit' Moody, who after his new computer arrived could talk without damning the machine with every other breath. Our semi-regular walks to the 'Onion' were a welcome break for both of us, and were filled with interesting and lively conversation.

I would like to thank Mike Walker for being the voice of reason/awesome, depending upon the situation, and all other member of the Jim Thomas and Mark Geoghegan groups past and present. I would like to also thank all the level 4 project students, of which there have been many, with special mention to Dan Chesman and Alex Matthews. The last, and some might say 'brightest', projects students I had the pleasure of working with.

Outside of work, I am also indebted to Dawn and Johnathan Was, for all their massive amounts of help and support with everything which has happened in my life. Tuesdays were what kept me going. Thank you. I would also like to express my gratitude to SJ Tonks and AJ Standerwick, whose sound council, discerning eye, and beautiful madness helped me get through. Last, and my no means least, I would like to thank my parents, Richard and Elaine Seddon, for their unfaltering support, and for giving me somewhere to live while I wrote this thesis.

Table of Contents

Abstract.....	i
Acknowledgements.....	iii
Table of Contents.....	vii
Table of Figures.....	xi
Table of Tables.....	xvi
List of Abbreviations.....	xvii
1. Introduction.....	1
1.1. Aim.....	5
1.2. Adhesion and nanotechnology.....	6
1.2.1. Mechanisms of adhesion.....	7
1.2.2. Chemistry of common types of adhesives.....	12
1.2.2.1. Epoxy resins.....	12
1.2.2.2. Silicones.....	13
1.2.2.3. Polyimides.....	14
1.2.2.4. Polyurethanes.....	15
1.2.2.5. Cyanate esters.....	15
1.2.2.6. Acrylics and acrylates.....	16
1.2.2.7. Non-curing adhesives.....	17
1.2.3. Advantages and disadvantages of traditional adhesives.....	17
1.2.4. The use of nanotechnology at the surface.....	19
1.2.5. Switchable adhesives.....	23
1.3. Polymers and polyelectrolytes.....	31
1.3.1. Free-radical addition and ‘living’ polymerisations.....	33
1.3.2. Nitroxide-Mediated Polymerisation.....	34
1.3.3. Atom transfer radical polymerisation.....	35
1.3.4. Reversible addition-fragmentation chain transfer polymerisation.....	36
1.3.5. Polyelectrolytes.....	38
1.3.6. Surface modification with polymer brushes.....	41
1.3.7. Polyelectrolyte brushes.....	42
1.4. Calix[4]resorcinarenes.....	44
1.5. Experimental techniques.....	46
1.5.1. Langmuir films and Langmuir-Schaefer deposition.....	46
1.5.2. Ellipsometry.....	50
1.5.3. Atomic force microscopy.....	51
1.5.4. Adhesion testing.....	52

1.5.4.1.	The peel test	52
1.5.4.2.	The probe test.....	53
1.5.4.3.	Probe test set-up for polyelectrolyte hydrogels.....	55
1.6.	Thesis outline.....	56
2.	Synthesis of Calixarene-Polyelectrolyte Adhesives using ATRP	57
2.1.	Introduction	57
2.2.	Synthesis of the mono-functionalised calix[4]resorcinarene.....	57
2.2.1.	Selective reprotection of hydroxyl calix[4]resorcinarene	60
2.2.2.	Alternative formation of protected hydroxyl calix[4]resorcinarene.....	60
2.3.	Synthesis of the polybasic adhesive via ATRP	62
2.4.	Synthesis of the polyacidic adhesive via ATRP	66
2.4.1.	Synthesis of the polyacid via protected monomer intermediate	70
2.5.	Summary.....	73
3.	Synthesis of Calixarene-Polyelectrolyte Adhesives using RAFT	75
3.1.	Introduction	75
3.2.	Synthesis of the RAFT agent.....	76
3.2.1.	Coupling of PETTC using acyl chloride intermediates	77
3.3.	Coupling of PETTC using activating reagents	78
3.4.	RAFT polymerisation	86
3.5.	Summary.....	87
4.	Deposition of Calixarene-Polyelectrolyte Adhesives.....	89
4.1.	Introduction	89
4.2.	Deposition of calixarene-polyelectrolyte adhesives from solution.....	90
4.3.	Langmuir-Schaefer deposition of adhesives.....	92
4.4.	AFM imaging of deposited brushes.....	101
4.5.	Spin-coating of PVAc films	114
4.6.	Summary.....	117
5.	Adhesion Measurements.....	119
5.1.	Introduction	119
5.2.	Adhesion force and work done	120
5.3.	Stress, strain, and elastic modulus	126
5.4.	Work of debonding.....	135
5.5.	Variation of load.....	140
5.5.1.	Stress-strain characteristic of the hydrogel under compression.....	147
5.6.	Comparison to previous studies.....	150
5.7.	Summary and conclusions	151

6.	Polyelectrolyte Multilayers and AFM Force Measurements.....	153
6.1.	Introduction	153
6.2.	Formation of polyelectrolyte films by layer-by-layer deposition.....	153
6.3.	AFM imaging of the deposited polyelectrolyte films.....	158
6.4.	Adhesion measurements of layer-by-layer polyelectrolyte films	162
6.5.	AFM force measurements of calixarene bonding strength.....	167
6.6.	Overall comparison of adhesives.....	171
6.7.	Summary and conclusions.....	174
7.	Conclusions and Future Work.....	177
7.1.	Introduction	177
7.2.	Findings and Implications	178
7.3.	Study Limitations and Final Conclusions.....	181
7.4.	Future Work.....	182
8.	Experimental.....	185
8.1.	Synthesis of mono-C-decenyl, tri-C-decyl calix[4]resorcinarene (1).....	187
8.2.	Synthesis of Boc-mono-C-decenyl, tri-C-decyl calix[4]resorcinarene (3).....	188
8.3.	Synthesis of Boc-mono-C-decanol, tri-C-decyl calix[4]resorcinarene (5).....	189
8.4.	Synthesis of mono-C-hydroxypropyl, tri-C-pentyl calix[4]resorcinarene (6).....	190
8.5.	Synthesis of Boc-mono-C-hydroxypropyl, tri-C-pentyl calix[4]resorcinarene (8) 191	
8.6.	Synthesis of mono-C-hydroxydecyl, tri-C-decyl calix[4]resorcinarene (9).....	192
8.7.	Synthesis of Boc-mono-C-decanol, tri-C-decyl calix[4]resorcinarene (5).....	193
8.8.	Synthesis of Boc-mono-C-bromisobutyloxydecyl, tri-C-decyl calix[4]resorcinarene (10).....	194
8.9.	Synthesis of Boc-mono-C-pDMAEMA-isobutyloxydecyl, tri-C-decyl calix[4]resorcinarene (11).....	195
8.10.	Synthesis of mono-C-pDMAEMA-isobutyloxydecyl, tri-C-decyl calix[4]resorcinarene (12).....	196
8.11.	Synthesis of decyl-2-bromo-2-methylpropanoate (13).....	197
8.12.	Synthesis of decyl-pDMAEMA-2-methylpropanoate (14).....	197
8.13.	Synthesis of sodium methacrylate (15).....	198
8.14.	Synthesis of decyl-pNaMA-2-methylpropanoate (16).....	198
8.15.	Synthesis of decyl-pMAA-2-methylpropanoate (17).....	199
8.16.	Synthesis of 1-ethoxyethyl methacrylate (18).....	200
8.17.	Synthesis of decyl-poly(1-ethoxyethyl methacrylate)-2-methylpropanoate (19). 200	
8.18.	Synthesis of decyl-p'BMA-2-methylpropanoate (20).....	201

8.19.	Synthesis of Boc-mono-C-ptBMA-isobutyloxydecyl, tri-C-decyl calix[4]resorcinarene (21).....	202
8.20.	Synthesis of mono-C-pMAA-isobutyloxydecyl, tri-C-decyl calix[4]resorcinarene (22)	203
8.21.	Synthesis of 4-cyano-4-[(phenethylthio)thiocarbonylthio] valerate (25)	203
8.22.	Synthesis of 4-cyano-4-[pMAA-(phenethylthio)thiocarbonylthio] valerate (26). 204	
8.23.	Synthesis of 4,4'-azobis(4-cyano-valeroyl chloride) (27).....	205
8.24.	Synthesis of 4,4'-azobis(decyl 4-cyano-valerate) (28).....	205
8.25.	Synthesis of decyl 4-cyano-4-[(phenethylthio)thiocarbonylthio] valerate (29)....	206
8.26.	Synthesis of decyl hexanoate (30)	207
8.27.	Synthesis of Boc-mono-C-4-cyano-4-[(phenethylthio)thiocarbonylthio] valerate, tri-C-decyl calix[4]resorcinarene (31)	207
8.28.	Synthesis of N-octyl 4-cyano-4-[(phenethylthio)thiocarbonylthio] valeramide (32) 208	
8.29.	Synthesis of 4,4'-azobis(Boc-mono-C-decyl-4-cyano-valerate, tri-C-decyl calix[4]resorcinarene) (33)	209
8.30.	Synthesis of decyl 4-cyano-4-[pMAA-(phenethylthio)thiocarbonylthio] valerate (34)	210
8.31.	Synthesis of Boc-mono-C-4-cyano-4-[pMAA-(phenethylthio)thiocarbonylthio] valerate, tri-C-decyl calix[4]resorcinarene (35)	210
8.32.	Synthesis of C-decenyyl calix[4]resorcinarene (36).....	211
8.33.	Synthesis of Boc-C-decenyyl calix[4]resorcinarene (37)	212
8.34.	Synthesis of Boc-C-hydroxydecyl calix[4]resorcinarene (38)	213
8.35.	Synthesis of Boc- C-decyl-3-triethoxysilylpropylcarbonamate calix[4]resorcinarene (39).....	214
8.36.	Synthesis of poly(methacrylic acid) hydrogels.....	215
8.37.	Synthesis of poly(diethylaminoethyl methacrylate) hydrogels	215
8.38.	Synthesis of poly(methacrylic acid)-poly(oligo(ethylene glycol) methyl ether methacrylate) double network hydrogels.....	215
8.39.	Preparation of silicon wafers	216
8.40.	Spin-coating of PVAc.....	216
8.41.	Preparation of layer-by-layer functionalised surfaces	217
8.42.	Preparation of APTES-calix[4]resorcinarene functionalised surfaces	217
9.	References	219

Table of Figures

Figure 1.1: Surface wetting of adhesives.....	7
Figure 1.2: Mechanical interlocking between two substrates.....	8
Figure 1.3: Electrical double layer at polymer–metal interfaces.....	9
Figure 1.4: Diffusion theory of adhesion.....	10
Figure 1.5: Model of weak boundary layers.....	11
Figure 1.6: Structure of diglycidylether of Bishenol-A/F epoxy resins.....	12
Figure 1.7: Mechanism of epoxy resin synthesis.....	13
Figure 1.8: General structure of silicone polymer.....	13
Figure 1.9: Synthesis of RTV silicone resins.....	14
Figure 1.10: Formation of polyimides.....	14
Figure 1.11: Formation of polyurethane.....	15
Figure 1.12: Formation of cyanate ester resin.....	15
Figure 1.13: Formation of cyanoacrylate polymers.....	16
Figure 1.14: Structure of poly(ethylene glycol dimethacrylate).....	16
Figure 1.15: Structure of poly(vinyl acetate).....	17
Figure 1.16: The processes of photolithography.....	21
Figure 1.17: Adsorption of alkanethiols onto Au(111).....	22
Figure 1.18: Silanisation of a hydroxylated substrate.....	22
Figure 1.19: Photograph and SEM images of Tokay gecko fibril structure.....	23
Figure 1.20: Switching of adhesion using a photoresponsive actuator.....	26
Figure 1.21: Switchable adhesion using expanded starch.....	28
Figure 1.22: pH switchable adhesion.....	29
Figure 1.23: Synthesis of polyelectrolyte brush.....	30
Figure 1.24: Step-growth polymerisation of ethylene glycol and terephthalic acid to give the polyester poly(ethylene terephthalate) and addition polymerisation of styrene to give poly(styrene).....	31
Figure 1.25: The molar mass distribution of a mono-modal polymer.....	32
Figure 1.26: Example of a free-radical addition polymerisation.....	33
Figure 1.27: Living radical polymerisation showing the equilibrium between the dormant (P_n-X) and active (P_n^*) species.....	34
Figure 1.28: Alkoxyamine based nitroxides.....	34
Figure 1.29: Polymerisation of styrene using nitroxide-mediated polymerisation.....	35
Figure 1.30: Overall Scheme of the ATRP reaction.....	35
Figure 1.31: RAFT equilibria. k_d is the rate constant for initiator decomposition.....	37
Figure 1.32: A polyelectrolyte that is dissociated into a polyion and small counter-ions in polar solvents.....	38
Figure 1.33: A polyelectrolyte chain showing the three different counter-ion regions.....	39
Figure 1.34: Conformations of neutral polymers in dilute solution.....	41
Figure 1.35: Scheme of planar and spherical polyelectrolyte brushes.....	42
Figure 1.36: Structures of calix[4]arene and calix[4]resorcinarene.....	44
Figure 1.37: Pathway for the acid catalysed condensation of resorcinol and aldehydes.....	46
Figure 1.38: Compression of amphiphiles to form a Langmuir film.....	47
Figure 1.39: A pressure-area isotherm showing three distinct ordering regions, as well as the collapse pressure (π_c).....	48
Figure 1.40: Langmuir-Blodgett deposition onto a hydrophobic substrate.....	48
Figure 1.41: Langmuir-Blodgett deposition onto a hydrophilic substrate.....	49

Figure 1.42: Langmuir-Schaefer deposition.	49
Figure 1.43: Ellipsometry set up.....	50
Figure 1.44: AFM set-up.	51
Figure 1.45: Schematic of a peel test.....	53
Figure 1.46: Schematic of a probe test.....	53
Figure 1.47: Normalised force displacement curve for the probe test showing the stress-strain characteristics of the adhesion.	54
Figure 1.48: Mechanical tester setup.	55
Figure 2.1: Target calixarene-adhesives.	57
Figure 2.2: Synthesis of calix[4]resorcinarenes 1 and 2	58
Figure 2.3: Synthesis of Boc protected calix[4]resorcinarenes 3 and 4	58
Figure 2.4: Synthesis of mono-hydroxyl calix[4]resorcinarene 5	59
Figure 2.5: Selective reprotection of the phenolic hydroxyls to give calix[4]resorcinarene 5	60
Figure 2.6: Synthesis of calix[4]resorcinarenes 6 and 7	61
Figure 2.7: Selective protection of the aromatic hydroxyls to give calix[4]resorcinarene 8	61
Figure 2.8: Synthesis of mono-hydroxyl calix[4]resorcinarene 9	61
Figure 2.9: Selective protection of the aromatic hydroxyls to give mono-hydroxyl calix[4]resorcinarene 5	62
Figure 2.10: Synthesis of bromo-initiator calix[4]resorcinarene 10	62
Figure 2.11: Synthesis of Boc-calix[4]resorcinarene-pDMAEMA 11	63
Figure 2.12: Thermal deprotection of Boc-calix[4]resorcinarene 4 to give the unprotected calix[4]resorcinarene 2	64
Figure 2.13: Acidic deprotection to give calix[4]resorcinarene-pDMAEMA 12	64
Figure 2.14: Basic deprotection to give calix[4]resorcinarene-pDMAEMA 12	64
Figure 2.15: Synthesis of decyl bromo-initiator 13	65
Figure 2.16: Synthesis of decyl-pDMAEMA 14	65
Figure 2.17: Synthesis of sodium methacrylate 15	66
Figure 2.18: Synthesis of decyl-pNaMA 16	66
Figure 2.19: Polymerisation using EDTDAA to give decyl-pMAA 17	68
Figure 2.20: Relative polymerisation rate vs. pH for methacrylic (A) and acrylic (B) acids at 60°C and rate vs. time at various pH values for methacrylic acid.	68
Figure 2.21: Illustration of the transition state structure for the propagation step.	69
Figure 2.22: Synthesis of EEMA 18 using phosphoric acid (H ₃ PO ₄).	70
Figure 2.23: Synthesis of EEMA 18 using phenothiazine and pyridinium <i>p</i> -toluene sulfonate (PPTS).....	70
Figure 2.24: Attempted polymerisation of EEMA 19 using ATRP.....	71
Figure 2.25: Synthesis of decyl- ¹ BMA 20	71
Figure 2.26: Synthesis of decyl-pMAA 17	71
Figure 2.27: Synthesis of Boc-calix[4]resorcinarene- ¹ BMA 21	72
Figure 2.28: Synthesis of calix[4]resorcinarene-pMAA 22	72
Figure 2.29: Overall synthetic route for the calix[4]resorcinarene adhesives.	73
Figure 2.30: Overall synthetic route for the decyl control compounds.....	74
Figure 3.1: Target calix[4]resorcinarene-pMAA (RAFT).	75
Figure 3.2: Synthesis of RAFT agent PETTC 25	76
Figure 3.3: RAFT polymerisation of methacrylic acid to give pMAA 26	76
Figure 3.4: Synthesis of 4,4'-azobis(4-cyano-valeroyl chloride) 27	77
Figure 3.5: Synthesis of diester 28	78

Figure 3.6: Radical cleavage of diester 28 to give decyl-PETTC 29	78
Figure 3.7: Radical decay product of diester 28	78
Figure 3.8: Formation of ester/acyl chloride using cyanuric chloride.	79
Figure 3.9: Formation of decyl hexanoate 30 using cyanuric chloride.....	79
Figure 3.10: Synthesis of calix[4]resorcinarene-PETTC 31 using CC.....	81
Figure 3.11: Synthesis of octyl-PETTC 32	82
Figure 3.12: Activation of PETTC 25 with cyanuric chloride.....	82
Figure 3.13: Synthesis of decyl-PETTC 29 using CDI.....	83
Figure 3.14: Synthesis of decyl-ACVA 28 using DCC.	85
Figure 3.15: Synthesis of calix[4]resorcinarene-ACVA 33	85
Figure 3.16: Decomposition of PETTC 25	85
Figure 3.17: Synthesis of decyl-PETTC 29	86
Figure 3.18: Synthesis of calix[4]resorcinarene-PETTC 31	86
Figure 3.19: RAFT polymerisation of methacrylic acid using decyl-PETTC 29 to give decyl-pMAA 34	86
Figure 3.20: RAFT polymerisation of methacrylic acid using Boc-calix[4]resorcinarene- PETTC 31 to give Boc-calix[4]resorcinarene-pMAA 35	87
Figure 3.21: Overall synthetic route for the Boc-calix[4]resorcinarene-pMAA 35	88
Figure 3.22: Overall synthetic route for decyl-pMAA 34	88
Figure 4.1: Calixarene adhesives 11 , 12 , and 22 , and decyl controls 14 and 17	89
Figure 4.2: Pressure-area isotherms of calixarene-pDMAEMA adhesive 12	94
Figure 4.3: Pressure-area isotherms of Boc-calixarene-pDMAEMA adhesive 11	95
Figure 4.4: Pressure-area isotherms of decyl-pDMAEMA control 14	96
Figure 4.5: Pressure-area isotherms of calixarene-pMAA adhesive 22	97
Figure 4.6: Pressure-area isotherms of decyl-pMAA control 17	98
Figure 4.7: Thicknesses of material deposited by Langmuir-Schaefer.....	99
Figure 4.8: AFM images of HMDS treated wafers.....	102
Figure 4.9: AFM images of deposited Boc-calix-pDMAEMA 11	103
Figure 4.10: AFM images of post-baked Boc-calix-pDMAEMA 11	103
Figure 4.11: AFM images of water sonicated Boc-calix-pDMAEMA 11	104
Figure 4.12: AFM images of deposited calix-pDMAEMA 12	105
Figure 4.13: AFM images of post-baked calix-pDMAEMA 12	106
Figure 4.14: AFM images of water sonicated calix-pDMAEMA 12	106
Figure 4.15: AFM images of deposited decyl-pDMAEMA 14	108
Figure 4.16: AFM images of post-baked decyl-pDMAEMA 14	108
Figure 4.17: AFM images of water sonicated decyl-pDMAEMA 14	109
Figure 4.18: AFM images of deposited calix-pMAA 22	110
Figure 4.19: AFM images of post-baked calix-pMAA 22	111
Figure 4.20: AFM images of water sonicated calix-pMAA 22	111
Figure 4.21: AFM images of deposited decyl-pMAA 17	112
Figure 4.22: AFM images of post-baked decyl-pMAA 17	113
Figure 4.23: AFM images of water sonicated decyl-pMAA 17	113
Figure 4.24: Predicted vs measured film thickness.....	116
Figure 4.25: AFM images of spin coated films of PVAc at 1750 rpm.	116
Figure 4.26: AFM images of spin coated films of PVAc at 4500 rpm.	117
Figure 5.1: Calixarene adhesives 11 , 12 , and 22 , and decyl controls 14 and 17	119
Figure 5.2: Adhesion and work done of Boc-calixarene-pDMAEMA 11	120
Figure 5.3: Adhesion and work done of calixarene-pDMAEMA 12	122

Figure 5.4: Adhesion and work done of decyl-pDMAEMA 14 .	123
Figure 5.5: Adhesion and work done of calixarene-pMAA 22 .	124
Figure 5.6: Adhesion and work done of decyl-pMAA 17 .	125
Figure 5.7: Adhesion and work done of PVAc.	126
Figure 5.8: Stress (max) and strain (max) of Boc-calixarene-pDMAEMA 11 .	127
Figure 5.9: Elastic moduli of Boc-calixarene-pDMAEMA 11 .	127
Figure 5.10: Stress (max) and strain (max) of calixarene-pDMAEMA 12 .	128
Figure 5.11: Elastic moduli of calixarene-pDMAEMA 12 .	129
Figure 5.12: Stress (max) and strain (max) of decyl-pDMAEMA 14 .	130
Figure 5.13: Elastic moduli of decyl-pDMAEMA 14 .	130
Figure 5.14: Stress (max) and strain (max) of calixarene-pMAA 22 .	131
Figure 5.15: Elastic moduli of calixarene-pMAA 22 .	132
Figure 5.18: a) Stress (max) and strain (max) of PVAc. b) Elastic moduli of PVAc.	133
Figure 5.19: Work of debonding for Boc-calixarene-pDMAEMA 11 .	135
Figure 5.20: Work of debonding for calixarene-pDMAEMA 12 .	136
Figure 5.21: Work of debonding for decyl-pDMAEMA 14 .	137
Figure 5.22: Work of debonding for calix-pMAA 22 .	138
Figure 5.23: Work of debonding for decyl-pMAA 17 .	138
Figure 5.24: Work of debonding for PVAc.	139
Figure 5.25: Effect of load upon the adhesion characteristics of Boc-calixarene-pDMAEMA 11 .	140
Figure 5.26: Effect of load upon the adhesion characteristics of calixarene-pDMAEMA 12 .	142
Figure 5.27: Effect of load upon the adhesion characteristics of decyl-pDMAEMA 14 .	143
Figure 5.28: Effect of load upon the adhesion characteristics of calixarene-pMAA 22 .	144
Figure 5.29: Effect of load upon the adhesion characteristics of decyl-pMAA 17 .	145
Figure 5.30: Effect of load upon the adhesion characteristics of PVAc tested with pDEAEMA hydrogel.	146
Figure 5.31: Effect of load upon the adhesion characteristics of PVAc tested with DN pMAA-pOEGMA hydrogel.	147
Figure 5.32: Stress-strain characteristics of DN pMAA-pOEGMA hydrogel under varying load.	148
Figure 5.33: Stress-strain characteristics of pDEAEMA hydrogels under varying load.	149
Figure 5.34: Comparison of Work of debonding and stress.	150
Figure 6.1: Total thickness of layer-by-layer films on silicon, arranged by deposition solution.	154
Figure 6.2: Thickness of pDMAEMA deposited on silicon at different deposition times.	155
Figure 6.3: Thickness of pMAA deposited on silicon-APTES at different deposition times.	157
Figure 6.4: Thickness of depositions from dichloromethane and 0.5 M NaCl _(aq) .	157
Figure 6.5: AFM images of the first deposited layer onto silicon (Si/+).	158
Figure 6.6: AFM images of the second deposited layer onto silicon (Si/+/-).	159
Figure 6.7: AFM images of the third deposited layer onto silicon (Si/+/-/+).	159
Figure 6.8: AFM images of the first deposited layer onto silicon-APTES (Si-APTES/-).	160
Figure 6.9: AFM images of the second deposited layer onto silicon-APTES (Si-APTES/-/+).	161
Figure 6.10: AFM images of the third deposited layer onto silicon-APTES (Si-APTES/-/+/-).	161

Figure 6.11: Adhesion characteristics of LbL depositions on silicon substrates tested with DN pMAA-pOEGMA hydrogels.	163
Figure 6.12: Thickness of films deposited onto silicon substrates before and after measurements.	164
Figure 6.13: Adhesion characteristics of LbL depositions on silicon substrates tested with pDEAEMA hydrogels.	165
Figure 6.14: Adhesion characteristics of LbL depositions on silicon-APTES substrates tested with pDEAEMA hydrogels.	166
Figure 6.15: Thickness of films deposited onto silicon-APTES substrates before and after measurements.	166
Figure 6.16: Adhesion characteristics of LbL depositions on silicon-APTES substrates tested with pDEAEMA hydrogels.	167
Figure 6.17: Synthesis of C-decenyl calix[4]resorcinarene 37	168
Figure 6.18: Synthesis of Boc-C-decenyl calix[4]resorcinarene 37	168
Figure 6.19: Synthesis of Boc-C-hydroxydecyl calix[4]resorcinarene 38	168
Figure 6.20: Synthesis of APTES calix[4]resorcinarene 39	169
Figure 6.21: AFM images of APTES-calixarene treated wafers.	170
Figure 6.22: Force mapping of APTES-calixarene surfaces.	171
Figure 4.4: Synthetic route for functionalising calixarene with dopamine.	183
Figure 4.5: Synthetic route for post-polymerisation modification with calixarene.	184

Table of Tables

Table 2.1: Summary of Reaction conditions used to synthesise pMAA.....	67
Table 3.1: Summary of conditions for formation of acyl chloride.....	77
Table 3.2: Summary of conditions for formation of decyl hexanoate 30 using cyanuric chloride.....	80
Table 3.3: Summary of conditions for formation of decyl hexanoate 30 using cyanuric chloride with varying reaction times.	80
Table 3.4: Summary of conditions for formation of RAFT esters using cyanuric chloride..	81
Table 3.5: Summary of conditions for formation of activated PETTC 25-CC using cyanuric chloride.....	83
Table 3.6: Summary of coupling conditions between varying alcohols and acids.	84
Table 4.1: Compounds deposited from solution showing thickness, number of chain units (N), radius of gyration (R_g), grafting density (σ), interchain distance (D), and reduced tether density (Σ).....	91
Table 4.2: Adhesion and Work done of calixarene adhesives deposited from solution.	92
Table 4.3: Compounds deposited from solution showing thickness, number of chain units (N), radius of gyration (R_g), grafting density (σ), interchain distance (D), and reduced tether density (Σ).....	100
Table 4.4: Compounds deposited from solution showing thickness, number of chain units (N), radius of gyration (R_g), grafting density (σ), interchain distance (D), and reduced tether density (Σ).....	101
Table 4.5: Surface roughness of Boc-calix-pDMAEMA 11 films.....	104
Table 4.6: Surface roughness and feature dimensions of calix-pDMAEMA 12 films.	107
Table 4.7: Surface roughness and feature dimensions of decyl-pDMAEMA 14 films.....	109
Table 4.8: Surface roughness and feature dimensions of calix-pMAA 22 films.	112
Table 4.9: Surface roughness and feature dimensions of decyl-pMAA 17 films.	114
Table 5.1: Adhesion properties of HMDS treated silicon wafers	120
Table 5.2: Elastic moduli of hydrogels.	147
Table 6.1: Surface roughness of layer-by-layer depositions onto silicon.	160
Table 6.2: Surface roughness of layer-by-layer depositions onto silicon-APTES.....	162
Table 6.3: Adhesion properties of APTES treated silicon wafers.....	162
Table 6.4: Comparison matrix for all adhesive systems investigated, and for the systems present in the literature.	172

List of Abbreviations

(3-aminopropyl)triethoxysilane	(APTES)
(1-[Bis(dimethylamino)methylene]-1H-1,2,3-triazolo[4,5-b]pyridinium 3-oxid hexafluorophosphate	(HATU)
1,1'-carbonyldiimidazole	(CDI)
1-ethoxyethyl methacrylate	(EEMA)
1-ethyl-3-(3-dimethylaminopropyl)carbodiimide	(EDC)
2-(diethylamino)ethyl methacrylate	(DEAEMA)
2-(dimethylamino)ethyl methacrylate	(DMAEMA)
2,2,6,6-tetramethyl piperidiny-1-oxyl	(TEMPO)
2,2'-bipyridine	(bipy)
2,2'-(Ethylenedithio)diacetic acid	(EDTDAA)
4,4'-azobis(4-cyanopentanoic acid)	(ACVA)
4-cyano-4-[(phenethylthio)thiocarbonylthio] valerate	(PETTC)
4-dimethylaminopyridine	(DMAP)
acetic acid	(AcOH)
acetonitrile	(MeCN)
acid dissociation constant	(pKa)
adhesion force	(Fa)
apparent fracture energy	($\Gamma_{app(v)}$)
aqueous sodium chloride	(NaCl(aq))
atom transfer radical polymerisation	(ATRP)
atomic force microscope	(AFM)
Avogadro's number	(N_A)
binary diffusivity	(D_g)
borane-dimethyl sulfide complex	($BH_3 \cdot Me_2S$)
borane-tetrahydrofuran complex	($BH_3 \cdot THF$)
brush thickness	(l)

carbon disulfide	(CS ₂)
collapse pressure	(π_c)
concentration of deactivator	([D])
concentration of initiator	([RX] ₀)
concentration of ions	(c_c)
constant (Schmidt number dependent)	(c)
controlled radical polymerisations	(CRP)
copper(I) bromide	(Cu ^I Br)
copper(I) chloride	(Cu ^I Cl)
copper(II)bromide	(Cu ^{II} Br)
crack velocity	(v)
cyanuric chloride	(CC)
debonding velocity	(V_{deb})
degree of polymerisation	(DP)
density	(ρ)
dichloromethane	(DCM)
diethyl ether	(Et ₂ O)
dimethylformamide	(DMF)
dispersity index	(\mathcal{D})
displacement	(h)
di- <i>tert</i> -butyl dicarbonate	(Boc ₂ O)
double network	(DN)
effective adhesion energy	($\Gamma(v)$)
elastic modulus	(λ)
ethanol	(EtOH)
ethyl 2-bromoisobutyrate	(EtBriBu)
ethyl acetate	(EtOAc)
final spin coated film thickness	(h_f)

formaldehyde	(CHO)
freeze-pump-thaw	(FPT)
friction force microscopy	(FFM)
gel permeation chromatography	(GPC)
grafting density	(σ)
hexamethyldisilazane	(HMDS)
hydrazine	(H ₂ NNH ₂)
hydrochloric acid	(HCl)
hydrogen peroxide	(H ₂ O ₂)
ideal gas constant	(R)
initial layer thickness	(h_0)
initial polymer concentration	(c_0)
initial solution viscosity	(η_0)
initial solvent mass fraction	(x_1^0)
interacting force	($F_{\text{interaction}}$)
interchain distance	(D)
kinematic viscosity	(ν_g)
layer-by-layer	(LbL)
less activated monomer	(LAM)
liquid crystalline elastomer	(LCE)
living radical polymerisations	(LRP)
mass average molar mass	(M_w)
mass transfer coefficient	(k_m)
maximum contact area	(A_{max})
maximum strain	(ϵ_{max})
maximum stress	(σ_{max})
methacrylic acid	(MAA)
methanol	(MeOH)

mixture parameters	$(a_m \text{ and } b_m)$
molar volume of the solvent	(V_1)
mole fraction of polymer	(x_{m2})
mole fraction of solvent	(x_{m1})
monomer conversion	(p)
more activated monomer	(MAM)
<i>N,N</i> -dicyclohexylcarbodiimide	(DCC)
<i>N,N</i> -Diisopropylethylamine	(DIPEA)
nominal strain	(ϵ)
nominal stress	(σ_N)
normal spring constant of the cantilever	(k)
number average molar mass	(M_n)
number of monomer units	(N)
oxalyl chloride	$((\text{COCl})_2)$
peak molar mass	(M_p)
phase transfer catalyst	(PTC)
plateau stress	(σ_p)
poly(2-(diethylamino)ethyl methacrylate)	(pDEAEMA)
poly(2-(dimethylamino)ethyl methacrylate)	(pDMAEMA)
poly(methacrylic acid)	(pMAA)
poly(methacrylic acid)-poly(oligo(ethylene glycol) methyl ether methacrylate)	(pMAA-pOEGMA)
Poly(methyl methacrylate)	(pMMA)
poly(oligo(ethylene glycol) methyl ether methacrylate)	(pOEGMA)
Poly(vinyl acetate)	(PVAc)
polydimethylsiloxane	(PDMS)
polymer density	(ρ_{pol})
polymer molecular weight	(M_2)

<i>p</i> -toluenesulfonic acid	(<i>p</i> -TsOH)
radius of gyration	(R_g)
rate constant of deactivation	(k_{deact})
rate constant of propagation	(k_p)
reduced tether density	(Σ)
retention factor	(R_f)
reversible addition-fragmentation chain transfer	(RAFT)
reversible deactivation radical polymerisation	(RDRP)
room temperature	(RT)
room-temperature vulcanising	(RTV)
salt concentration	(c_a)
scanning tunnelling microscope	(STM)
segment length	(b)
self-assembled monolayer	(SAM)
silicon/pDMAEMA/pMAA/pDMAEMA	(Si/+/-/+)
silicon-APTES/pMAA/pDMAEMA/pMAA	(Si-APTES/-/+/-)
size exclusion chromatography	(SEC)
sodium azide	(NaN ₃)
sodium chloride	(NaCl)
sodium hydride	(NaH)
sodium hydroxide	(NaOH)
sodium methacrylate	(NaMA)
solid iodine	(I ₂)
solvent mass fraction (equilibrium - gas phase)	($x_{1\infty}$)
solvent molecular weight	(M_1)
spin speed	(ω)
strain release rate	(\mathcal{G})
surface roughness	(R_a)

temperature	(T)
<i>tert</i> -butoxycarbonyl	(Boc)
<i>tert</i> -butyl methacrylate	(^t BuMA)
tetrahydrofuran	(THF)
thin-layer chromatography	(TLC)
thionyl chloride	(SOCl ₂)
triethylamine	(Et ₃ N)
trifluoroacetic acid	(TFA)
trifluoromethanesulfonyl chloride	(TfCl)
ultraviolet	(UV)
vapour pressure (pure solvent)	(p_1^0)
vertical cantilever deflection	(Δz)
wet film thickness	(h_w)
width of peeled strip	(w)
work done	(W)
work of debonding	(W_{deb})

1. Introduction

Adhesives are ubiquitous, and have proven to be a versatile means of joining disparate materials for millennia. The oldest discovered use of an adhesive is the use of birch-bark-tar on stone flakes from the Mid-Pleistocene era (circa 200,000 years ago).¹ Until the twentieth century, adhesives were made from naturally derived products; such as egg whites (tempura), plant resins, and animal collagen. One such use of these natural adhesives which is still in use is artists' gesso, which is a mixture of an animal glue binder (usually rabbit-skin glue) and chalk, gypsum, and pigment.²

With the introduction of synthetic polymer-based adhesives, their increased versatility and strength has cemented their position in the modern world. Adhesives are used for joining together complex assemblies and greatly differing materials, forming joints which could not otherwise be achieved by traditional fastenings. They are utilised in a variety of products and manufacturing; such as the automotive and aerospace industries, the construction of composite materials and filters, electronics and electric motors, and many more.³ The adhesives market is sizeable, with a forecasted turnover of ~\$50 billion for the global adhesives market in 2019.⁴

Adhesives offer many advantages, for example, due to their amorphous nature adhesives form continuous seals, rendering the joints they form leak proof. These continuous bonds also distribute stress evenly, provide stiff structures, and reduce susceptibility to vibration and fatigue.^{5,6} Most of the advantages of adhesives come from their ability to join disparate materials and avoid some of the problems caused by mechanical fastening, e.g. galvanic corrosion caused by two metals with differing galvanic potentials, such as steel and aluminium.

As most adhesives are polymer based, they also suffer the same disadvantages as polymers. They lack the mechanical strength of metals but compensate with a high area of surface contact. When heated to their glass transition temperature, the polymer bond strength decreases as the polymers become more fluid and can move away from the interface with greater ease. Bonded joints do not acquire full strength instantly, and must be supported until fully cured. Once formed, a bonded joint is permanent and cannot be corrected or dismantled.^{5,6} The advantages and disadvantages of traditional adhesives are discussed in greater detail in section 1.2.2.

Some of these disadvantages have led to the development of switchable adhesives, which bond and de-bond in response to an external, controllable, stimulus.⁷ The ability to reverse an adhesive joint offers the capacity to disassemble components, either for more efficient repair or replacement, or for easier end-of-life decommissioning and recycling. The properties of the adhesive can be altered depending upon their intended use, for example, operating underwater.⁸

Two areas which could benefit from the use of switchable adhesives are the automotive and aerospace industries. In the automotive industry, adhesives are becoming more prevalent as companies strive to decrease costs and improve durability.⁹ There is also a move towards improving vehicle end-of-life recycling, driven by the increasing legislation concerning this area, for example the ELV directive in the European Union.¹⁰ The use of adhesives allows the reduction of weight compared to traditional fastenings or welding, and offer greater stiffness, superior packaging, and greater long-term refinement.¹¹

One of the greatest benefits is in comparison to welded joints, as adhesives are vastly cheaper and can be applied to give excellent consistency. As adhesives spread the stress evenly throughout the joint, they allow thinner gauge materials to be used in comparison to spot welding, which gives weight and cost savings. Adhesives also age better than spot welds, which can develop micro fractures when subjected to environmental vibration as well as over successive heating and cooling cycles, leading to an increased flexing of the body. As adhesives do not suffer from localised fatigue, the structure maintains its integrity and so remains safer over the course of its lifespan. The energy absorption capabilities of adhesives also improves the crash worthiness of the newer lightweight structures which are coming into use.¹¹

From the above it can be seen that a major problem with the use of traditional spot-welded joints in vehicles is the fatigue and weight of the material. Although traditional adhesives help resolve the problem of failure due to fatigue of the joint, metal fatigue in the component body will still curb the ultimate life-span of the vehicle. If these adhesives could be reversed, then fatigued components could be replaced, extending the life-span of vehicles whilst maintaining the light-weight joints and components required.

Similar advantages could be observed in the aerospace industry, which shares many of the same problems as the automotive industry. However, these problems are generally on a much greater scale as the materials have to contend with fatigue from: extremes of environmental temperature cycles, harsh environmental vibrations, and repeated pressurisation cycles from ground level to high altitude. Therefore, the costs involved are far greater. The list price of a commercial aircraft produced by Boeing ranges from \$82.4 million (737-700), to \$408.8 million (777-9),^{12,13} with a single engine of the 777 costing \$24 million.¹⁴

The aerospace industry makes extensive use of structural adhesives, which are used for bonding a variety of composite materials; primarily to bind a sandwich structure comprised of a metal honeycomb and metallic skins.¹⁵ For example, they are used for local reinforcement on primary structures and structural components. They are also used for engine components where vibration absorption is critical. Similar to the automotive industry, adhesives offer advantages of lighter weight and improved fatigue resistance over mechanical fastenings.¹⁵ New adhesives are being developed for structural metal and composite bonding and repairs which maintain the mechanical properties required for aircraft at the large variation of operating temperatures.¹⁶

The major limiting factor on the lifespan of an aircraft is the number of pressurisation cycles it endures. For example, a Boeing 747 can endure approximately 35,000 pressurisation cycles before metal fatigue weakens the structure and makes the aircraft unsafe to fly. When aircraft are grounded they are sent to ‘boneyards’ to be assessed and either returned to service, or dismantled for parts for other aircraft. The largest aircraft boneyard in the world is the 209th Aerospace Maintenance and Regeneration Group (AMARG) at Davis-Monthan Air Force Base close to Tucson, Arizona. AMARG contains approximately \$32 billion worth of outdated planes. In the period 2009-2011, ~\$2.5 billion worth of salvaged parts entered the market.¹⁷⁻¹⁹

If the process of disassembly and removal of useful material could be facilitated by the use of switchable adhesives, then more material could be reclaimed quicker and without damage to components. The use of switchable adhesives would also facilitate the replacement of parts on in-service aeroplanes; either through ease of removal and placement of a part, or through reversible access to closed areas of the aircraft which does not weaken the superstructure through cuts and repairs.

Thus far, most switchable adhesives which have been developed are produced in a laboratory environment. They require stringent conditions; such as using cleanroom techniques,²⁰⁻²⁴ or involved multi-step processes,²⁵⁻²⁹ many of which require an inert or deoxygenated atmosphere.²⁷⁻²⁹ The current research into switchable adhesives is discussed in greater detail in section 1.2.4. Although these adhesives prove promising for future applications, many are not currently suitable for commercialisation.

Some switchable adhesives are starting to be developed for commercial applications. Examples are readily applicable, but can only be switched 'off', and are not reversible.³⁰ Others can be recycled, but not in situ.³¹ Although one of the adhesives is appropriate for the textile industry for which it was developed,³¹ it would not be suitable for applications such as the removal or exchange of mechanical components. Another adhesive shows promise as a mechanical manipulator,³² but would not be applicable on a large scale, or for use as a 'permeant' bond as the material relaxes to the 'off' state over time. These adhesives are discussed in more detail in section 1.2.4.

This work looks at developing pH switchable adhesives from a laboratory technique towards an applicable coating. pH switchable adhesives operate through the use of polyelectrolytes: polymers which change their adhesive properties upon varying the environmental pH. They are discussed in further detail in section 1.2.4. Previous work within the research group has investigated pH switchable adhesion using polyelectrolytes grown from surfaces.^{8,27,33,34} pH switchable adhesives have been shown to display strong adhesion which can be switched reversibly over multiple cycles. This repeatable nature makes them useful candidates for applications where components need to be reassembled, such as the replacement of fatigued or broken parts within a larger matrix. As the adhesion can be switched using either acid or base, the method for disassembly can be tailored to the required application.

Currently, the limiting factor on these adhesives is the requirement to grow the polyelectrolyte brush from the surface. Growth of these polymers from the surface is not trivial, and requires the use of reactive chemicals, metal catalysts, and both anhydrous and deoxygenated conditions over the course of the synthesis. Although this is achievable in a laboratory environment on a relatively small scale, this process would be difficult to translate to large components in a commercial environment.

This work looks at developing a polyelectrolyte adhesive which can be prepared in advance of its application to a surface of interest. This would allow it to be synthesised as a bulk material and stored until required, bringing the cost benefits of batch or continuous flow production. By comparison, bespoke synthesis on each component that is to be coated engenders a large amount of waste, and therefore excess cost. By making the adhesive an applicable coating, it could be used in existing manufacturing processes without a dramatic shift in the method. It could also be used with existing infrastructure. When components held together by traditional means need replacing, the joint could be replaced with the switchable adhesive at the same time, making further replacements easier.

Most switchable adhesives are in the early stages of research and development, with the focus on generating and improving the switchable response.^{8,20,29,33,34,21–28} The adhesives developed for market thus far have concentrated on switching ‘off’ a traditional adhesive, generally in a non-reversible fashion.^{30,31} Transferring switchable adhesives from the laboratory to the market comes with a variety of challenges, such as introducing a coating method or functionality, and balancing how that method may have an effect on the adhesiveness of the material. This work looks at overcoming those initial challenges of how to deliver the pH switchable adhesive to the surface, and the effect upon the adhesion compared to the brush system grown from the surface.

1.1. Aim

This thesis looks at the development of a new type of pH switchable adhesive which can be applied directly to a surface, and the comparison of the strength of this physical bond to the chemical bond used in the ‘grafted-from’ techniques in the literature.

This involves transferring the established pH switchable adhesive from a system where the adhesive polyelectrolyte is synthesised on the surface, to a system where the adhesive polyelectrolyte is pre-synthesised and then applied to the surface using a surface-active functionality. In this work a calix[4]resorcinarene is used as a novel surface-active head group for these polymer adhesives. This thesis poses the questions:

- a) *Can a calix[4]resorcinarene be used as a surface-active head group for the direct attachment of polyelectrolyte adhesives to surfaces?*
- b) *Is the deposited material adhesive? If so, how does it compare to polyelectrolyte adhesives generated using ‘grafted-from’ techniques?*

To answer these questions, they were broken down into three key objectives. The key objectives for this project are:

- *Synthesis of mono-functional calixarenes, which can then be used to grow pDMAEMA and pMAA polyelectrolyte adhesives.*
- *Deposition of these adhesives to form an ordered brush monolayer using a physical bond.*
- *Evaluation of the adhesive strength of the deposited brushes, and comparison of the strength of the physical bond to the chemical bond used in 'grafted-from' brushes.*

In addition to these objectives, a comparison to material deposited by layer-by-layer deposition, and the strength of the calixarene head group, will also be investigated. The first objective covers generating a new material which fills the requirement for a polyelectrolyte which can be applied directly to a surface, which is currently missing from this area of work. This, combined with the second objective, work towards answering the first thesis question a). The third objective covers how the material behaves, and if it usefully compares to those in the wider literature, and answers the second thesis question b).

The rest of this chapter presents a review of the relevant background information, and expands upon the topics mentioned thus far. It describes the mechanisms of adhesion, and the advantages and disadvantages of traditional adhesives, which have led to the development of switchable adhesives. The current research into switchable adhesives is then presented, with examples of the current commercialised switchable adhesives and a more detailed explanation of the current pH switchable adhesive system. The polyelectrolytes used to generate the pH switching are then described in more detail, along with the techniques used to produce them, and the formation and properties of the polymer brushes used in the current system. The important experimental techniques are then briefly described, with an explanation of the experimental setup for measuring adhesion.

1.2. Adhesion and nanotechnology

The phenomenon of adhesion is complex, and still an area of much research. There have been many models which have attempted to explain adhesion. The most important models are reviewed here to provide a background, and to highlight the importance of the adhesive interface. As surface effects are an important aspect of adhesion, and form a large part of how switchable adhesives operate, the use of nanotechnology and surface chemistry is then briefly introduced. The current research into switchable adhesives is then described, with a focus on the pH switchable adhesives which are the target of this work. Current switchable adhesives which have been developed for market are also examined and compared to the targets for this work.

1.2.1. Mechanisms of adhesion

Adhesives join surfaces of materials together and resist separation. The material which is being bonded together is usually termed the adherend or substrate. To form an adhesive bond the adhesive must sufficiently wet the surfaces of the substrates, spreading across the material with a contact angle approaching zero (Figure 1.1). This is normally achieved using an adhesive of relatively low viscosity, the exception to this is the use of gap filling adhesives, which require a high viscosity. Once the adhesive has sufficiently wetted the surfaces it must harden to form a strong cohesive bond. There are various ways to form this bond, including chemical reaction, loss of solvent or water, or by the cooling of hot melts. The exception to this is pressure sensitive adhesives which are permanently sticky.⁵

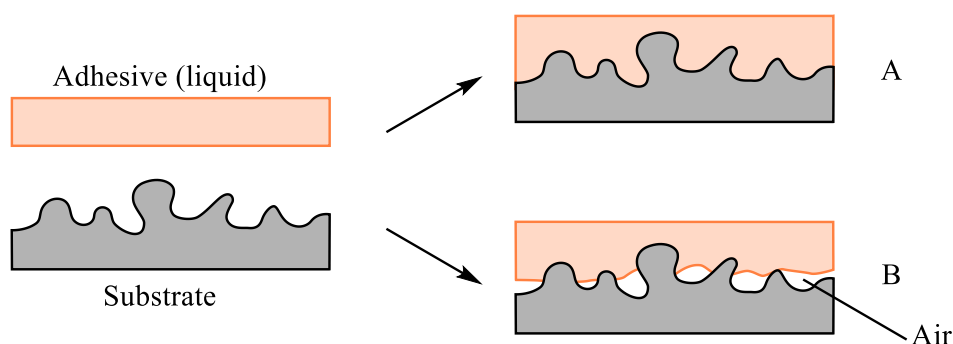


Figure 1.1: (Based on G. Fourche³⁵) Surface wetting of adhesives. (A) Good wetting. (B) Poor wetting

Traditional adhesives are based upon polymers which are either already present in the adhesive, or are formed when the adhesive bond cures. These polymers give the bond cohesive strength and can be either linear, branched, or crosslinked. Linear and branched polymers will flow at high temperatures. However, highly crosslinked polymers have very different flow properties, as they cannot entangle in solution. Linear and branched polymers are also soluble in appropriate solvents. It is these properties which form the basis for hot-melt and solvent based adhesives, respectively. Crosslinked polymers, on the other hand, do not flow upon heating and will only swell upon addition of solvents. These properties make crosslinked polymer adhesives the primary form of structural adhesive, as they are not susceptible to creep. Many traditional adhesives contain additives such as stabilisers against degradation and plasticisers which increase the flexibility.⁵

The interface region between an adhesive material and the substrate is normally the weakest part of the joint. The discontinuity in the material properties of the two materials can cause abrupt changes in the stress distribution, generating stress points at the edges, or localised points, of the interface region.³⁶ The surface topography of the substrate must be carefully controlled to maximise the load bearing capacity and deformational characteristics of the joints formed. These factors result in the quality of the interface between the adhesive and the substrate being the governing factor in the strength of an adhesive bond.^{36,37}

Several mechanisms have been proposed for the process of adhesion. These include; mechanical interlocking, electrostatic interactions, polymer interdiffusion, the thermodynamic or wetting model (physical adsorption), rheological effects, chemical bonding, and the weak boundary layer interactions. A distinction is usually made between mechanical and specific adhesions, as mechanical interlocking is not an adhesion mechanism at the molecular level, but rather an associated increase in the adsorption of the adhesive on the substrate. Physical adsorption must always be a contributing factor to any adhesion, as the molecules will always be in intimate contact.^{5,37}

The mechanical interlocking mechanism was introduced by McBain,³⁸ and is based upon the mechanical keying of the fluid adhesive material into the rough irregularities of the hard substrate surface (Figure 1.2).^{38,39} This interlocking is the most obvious when using porous substrates such as wood, fabric, and some metals, such as anodised aluminium. The anodization of aluminium forms an oxide with a network of hexagonal cells, which adhesives can readily penetrate. The wetting ability of the adhesive combined with the roughness and porosity of the substrate will determine the bond strength, with a greater wetting ability improving the flow of the adhesive into surface asperities.³⁷

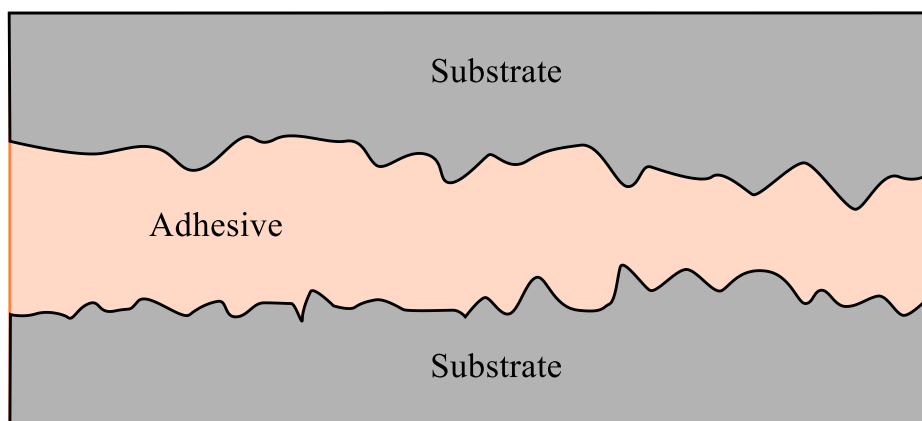


Figure 1.2: (Based on F. Awaja et al.⁴⁰) Mechanical interlocking between two substrates.

Chemical bonding, or specific adhesion, is similar to physical adsorption, but is based upon ‘primary’ bonding forces instead of ‘secondary’ physical non-bonding forces between the substrate and the adhesive. These primary forces include; covalent, ionic, and metallic bonding, similar to those found in bulk materials.^{37,40} An example of chemical bonding is the use of silane coupling agents, which form bonds with the substrate.⁵

The electrostatic model is based upon differing electronic structures between the two materials at the interface, resulting in a transfer of electrons.⁴¹ The model treats the system as an electrical double layer which forms when two materials of a different nature are brought into contact (Figure 1.3). This is only applicable to incompatible materials, such as polymers and metals. As a result of this interaction, an electrostatically charged double layer of ions forms at the interface, resulting in attraction between the two components.^{37,39} The energy of adhesion of the system is equal to the energy of separation of the two ‘capacitor’ faces. Although this theory only describes incompatible materials, it does demonstrate that a strong adhesive bond can be formed by using two oppositely charged surfaces, such as those used in pH switchable adhesion.

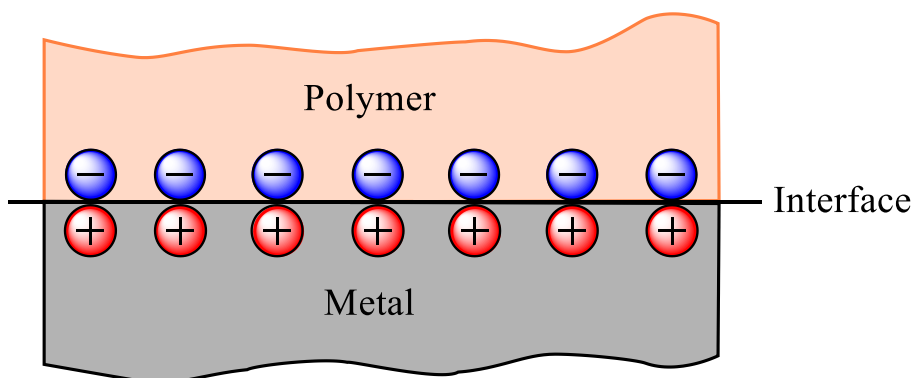


Figure 1.3: (Based on G. Fourche³⁵) Electrical double layer at polymer–metal interfaces.

If the adhesive and substrate are both polymers then they can bond via diffusion. The diffusion theory was proposed by Voyutski,⁴² and explains adhesion between polymers as an interdiffusion of the polymer chains until the initial boundary between the two regions is removed, resulting in a smooth transition zone between the two regions (Figure 1.4). Interdiffusion will only occur if the polymer chains are very mobile (i.e. above their glass transition temperature) and mutually miscible. If the two polymers are identical, then the process is known as autohesion. The smooth transition zone will reduce the abrupt change in stress distribution across the interface and provide increased bond strength.⁴³ The diffusion model will only occur if the conditions for interdiffusion are met, and so is only useful for autohesion and adhesion of compatible polymers, as well as the ‘welding’ of thermoplastics.

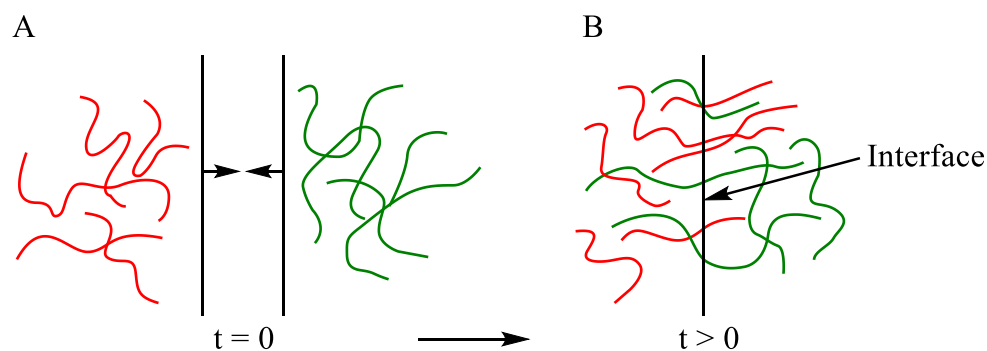


Figure 1.4: (Based on G. Fourche³⁵) Diffusion theory of adhesion (A) Interdiffusion of polymer chains (B) substrate molecules after an interface as formed.

The interdiffusion of compatible polymer chains only occurs when the adhesive and the adheree are in perfect contact. When this happens, the short range intermolecular forces are strong enough to generate adhesion irrespective of whether diffusion can occur or not. This concept was developed into the thermodynamic adsorption, or wetting, model, which was first described by Sharpe and Schonhorn.⁴⁴

The thermodynamic adsorption model is based upon the non-bonding interatomic and intermolecular forces between the surface and the adhesives when they are brought into intimate contact.^{39,44} These forces include van der Waals interactions and hydrogen bonding between permanent or induced dipoles.^{5,37,39} These intermolecular forces have ranges in the same order of magnitude as molecular distances, hence why intimate contact is required. The intimate contact is dependent upon the degree of the mechanical interlocking, and therefore the wetting ability of the adhesive. This makes the wetting ability of an adhesive key to its physical bonding.^{35,37}

The rheological model expands upon the thermodynamic adsorption model by establishing a quantitative relationship between the failure energy of an assembly, and the reversible energy of adhesion. Peel tests show that the failure energy varies depending on the separation rate and the temperature of the system. From this, adhesion can be shown to be closely dependent on the rheological, and therefore bulk, properties of the adhesive. However, the surface characteristics still play a role in the observed adhesion.³⁵

Chemical adhesion of an adhesive to a substrate generates much stronger bonds than physical bonding, $60\text{-}700\text{ kJ mol}^{-1}$ compared to $2\text{-}40\text{ kJ mol}^{-1}$, respectively.³⁵ These bonds can be observed between rubber and brass and between vulcanised (sulfur rich) rubber and copper. The chemical bond can also be formed using coupling agents, such as silanes for glass-adhesive bonding, which bridge between the surface and the adhesive polymer.³⁵

When an adhesive bond fails, the fracture is most likely to be propagated cohesively through material in the joint. This means that the strength of the adhesive bond is normally dependent upon bulk properties of the material. However, fracture can occur through a weak interfacial layer between the two materials if there are sufficient imperfections in the interface. These weak boundaries were first categorised by Bikerman.⁴⁵ The weak boundary layer mechanism is based upon surface contamination reducing the strength of an adhesive bond.⁵ It proposes that a clean surface gives the strongest possible bond, and contamination such as oils and loose oxide layers can increase the risk of bond failure (Figure 1.5).

The weak boundary conditions consist of: (1) air pockets at the surface when the substrate is poorly wetted by the adhesive; (2 & 3) contamination, such as impurities or additives, moving towards the interface, and present in either the adhesive (2) or substrate (3); (4-7) the products of reaction between air and the adherates (4, 5, & 7), or between the two adherates (6). These models of weak boundaries introduce the importance of ‘interphase’ regions at the adhesive interface, the properties of which can determine the joint strength. For example, in polymer-copper assemblies a weak interfacial layer is formed by the copper catalysed oxidation of the polymer.^{35,37,45}

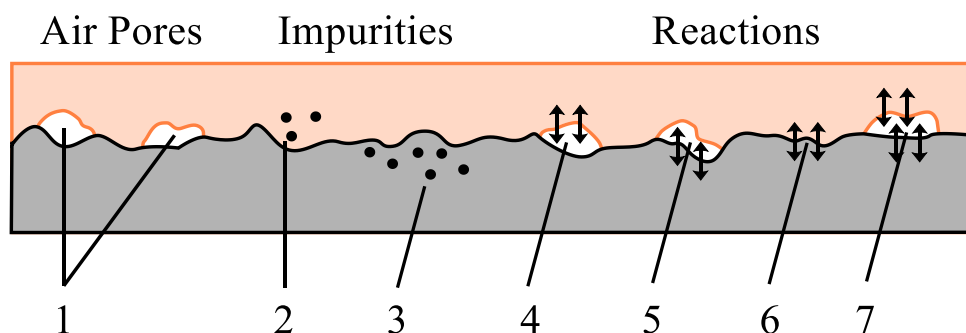


Figure 1.5: (Based on G. Fourche³⁵) Model of weak boundary layers: (1) air pores; (2 & 3) impurities at the interface; (4,5, and 7) reactions between air and adherates; (6) reaction between adherates, which may result in a strengthening or weakening of adhesion, depending upon the products.

In general, adhesives function by wetting a substrate and forming intimate contact over an increased surface area. This large contact area allows for the multiplication of weak physical non-bonding interactions, or for the formation of chemical bonds to the surface. Although most adhesive bonds fail through cohesive failure of the bulk material, the interface between the two adherates is critical in forming the initial adhesion and in determining where the adhesion will fail.

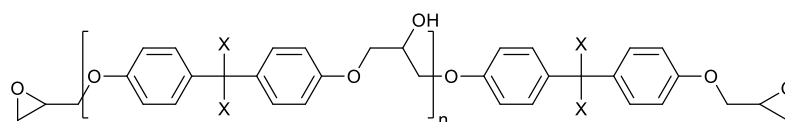
As most adhesion is through multiplication of weak interactions, if these interactions can be modified using a surface structure which can alter its surface area, then adhesion can be controlled. This is the basis of how the Tokay gecko sticks reversibly, and is the inspiration for many topographical switchable adhesives. Alternatively, some adhesion relies on the formation of a small number of strong interactions, such as electrostatic or chemical bonds, which when harnessed reversibly gives the basis for chemical switchable adhesives. Adaptation of these properties means that less material needs to be used, and adhesive properties can be tailored to the desired application.

1.2.2. Chemistry of common types of adhesives

1.2.2.1. Epoxy resins

Epoxy resin adhesives are one of the most ubiquitous for forming strong adhesive joints between a variety of surfaces. They can be available as one- or two-part adhesives, or in a pre-prepared film form.⁶ By variation of the resin and hardener, the resulting adhesive can be tailored to a variety of applications, such as electronics assembly.⁴⁶ These adhesives cure by reaction of terminal epoxy groups with a variety of nucleophilic functionalities, such as; phenols, amines, amides, anhydrides, and Lewis acid or base complexes.⁴⁶

The most commonly used epoxy resins are based upon the diglycidylethers of bisphenol-A or bisphenol-F (Figure 1.6).⁴⁶⁻⁴⁹ In these curing reactions the hardener, or curing agent, is the phenol group of bisphenol, normally under basic conditions using sodium hydroxide.



Bisphenol-A X = CH₃
Bisphenol-F X = H

Figure 1.6: Structure of diglycidylether of Bisphenol-A/F epoxy resins.

The curing reaction involves a step-growth polymerisation (Figure 1.7).⁴⁶⁻⁴⁹ This starts with deprotonated bisphenol displacing the chloro- group on epichlorohydrin to give the major intermediate **1**. This intermediate can react further with additional molecules of intermediate **1** to give the diglycidylether of bisphenol epoxy resin. The polymerisation is terminated by an excess of epichlorohydrin, which reacts with the propagating hydroxyl anion to terminate the polymerisation.⁴⁶⁻⁴⁹

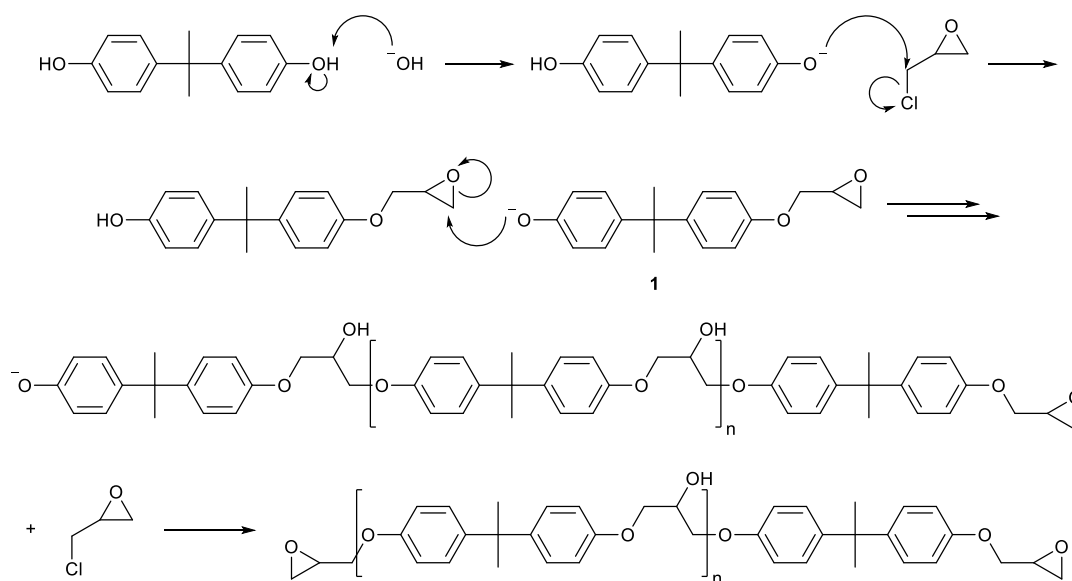


Figure 1.7: Mechanism of epoxy resin synthesis.

1.2.2.2. Silicones

Instead of the carbon-carbon backbone commonly encountered in adhesive polymers, silicones utilise a siloxane (-Si-O-Si-O-) backbone. This gives them very high thermal stabilities, with some polymers stable up to 300°C, and many remaining flexible down to temperatures of -80°C. This large operational range, along with high-voltage electrical insulating properties, has made them useful in a large number of applications.⁴⁶

The siloxane backbone of silicones may have a variety of pendant groups, depending upon the intended application. Commonly, they are either: methyl, phenyl, allyl, or vinyl, and have the general structure shown in Figure 1.8.⁴⁶

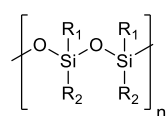


Figure 1.8: General structure of silicone polymer.

Silicones can be cured either by room-temperature vulcanising (RTV), or by addition polymerisation. Both heat-cured and RTV silicones are formed by condensation polymerisation. Hydrolysis of mono-, di-, and trichlorosilanes generates hydroxysilanes, which react via condensation to generate the hydroxyl terminated alkylpolysiloxanes (Figure 1.9). Further reaction with alkoxy silanes cross links these resins to give the RTV silicones.^{46,50}

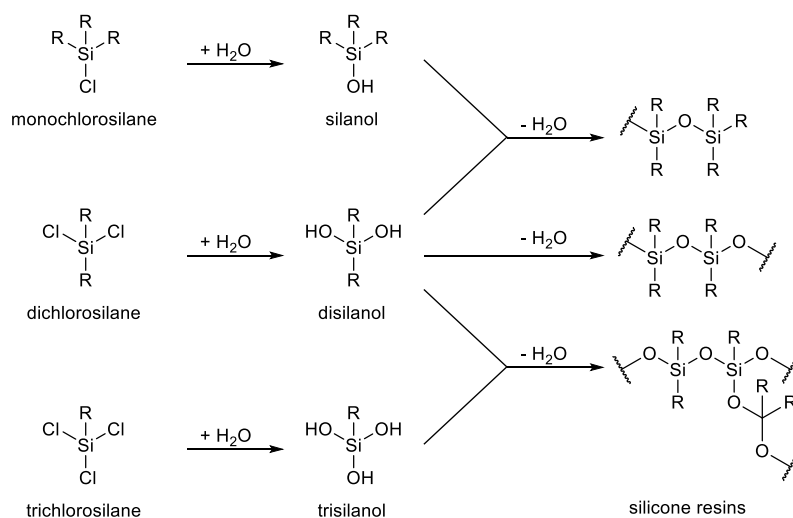


Figure 1.9: Synthesis of RTV silicone resins.

1.2.2.3. Polyimides

Polyimides are high heat-resistant polymers formed from polyamic acids or esters. These polyamic structures are formed by the reaction of aromatic diamines with aromatic dianhydrides. Curing of these polyamic structures at high temperatures results in dehydration to give the polyimide (Figure 1.10).⁴⁶

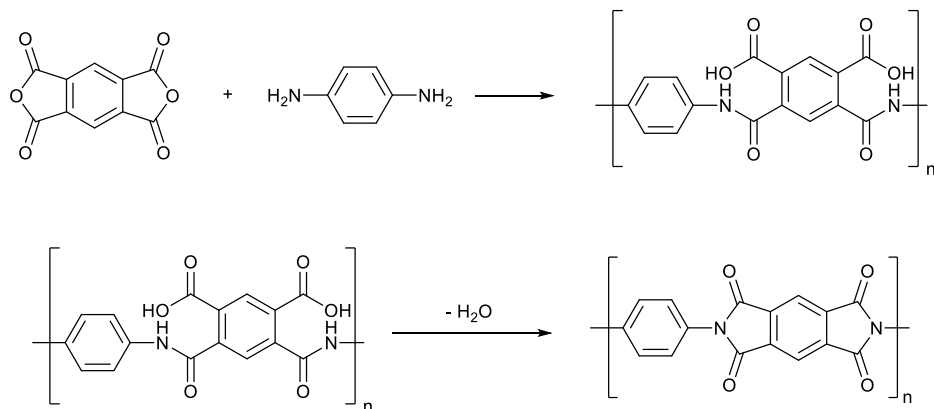


Figure 1.10: Formation of polyimides.

1.2.2.4. Polyurethanes

Polyurethanes are two-part fast-curing adhesives containing repeating units of the urethane group. Polyurethanes generate strong joints resistant to impact, so are useful for bonding glassfibre-reinforced plastics.⁶ Polyurethanes can also be thermoplastics, unlike epoxy resins, so can be reworked if required, this is dependent upon the type of monomer used. The monomers used for polyurethanes can contain a wide variety of groups, including: aliphatic and aromatic hydrocarbons, ester, amides, urea, and allophanate groups. Polyurethanes are formed from the reaction polyalcohols, such as ethylene glycol, with di- or polyisocyanates. Common isocyanates include toluene diisocyanate and methylene-4,4'-di(phenylisocyanate). An example of the polyurethane reaction is shown in Figure 1.11.⁴⁶

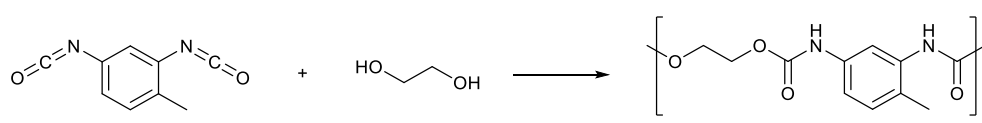


Figure 1.11: Formation of polyurethane.

1.2.2.5. Cyanate esters

Cyanate-ester adhesives are used to produce highly cross-linked resins made from triazine networks. Similar to polyimides, the structure of cyanate esters gives the cured adhesive a high thermal stability. However, this can require high curing temperatures for prolonged periods of time. Cyanate esters form through cyclotrimerization of cyanate groups to generate the highly cross-linked network (Figure 1.12).^{46,51}

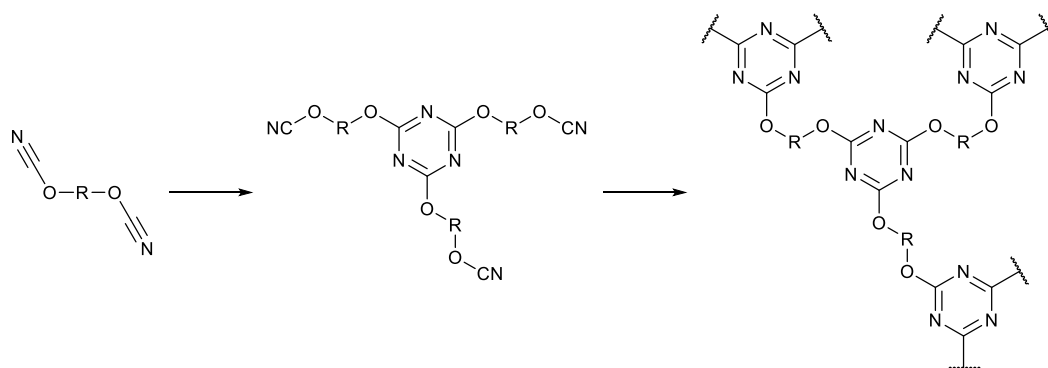


Figure 1.12: Formation of cyanate ester resin.

1.2.2.6. Acrylics and acrylates

Acrylic based adhesives are based upon reactive vinyl monomers or oligomers which cure via addition polymerisation, commonly involving free-radical polymerisation. The most widespread acrylate-based adhesives are cyanoacrylates, however other monomers include methylmethacrylate, diethyleneglycol dimethacrylate, and butyl methacrylate.^{6,46,52,53}

There are four broad classes of acrylic adhesive, based upon the curing mechanism or application: cyanoacrylate, UV curing, anaerobic, and toughened adhesives. Cyanoacrylates are highly polar thermoplastic polymers which polymerise in seconds in contact with weak bases such as water and blood (Figure 1.13), making them famously useful as wound sealants in humid environments.^{6,46,52,53}

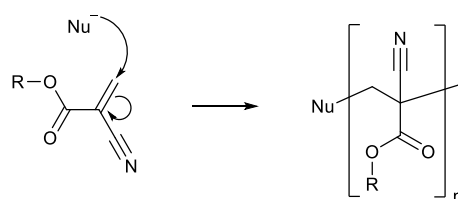


Figure 1.13: Formation of cyanoacrylate polymers.

UV curing acrylics polymerise by free-radical polymerisation initiated either directly by absorbance of UV by the monomer, or indirectly by the decomposition of sensitiser, which generate the radicals to initiate polymerisation.⁵³ Anaerobic curing acrylates are almost exclusively based upon poly(ethylene glycol dimethacrylate) (Figure 1.14), which polymerises spontaneously under anaerobic conditions to generate hard thermoset plastics.^{53,54} Toughened adhesives are not defined by a formation mechanism, but can be considered to be an adhesive where the load is borne by the glassy portion of the structure, and where fracture energy is absorbed and dissipated in a dispersed, rubbery phase.⁵³

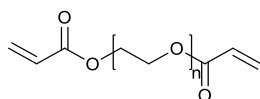


Figure 1.14: Structure of poly(ethylene glycol dimethacrylate).

1.2.2.7. Non-curing adhesives

As well as adhesives that cure by the formation of chemical bonds, many adhesives form adhesive joints by undergoing a phase transition upon heating past the glass transition temperature, allowing them to interface with the substrates before returning to a solid phase upon cooling. Many other adhesives also ‘cure’ by evaporation of a solvent medium, leaving the adhesive polymer in the joint, making these types of adhesive useful for porous substrates. One particular example of an adhesive which cures by solvent loss is poly(vinyl acetate), which cures by evaporation of water (Figure 1.15).⁶

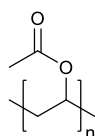


Figure 1.15: Structure of poly(vinyl acetate).

1.2.3. Advantages and disadvantages of traditional adhesives

Adhesives have a variety of advantages over other methods of creating a bond (such as welding, riveting, bolting, etc.), but they also have certain disadvantages when compared to those other methods. It is this balance which has maintained the importance of adhesives, without leading to their dominance. The advantages and disadvantages of adhesives are listed below, with one major disadvantage, the removal and disassembly of components, being the focus of switchable adhesives.

Adhesives can join greatly disparate materials; such as glass, ceramics, plastics and metals, and components with differing sizes or geometries can be joined. As adhesives do not usually require any force to form the joint, such as in riveting, there is no mechanical aggravation to the substrate, which avoids damage to the components. It also prevents deformation in the substrates, removing the requirement to correct the aesthetics through processes such as metal grinding, which reduces the manufacturing costs. Manufacturing costs can also be reduced by the reduction of the number of mechanical fastenings required when an adhesive is used to form the bond. This also leads to a reduction in weight of the product, which, as was described earlier, is a major advantage desired by the automotive industry.¹¹ Due to the intimate contact of adhesives, the joints form continuous seals, rendering the joints they form leak proof. These continuous bonds also distribute tension evenly throughout the bond, eliminating stress concentrations, which can initiate fractures. This distribution of forces throughout the joint also reduces noise and vibration, and increases the impact and fatigue resistance of the joint. Adhesives are also useful for joining dissimilar metals which are at risk of corrosion due to differing galvanic potentials, such as steel and aluminium.^{5,6,48}

Although adhesives have a number of advantages over other fastenings, there are also a number of drawbacks to their use. Similar to painting, the substrate surface needs to be clean and free from contamination, and may require specific preparation depending on the adhesive. This is due to the presence of contaminants causing the formation of weak boundary layers, which can cause a poor adhesive joint.⁴⁵ Although the majority of adhesives are simple to apply, some require specialist processes, similar to welding, depending on the complexity of the adhesive assembly.^{5,6,48}

As adhesives are reactive chemical compounds which cure, or materials which require solvents for application, there can be safety concerns over exposure to these compounds and the management of the waste generated. Unlike mechanical fasteners, which achieve their final strength immediately, adhesives do not reach full strength immediately, and after an initial bond require time to harden. The structure being bonded must be supported until the adhesive bond acquires full strength, this time varies depending upon the adhesive and the environmental conditions, such as temperature and relative humidity. Temperature resistance can also be a problem for linear or branched polymer adhesives, as temperatures close to or exceeding the glass transition temperature of the adhesive results in a reduction in the relative viscosity, and results in creep within the joint. Certain adhesives, such as crosslinked polymers and silicone-based adhesives, have a much higher temperature resistance, and resist creep.

Nearly all forms of joint age over time. Adhesives can be degraded by exposure to physical and chemical action in the environment; such as degradation by ultraviolet (UV) light, reactive chemical species in the environment, and water ingress from moisture.^{5,6,48}

Similar to other permanent methods of fastening, such as welding or riveting, adhesive joints cannot be easily undone. Disassembly of adhered structures often results in damage to, or distortion of, the components, and can be an expensive process which may require specialist chemicals or solvents to remove.^{5,6,48} For example, the removal of cured UV adhesives and resins, which are crosslinked thermosets that do not melt, and require harsh conditions to remove. These adhesives are normally removed by exposing the adhesive to extremes of temperature, or through the use of solvents, such as dichloromethane or acetone, to swell the polymer matrix.⁵⁵ It is this limitation of traditional adhesives which has led to the development of switchable adhesives, which combine the advantages of traditional adhesives with the reversibility of mechanical fasteners. Many of the switchable adhesives developed so far exploit advances in nanotechnology, which allows for the manipulation of unusual properties only observed at these length scales and at the surfaces of materials.

1.2.4. The use of nanotechnology at the surface

Nanotechnology encompasses a variety of methods which generate or otherwise use structures, devices, and systems in the 0.1-100 nm scale; which covers the atomic, molecular, and macromolecular length scales.⁵⁶⁻⁵⁸ Systems developed at these length scales can produce novel functional properties,⁵⁸ such as semiconducting quantum dots⁵⁹ and carbon nanotubes.⁶⁰

At the ≤ 100 nm scale, materials are reaching the so-called 'quantum realm', where the effects of quantum mechanics upon the system become significant.^{61,62} For example, the Casimir effect⁶³ generates a force of hundreds of piconewtons between two uncharged plates in a vacuum through fluctuations in the ground state energy of the electromagnetic field, but only when the plates are separated by up to a few micrometres.⁶¹

As well as the predominant position quantum mechanical effects occupy at the sub-100 nm range, the physical properties of materials can vary greatly from that presented within the bulk. For example, the surface area to volume ratio is dramatically increased at the nanoscale. This can result in differing melting points and enthalpies of fusion when compared to the bulk. The size confinement can also lead to selective formation of metastable states and thermodynamic stabilisation of normally metastable phases.⁶⁴

With a large increase in surface area to volume ratio the reactivity of the material will also increase due to an increased number of reaction sites, potentially leading to new catalytic pathways using materials which are inert in the bulk phase. The most prominent example of this is gold, which is insoluble and inert at the macro scale, but is both soluble and catalytically active at the nanoparticle scale.⁶⁵ The large increase in surface area generated by nanoscale features greatly increases the number of weak intermolecular forces per unit area. This multiplication of forces, combined with manipulation of the available surface, is the basis of topographical adhesives.^{20-22,24,25,66-68}

By reducing the size of a functional material, it can be incorporated into other material systems or interact with targets at the biological scale. For materials designed for drug delivery, keeping the nanoparticle size small means it can remain within the biological system and travel to its desired target.⁶⁹ Many of the unusual effects demonstrated at the nanoparticle scale would be difficult or impossible to reproduce in any useful fashion at the macromolecular scale. It is these novel properties, combined with their inherently compact nature, which has brought nanotechnology to the forefront of material development.

There are many techniques available to modify a surface at the nanoscale. Nearly all techniques fall into two categories: ‘top-down’ and ‘bottom-up’.⁵⁶ Top-down techniques utilise fabrication tools controlled externally at the macroscopic level to generate nanoscopic features and devices by reducing the dimensions of the starting material down to the required size. The majority of these techniques involve a form of lithography to selectively protect a substrate before removal of unwanted material to leave the desired structure.^{56,70,71} Bottom-up techniques utilise the ordered assembly of atomic or molecular components into larger more complex nanoscale structures.^{56,72–74} Both have found use in the preparation of switchable adhesives, with top-down techniques, such as lithography, being used to generate topographical switchable adhesives,^{20–22,24,25,68} and bottom-up techniques, such as self-assembled monolayers, being used to generate chemical switchable adhesives.^{8,27,33,34,75}

A variety of lithographic techniques have been developed for the generation of nanoscale features, with many newer techniques focusing on reducing the lower limit on feature size. There are also techniques which allow for the patterning of two-dimensional features.^{56,70,71} In most forms of conventional lithography, the substrate is protected by a mask or resist, which is then patterned with the desired features. This selective patterning allows for the desired features to be protected, while the exposed material is etched away. Various etching techniques exist, and include either chemical etching with acids, or mechanical etching with UV radiation, X-rays, or electron beams. The limits of the patterning of the mask as well as the etching technique will determine the feature resolution of the structures formed.

When optical lithography is used, a photoresist is used to generate the mask. The resist can be developed in two ways depending upon how the resist reacts to light. In a positive resist, the regions exposed to light will be removed in the development stage. In a negative resist, the regions exposed to light will not be removed in the development stage, giving the inverse of the exposed pattern. Once the resist has been developed, excess material can be etched away, or a new layer of material can be deposited on the exposed regions. Removal of the resist at the end of the process reveals the nanoscale structures (Figure 1.16).^{56,70,71}

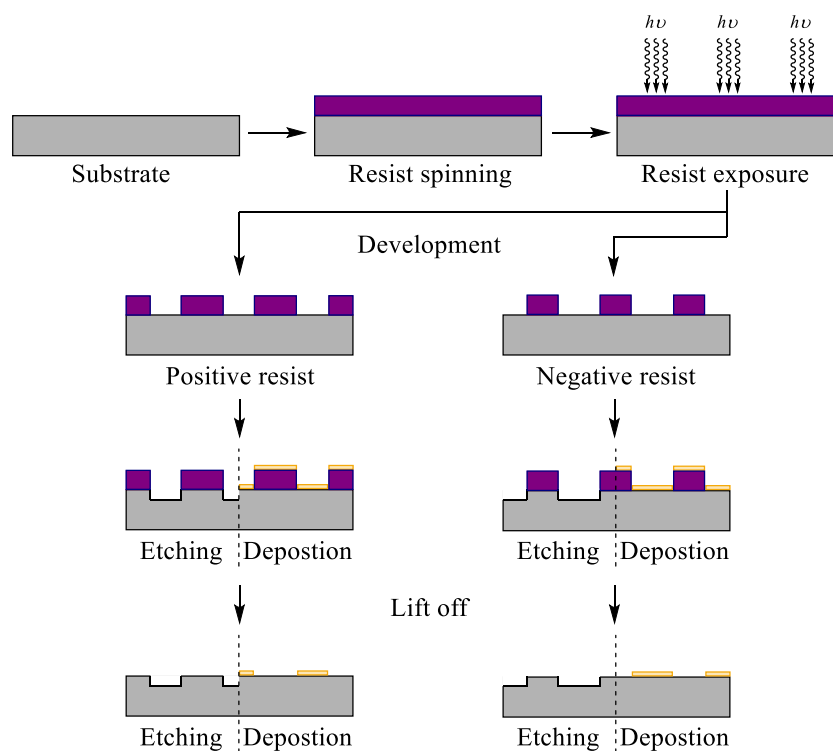


Figure 1.16: The processes of photolithography, showing the difference in positive and negative resist techniques.

Self-assembly is the spontaneous organisation of two or more components into larger structures using covalent and/or noncovalent bonds.^{73,76} Self-assembly can occur in two or three dimensions, when this process occurs at a surface in two dimensions the generated structure is called a self-assembled monolayer (SAM). Self-assembled monolayers are ordered assemblies formed by the adsorption of an active functionality onto a solid substrate.^{56,70,74} Most SAMs adsorb from solution onto an immersed substrate, depositing a layer of material one molecule thick. The simplicity of this technique makes it readily applicable to manufacturing, and an attractive way to deliver functional material to a substrate without waste or needing to remove material from the substrate.^{56,74}

Two of the most common functionalities for forming SAMs are thiols and silanes.^{56,77} Sulfur has a strong affinity to transition metal surfaces,^{78–80} and can form multiple bonds with surface metal clusters.⁸¹ The most common thiol SAM is alkanethiols on Au(111) substrates.⁷⁴ Thiols adsorb onto gold with two distinct adsorption kinetics; an initial fast step, which occurs in minutes, where the monolayer reaches 80–90% of its maximum thickness, and a second slow step, which takes several hours, where the monolayer reaches maximum thickness.⁸² The first step is diffusion controlled adsorption, and is strongly concentration dependant. The second step is the surface crystallisation of the monolayer, where the chains rearrange from a disordered state into unit cells, forming a two-dimensional crystal (Figure 1.17).^{74,82}

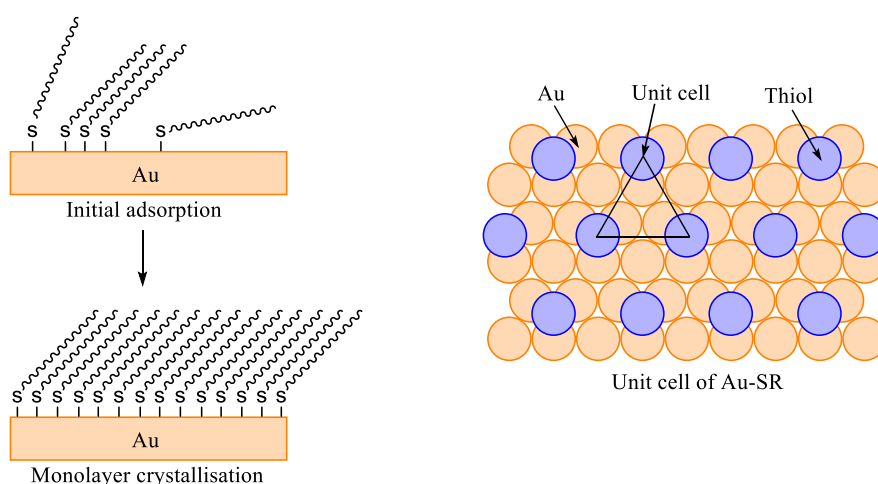


Figure 1.17: Adsorption of alkanethiols onto Au(111) showing the two stages of monolayer development (left) and the hexagonal coverage of the alkanethiol (right).

Organosilanes are capable of forming monolayers on a variety of surfaces as long as it is hydroxylated. SAMs of organosilanes have been prepared on silicon oxide,^{83–86} aluminium oxide,^{87,88} quartz,^{89,90} and glass,⁸⁶ among other substrates.⁷⁴ The driving force for the self-assembly of organosilanes is the formation of polysiloxane, which is connected to the surface silanol groups (when on silicon), and each other, by Si-O-Si bonds (Figure 1.18).⁷⁴

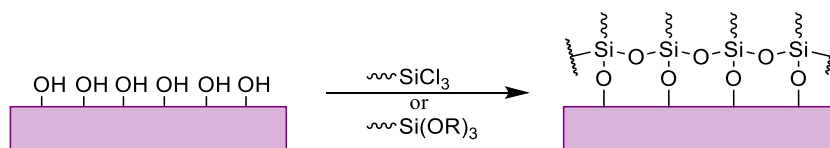


Figure 1.18: Silanisation of a hydroxylated substrate to form a monolayer of polysiloxane.

SAMs of reactive organosilanes, such as alkyltrichlorosilanes, require the control of the quantity of water present. In the absence of water monolayers can fail to form completely,⁸⁵ while in the presence of excess water the organosilane polymerises and deposits polysiloxane on the surface.⁸⁹ The use of silyl ethers reduces the effect water has upon the monolayer. This, combined with their easier handling, has made them popular choices for surface functionalisation.^{91–93}

1.2.5. Switchable adhesives

Switchable adhesives have the capability to de-bond as well as bond when an external stimulus is applied. This stimulus can be mechanical,^{22,67,68} thermal,^{21,24,26,66,75,94–97} electromagnetic,^{20,25,95,98,99} or chemical^{8,23,27,33,34,100–103} in nature. In some circumstances, the adhesive joint will need to bond and de-bond rapidly. The original inspiration for switchable adhesion came from natural examples, the Tokay gecko's foot being the most famous. The gecko utilises a hierarchical system of ever smaller hair follicles, starting with fibrils which then are divided repeatedly until they end with tiny spatula shaped structures 200-500 nm in size (Figure 1.19). This topography gives the gecko a substantially large contact area for adhesion, while at the same time allowing it to quickly remove its feet simply by curling its toes.^{25,104}

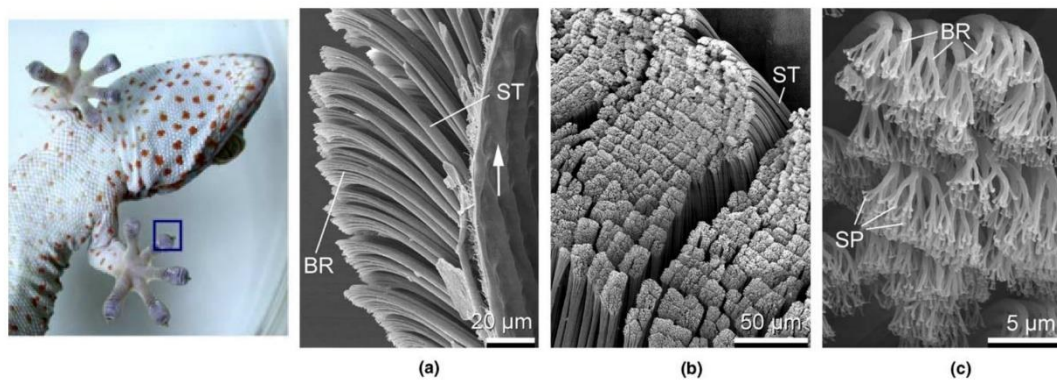


Figure 1.19: (From H. Gao et al.¹⁰⁴) Photograph and SEM images of Tokay gecko (*Gekko gecko*) fibril structure. Each toe contains hundreds of thousands of setae and each seta contains hundreds of spatulae. (a) and (b) Scanning electron micrographs of rows of setae at different magnifications. (c) Spatulae, the finest terminal branches of seta. ST: seta; SP: spatula; BR: branch. Image copyright Elsevier.¹

¹ Reprinted from *Mechanics of Materials*, Vol 37, Huajian Gao, Xiang Wang, Haimin Yao, Stanislav Gorb, Eduard Arzt, *Mechanics of hierarchical adhesion structures of geckos*, Pages 275-285, Copyright (2004), with permission from Elsevier.

This reversibility is achieved using the hierarchical structure of the setae and spatulae. Each seta contains hundreds of spatulae, and hundreds of thousands of setae multiply the adhesion strength of the spatula to provide the attachment strength needed. The spatulae act as a cohesive layer over the end of the seta. This cohesive energy is made up of van der Waals and elastic energies. Based upon this hierarchy, there are two methods of adhesive failure. Either sliding with respect to the substrate at angles $<30^\circ$, or detachment for angles $>30^\circ$. The maximum attachment force is observed when force is exerted at 30° . The gecko applies muscular force at 30° to adhere strongly to surfaces, then a pull-off force at 90° (toe-curling) to debond from the surface, as this force is an order of magnitude smaller than the maximum force at 30° .¹⁰⁴

Of the methods developed for switchable adhesion, most fall into two broad categories: topographical or chemical. They are controlled by either tuning the composition of the adhesive, or the morphology of either the adhesive or the substrate. Switchable topographical adhesion is based upon surface geometry, and is controlled by changing the morphology of either the adhesive or the substrate using a lock and key effect upon patterned surfaces.²⁵ Switchable chemical adhesion is based upon the composition of the surface, and is controlled by changing the properties of the responsive adhesive using an external stimulus.⁸

Switchable topographical adhesives have their adhesive strength altered by maximising and minimising the degree of contact area in a reversible process. They have been developed to respond to a variety of stimuli; including temperature,^{21,24,66} magnetic and electric fields,^{20,25} and mechanical stretching.^{22,67,68} The general principle of most designs of topographical adhesive is the maximization and minimization of the contact area in a switchable fashion.²²

Temperature-sensitive switchable adhesives often utilise thermosensitive shape memory polymers to alter the amount of the adhesive surface available for bonding.^{21,24,66} These adhesives utilise the glass transition temperature of a moulded polymer array. When the polymer is heated above its glass transition temperature, it can be deformed into a non-bonding conformation. When the polymer is cooled below its transition temperature, with the load still applied, this conformation is 'locked', resulting in a temporary non-adhesive surface due to the greatly reduced contact area. When the polymer is reheated to above its glass transition temperature, the surface recovers its original, highly adhesive, conformation.^{21,24,66}

Adhesives which switch using magnetic and electric fields utilise the magnetic switching of nickel cantilevers coated with vertically aligned polymer nanorods, or the electrically controlled capillary action of water surface tension.^{20,25} For magnetic switching, the nickel cantilevers can be reoriented using a magnetic field to rotate the ends away from the surface, greatly decreasing the contact area, and therefore the adhesion force.²⁵ Electrical switching relies on moving multiple water contacts into and out of contact with the surface. The large number of contacts multiply the adhesion caused by surface tension. A low-voltage pulse is used to reversibly drive the water through the capillary contacts by electroosmotic flow, allowing the device to make and break adhesive contact with the substrate.²⁰

Switchable adhesion by mechanical switching encompasses a variety of methods, all of which utilise a mechanical stimulus.^{22,67,68} For example, mechanical stretching utilises a fibrillar array, which is held taut to adhere to the surface, and allowed to relax to a wrinkled conformation to detach from the surface due to a low contact area. Adhesion is effected by orientating the fibrillar array normal to the surface whilst stretched under tension, which generates a large contact area. Removing the tension causes the film to relax to its original wrinkled configuration, causing the fibrillar array to become mismatched with the surface, greatly reducing the contact area and breaking the adhesive contact.²²

Some of these topographical adhesives are being developed towards specific applications, a recent example is a photocontrollable microstructured transport device inspired by the gecko foot architecture.³² This material consists of a three-layered structure made of: a moulded polydimethylsiloxane (PDMS) adhesive, which contains ‘mushroom’ shaped features similar to gecko setae; a photoresponsive actuator, consisting of azobenzene-containing crosslinked liquid crystalline elastomers (LCEs); and a second PDMS backing layer to seal the device. The LCE film acts as a muscle-like actuator upon irradiation. When illuminated with 320-380 nm UV light the azobenzene groups undergo a reversible trans-cis isomerisation, causing a macroscopic deformation of the LCE material. When the material is illuminated with 420-480 nm visible light, or exposed to thermal stimuli, the isomerisation is reversed, and the LCE material relaxes to its original conformation. This photocontrollability allows the composite material to either create an adhesive contact, by bringing the material into contact with the substrate, or cause the detachment from a substrate, by causing the adhesive to peel away from the surface (Figure 1.20).

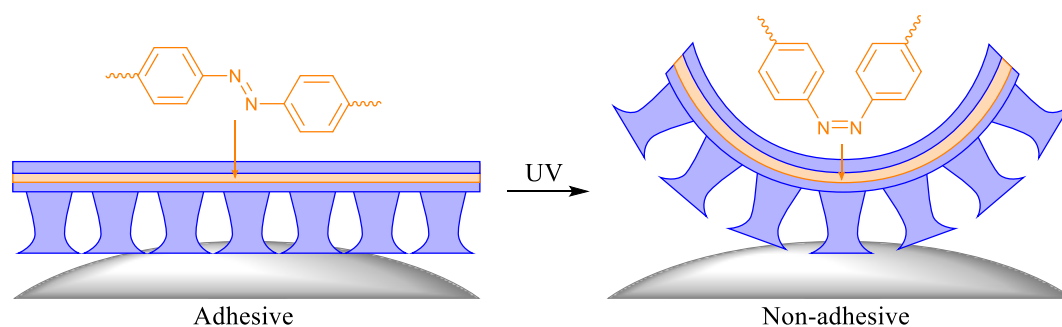


Figure 1.20: Switching of adhesion using a photoresponsive actuator to deform a PDMS adhesive layer, causing a reduction of contact area and an associated reduction in adhesion.

It was found that the device only required UV irradiation to activate the deformation, and when the illumination is removed the device relaxes to the initial state without further stimulation. This was attributed to a combination of the elastic muscle-like nature of the composite material, and the high thermal capacity of the material, causing thermal cis-trans isomerisation from heat build-up.³² This material proves promising for use as a multifunctional manipulator for the transportation of various materials, especially at the micro-scale. However, its involved production and its quick relaxation would make it unsuitable as a large-scale structural adhesive.

Switchable chemical adhesives are based upon manipulating the molecular interactions between the adhesive and the substrate. These interactions can include hydrogen bonding, electrostatic interactions, or hydrophobic interactions. The switching is usually achieved by using stimuli responsive polymers. They have been developed to respond to a variety of stimuli; including temperature,^{26,75,94–97} light,^{95,98,99} solvent,^{23,100,101} and pH.^{8,27,33,34,102,103}

Temperature-sensitive switchable adhesives utilise a phase transition in polymers such as glass transitions, melting, and crystallising.^{26,75,94–97} Transitions between highly ordered smectic phases and disordered isotropic phases results in an associated transition from a hard to a soft material. This affects the ‘tack’ properties and the wetting ability of the polymer.²⁶ Fluorinated liquid crystalline polymers have been used to achieve temperature switching. These polymers undergo a first-order phase transition from a crystalline smectic phase to an amorphous isotropic phase upon heating, and importantly, transition back to the ordered smectic phase upon cooling.

In the smectic liquid crystalline phase the polymer shows no adhesive response, however in the isotropic phase the polymer shows a strong adhesive response. If the material is heated further, then the adhesion drops off again. This is because in the isotropic phase the polymer has a greater degree of mobility, so can increase the contact with the substrate and orientate the polymer functionalities to maximise adhesive interactions. However, this is a delicate balance between the factors which increase and decrease tack, so at higher temperatures factors which decrease the tack, such as increased flow, reduce the adhesion.⁹⁴ These polymers are relatively straightforward to prepare and apply to substrates, making them good candidates for commercialisation. However, their use would be restricted to use within a comparatively narrow temperature range, so would not be suitable for the aerospace or automotive industries, which require a large operational temperature range.

Light-switching based adhesives use polymers which crosslink upon exposure to light, causing it to harden and reduce its bonding strength.^{95,98,99} These adhesives are used as traditional adhesives until they need to be removed, the only difference being that they must be shielded from light until removal, which is normally achieved via an opaque backing. When the adhesive needs to be removed, the adhesive is exposed to visible light to cause a free radical crosslinking process using a photoinitiator and a crosslinking agent, which are present in the adhesive. This crosslinking causes the material to harden, greatly reducing its adhesive strength. The safety and ease of use of this process have made it useful in the development of removable wound dressings.^{95,99}

Solvent switching adhesives are based upon the properties of mixed glassy polymer brushes. These brushes are switched by exposure to selective solvents, making them mobile, and frozen in either a bonding or non-bonding state.^{23,100,101} The adhesive works by combining two types of polymer brush in the mixed layer, one bonding (generally hydrophilic), and one non-bonding (generally hydrophobic). The mixed polymer film morphology is dependent upon the lateral and vertical phase separation of the polymers. This phase separation is altered by use of differing solvents which preferentially solvate one of the two polymers. Upon exposure to the solvent, the polymer which is solvated preferentially occupies the upper fraction of the layer, presenting its functionality at the surface, whilst the other polymer is desolvated and collapses to the lower fraction of the layer. By switching solvents, the adhesive polymers can be brought to the surface, making the material adhesive, or collapsed to the bottom of the layer, making the material non-adhesive.²³

Some of these chemical adhesives are being developed towards specific applications. For example, an adhesive has been developed for carpet tiles which can be switched off to enable recycling at the end of the life of the tile.³¹ The adhesive consists of expanded starch which has been hydrophobically modified by acetylation to increase the hydrophobicity of the adhesive, which improves the wash resistance of the adhesive. Corn starch is gelatinised in hot water and allowed to crystallise. The water is then replaced with ethanol, which prevents the collapse of the pore structure formed when the gel is dried. This process creates a metastable form of starch with a much higher surface area and porosity compared to the native starch. Hydrophobic modification of the generated material by acetylation protects the metastable structure from collapse due to atmospheric moisture. The high porosity facilitates mixing of the adhesive solution, and hence plasticisation.

The adhesive is utilised in the same manner as traditional adhesives, making use of a high surface area and suitable viscosity and wetting characteristics to enable good penetration and intimate contact with the carpet fibres. When the structure needs to be debonded, the adhesive is exposed to hot water or steam, which overcomes the hydrophobic modification and causes the material to rapidly collapse to a low surface area solid, which minimises the adhesion (Figure 1.21).³¹ This system is an excellent solution to the recovery of nylon from bonded carpet tiles, which makes use of renewable materials in a simple process. However, although the adhesion can be switched off, it is not reversible. The adhesive also relies on traditional adhesive mechanisms of wetting and viscosity to resist separation. Although this is suitable for adhering fabric, it would not be suitable for non-porous substrates. The lack of reusability also makes it unsuitable for use in component exchange across the lifetime of an assembly.

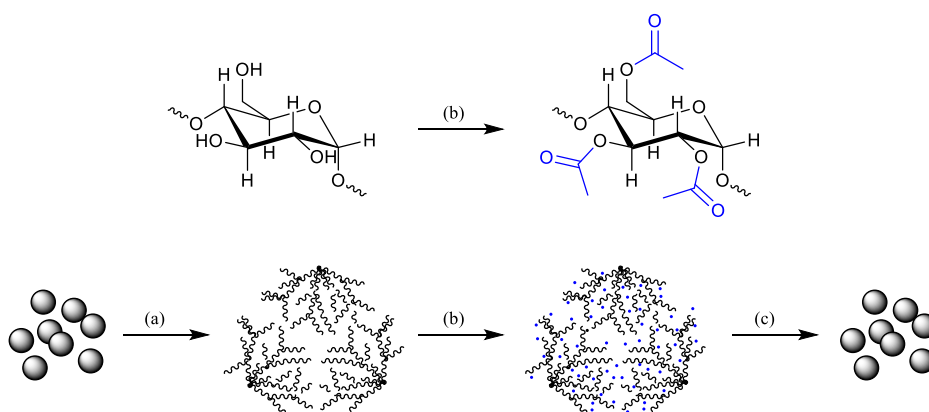


Figure 1.21: Switchable adhesion using expanded starch. (a) Expansion of starch matrix using hot water. (b) Hydrophobic modification of expanded starch by acetylation. (c) Collapse of expanded starch upon treatment with hot water to reverse adhesion.

pH switchable adhesives consist of weak polyelectrolyte polymers which change their charge state, and undergo conformational transitions with changing solution pH.^{8,27,33,34,102,103} These polymers are capable of becoming electrically charged via the protonation or deprotonation of the polymer chains at varying proton concentrations, i.e. varying pH ranges. The increased charge along the polymer causes it to extend due to Coulombic repulsion or osmotic pressure from the associated counter-ions.^{8,27,33,34}

Weak polyelectrolytes are required, so that the degree of polymer charge can be controlled by the solution pH, as strong polyelectrolytes are predominately dissociated over most pH ranges. When a positively charged polyelectrolyte brush or gel is brought into contact with a negatively charged polyelectrolyte brush or gel the two are held together via electrostatic interactions, forming a system similar to an electrical double layer between the two surfaces. Adhesion can also be effected using one charged polyelectrolyte and one uncharged polymer through the formation of hydrogen bonds and van der Waals interactions.^{8,27,33,34}

In solution, these polyelectrolytes undergo a transition from an extended charged hydrophilic state to a neutral state when the solution pH changes, resulting in the polymer brush collapsing out of the solution. This reduction in charge, and the associated shape transition, causes the adhesive bonds, electrostatic or hydrogen, to fail at the interface. This results in the system debonding without damage to the interface. When the pH is reversed so that the charge is restored, the system becomes bonding again (Figure 1.22).^{8,27,33,34}

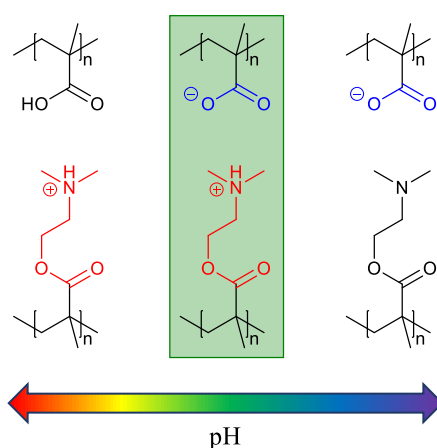


Figure 1.22: pH switchable adhesion. As the pH of the system is altered the charge state of the two polyelectrolytes varies, with both polymers charged and adhesive at \sim pH7 (green box).

Recent work has shown that this process is reversible and can be cycled a number of times whilst still giving adhesion.³³ Much of the previous work conducted has used polyelectrolyte brushes grown directly from a silicon surface, which have been tested for switchable adhesion using a polyelectrolyte hydrogel with the opposite charge.^{8,27,33} As the pH is altered the gel can be switched between adhering to the brush layer and dissociating from it. This system shows great promise as a truly reversible switchable adhesive which could potentially have applications in the disassembling and reassembling of structures multiple times over the lifespan of an assembly. However, the polymer brushes used to generate the pH and conformational changes must currently be synthesised on the substrate.

The synthesis of the polyelectrolyte brushes (Figure 1.23) requires the use of reactive chemicals, metal catalysts, and both anhydrous and deoxygenated conditions over the course of the synthesis.^{8,27,33,34} Although this is achievable in a laboratory environment on a relatively small scale, this process would be difficult to translate to large components in a commercial environment. This work looks at taking the functional polyelectrolytes required, and making them applicable in one coat. This will reduce costs by allowing the adhesive to be produced in bulk and stored until required. It will also make them useful as an applicable coating, which could be used in existing manufacturing processes without a dramatic shift in the method.

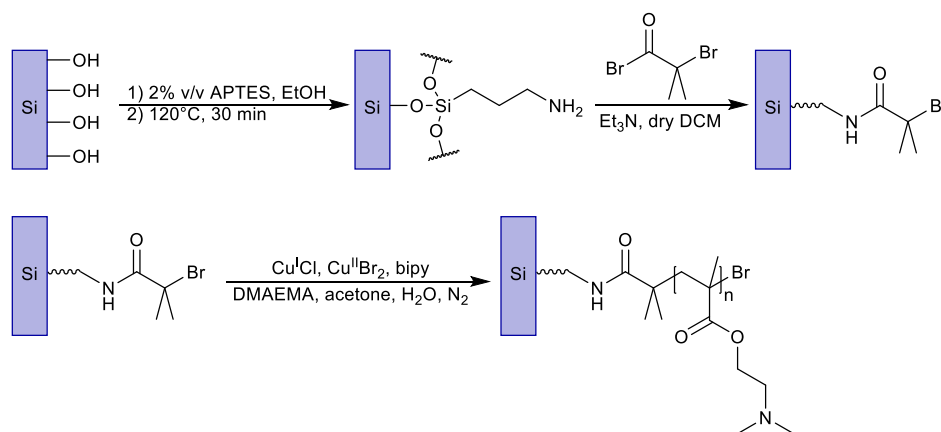


Figure 1.23: Synthesis of polyelectrolyte brush. The substrate is cleaned and hydroxylated and (3-aminopropyl)triethoxysilane (APTES) is deposited and annealed. The polymerisation initiator α -bromoisobutyryl bromide is coupled to the activated surface using triethylamine (Et_3N) under anhydrous conditions. The polyelectrolyte 2-(dimethylamino)ethyl methacrylate (DMAEMA) shown) is then grown from the surface using copper catalysed (copper(I) chloride ($\text{Cu}^{\text{I}}\text{Cl}$), copper(II)bromide ($\text{Cu}^{\text{II}}\text{Br}$), 2,2'-bipyridine (bipy)) atom transfer radical polymerisation (ATRP) under inert atmosphere (nitrogen).

1.3. Polymers and polyelectrolytes

Polymers are large macromolecules constructed from repeating units, or monomers. The large size of these macromolecules gives them properties not generally observed with smaller molecules.^{105,106} Polymers have proven a vital component of modern adhesives, increasing their strength and versatility. This has mostly been due to the ability of polymers to flow and wet a substrate, and then cure to a harder, yet flexible, material.⁵ This is normally achieved through manipulation of the thermal properties of the polymer or through secondary crosslinking reactions. As polymer technology has developed, with an ever-increasing control over, and functionality of, polymers, new properties and applications have been developed. Such developments include the use of polymers for switchable adhesion.^{8,21,67,68,75,94–100,22,101–103,23,24,26,27,33,34,66}

The majority of new polymer functionality is achieved through manipulation of novel monomers, or the combination of existing polymers. Monomers are the essential building block of polymers, and require two or more bonding sites through which they can be linked to other monomers, forming the polymer chain. More complex or crosslinked structures can be formed by using monomers with more than two bonding sites. The number of monomers in the polymer chain formed is known as the degree of polymerisation (DP), and is represented by n in chemical structures.^{105,106}

There are two major categories of polymerisation, depending upon how the monomer units bond. These are step-growth and addition polymerisation (Figure 1.24). Step-growth polymerisations are predominately, but not always, condensation reactions between alcohols and carboxylates, with the resultant loss of a small molecule in each step. Addition polymerisations utilise unsaturated bonds, such as alkenes and alkynes, and open the unsaturated bond using a free radical or ionic initiator. As this is a bond opening process there is no loss of a small molecule in the polymerisation.^{105,106}

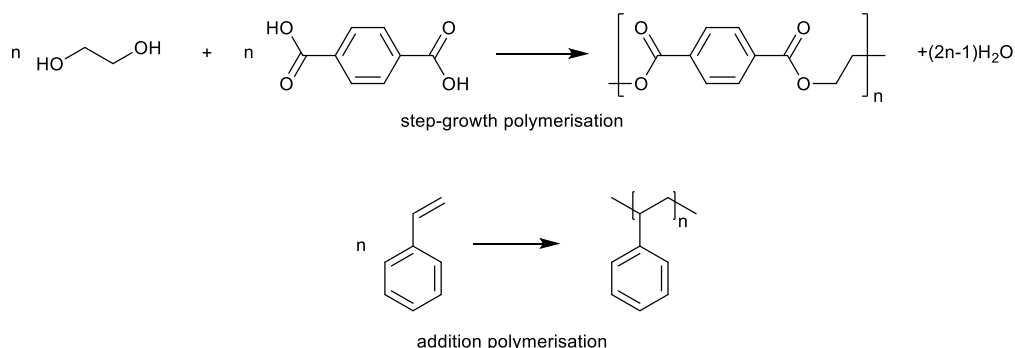


Figure 1.24: (top) Step-growth polymerisation of ethylene glycol and terephthalic acid to give the polyester poly(ethylene terephthalate). (bottom) Addition polymerisation of styrene to give poly(styrene).¹⁰⁵

One of the major differences between polymers and simple molecules is the lack of an exact molar mass. This is because the length of the chain formed by polymerisation is governed by random events controlled by the availability of reactive groups and the lifetime of reactive radicals. Due to this random component to the formation of polymers, there is a distribution of chain lengths formed. Therefore, polymers are characterised by molar mass averages and the distribution of masses.^{105,106} This is best conducted using gel permeation chromatography (GPC), a form of size exclusion chromatography (SEC). GPC separates the analytes based upon size by passing it over microporous beads. Small molecules can enter the pores of the beads whereas larger molecules cannot, so small molecules therefore have a higher retention time. This technique determines a range of mass averages and the dispersity index (\mathcal{D}) of polymers (Figure 1.25).^{105,107}

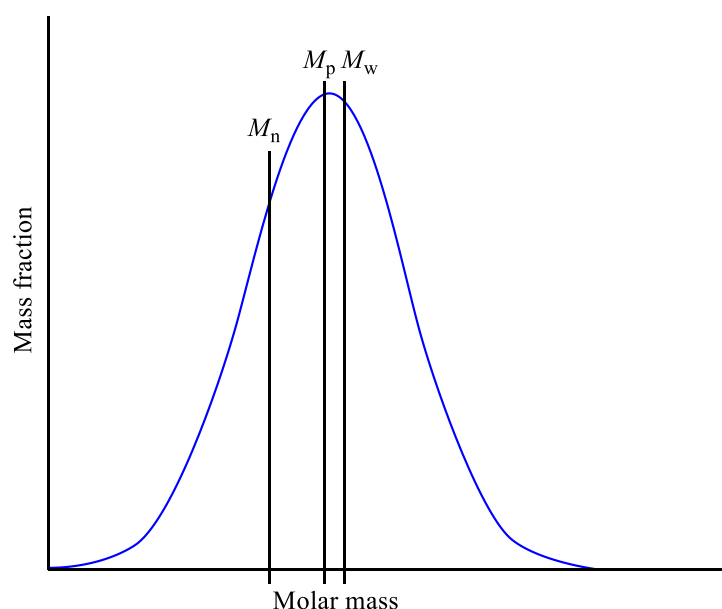


Figure 1.25: The molar mass distribution of a mono-modal polymer.

The peak molar mass (M_p) is the largest mass fraction of the polymer, and represents the modal value for the polymer molar mass. The number average molar mass (M_n) is the mean value for the polymer, and for a symmetrical distribution marks the mass at which there are equal numbers of molecules on each side at higher and lower masses. The value of M_n influences the thermodynamic properties of the molecule. The mass average molar mass (M_w) is the mass at which there are equal masses of molecules on each side at higher and lower masses. M_w is sensitive to large molecules and influences the bulk properties and the toughness of the polymer. The ratio of M_w to M_n is used to calculate the dispersity index of the polymer, which gives an indication of the range of molecular masses. The broader the molecular mass distribution, the larger the dispersity index. A molecule with no dispersity would have a dispersity index of 1.^{105,107}

1.3.1. Free-radical addition and ‘living’ polymerisations

Traditional addition polymerisation has been utilised successfully on an industrial scale for decades to produce important polymers from alkene-based monomers. The reactivity of the π -bonds leads to rearrangement when activated by a free-radical or ionic initiator. The new active species generated by this rearrangement can then react further with other monomers, leading to propagation of the reaction, and formation of a single macromolecule. The growth of this macromolecule is stopped when the propagating active species is neutralised by a termination reaction. The polymerisation process can be characterised by three distinct stages: activation, where the initiator forms the initial active species; propagation, where the formed active species reacts further with other monomers in a kinetic chain, forming many repeat additions of monomer to the growing macromolecule; and termination, where the chain propagation is stopped by neutralisation or transfer of the active species (Figure 1.26).¹⁰⁵

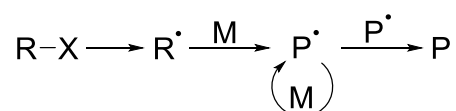


Figure 1.26: Example of a free-radical addition polymerisation. The first step is formation of the radical initiator (R^{\bullet}) which activates the monomer (M). The second step is the propagation of the polymer (P^{\bullet}) which grows the macromolecule. The third step is termination with another radical, such as another propagating chain, to give the final polymer (P).

Traditional free-radical polymerisations are, however, difficult to control due to the numerous fast, irreversible, chain transfer and termination reactions that occur. Various side reactions lead to products with a broad molar mass distribution, and lower than predicted molar masses. As a greater degree of control is desired by many newer applications, techniques to control the polymerisation have been developed. These controlled radical polymerisations (CRP), or ‘living’ radical polymerisations (LRP), produce structurally well-defined polymers with a low dispersity.

The major difference between traditional free-radical polymerisations and living radical polymerisations is the formation of a rapid dynamic equilibrium between a small quantity of active chain-growing free radicals, and a much larger excess of inactive dormant species (Figure 1.27). The dormant species ($\text{P}_n\text{-X}$) is terminated by a group (X) capable of reversibly terminating with the propagating polymer chain end (P_n^{\bullet}) without initiating further polymerisations. Because the capping radical (X^{\bullet}) cannot initiate chain growth, only the polymer radical (P_n^{\bullet}) can propagate the chain, leading to controlled growth of a small number of polymer chains at any one time.¹⁰⁵

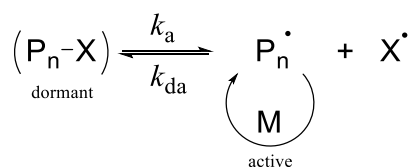


Figure 1.27: (Based on J.M.G. Cowie and V. Arrighi¹⁰⁵) Living radical polymerisation showing the equilibrium between the dormant ($\text{P}_n\text{-X}$) and active ($\text{P}_n\cdot$) species. Here k_a and k_{da} are the activation and deactivation rate constants, respectively.¹⁰⁵

These polymerisation techniques include; nitroxide-mediated polymerisation, atom transfer radical polymerisation (ATRP),¹⁰⁸ and reversible addition-fragmentation chain transfer (RAFT).¹⁰⁹ ATRP and RAFT have the advantage that the initial growth point of the polymer chain can be coupled to a molecule of interest, allowing the polymer to be grown from a specific functionality, in this work the surface-active calix[4]resrocinarene.¹⁰⁵

1.3.2. Nitroxide-Mediated Polymerisation

Nitroxide-mediated polymerisations are a class of dissociation-combination polymerisations, and epitomise this type of polymerisation. Early examples utilised 2,2,6,6-tetramethyl piperidiny-1-oxy (TEMPO) as the mediating stable free radical. However, TEMPO gives poor yields of polymer, and the resulting material contains several by-products which are difficult to remove. The TEMPO-based system has been improved upon by modifying the nitroxide and through the inclusion of additives, such as acetic acid. The most significant new nitroxides developed have been the alkoxyamine type structures (Figure 1.28). These nitroxides can polymerise a greater variety of monomers, and give a greater control over the molecular weight of the polymer, with a current upper limit of $M_n \leq 200,000$ whilst retaining ‘living’ character.¹⁰⁵

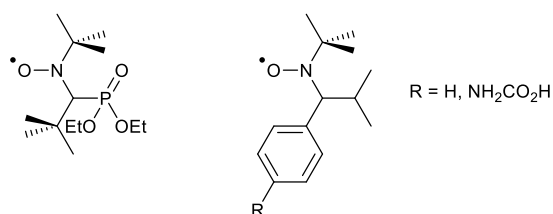


Figure 1.28: Alkoxyamine based nitroxides.

An example of a TEMPO mediated nitroxide-mediated polymerisation is shown in Figure 1.29. The polymerisation is started by the decomposition of a unimolecular-initiating species ($\text{P}_n\text{-X}$), which generates the chain initiating radical $\text{P}_n\cdot$ and the mediating radical $\text{X}\cdot$. A small degree of $\text{P}_n\cdot$ radicals irreversibly terminate, generating a small excess of $\text{X}\cdot$. This controls the reaction by through the reversible effect of the persistent radical $\text{X}\cdot$.¹⁰⁵

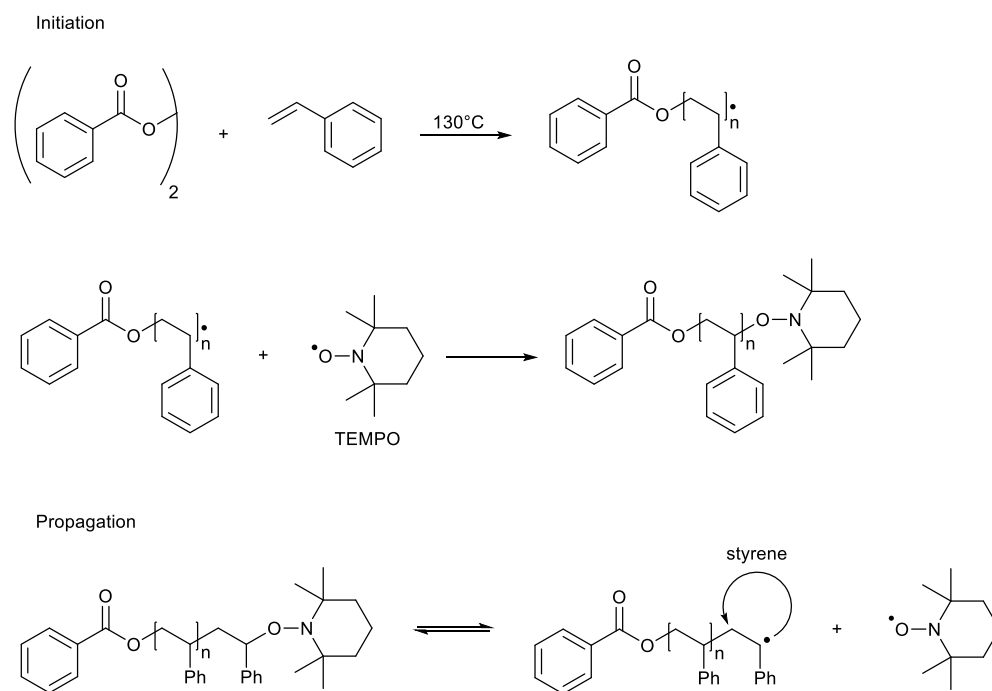


Figure 1.29: Polymerisation of styrene using nitroxide-mediated polymerisation.

1.3.3. Atom transfer radical polymerisation

Atom transfer radical polymerisation gives a uniform chain growth, and hence a lower dispersity, due to its metal-based catalyst. This catalyst generates an equilibrium between an active propagating form and an inactive dormant form of the polymer (Figure 1.30). The inactive state is vastly preferred in the equilibrium so only a few monomer units are added at any one time in order to maintain control. This equilibrium lowers the concentration of propagating radicals, suppressing unintentional chain termination and controlling molar masses. It is this slow propagation rate, combined with termination only occurring when the polymerisation approaches complete conversion, that gives low dispersity.^{105,108}

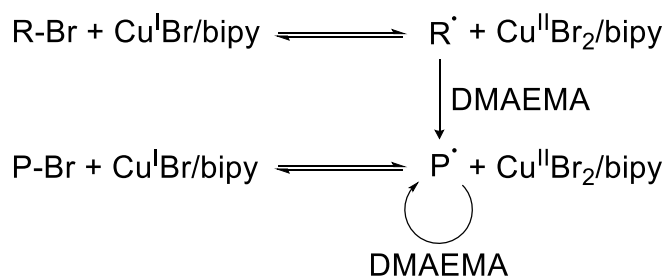


Figure 1.30: Overall Scheme of the ATRP reaction. R-Br is the initiator. $\text{Cu}^{\text{I}}\text{Br/bipy}$ and $\text{Cu}^{\text{II}}\text{Br}_2/\text{bipy}$ are the two oxidation states of the catalyst. R^{\cdot} is the radical initiator. DMAEMA is the monomer (2-(dimethylamino)ethyl methacrylate). P^{\cdot} is the propagating active polymer. P-Br is the dormant polymer.^{105,108}

Methacrylate-based monomers are well suited to ATRP as its substituents can stabilise the propagating radical by delocalisation of the radical over two or more atoms. The metal catalyst determines the equilibrium constant between the active and dormant species, which in turn determines the polymerisation rate. If the equilibrium constant is too small, it may inhibit the polymerisation, as there will only be a small amount of material able to react with the monomers. If it is too large, it can lead to a high distribution of chain lengths as there will be a large amount of propagating species. The metal catalyst itself needs: two accessible oxidation states separated by one electron, a relatively high affinity for halogens, a strong ligand complexation, and an expandable coordination sphere when oxidised to accommodate the halogen. These characteristics allow the catalyst to cleave the C-Br bond and generate the propagating radical (R' or P'), as the bromine atom can be readily accommodated by the metal catalyst. Copper based catalysts have proven to be the most versatile for ATRP.¹⁰⁸

1.3.4. Reversible addition-fragmentation chain transfer polymerisation

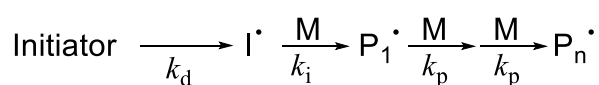
Reversible addition-fragmentation chain transfer is a reversible deactivation radical polymerisation (RDRP) which has a strong living character, giving good control over molar masses and low dispersities. The RAFT process gives reversible deactivation of the propagating radicals by degenerate chain transfer, which involves the exchange of functionality between two species differing only in molar mass. There are a variety of RAFT agents, most of which centre around thiocarbonylthio compounds.

The variation in RAFT agents allows for selection of an appropriate RAFT agent for: the monomer, the reaction conditions, and the required functionality of the final product. In addition to the processes normally observed in free-radical polymerisation, RAFT polymerisation also includes specific addition-fragmentation equilibria (Figure 1.31). It is important to note that the RAFT process does not generate or destroy any radicals, hence an external initiator is required to supply the radicals required for polymerisation.^{105,109,110}

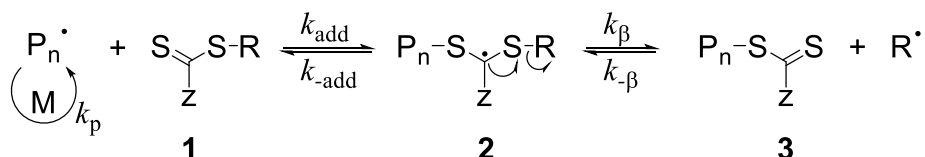
The RAFT agent can be tailored to the monomer and reaction conditions by altering the Z and R groups. The Z group alters the rate of addition of propagating radicals (P_n^{\cdot}) to the thiocarbonyl of **1** and **3**, and the rate of fragmentation of the intermediates **2** and **4**. The rate constant k_{add} can be altered over ~5 orders of magnitude by changing the Z group. Monomers can be classed as either 'more activated' monomers (MAMs) or 'less activated' monomers (LAMs).

Propagating radicals with a terminal MAM are less reactive in radical addition (lower k_p and k_{add}), so a more active RAFT agent is required to maintain good control. These propagating radicals are good homolytic leaving groups, so polymerisation retardation by slow fragmentation is unlikely. Propagating radicals with a terminal LAM are much more reactive in radical addition (higher k_p and k_{add}), so a less active RAFT agent is required to maintain good control. As the propagating poly(LAM) radical is a poor homolytic leaving group when more active RAFT agents are used, fragmentation is slow and inhibition or retardation is likely.^{109,110}

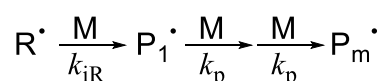
Initiation:



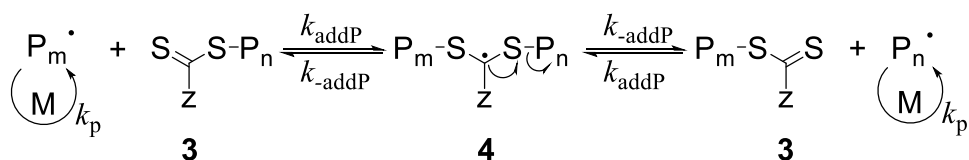
Initialisation:



Reinitiation:



Main equilibrium:



Termination:

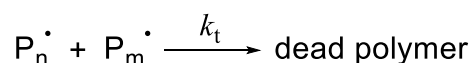


Figure 1.31: (Based on D.J. Keddie et al.^{109,110}) RAFT equilibria. k_d is the rate constant for initiator decomposition. k_i is the rate constant for initiation. k_p is the rate constant for polymerisation/monomer addition. k_{add} is the rate constant for radical addition of P_n^\bullet and **1**. k_{-add} is the rate constant for fragmentation of P_n^\bullet and **1**. k_β is the rate constant for fragmentation of R^\bullet and **3**. $k_{-\beta}$ is the rate constant for radical addition of R^\bullet and **3**. k_{iR} is the rate constant for reinitiation. k_{addP} is the rate constant for radical addition of P^\bullet and **3**. k_{-addP} is the rate constant for fragmentation of P^\bullet and **3**. k_t is the rate constant for termination.

The R group needs to be a good homolytic leaving group compared to the propagating radicals (P_n^\bullet), so that when P_n^\bullet adds to **1**, the intermediate **2** fragments rapidly and partitions in favour of **3** and R^\bullet . The radical expelled (R^\bullet) needs to be able to efficiently reinitiate polymerisation ($k_{iR} > k_p$), otherwise retardation may occur. The stability of the radical formed is important in determining the fragmentation rate, and is predominately determined by how well the R group can stabilise the radical, for example through increased substitution.^{109,110}

1.3.5. Polyelectrolytes

Polyelectrolytes are polymers consisting of ionisable monomers. They are usually soluble in water and ionising solvents. In these solvents, they dissociate into macromolecular polyions carrying multiple charges and an equivalent amount of small molecule counter-ions (Figure 1.32).¹¹¹ When in an electrolyte solution, co-ions of the same charge as the polyion will be present in the solution. For example, for the sodium salt of poly(styrene sulfonic acid) in solution with sodium chloride (NaCl), the Na^+ ions are the counter-ions and the Cl^- ions are the co-ions.¹¹² Polyelectrolytes exist in a variety of conformations including rods, globules, pearl-necklace structures, torii, and helices depending upon the properties of the molecule and the balance between the electrostatic and solvent-induced interactions.¹¹³

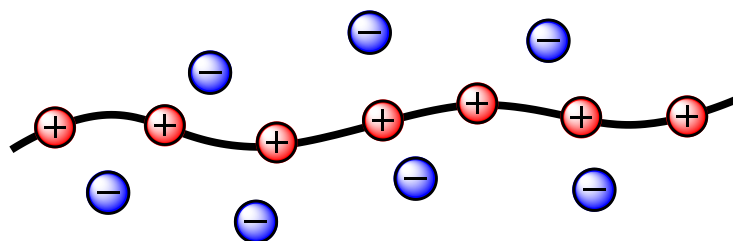


Figure 1.32: (Based on D. Hinderberger et al.¹¹¹) A polyelectrolyte that is dissociated into a polyion and small counter-ions in polar solvents.

The physicochemical properties of polyelectrolytes in solution are not simply intermediate between the properties of small molecule electrolytes and neutral polymers.¹¹² On the contrary, they differ significantly from the properties of these materials and are the result of the balance between the solvent-induced hydrophobic interactions of the backbone and the electrostatic interactions of the ionisable side groups.¹¹³ Polar solvents are usually used to dissolve polyelectrolytes due to their polar side groups. However, these are poor solvents for the polymer hydrocarbon backbone. This poor solubility is equivalent to an attractive hydrophobic interaction, which favours a more collapsed conformation.¹¹¹

The gain in entropy from the dissociation of counter-ions from the side groups results in a highly charged polymer, and the electrostatic repulsion between the like charges leads to a preference for an extended conformation of the polymer chain.¹¹¹ Intramolecular interactions are also an important factor because bond-angles and torsional potentials will have an effect on the presentation of the charged groups in solution.¹¹³

In polyelectrolyte solutions, the activity (effective concentration) and the mobility of the counter-ions are reduced below the bulk values, while the activity of water is high due to a low osmotic pressure. When an external field is applied to a polyelectrolyte solution, some of the counter-ions move as part of the polyion. In contrast to small molecule electrolyte solutions, the discrepancy between the observed and ideal systems increases with dilution of the polyelectrolyte. The reduced viscosity also increases upon dilution, whereas the opposite is true for neutral polymers.¹¹⁴ The ion specific effects caused by water rearrangement upon dilution can alter the values for the heats of dilution, which electrostatic theory predicts should be exothermic, but can be either positive or negative.¹¹²

The properties of polyelectrolytes strongly rely upon the distribution of small ions in the vicinity of the polyions. There are two types of interaction between counter-ions and polyions. One is the Coulomb attraction of counter-ions to polyions, in which they are territorially bound, and the other is a specific interaction between individual charge sites on the chain and the counter-ions called site binding (Figure 1.33).

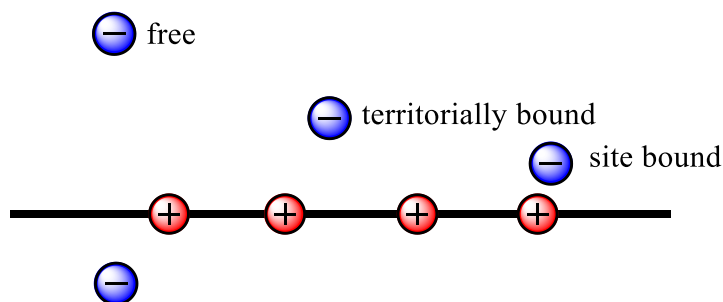


Figure 1.33: (Based on D. Hinderberger et al.¹¹¹) A polyelectrolyte chain showing the three different counter-ion regions.

The Coulombic attraction traps the counter-ions in an electrostatic field around the polyions, which makes the osmotic coefficient of the solution very low and reduces the effective charge density.^{111,112} The proportion of counter-ions in either the free or site bound states is determined by the opposing electrostatic and entropic effects. The Coulomb energy decreases when the counter-ions are very close to the polyion chain, but the reduction of effective system volume is counteracted by entropy maximisation.¹¹¹

The specific site-binding of counter-ions may displace the water molecules between the two interacting charges and is ion specific. The nature of the counter-ion and the charged group on the polyion, as well as any hydrophobic groups, will have an effect upon the water rearrangement between the approaching charges. These effects are even observable with strong polyelectrolytes such as poly(styrene sulfonic acid).¹¹²

For neutral polymers, one component systems qualitatively describe the conformational and thermodynamic properties. In good solvents the characteristic chain size scales with the degree of polymerisation, and the scaling exponent is changed as the quality of the solvent decreases. Polyelectrolyte solutions contain at least three key components: the polymer, the counter-ion, and the solvent. The conformational properties of the polyelectrolyte depend upon the charge on the polymer, the concentration of added salt, and the nature of the salt ions.¹¹³

In a one component system the intermolecular interactions between the polymer sites are affected by the solution properties. Any added salt affects the screening between charges on the chains. The degree of dissociation of the ionisable groups can also change, altering the net charge on the polymer molecules.¹¹³ The screening of intramolecular electrostatic repulsion within the polyion by counter-ions, especially multivalent counter-ions, can lead to a dominance of hydrophobic attraction. This can result in a more collapsed, globular, chain conformation.¹¹¹

In dilute solutions polymers exist as single chains (Figure 1.34). For neutral polymers in a θ -solvent the polymer coils act like ideal chains and adopt a random walk conformation. When two polymer chains approach each other there is only three-body repulsion and some temporary association which affects some properties. If there is zero net excluded volume, i.e. the chains can come into contact, they are able to overlap and temporarily entangle. For dilute neutral polymers in a good solvent, the excluded volume between the chains keeps them separated in an expanded self-avoiding walk conformation.¹¹⁵

In dilute polyelectrolyte solutions without salt, the polymer is dominated by charge repulsion, which keeps the chains separate and stretched into a directed random walk of electrostatic blobs. Along the chain axis the conformation is determined by charge repulsion, but in the other two orthogonal directions the chain is subject to random walks. As the concentration is raised, the conformations of individual chains begin to overlap each other.¹¹⁵

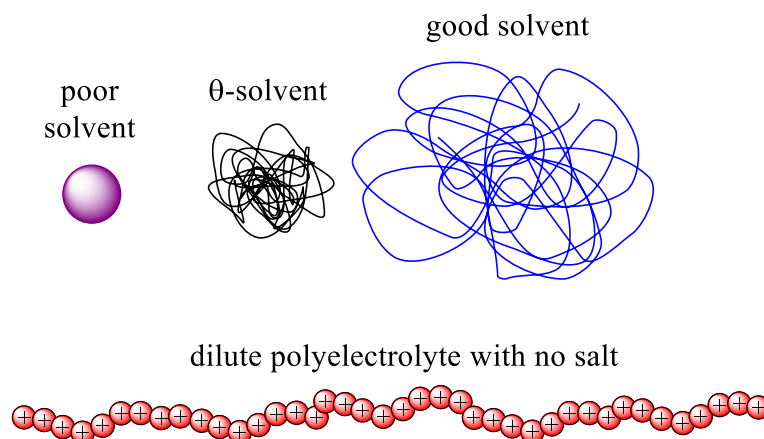


Figure 1.34: (Based on R. H. Colby¹¹⁵) Conformations of neutral polymers in dilute solution. In poor solvents, they collapse into dense coils (purple). In θ -solvents, they adopt random walks (black). In good solvents, they adopt self-avoiding walks (blue). Polyelectrolytes with no salt adopt the highly extended directed random walk conformation (red).

1.3.6. Surface modification with polymer brushes

Polymer brushes can be prepared through either physisorption or covalent attachment. Covalent attachment is often preferred as it overcomes the thermal solvolytic instability of physisorption.¹¹⁶ There are two ways of forming a layer of covalent end-grafted polymer chains, either by ‘grafting-from’ or ‘grafting-to’ the surface. In grafting-from techniques, a monolayer of initiators is attached to the surface of the substrate and the polymer chain is grown via surface-initiated polymerisation. This polymerisation technique is not hindered by the same kinetic or thermodynamic barriers as grafting-to the surface due to its step-wise addition.¹¹⁷

Atom transfer radical polymerisation can be used to give control over the brush thickness via its narrow molar mass distributions. However, there are certain functionalities that ATRP cannot be used for, such as the acid of (meth)acrylic acid, as it poisons the ATRP catalyst.¹¹⁶ Using this technique, polyelectrolyte brushes can be prepared by polymerising charged monomers on solid surfaces. Polyelectrolyte brushes can also be prepared by first growing a neutral polymer monolayer and then converting it into a charged brush by a quaternisation step.¹¹⁷

In grafting-to techniques, the charged or neutral polymers are attached to the substrate via a chemical bond between the end group of the polymer and the surface. This is normally achieved through the formation of self-assembled monolayers using specific end groups such as trichlorosilane.

Grafting-to techniques offer several advantages. For example, the polyelectrolytes can be synthesised and characterised prior to attachment. This allows a layer of well-defined linear polymers to be built up. However, as the monolayer forms, the adsorbed amount and the thickness of the brush layer becomes limited by thermodynamic and kinetic hindrances. Once the surface is covered with grafted chains the diffusion of additional chains into the layer against the concentration gradient becomes very slow. The polymer chains already grafted to the surface must also stretch to accommodate further chains in the monolayer. This chain stretching is an entropically unfavourable process and creates a barrier to further grafting.¹¹⁷

Neutral brushes can be converted to polyelectrolyte brushes after they have been grafted from the substrate by chemical treatment, for example by sulfonation. However, these treatments generally require harsh conditions which may result in side reactions and a limited degree of conversion, the notable exception being the quaternisation of substituted ammonia groups which can achieve nearly full conversion.¹¹⁷

1.3.7. Polyelectrolyte brushes

A polyelectrolyte brush is formed when a long linear polyelectrolyte chain is grafted densely to a solid surface. The polyelectrolyte chains can be grafted to either flat surfaces or to curved surfaces, such as colloidal particles (Figure 1.35). The strong electrostatic interaction between the polymer chains results in several properties not observed in monolayers of end-grafted uncharged macromolecules.¹¹⁷

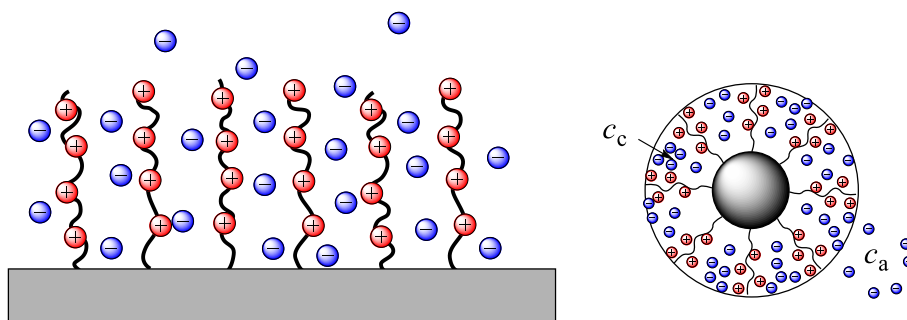


Figure 1.35: (Based on M. Ballauff and O. Borisov¹¹⁷) Scheme of planar and spherical polyelectrolyte brushes. The concentration of ions (c_c) within the brush layer can be markedly different than the salt concentration (c_a) outside.

There are two broad classes of polyelectrolyte brushes. If the grafted chains are strongly dissociating, e.g. poly(styrene sulfonic acid), then the polyelectrolyte is a quenched brush. The degree of dissociation of the ionisable side groups is less dependent on the pH of the system and is more influenced by the nature of the polyelectrolyte. If the grafted chains are weakly dissociating, e.g. poly(acrylic acid), then the polyelectrolyte is an annealed brush. The degree of dissociation of the ionisable groups depends directly upon the local pH, which itself relies upon both the pH and ionic strength of the bulk solution. Both classes of brush can be tuned by changing the ionic strength of the system.¹¹⁷

The Debye length is a measure of the net electrostatic effect of a charge carrier in solution, as well as the persistence length of those effects. At low concentrations of added salt (c_a), the Debye length is large and the brush properties are predominately determined by electrostatic interactions. At high concentrations of added salt there is a strong screening of the electrostatic interactions and the brush properties will be similar to those of a neutral polymer brush. The pH and c_a are therefore the two external variables which will have an effect upon the brush properties, such as swelling behaviour in water.¹¹⁷

The polyelectrolyte brush may also respond to the strength of the solvent used as well as specific interactions with the counter-ions. The essential properties of polyelectrolyte brushes are determined by the confinement of a major fraction of counter-ions compensating for the electrostatic charge of the polyion chains within the brush layer. The stretching of the polyelectrolyte chains is therefore controlled by the high osmotic pressure of the confined counter-ions.¹¹⁷

Two polyelectrolytes of opposite charge are used in this study to form the pH switchable adhesive. A polybasic polyelectrolyte is used to form a positively charged layer and a polyacidic polyelectrolyte is used to form a negatively charged layer. This provides an electrostatic interaction for adhesion. The polymers need to be weak polyelectrolytes so that they are both charged, and strongly adhesive, at intermediate pH (~ 6), and one or the other is uncharged at the extremes of pH, which reduces the strength of the adhesive interaction and causes the polymer to collapse away from the adhesive interface.

The polybase selected was poly(2-(dimethylamino)ethyl methacrylate) (pDMAEMA) and the polyacid selected was poly(methacrylic acid) (pMAA). These two polymers are both weak polyelectrolytes and will be charged at intermediate pH (pK_a 7.5 and 5.7 respectively),^{118,119} whilst at higher or lower pH one will be uncharged, and will collapse due to the hydrophobic effects of the methyl groups along the polymer backbone.^{8,27} These polymers have been shown to exhibit switchable adhesive behaviour in previous studies as 'grafted-from' brushes or gels.^{8,27,33,34}

1.4. Calix[4]resorcinarenes

The use of polyelectrolytes grafted from surfaces has been shown to provide a viable route to switchable adhesion. However, ‘grafted-from’ brushes require stringent laboratory conditions, such as anhydrous or deoxygenated environments,^{27–29} limiting their potential usefulness in mass market applications. If the polyelectrolyte brushes can be ‘grafted-to’ the surface of interest as a ‘dip-and-dry’ coating, then this will increase their ease of use. By making the adhesives an applicable coating, they can be used directly on large or more complex surfaces more readily than if they were generated in situ.

Calixarene, specifically calix[4]resorcinarene, was selected to provide a surface attachment group from which a polyelectrolyte could be grown. Calixarenes are a class of cyclic macromolecules formed from the condensation of phenols with aldehydes under acidic conditions to give cyclic oligomers of aryl units linked by alkylene bridges. Calixarenes are named for the Greek word *calix*, meaning chalice, with the *arene* suffix showing the presence of aromatic rings in the resulting molecule. The term was first noted by C. Gutsche and R. Muthukrishnan in 1978,¹²⁰ and relates to the bowl-like shape adopted by the molecules. This can be seen in Figure 1.36, which shows the structures of calix[4]arene and calix[4]resorcinarene. The bracketed number indicates the number of aromatic units in the cyclic oligomer.

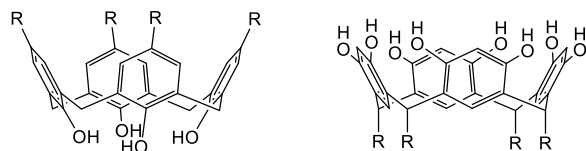


Figure 1.36: Structures of calix[4]arene (Left) and calix[4]resorcinarene (Right).

The three-dimensional structure of calixarenes results in a hydrophobic molecular cavity, or annulus, leading to their use in host-guest chemistry,^{121–127} and as synthetic ionophores,^{128–135} catalysts,^{136,137} and sensors.^{138–142} The internal directionality of calixarene macromolecules has also made them popular as surface modifiers. Calixarenes with modified alkyl substituents have been used to form monolayers on surfaces with the bowl facing away from the surface. For example, use of alkyl thiols allows for the formation of well-ordered monolayers on gold substrates,^{143–146} which exhibit host-guest behaviours.^{147–150}

Calixarenes have phenolic hydroxyl residues on one rim of the bowl. These residues can hydrogen bond to each other and to other hydrogen bond donors and acceptors. The conformation of the hydroxyl residues is determined by which aromatic compound is used to form the calixarene. If phenol is used, then the calixarene will adopt a ‘cone’ conformation with the hydroxyls facing inward towards the annulus¹⁵¹ on the narrower lower rim. These calixarenes can also adopt three other conformers; the partial cone, the 1,2-alternate, and the 1,3-alternate.^{151,152} These conformations can be locked or altered by changing the alkyl substituents or modifying the phenolic hydroxyls.¹⁵¹

Calix[4]resorcinarenes have eight phenolic hydroxyl residues which adopt a ‘crown’ conformation with the hydroxyls facing outwards away from the annulus on the wider upper rim.¹⁵¹ This ‘crown’ conformation is only formed upon prolonged heating under acid-catalysed reaction conditions. This results from the initially formed kinetically favoured isomers being converted into the more thermodynamically stable ‘crown’ isomer.^{153,154}

The phenolic hydroxyl residues on calix[4]resorcinarenes can hydrogen bond both to each other and to polar surfaces, such as silicon, leading to multi-point adsorption from solution.^{153,155} This makes calix[4]resorcinarenes useful for functionalising polar surfaces bowl down, and can be used to change the surface properties,^{156–159} such as rendering it hydro- and oleophobic,¹⁶⁰ or efficiently delivering functional material to a surface as a monolayer.^{153,155,161–163}

This capacity to readily modify surfaces under ambient conditions makes calix[4]resorcinarene well suited to use as a ‘dip-and-dry’ surface modifier for attaching polyelectrolytes to surfaces. The defined macrostructure of calixarene, with the adsorbing phenolic hydroxyls on the upper rim and the lower rim vacant for functionalisation, also makes it a useful molecular framework. It allows the polyelectrolyte to be orientated away from the surface attachment hydroxyls within the molecule.

Calix[4]resorcinarenes are formed from the condensation of four resorcinol units with an equivalent amount of the corresponding aldehydes. The acidic condensation of resorcinol with aldehyde to form calix[4]resorcinarene takes place as a series of electrophilic aromatic substitutions with cationic intermediates, as shown in Figure 1.37. Kinetic and molecular modelling studies¹⁶⁴ have shown that the ring closure to the calix[4]resorcinarene is at least as fast as chain propagation. This results in the four-membered macrocyclic product being the thermodynamic sink of the reaction, with linear oligomers longer than four aryl units depolymerising fast in comparison with ring opening. These factors promote the formation of the cyclic tetramer, hence the majority of the material is converted to the calix[4]resorcinarene.¹⁶⁴

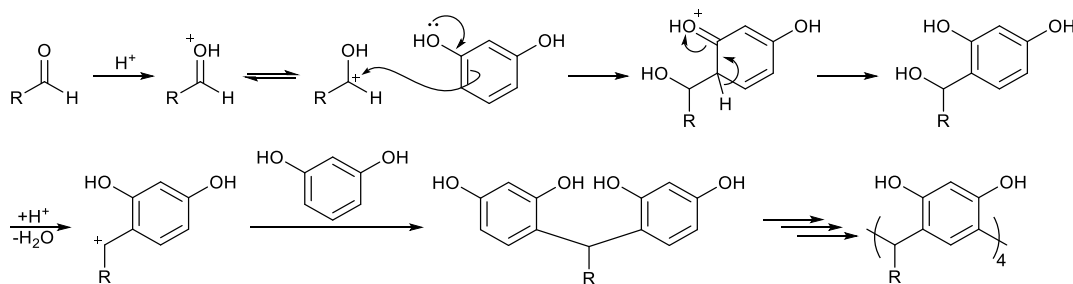


Figure 1.37: Pathway for the acid catalysed condensation of resorcinol and aldehydes.

1.5. Experimental techniques

The synthesis of the target adhesive was performed using established experimental techniques, with the two polymerisations methods used discussed in sections 1.3.3 and 1.3.4. The deposition and analysis of adhesives prepared was achieved using techniques including a mechanical tester set-up for measuring adhesion (probe test), and are briefly summarised below. Langmuir-Schaefer deposition was used to deposit ordered monolayers of the adhesive molecules, and ellipsometry was used to determine the thickness of these layers without causing damage to the films. The mechanical tester was fitted with a hydrogel of an opposite charge to the prepared layers, and was used to measure the adhesive force between the brush and the gel.

1.5.1. Langmuir films and Langmuir-Schaefer deposition

Langmuir films are formed when amphiphilic molecules are trapped at the interface between two dissimilar phases, either liquid-liquid or liquid-gas, with the water-air interface being the most common. When the amphiphile, dissolved in appropriate volatile organic solvent, is deposited onto the water surface the organic solvent will evaporate, leaving the amphiphilic molecules orientated at the water-air interface. The hydrophilic component will orientate into the water subphase, while the hydrophobic component will orientate into the air superphase. A surface monolayer will only be achieved if the balance between these two components is suitable. By sweeping a barrier over the surface of the water, the molecules are forced together and are eventually compressed to form an ordered monolayer, which is also known as a Langmuir film (Figure 1.38).¹⁶⁵

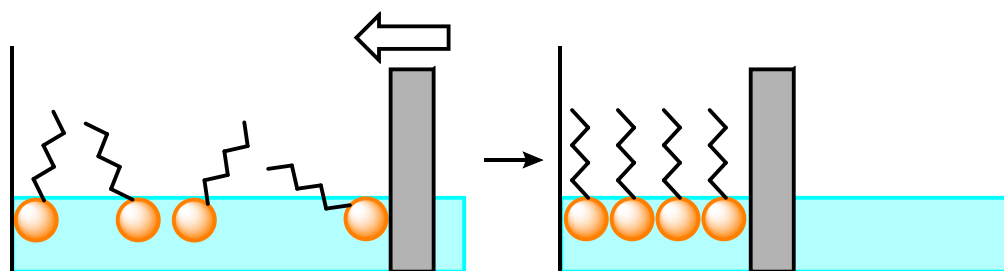


Figure 1.38: Compression of amphiphiles to form a Langmuir film.

When amphiphiles accumulate at the interface the surface tension drops. This is because this accumulation favours expansion of the interface. This behaviour allows the surface pressure to be monitored as a function of the area occupied by the monolayer. The surface pressure is monitored using a Wilhelmy plate attached to a microbalance.

The plot of surface pressure versus area gives a pressure-area isotherm (Figure 1.39). The isotherm shows three distinct regions: two-dimensional gas, two-dimensional liquid, and two-dimensional quasi-solid. After the amphiphile has been spread on the surface, and before any external pressure is applied, the molecules behave as a two-dimensional gas. During this region, the isotherm shows no increase in pressure for decreasing area, as the molecules are not interacting. As the area is decreased, and the monolayer starts to be compressed, the amphiphiles begin to order, and behave as a two-dimensional liquid. During this region, the isotherm shows a gradual increase in pressure for decreasing area, as the molecules begin to interact. With continued decreasing of the area, the increasing pressure causes further ordering, and the monolayer behaves as a quasi-solid. Eventually a collapse pressure (π_c) is reached, at which point the film irretrievably loses its monolayer form. The pressure is too high for the molecules to be confined in two dimensions, so are pushed out of the monolayer plane into either the subphase or superphase.¹⁶⁵

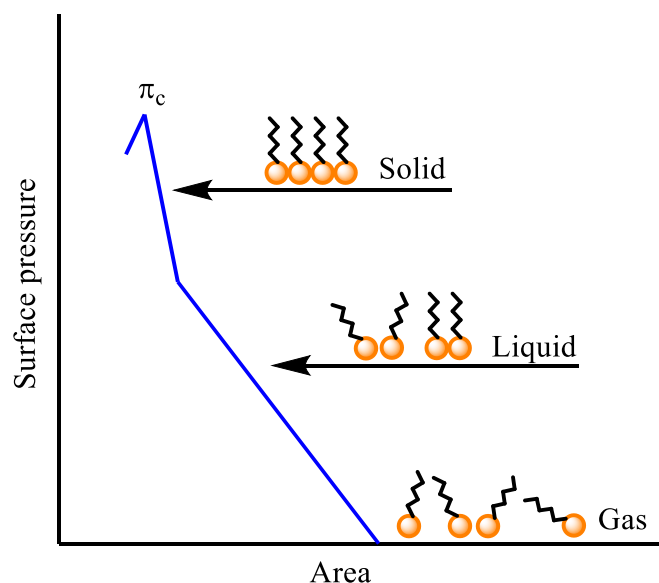


Figure 1.39: (Based on P. Martin and M. Szablewski¹⁶⁵) A pressure-area isotherm showing three distinct ordering regions, as well as the collapse pressure (π_c).

There are two major techniques for depositing the compressed monolayer onto a substrate, Langmuir-Blodgett and Langmuir-Schaefer. Langmuir-Blodgett films are deposited by lowering the substrate orthogonally into the water subphase. If the substrate is hydrophobic, one monolayer will deposit on the down stroke, making the substrate hydrophilic, and another will deposit on the upstroke, making the substrate hydrophobic again (Figure 1.40).¹⁶⁵

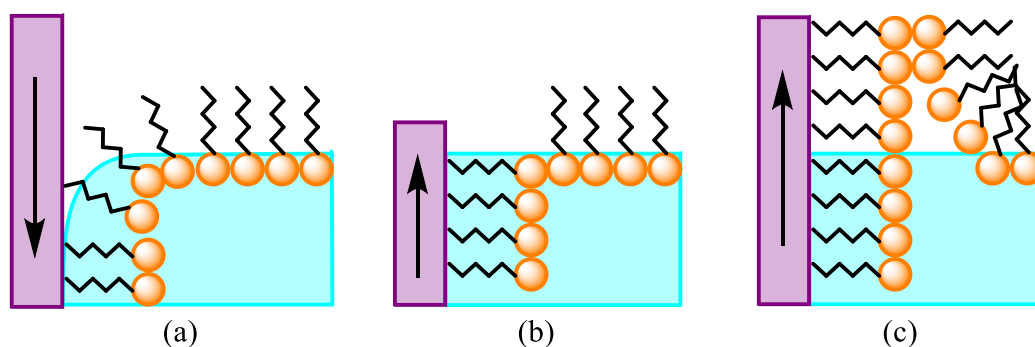


Figure 1.40: Langmuir-Blodgett deposition onto a hydrophobic substrate. (a) Deposition of the first monolayer on the down stroke. (b) The direction of travel of the substrate is reversed. (c) The second monolayer is deposited.¹⁶⁵

If the substrate is hydrophilic, no material will deposit on the down stroke, as the curvature of the meniscus and the direction of substrate travel do not coincide. Material will be deposited on the upstroke, as the curvature of the meniscus and the direction of substrate travel do coincide, giving a single monolayer and rendering the surface hydrophobic (Figure 1.41).¹⁶⁵

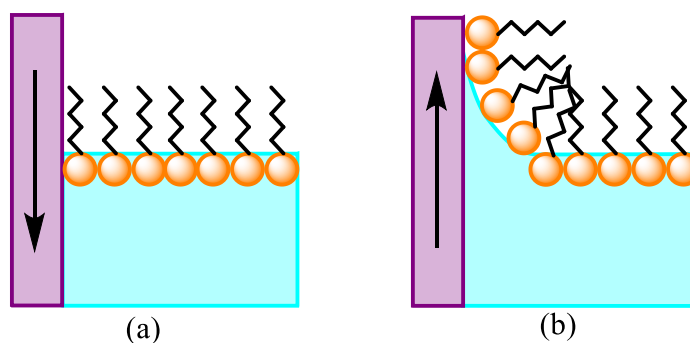


Figure 1.41: Langmuir-Blodgett deposition onto a hydrophilic substrate. (a) No deposition occurs on the down stroke as the curvature of the meniscus and the direction of substrate travel do not coincide. (b) Deposition of the first monolayer on the upstroke.¹⁶⁵

If a single hydrophilic monolayer is required, then Langmuir-Schaefer deposition is used. Langmuir-Schaefer films are deposited by bringing the substrate into contact parallel with the water subphase, and then withdrawing it by reversing the direction of travel. This deposits a single monolayer with the hydrophilic component at the substrate-monolayer interface (Figure 1.42). This technique can be used on either hydrophilic or hydrophobic substrates, but generally gives better depositions onto hydrophobic substrates.^{165,166} Langmuir-Schaefer deposition was chosen for this work as the adhesive was hydrophilic and the surface attachment group hydrophobic. Hence, a single monolayer of hydrophobic surface attachment groups deposited at the surface and hydrophilic adhesive at the surface was required.

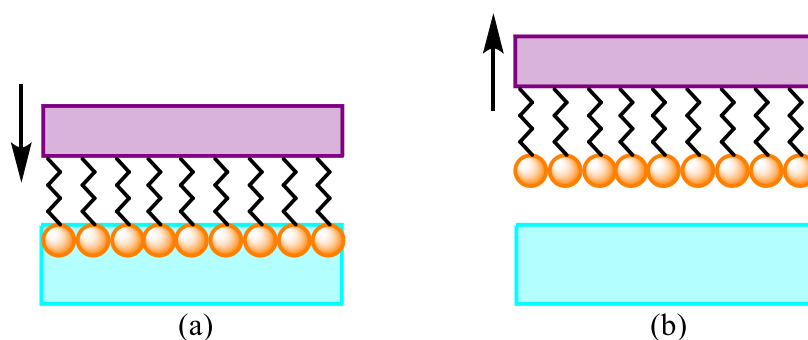


Figure 1.42: Langmuir-Schaefer deposition. (a) The substrate is brought into contact parallel with the monolayer. (b) The direction of travel is reversed and the substrate is removed, taking a deposited monolayer with it.

1.5.2. Ellipsometry

In ellipsometry a polarised beam of light is reflected from a surface and the difference between the amplitude and phase of the incident and reflected beams is measured (Figure 1.43). This is used to determine the thickness and optical properties of surfaces, interfaces, and thin film systems.¹⁶⁷

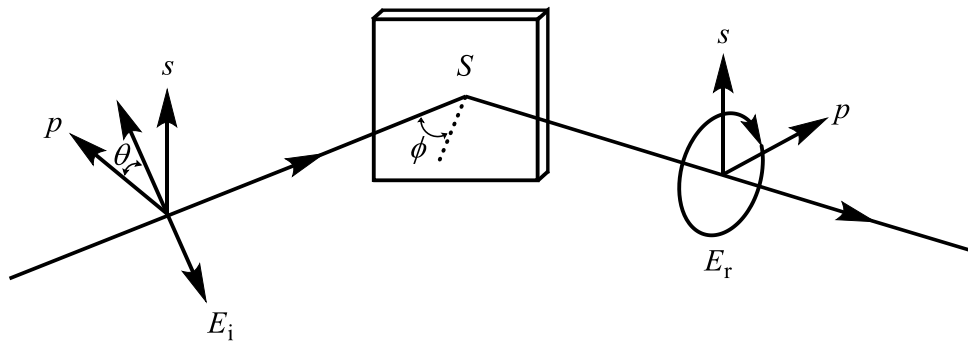


Figure 1.43: (Based on M. Bass et al.¹⁶⁷) Incident linearly polarised light of arbitrary azimuth θ is reflected from the surface S with an angle of incidence ϕ as an elliptically polarised beam with polarisations directions p and s . Where E_i and E_r are the electric field components for the incident and reflected waves, respectively.

The incident light is a monochromatic collimated beam with a known linear polarisation. The electric field (E) of a light wave always travels orthogonal to the propagation direction of the wave, meaning its x- and y- components can be used to describe the characteristics of the z-direction of the wave. Polarised light follows a specific path and trace, linearly polarised light results from the two orthogonal waves oscillating in phase. This linearly polarised light is reflected off the sample surface and analysed. The reflected light is elliptically polarised, i.e. the phase and amplitude of the two orthogonal waves is offset by an arbitrary amount, resulting in an 'elliptical' trace.^{167,168}

The changes in the phase and amplitude of the reflected light give the ratios of complex reflection coefficients for the sample surface. As one of the orthogonal components acts as a reference to the other, the measurements are relative, and hence highly accurate. Analysis of the measured ratios gives information on the structural and optical properties of the sample system. This is done using an iterative model fitting approach based upon the types of material that each layer is believed to be comprised of and their relative thicknesses.¹⁶⁷ Ellipsometry is a non-destructive technique, which allows the thickness of the deposited films to be determined without damaging them. The deposited films can then be used directly in the adhesion measurements with an accurate knowledge of the thickness.

1.5.3. Atomic force microscopy

The atomic force microscope (AFM) was developed by IBM, and combines the principles of the scanning tunnelling microscope (STM) and the stylus profilometer.¹⁶⁹ Unlike the STM, which measures the tunnelling current of a conductive sample, the AFM measures the force between a cantilever beam with a very small tip and the surface by the elastic deformation of the cantilever. As the sample is not required to be conductive, AFM can be performed on a much wider variety of surfaces.¹⁷⁰

By using an ultrasmall mass for the cantilever tip, the force required to move the probe through measurable distances (10^{-4} Å) can be as low as 10^{-18} N. As such, this technique can be used to measure the inter-atomic forces between single atoms.¹⁶⁹ In addition to the measurement of the vertical forces, and by extension the topography, of the surface, AFM can also be used to measure the lateral forces between the tip and the sample. Measurement of these lateral forces is usually described as friction force microscopy (FFM).¹⁷⁰

In a general AFM set-up (Figure 1.44), a flexible cantilever with a small sharp tip is brought into close contact with the substrate being measured. This causes the cantilever to bend due to the forces interacting between the tip and surface. The cantilever will bend either towards or away from the surface depending upon the force acting upon the tip, i.e. attractive or repulsive. The deflection of the tip is measured by reflecting a laser from the back of the cantilever into a four-quadrant photodiode detector.^{170,171}

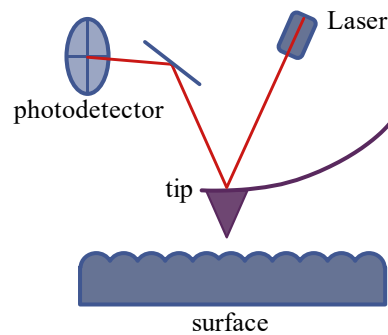


Figure 1.44: AFM set-up. The tip is in contact with the surface, causing the tip to bend. A laser beam is reflected off the back of the cantilever into a four-quadrant photodiode to determine tip deflection.

Commercially available cantilevers normally consist of silicon or silicon nitride, and are available with a variety of force constants (~ 0.01 - 100 N m⁻¹).¹⁷⁰ If the normal spring constant of the cantilever (k) is known, the interacting force ($F_{\text{interaction}}$) can be calculated using Hooke's Law:¹⁷¹

$$F_{\text{interaction}} = -k \times \Delta z \quad (1.1)$$

where k is the cantilever stiffness and Δz is the vertical cantilever deflection.

1.5.4. Adhesion testing

Adhesives are commonly tested for adhesive strength using the peel test or the probe tack test. These tests measure the structural response of an adhesive joint during debonding and provide a global response, rather than a detailed elucidation of debonding mechanism.¹⁷²

The weak adhesion of elastic soft materials has been the subject of much study, normally examining the contact mechanics between a sphere and a flat surface, or two crossed cylinders. This method of examining the materials allows the elastically deformed volume in the bulk to be distinguished from length scales typically encountered for dissipative interfacial processes. The analysis can therefore be treated as a classical interfacial fracture propagation, which can be modelled using JKR contact mechanics.¹⁷³ In these experiments, the crack velocity (v) is measured under an imposed energy release rate. This generates a unique effective adhesion energy curve ($\Gamma(v)$), which characterises the adhesive properties at the interface.^{172,174}

Nevertheless, if the material is too adhesive, or it is more viscoelastic in the bulk within the timeframe of the experiment, the adhesion energy cannot be separated from the energy dissipated in the bulk, as the strain release rate (\mathcal{G}) is dependent upon the load history. In these cases, JKR contact mechanics cannot adequately model the adhesion. For more strongly adhesive material, the peel test or probe test are used.¹⁷²

1.5.4.1. The peel test

The peel test uses the peel force per unit width to determine the adherence energy, and is commonly used for testing adhesive tapes (Figure 1.45). The tape being studied is usually conducted at a constant peel angle of either 90° or 180°, at either a constant velocity or load, with constant velocity being a standard industrial test. The peel test is deceptively simple, in that the debonding front contains a relatively complex strain field. This is the result of coupling between the stiffness of the backing material and the mechanical properties of the adhesive being tested. The Peel-test has the advantage that it can be used to study the steady-state crack propagation instead of the crack nucleation. If the peel angle is larger than a few degrees, then the strain release rate (\mathcal{G}) is given by:¹⁷²

$$\mathcal{G} = \frac{F}{w} (1 - \cos \theta) \quad (1.2)$$

where F is the force and w is the width of the peeled strip.

Peel tests usually give the steady-state peel force as a function of peel velocity. Under quasistatic steady-state peeling, normalising the peel force by the width of the strip generates an apparent fracture energy ($\Gamma_{\text{app}}(v)$). Although this value is useful for direct comparisons with other materials tested using the same method, without additional information about the properties of the adhesive further information on the interface cannot be determined. It is also strongly dependent upon the thickness of the material being studied, and the peel angle used.^{172,175}

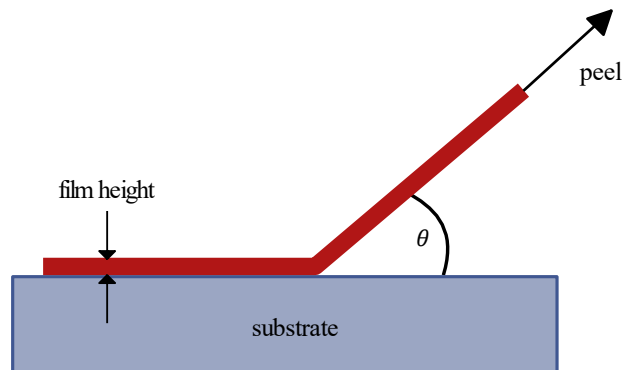


Figure 1.45: Schematic of a peel test.

1.5.4.2. The probe test

In the probe test, the adhesive being studied is compressed between the flat end of a cylindrical probe of contact radius a and a hard surface with a defined load (Figure 1.46). This load is maintained for a pre-set duration, after which the probe is withdrawn at a constant velocity (V_{deb}). At this point the adhesion force (F_a) is measured as a function of distance or time. Unlike the peel test, a well-defined displacement field can be applied to the adhesive being tested, due to the negligible bending of the equipment. In addition to this, a defined strain history can be applied to the material before the debonding phase of the measurement.¹⁷²

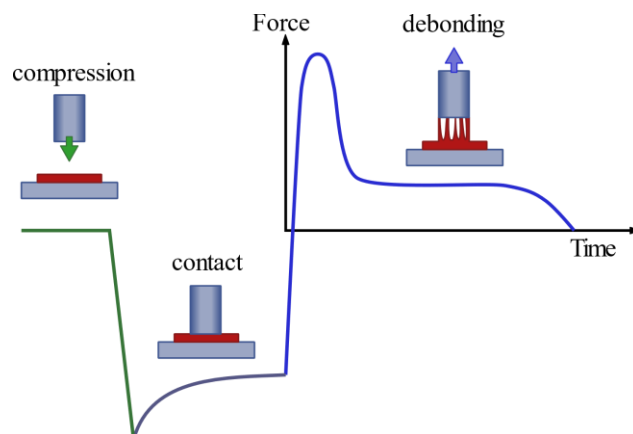


Figure 1.46: Schematic of a probe test.

Probe tests generate force-displacement curves for the adhesive being tested. These curves are normally converted into stress-strain curves (Figure 1.47) by dividing the force by the maximum contact area (A_{\max}) during compression, and by dividing the displacement (h) by the initial layer thickness (h_0):¹⁷²

$$\sigma_N = \frac{F_a}{A_{\max}}, \varepsilon = \frac{h - h_0}{h_0} \quad (1.3)$$

where σ_N is the nominal stress, and ε is the nominal strain.

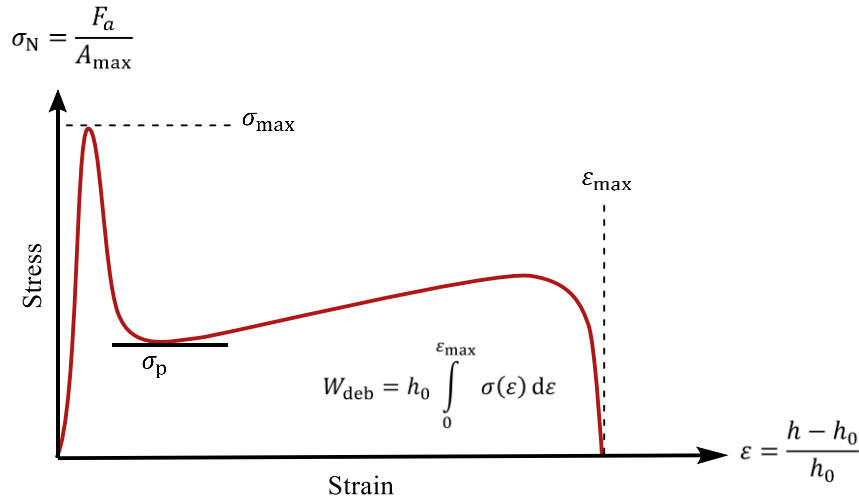


Figure 1.47: Normalised force displacement curve for the probe test showing the stress-strain characteristics of the adhesion.

As the debonding mechanism for soft adhesives is not simply crack propagation from the edge towards the centre of the sample, the data obtained cannot be quantitatively compared to a model. Nevertheless, the stress-strain curve yields information about the deformation mechanisms. The curves normally contain: the peak stress σ_{\max} , the maximum strain ε_{\max} , the plateau stress σ_p , and the work of debonding W_{deb} , which is determined from the area under the curve multiplied by the initial layer thickness. These values can be compared between materials and conditions, giving more information than the peel force alone. However, like the peel test, investigations into the deformation and failure mechanisms are also required for further interpretation.¹⁷²

Probe test geometry can be either spherical or flat. The spherical geometry is commonly used for non-fibrillating elastic rubbers as it is insensitive to small misalignments, and it generates well-defined crack propagation geometry. The flat-ended probe is more commonly used for soft viscoelastic adhesives, as the spherical probe imposes a more complex stress field on these types of material.¹⁷²

1.5.4.3. Probe test set-up for polyelectrolyte hydrogels

The adhesion between the deposited material and a polyelectrolyte hydrogel of an opposite charge was measured using a mechanical tester.^{33,34} The mechanical tester was used to perform pull-off experiments by bringing a hemispherical piece of polyelectrolyte hydrogel into contact with the deposited brush in Milli-Q water (Figure 1.48). The probe used to measure adhesion was fitted with a plastic jacket which held the hydrogel in place during the measurement. This probe is brought into contact with the test surface and a pre-set load pressure is applied for a specific duration. After the load pressure has been applied, the probe is withdrawn from the surface and the difference in the applied force and the pull-off force is measured. This allows determination of the adhesion between the substrate and the hydrogel at the specified load pressure.^{33,34} This technique allows for the direct measurement of adhesion, removing the requirement for its determination mathematically.

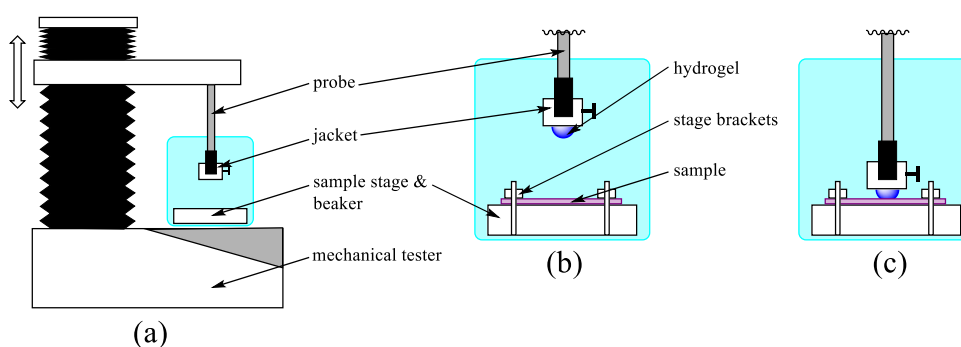


Figure 1.48: Mechanical tester setup. (a) Mechanical tester showing vertical motion of the probe and the sample stage, which is immersed in Milli-Q water. (b) Detail of probe and sample stage setup. The hydrogel is held in place using a plastic jacket. The sample is held in place using two brackets which hold it to the sample stage. (c) Detail of the probe when the hydrogel is brought into contact with the sample surface with an applied load. Only the hydrogel and sample come into contact, the probe and sample stage do not interact.

As the charged hydrogel is not expected to adhere strongly to a plain HMDS treated wafer under the test conditions, any observed adhesion from the calixarene-brush treated surfaces will be due to the effect of the deposited brush layer. The adhesion characteristics of the system are a combination of the surface and the mechanical properties of the hydrogel. The adhesive bonding itself is between the opposing polyelectrolyte chains over a few nm at the interface of the hydrogel and the brush, especially for brushes of the thicknesses used in this study, where the interdigitation is small.³⁴

1.6. Thesis outline

On order to answer the questions posed by this thesis, namely the use of a calixarene to deposit polyelectrolyte adhesives and compare them to chemically tethered ones, a new synthetic route had to be developed to generate the novel material required. The exploration of this synthetic route is examined in chapters 2 and 3. Chapter 2 details the preparation of a monofunctional surface-active calixarene, from which the functional polymers required are grown, producing polyelectrolytes functionalised with a surface tether. In chapter 3, an alternative method to prepare the calixarene-polyacid is developed, one in which a protected monomer is not required.

Once the surface-active adhesives had been synthesised, monolayers of adhesive were deposited and evaluated for film quality and adhesive strength. Chapter 4 details the deposition of the calixarene-polyelectrolyte adhesives, and the characterisation of these films to determine grafting density, polymer conformation, and surface roughness and topography. Chapter 5 fully characterises the adhesive properties of these deposited films using the probe test, and compares the results with the chemically tethered polyelectrolyte adhesives present in the literature.

In chapter 6, polyelectrolytes are deposited as sequential multilayers to determine how the deposition configuration affects the adhesive response, and the strength of the calixarene head-group is examined using AFM force pull-off measurements. Chapter 7 presents the conclusions drawn from this work, and briefly examines some possibilities for further investigation.

2. Synthesis of Calixarene-Polyelectrolyte Adhesives using ATRP

2.1. Introduction

The target calixarene-adhesives are shown in Figure 2.1, and comprise a calix[4]resorcinarene with either pDMAEMA or pMAA grown from the lower rim using atom transfer radical polymerisation (ATRP). This chapter details the synthesis of these two adhesives as well as the associated control compounds. The control compounds consist of replacing the calixarene with a decyl chain to demonstrate the effect of the calixarene upon surface adherence and overall adhesion of the system. These compounds fulfil the first objective, to synthesize mono-functional calixarenes, which can then be used to grow pDMAEMA and pMAA.

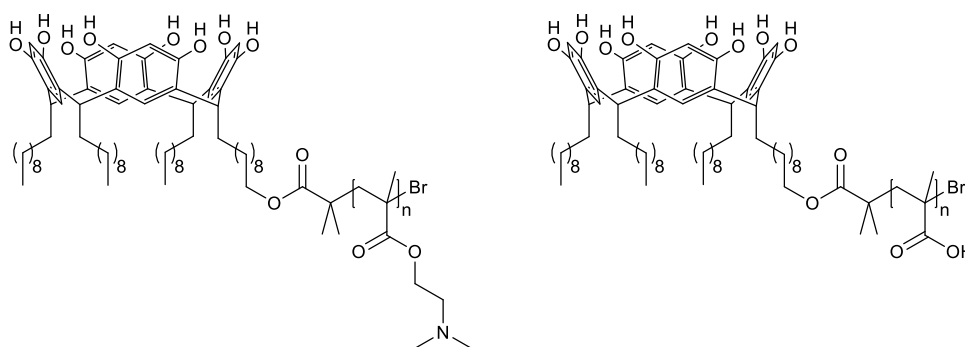


Figure 2.1: Target calixarene-adhesives. (Left) calix[4]resorcinarene-pDMAEMA. (Right) calix[4]resorcinarene-pMAA.

2.2. Synthesis of the mono-functionalised calix[4]resorcinarene

The first step in the synthesis of the calixarene-adhesives was to form the calix[4]resorcinarene, as this is the molecular framework from which the polyelectrolyte is grown. As only one polyelectrolyte chain per molecule was required, a monofunctional calixarene was required. This was achieved via the statistical incorporation of differing aldehydes, giving a mixture of mono- and unfunctionalized lower rim calixarenes.¹⁷⁶

The monoalkene functionalised calix[4]resorcinarene **1**, and the tetra-alkane calix[4]resorcinarene **2**, were prepared by refluxing resorcinol with two structurally similar aldehydes, undecenal and undecanal, in acidic (hydrochloric acid (HCl_(aq))) ethanol (EtOH) overnight (Figure 2.2).¹⁷⁶

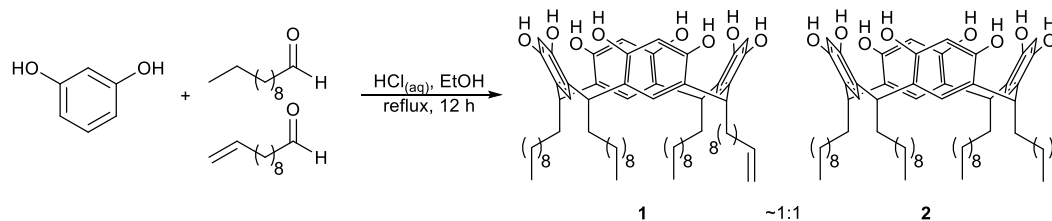


Figure 2.2: Synthesis of calix[4]resorcinarenes **1** and **2**.

The structural similarity of the aldehydes was used to maintain the bowl conformation.¹⁴⁶ The reagents were used in a 5:1:4 ratio of resorcinol:undecenal:undecanal. Based upon the statistical incorporation of the aldehydes, a maximum proportion of ~40% of the overall yield will be the desired monofunctionalised calix[4]resorcinarene **1** for aldehyde ratios between 1:2.1 and 1:4.

A lower ratio of undecenal to undecanal was used to minimise the formation of calix[4]resorcinarenes with more than one alkene incorporated. However, this does drop the effective yield to ~40% of the overall yield.¹⁷⁶ In the ¹H NMR spectrum the signals of the aromatic hydrogen atoms originally from resorcinol have large separation at $\delta = 6.28$ and 7.52 ppm, indicating that the molecule has the open bowl C_{4v} symmetry.¹⁵³

The phenolic hydroxyls on the upper rim of the calix[4]resorcinarenes **1** and **2** were protected with *tert*-butoxycarbonyl (Boc). Boc protection was effected by refluxing the calix[4]resorcinarenes **1** and **2** with di-*tert*-butyl dicarbonate (Boc_2O) and a catalytic quantity of 4-dimethylaminopyridine (DMAP) in acetone for 24 h to give the Boc protected calix[4]resorcinarenes **3** and **4** (Figure 2.3).¹⁷⁷

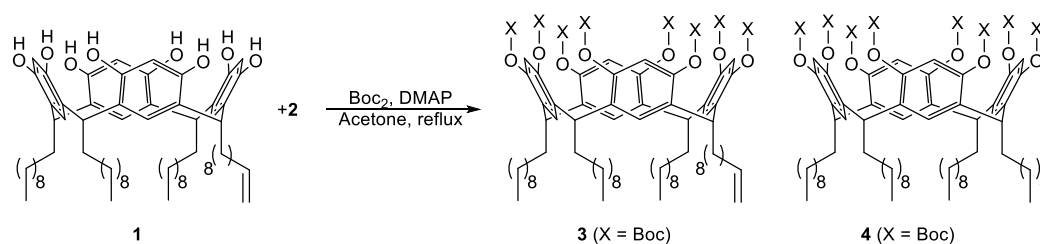


Figure 2.3: Synthesis of Boc protected calix[4]resorcinarenes **3** and **4**.

Boc protection allows for the chromatographical separation of the compounds, as the surface adhering properties of the phenolic hydroxyls prevent separation using standard silica gel chromatography. The Boc groups also prevent the ATRP initiator from coupling to the phenolic hydroxyls in the esterification step, allowing for the lower rim to be selectively functionalised with the desired polymer. This keeps the upper rim free to bind to surfaces.

The *tert*-butyl groups of Boc give a large sharp singlet signal in the ^1H NMR spectrum, making determination of the number of attached groups possible. The terminal functionality of the lower rim chains of calix[4]resorcinarene is far enough removed that it does not impact upon the chemical shifts of the bowl. The Boc singlet at $\delta = 1.5$ ppm can therefore be integrated against the methanetriyl bridge triplet at $\delta = 4.3$ ppm to give the fraction of phenolic hydroxyls protected. This integration showed that all the phenolic hydroxyls were Boc protected.

Once the upper rim had been protected, the lower rim alkene chain of **3** was converted to the hydroxyl by hydroboration with borane-tetrahydrofuran complex ($\text{BH}_3 \cdot \text{THF}$) in anhydrous tetrahydrofuran (THF) under nitrogen overnight. The excess borane was quenched with water, and the alkylborane was oxidised by the addition of sodium hydroxide (NaOH) and hydrogen peroxide (H_2O_2) to give the mono-hydroxyl calix[4]resorcinarene **5** (Figure 2.4).¹²⁹

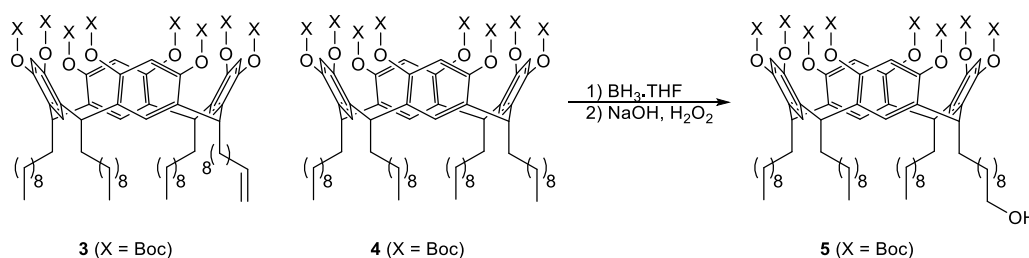


Figure 2.4: Synthesis of mono-hydroxyl calix[4]resorcinarene **5**.

The introduction of the hydroxyl group results in a polarity change that allows the mono-hydroxyl calix[4]resorcinarene **5** to be separated from the tetra-alkyl calix[4]resorcinarene **4**. The tetra-alkyl calix[4]resorcinarene **4** remains at a high R_f (0.76; eluent 20% ethyl acetate:petroleum ether 40-60) value while the mono-hydroxyl calix[4]resorcinarene **5** shifts to a lower R_f (0.19).

Use of gradient chromatography (10% ethyl acetate:petroleum ether 40-60, increasing to 40% ethyl acetate:petroleum ether 40-60) allows for the separation of multi-gram quantities by selectively eluting the tetra-alkyl calix[4]resorcinarene **4** at a low polarity before increasing the polarity to elute the mono-hydroxyl calix[4]resorcinarene **5**. In the ^1H NMR spectrum the alkene signals at $\delta = 4.9$ and 5.8 ppm disappear and are replaced by the oxy methylene triplet at $\delta = 3.6$ ppm.

2.2.1. Selective reprotection of hydroxyl calix[4]resorcinarene

The oxidising conditions used to cleave the alkyl-borane can also lead to cleavage of the O-Boc protecting group bond. This results in material with differing numbers of protecting groups around the upper rim. This showed as an increased number of spots observed by thin-layer chromatography (TLC) and a decreased isolated yield of the *per*-Boc hydroxy calix[4]resorcinarene **5**. The phenolic hydroxyls of the calixarene bowl were selectively protected in the presence of the alkyl hydroxyl.¹⁷⁸ This is achieved by maintaining the pH of the solution at \sim pH8 so that only the resorcinol hydroxyls ($pK_a = 9.15$)¹⁷⁹, and not the alkyl hydroxyl ($pK_a = 16.1$)¹⁸⁰, are ionised.

Initially, the method reported by V. Srivastava et al.¹⁷⁸ for selectively acylating phenols in the presence of alkyl alcohols was used. This involves adding a concentrated solution of sodium hydroxide to the phenol dissolved in isopropyl alcohol to produce a pH8 solution, followed by addition of the anhydride and stirring at room temperature for 30 min.

When these reaction conditions were used with calix[4]resorcinarenes **1** and **2** and di-*tert*-butyl dicarbonate, the reaction failed to give the *per*-Boc calix[4]resorcinarenes **3** and **4**. This was attributed to a lack of solubility of the calix[4]resorcinarene in isopropyl alcohol and the lower reactivity of di-*tert*-butyl dicarbonate compared to acetic anhydride. The solvent was replaced with acetone and the reaction was refluxed to effect Boc protection. When used with partially Boc protected calix[4]resorcinarenes **4a** and **5a**, this gave the *per*-Boc mono-hydroxyl calix[4]resorcinarene **5** (Figure 2.5).

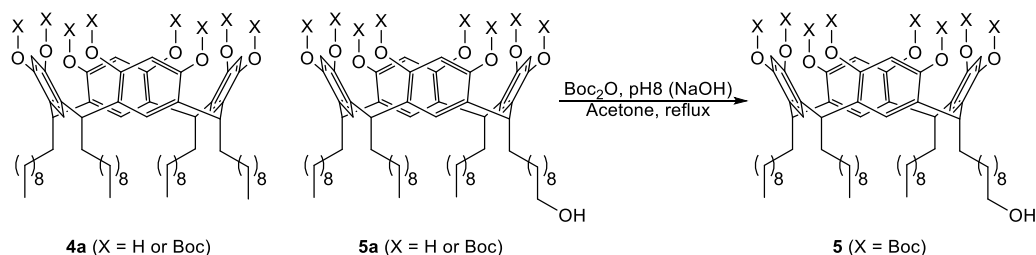


Figure 2.5: Selective reprotection of the phenolic hydroxyls to give calix[4]resorcinarene **5**.

2.2.2. Alternative formation of protected hydroxyl calix[4]resorcinarene

With the successful implementation of the selective reprotection reaction, an alternative route to the mono-hydroxyl calix[4]resorcinarene was determined. By using a cyclic enol ether (2,3-dihydrofuran) instead of an alkene terminated aldehyde in the preparation of the calix[4]resorcinarene, the terminal alcohol functionality was introduced at the initial synthesis of the material to give hydroxy calix[4]resorcinarene **6** (Figure 2.6).¹⁸¹

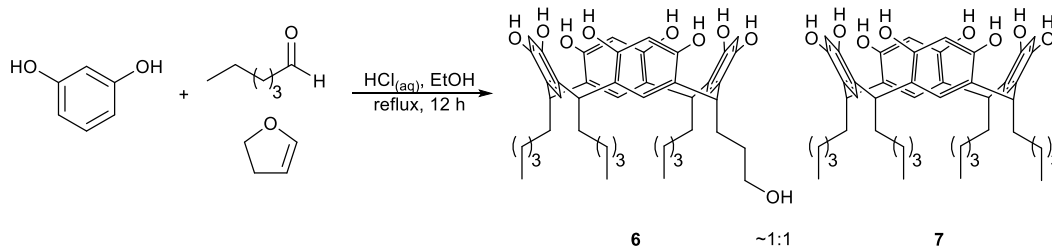


Figure 2.6: Synthesis of calix[4]resorcinarenes **6** and **7**.

Using the selective protection of the aromatic hydroxyls, the hydroxy calix[4]resorcinarene **6** were selectively protected to give Boc-protected mono-hydroxyl calix[4]resorcinarene **8** (Figure 2.7). This gives a Boc-protected mono-hydroxyl calixarene without the loss of Boc protecting groups. However, the lower rim chains are much shorter than those of mono-hydroxyl calix[4]resorcinarene **5**, especially the hydroxyl chain. This may impact upon the ability of the calixarene to form ordered monolayers.

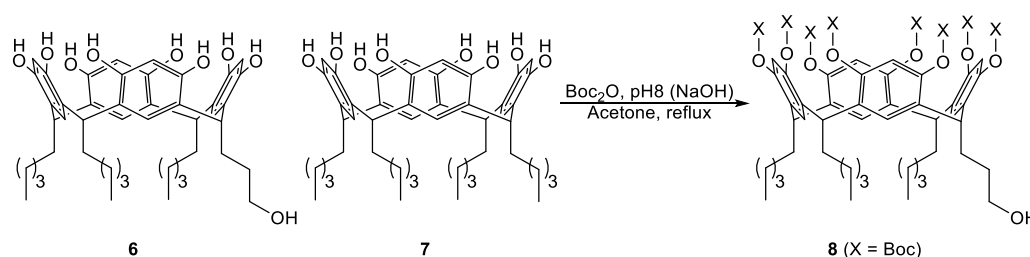


Figure 2.7: Selective protection of the aromatic hydroxyls to give calix[4]resorcinarene **8**.

The selective protection of calix[4]resorcinarene **6** demonstrates that the entire upper annulus can be protected in the presence of a terminal alkyl hydroxyl. This was applied to the synthesis of Boc mono-hydroxyl calix[4]resorcinarene **5**. By oxidising the terminal alkene of calix[4]resorcinarenes **1** before the selective protection of the upper annulus, the loss of material due to basic hydrolysis can be avoided. Calix[4]resorcinarene **1** was oxidised using the same hydroboration-oxidation procedure previously described to give the mono-hydroxyl calix[4]resorcinarene **9** (Figure 2.8).

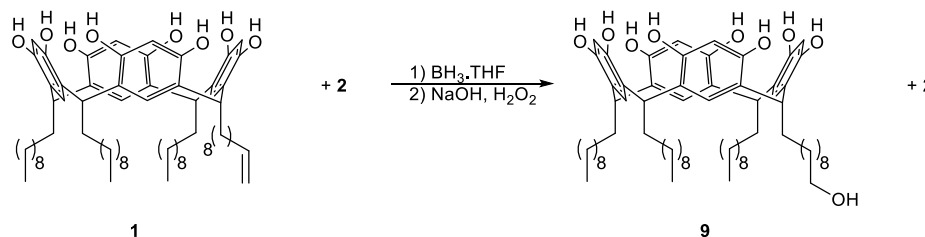


Figure 2.8: Synthesis of mono-hydroxyl calix[4]resorcinarene **9**.

To protect the mono-hydroxyl calix[4]resorcinarene **9**, the selective protection procedure was altered to improve the solubility of the materials. Pyridine was used as the base, as the pK_a difference between pyridine ($pK_a = 5.2$)¹⁸² and the alkyl hydroxyl ($pK_a = 16.1$)¹⁸⁰ is large enough to suppress reaction at the terminal alkyl hydroxyl. The pK_a difference between pyridine and the resorcinol hydroxyls ($pK_a = 9.15$)¹⁷⁹ is much smaller, promoting reaction at resorcinol hydroxyls instead. The mono-hydroxyl calix[4]resorcinarene **9** was refluxed with di-*tert*-butyl decarbonate and pyridine in acetone overnight to give the Boc protected mono-hydroxyl calix[4]resorcinarene **5** (Figure 2.9).

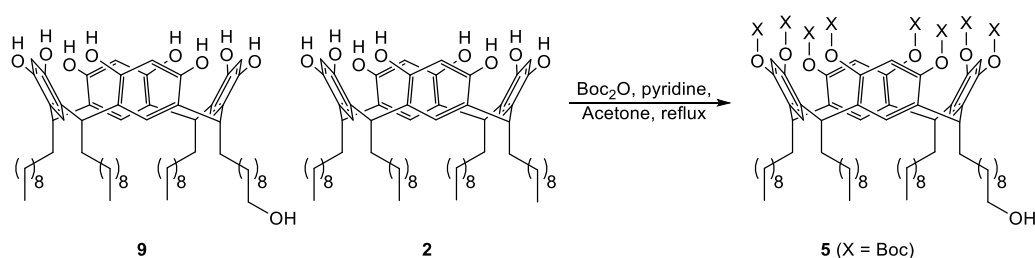


Figure 2.9: Selective protection of the aromatic hydroxyls to give mono-hydroxyl calix[4]resorcinarene **5**.

The mono-hydroxyl calix[4]resorcinarene **5** was then selectively coupled to a polymerisation initiator on the lower rim. The phenolic hydroxyls on the upper rim are screened from reaction by Boc protection, and the alkyl hydroxyl introduced on the lower rim is a synthetic handle to which the initiator can be attached.

2.3. Synthesis of the polybasic adhesive via ATRP

The synthesis of the mono-hydroxyl calix[4]resorcinarene **5** gave the molecular framework needed to grow the polyelectrolytes. The polymer initiator was selectively attached to the lower rim, and the polyelectrolytes of interest can then be grown from the surface attachment group. The ATRP initiator bromoisobutyl was attached to mono-hydroxyl calix[4]resorcinarene **5** using α -bromoisobutyryl bromide and pyridine in THF, which gave the bromo-initiator calix[4]resorcinarene **10** (Figure 2.10).

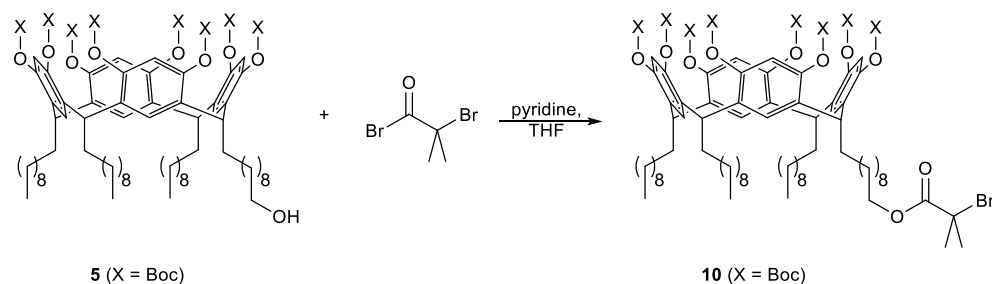


Figure 2.10: Synthesis of bromo-initiator calix[4]resorcinarene **10**.

The bromoisobutyl ester allows the polyelectrolyte chain to be grown from the lower rim of the calix[4]resorcinarene bowl. The acyl halide functionality allows for easy attachment to the terminal alkyl hydroxyl with a pyridine catalyst. The bromoisobutyl ester is an excellent initiator for radical polymerisation as the α -carbonyl activates the alkyl bromide. The alkyl bromide is also more reactive than the alkyl chloride, and the radical formed is stabilised by the tertiary carbon centre. These properties give good molar mass control.¹⁰⁸ In the ^1H NMR spectrum the oxy methylene triplet shifted from $\delta = 3.6$ ppm to $\delta = 4.2$ ppm, confirming that the ester linkage to the initiator had been formed.

The bromo-initiator calix[4]resorcinarene **10** was then used to grow the polyelectrolytes required to form the adhesives. The first polyelectrolyte grown was Boc-calix[4]resorcinarene-pDMAEMA **11** using ATRP (Figure 2.11). The ^1H NMR spectrum of Boc-calix[4]resorcinarene-pDMAEMA **11** showed the loss of the monomer alkene signals at $\delta = 5.5$ and 6.1 ppm, and the appearance of the polymer backbone signal at $\delta = 1.9$ ppm. The other original monomer signals at $\delta = 1.8$, 2.3, 2.6, and 4.1 ppm showed the peak broadening associated with polymers, which is due to the conformational restrictions present in the chain versus the free monomer in solution. The conformational restrictions reduce the molecular motion of the polymer, which leads to line broadening.¹⁰⁵

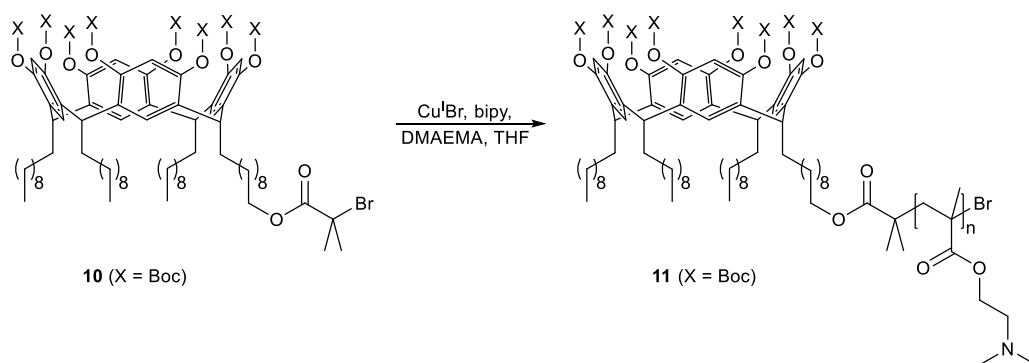


Figure 2.11: Synthesis of Boc-calix[4]resorcinarene-pDMAEMA **11**. ATRP catalyst: copper(I) bromide ($\text{Cu}^{\text{I}}\text{Br}$) and 2,2'-bipyridine (bipy).

Once the polymer had been prepared the Boc protecting groups were removed to reveal the phenolic hydroxyls on the upper rim. Initially thermolysis was attempted, as the calix[4]resorcinarene O-Boc group has been shown to thermally decompose at high temperature under vacuum to give carbon dioxide, isobutylene, and the liberated phenol (Figure 2.12).^{183,184} When thermolysis was used to remove Boc from Boc-calix[4]resorcinarene-pDMAEMA **12**, the resulting material became charred and insoluble in a range of solvents. This was attributed to thermal decomposition of the pDMAEMA polymer chain.

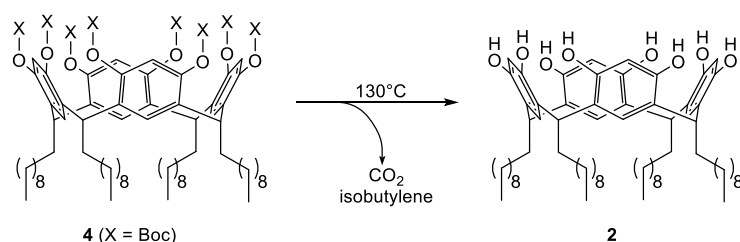


Figure 2.12: Thermal deprotection of Boc-calix[4]resorcinarene **4** to give the unprotected calix[4]resorcinarene **2**.

An alternative method for the removal of phenolic Boc is the acidic, or basic, cleavage of O-Boc. Acidic cleavage using HCl/dioxane gave the deprotected polymer calix[4]resorcinarene-pDMAEMA **12** (Figure 2.13).¹⁸⁵ Basic cleavage using sodium metal (Na) in methanol (MeOH) and dichloromethane (DCM) also gave the deprotected polymer calix[4]resorcinarene-pDMAEMA **12** (Figure 2.14).¹⁸⁶ Acidic cleavage was chosen as the predominate method as it was more convenient, does not involve flammable metals, and is less likely to cleave the calix-ester or polymer side chain ester bonds.

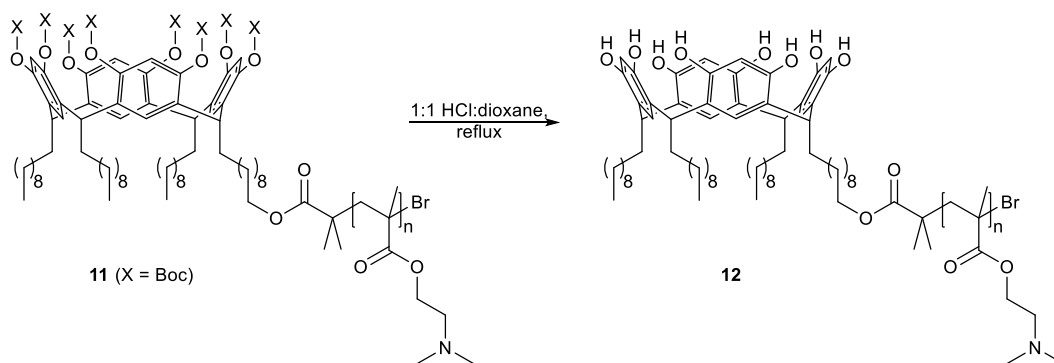


Figure 2.13: Acidic deprotection to give calix[4]resorcinarene-pDMAEMA **12**.

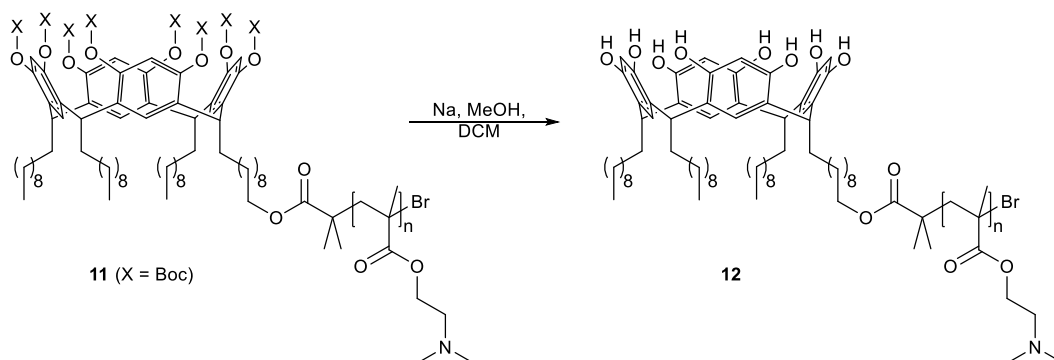


Figure 2.14: Basic deprotection to give calix[4]resorcinarene-pDMAEMA **12**.

In addition to the calixarene-based adhesive **12**, a control compound using decane instead of calix[4]resorcinarene was also prepared using the same synthetic methods. This was done to compare the impact of growing the polyelectrolyte from the calix[4]resorcinarene and to provide a control compound in adhesion studies. The decyl group is analogous to a calixarene ‘leg’, but lacks the surface attachment or molecular framework capabilities of the full calix[4]resorcinarene. The decyl bromo-initiator **13** was prepared in the same way as the bromo-initiator calix[4]resorcinarene **10** (Figure 2.15), and was then used to grow decyl-pDMAEMA **14** using ATRP (Figure 2.16).¹⁸⁷

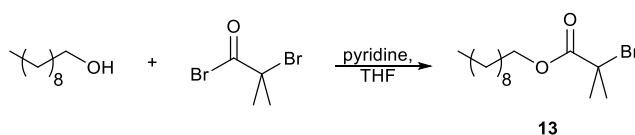


Figure 2.15: Synthesis of decyl bromo-initiator **13**.

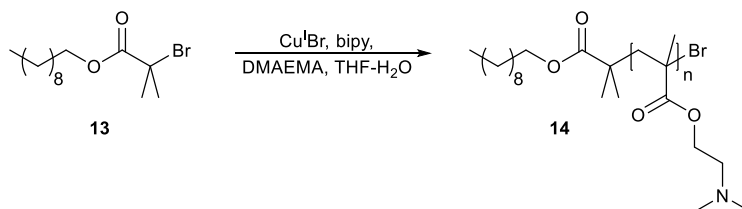


Figure 2.16: Synthesis of decyl-pDMAEMA **14**.

Once the polymers had been synthesised, they were analysed using Gel Permeation Chromatography (GPC). The target degree of polymerisation (DP) was 30 units. The DP for Boc-calix[4]resorcinarene-pDMAEMA **11**, and hence calix[4]resorcinarene-pDMAEMA **12**, was determined to be 51 units long with a dispersity index (\bar{D}) of 1.28. The DP for the decyl-pDMAEMA control **14** was determined to be 59 units long with a dispersity index of 1.34. The degree of polymerisation is similar for both chains. This shows that the calix[4]resorcinarene does not impact upon the growth of the polymer chain, as the degree of polymerisation was relatively unchanged between the two compounds. When the target DP was increased to 60 units, the measured DP increased to 82 units long.

The DP determined by GPC was greater than that targeted, suggesting reduced initiator efficiency. The dispersity indexes were also slightly higher than expected for traditional ATRP (~ 1.2).¹⁰⁸ This is due to the polymer chains being shorter than those normally reported. At the start of the polymerisation several monomer units are added at each activation step, as the polymerisation increases the chain uniformity also increases due to exchange reactions. So, at low lengths the dispersity is governed more by the effects of monomer addition rather than exchange reactions. This is shown by¹⁰⁸

$$M_w/M_n = 1 + \left(\frac{[RX]_0 k_p}{k_{\text{deact}}[D]} \right) \left(\frac{2}{p} - 1 \right) \quad (2.1)$$

where M_w/M_n is the dispersity index, $[RX]_0$ is the concentration of initiator, $[D]$ is the concentration of deactivator, k_p is the rate constant of propagation, k_{deact} is the rate constant of deactivation, and p is the monomer conversion. At shorter chain lengths, there is a higher concentration of initiator $[RX]_0$, hence there is a higher dispersity index.

2.4. Synthesis of the polyacidic adhesive via ATRP

The target polyelectrolyte adhesive system is comprised of two oppositely charged polymers. In addition to the polybasic adhesives **11** and **12**, and the associated control **14**, the polyacidic compounds were also required. These were prepared using the same molecular frameworks as for the polybasic material.

To synthesise the polyacid using a $\text{Cu}^{\text{I}}\text{Br}/\text{bipy}$ system, the methacrylic acid (MAA) monomer must first be protected, as the acid functionality ($\text{p}K_{\text{a}}[\text{MAA}] = 4.36$ and $\text{p}K_{\text{a}}[\text{p(MAA)}] = 5.7$)¹⁸⁸ will protonate the bipyridine ligand ($\text{p}K_{\text{a}}[\text{bipy}] = 4.33$),¹⁸⁹ causing the ATRP catalyst to precipitate from solution. An alternative route to the direct formation of the polyacid is via the use of the sodium salt of the acid, sodium methacrylate **15** (NaMA), which was prepared from the acid monomer by treatment with sodium hydroxide (Figure 2.17).^{190,191}

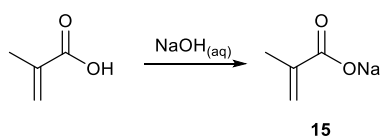


Figure 2.17: Synthesis of sodium methacrylate **15**.

The initial polymerisation used a similar procedure to the one used for decyl-pDMAEMA **14**. DMAEMA was replaced with NaMA **15** and a THF:H₂O solvent system was used to solubilise the monomer, this gave decyl-pNaMA **16** (Figure 2.18, Table 2.1: Entry 1). The catalyst was observed to have become oxidised within approximately 1 h. This was attributed to the nitrogen purge failing to fully deoxygenate the water used in this system. Analysis of the recovered material by aqueous GPC showed no significant polymerisation had occurred, as $M_w = 660 \text{ g mol}^{-1}$, which equates to $n = 3$.

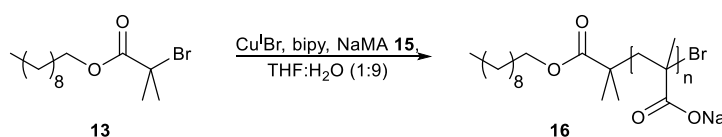


Figure 2.18: Synthesis of decyl-pNaMA **16**.

A more rigorous degassing procedure was then incorporated. The solution of NaMA **15** dissolved in water was separately deoxygenated using a minimum of three freeze-pump-thaw (FPT) cycles to remove dissolved gases.^{191–193} This prevented the premature oxidation of the catalyst, and there was no visible oxidation after 12 h. However, analysis by ¹H NMR and GPC of the product showed no polymerisation (Table 2.1: Entry 2).

The pH of the reaction solution was then investigated, as a basic pH is required to maintain the solubility of the Cu^IBr/bipy complex and allow for polymerisation under aqueous conditions. The pH of the reaction solution was adjusted to ~pH8 using 0.1 M NaOH. This still resulted in no significant polymerisation, with $M_w = 653 \text{ g mol}^{-1}$, $n = 3$. (Table 2.1: Entries 3 and 4). Increasing the temperature of the reaction from room temperature to 90°C showed no change in the degree of conversion, with $M_w = 685 \text{ g mol}^{-1}$, $n = 3$. (Table 2.1, Entries 5 and 6). However, the monomer is susceptible to non-living thermally initiated polymerisation if heated for prolonged periods of time.¹⁹¹ The degassing method, monomer, and recovery method were then varied to investigate the effects of different combinations of techniques (Table 2.1, Entries 7 and 8). However, all failed to polymerise, with the largest $M_w = 636 \text{ g mol}^{-1}$, $n = 3$.

Table 2.1: Summary of Reaction conditions used to synthesise pMAA. Degassing is either with nitrogen bubbling or freeze-pump-thaw cycles.

Entry	Degassing	pH	Temperature (°C)	Monomer	THF:H ₂ O
1	N ₂ Purge		25	NaMA	1:9
2	FPT		25	NaMA	1:9
3	FPT	8	25	NaMA	0:1
4	FPT	8	25	NaMA	1:9
5	FPT		90	NaMA	1:3
6	FPT	10	90	NaMA	1:4
7	FPT		25	NaMA	1:9
8	N ₂ Purge		25	MAA	1:0

Another method to polymerise acidic monomers by ATRP is to use ligands which are not basic, and therefore cannot be protonated. The ligand must also be able to coordinate to both Cu^{I} and Cu^{II} , giving soluble complexes with the appropriate electrode potential and halogen philicity of the Cu^{II} complex. 2,2'-(Ethylenedithio)diacetic acid (EDTDAA) is an acidic ligand and cannot be protonated by MAA, so will still coordinate the copper for polymerisation.¹⁹⁴ EDTDAA was used to polymerise MAA using decyl bromo-initiator **13** for 17 days with monitoring by ^1H NMR to give decyl-pMAA **17** (Figure 2.19).¹⁹⁴ However, the EDTDAA/MAA catalyst system polymerises much slower than bipy/DMAEMA, with the polymerisation only reaching $60.0 \pm 0.3\%$ after seventeen days (EDTDAA/MAA), compared with 99% after 12 h (bipy/DMAEMA). This is attributed to the lower polymerisation rates observed for MAA at neutral pH, and an increased resistance to oxidation.¹⁹⁵ This lower polymerisation rate can lead to broadening of the molecular weight distribution, and does not generate synthetically useful material within a reasonable timeframe.

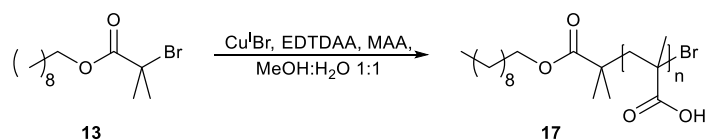


Figure 2.19: Polymerisation using EDTDAA to give decyl-pMAA **17**.

The pH of the reaction solution and the monomer concentration are very important in maintaining the solubility of the $\text{Cu}^{\text{I}}\text{Br}/\text{bipy}$ complex and determining the rate of polymerisation of the monomer. Between pH4 and 6 the polymerisation rate for methacrylic acid decreases by a factor of 15, it then passes through a minimum at pH6-7, and increases between pH6 and 9 by a factor of nearly 2 to a constant value at pH9-12 before decreasing again (Figure 2.20).^{195,196}

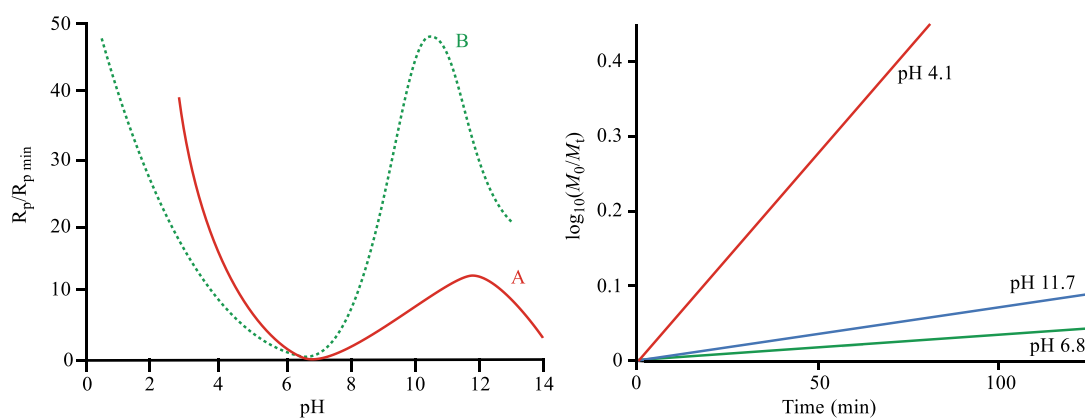


Figure 2.20: (Left, based on V.A. Kabanov et al.¹⁹⁵) Relative polymerisation rate vs. pH for methacrylic (A) and acrylic (B) acids at 60°C . (Right, based on G. Blauer¹⁹⁶) Rate vs. time at various pH values for methacrylic acid.

The high pH required to prevent protonation of the bipy ligand results in a depressed maximum polymerisation rate, resulting in chain death due to oxidation from oxygen ingress before an acceptable degree of polymerisation can be reached. This reduction in polymerisation rate is due to friction of the transition state structure, which varies with pH and monomer structure.^{195,197}

The variation in polymerisation rate with changing pH is due to the changing degrees of monomer ionisation and counter-ion concentration. These variables affect the amount of friction to the internal rotation of the transition state structure, as the counter-ions attract the carbonyl groups to one place in their molecular environment. This results in a reduction of the free radical propagation coefficient (Figure 2.21).^{195,197–200}

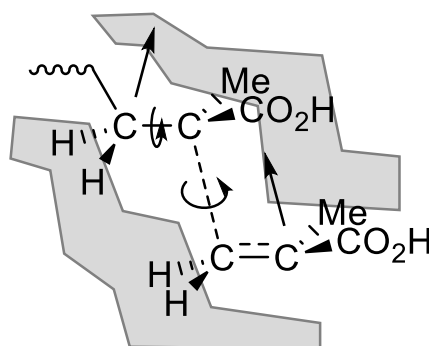


Figure 2.21: (Based on S. Beuermann et al.¹⁹⁷) Illustration of the transition state structure for the propagation step. The arrows indicate rotational and bending motions and the shaded areas the molecular environment, which can contain a varying quantity of counter-ions.

At low pH, there is no charge on the polymer and no counter-ions in the solution, so there is no friction to retard polymerisation. At neutral values of pH, near the pK_a of the polymer, the polymer is partially charged and there is an increase in the number of counter-ions. This results in a decrease in the polymerisation rate through friction between the transition state and the counter-ions in the environment, which attract the carbonyl groups to one place in their molecular environment. At high pH, there is an increase in polymer charge and counter-ion concentration. This results in an increase in the polymerisation rate as there is a uniform distribution of counter-ions in the environment. This provides additional counter-ions in the molecular environment for the transition state anionic carboxyl groups to interact with, reducing the rotational friction.^{195,197–200}

Intramolecular friction can also be caused by the α -methyl groups on the polymer backbone, resulting in a difference in polymerisation rate between MAA and acrylic acid at high degrees of ionisation, and therefore pH, as shown by Figure 2.20,^{195,197} resulting in the reduced polymerisation rate observed for the $\text{Cu}^{\text{I}}\text{Br}/\text{bipy}$ complex at high pH.

2.4.1. Synthesis of the polyacid via protected monomer intermediate

ATRP proved successful in the polymerisation of 2-(dimethylamino)ethyl methacrylate (**11**), but proved unsuccessful in polymerising methacrylic acid directly. Use of the sodium salt of methacrylic acid (**15**) to protect the acidic functionality also failed to allow polymerisation. Protection of the acid through the use of a protecting group removes the acidic functionality from the polymerisation completely, and does not require the pH of the solution to be controlled. Use of a chemically modified monomer instead of the sodium salt also allows the polymerisation to be conducted in organic solvents.

Two protecting groups were selected for investigation. The first is protection with ethyl vinyl ether to give 1-ethoxyethyl methacrylate (EEMA), which is cleaved by thermolysis at 150°C.^{201,202} The second is the use of *tert*-butyl methacrylate (*t*BuMA), which is cleaved by acid hydrolysis to give the methacrylic acid.

1-ethoxyethyl methacrylate was first prepared according to the method reported by A.J. Parnell et al²⁰¹ to give 1-ethoxyethyl methacrylate **18** (Figure 2.22). The isolated yield was negligible (0.5%), so the reaction was repeated with an increased quantity of catalyst. However, this failed to significantly increase the yield (4%).

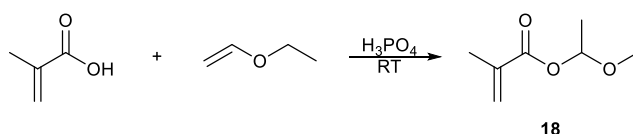


Figure 2.22: Synthesis of EEMA **18** using phosphoric acid (H₃PO₄).

1-ethoxyethyl methacrylate was then prepared according to the method reported by F. Urano²⁰³ to give 1-ethoxyethyl methacrylate **18** (Figure 2.23). Analysis of the recovered material showed a large portion of methacrylic acid contamination. This contamination was difficult to completely remove from the monomer, and was sufficient enough to poison the catalyst when polymerisation was attempted (Figure 2.24).

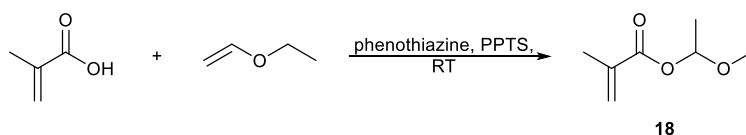


Figure 2.23: Synthesis of EEMA **18** using phenothiazine and pyridinium *p*-toluene sulfonate (PPTS).

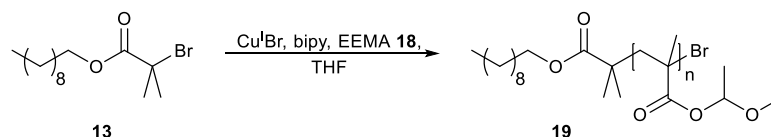


Figure 2.24: Attempted polymerisation of EEMA **19** using ATRP.

The other protecting group investigated was the *tert*-butyl ester of methacrylic acid, *tert*-butyl methacrylate (^tBuMA). The *tert*-butyl methacrylate monomer is commercially available, removing the need to separate residual methacrylic acid from a protecting group addition reaction.

The polymerisation of ^tBuMA by ATRP was first tested using the decyl bromo-initiator **13** control, which polymerised successfully to give decyl-p^tBMA **20** (Figure 2.25).²⁰⁴ The ¹H NMR spectrum of decyl-^tBMA **20** showed the same peak changes as observed for Boc-calix[4]resorcinarene-pDMAEMA **11** and decyl-pDMAEMA **14**. It showed the loss of the monomer alkene signals at $\delta = 5.5$ and 6.1 ppm, and the appearance of the polymer backbone signals at $\delta = 1.1$ -1.3 ppm. The *tert*-butyl signal at $\delta = 1.5$ ppm also showed the peak broadening associated with polymers.¹⁰⁵

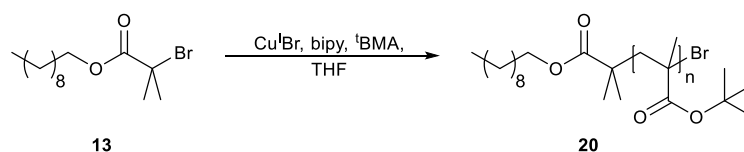


Figure 2.25: Synthesis of decyl-^tBMA **20**.

The polymer decyl-^tBMA **20** was then deprotected by acid hydrolysis to yield the polyacid using refluxing HCl:dioxane to give decyl-pMAA **17** (Figure 2.26). The ¹H NMR spectrum of decyl-pMAA **17** showed the loss of the *tert*-butyl signal at $\delta = 1.5$ ppm, confirming the cleavage of the *tert*-butyl ester to the acid.

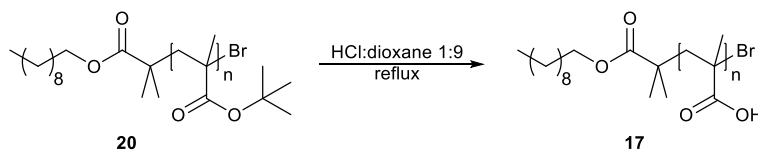


Figure 2.26: Synthesis of decyl-pMAA **17**.

Once the use of *tert*-butyl methacrylate had been shown to be successful in the formation of poly(methacrylic acid), it was applied to the calix[4]resorcinarene bromo-initiator **10** to give the polymer Boc-calix[4]resorcinarene-*p*^tBMA **21** (Figure 2.27).²⁰⁴ The ¹H NMR spectrum showed the same peak changes as observed for decyl-^tBMA **21**, with the loss of the monomer alkene signals, the appearance of the polymer backbone signals, and the *tert*-butyl signal peak broadening. The degree of polymerisation was determined to be 85 units long using GPC, with a dispersity index of 1.49 for 60 equivalents of monomer.

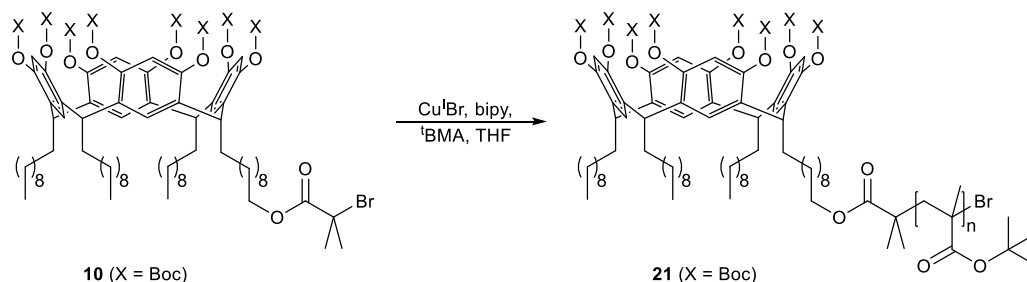


Figure 2.27: Synthesis of Boc-calix[4]resorcinarene-*p*^tBMA **21**.

The polymer Boc-calix[4]resorcinarene-*p*^tBMA **21** was then deprotected by acid hydrolysis to yield the polyacid calix[4]resorcinarene-*p*MAA **22** (Figure 2.28). The acid deprotection also removes the Boc protecting groups from the calix[4]resorcinarene bowl. The ¹H NMR spectrum of calix[4]resorcinarene-*p*MAA **22** showed the loss of the *tert*-butyl signal at $\delta = 1.5$ ppm, confirming the cleavage of the *tert*-butyl ester to the acid and the calixarene O-Boc to the aromatic alcohol. As the poly(methacrylic acid) is derived from the poly(*tert*-butyl methacrylate), it will have the degree of polymerisation and dispersity index as Boc-calix[4]resorcinarene-*p*^tBMA **21**.

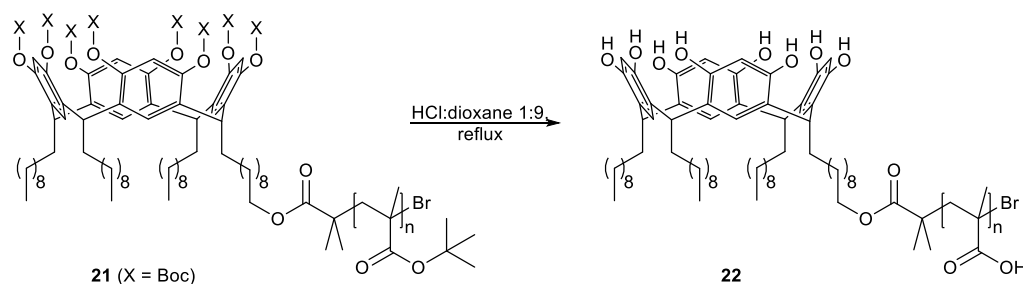


Figure 2.28: Synthesis of calix[4]resorcinarene-*p*MAA **22**.

With the successful synthesis of the decyl-*p*MAA **17** and calix[4]resorcinarene-*p*MAA **22** polymers, all the adhesives required had been prepared.

2.5. Summary

In this chapter, three calixarene-based adhesives were prepared, completing the first objective. Preparation of the Boc protected mono-hydroxyl calixarene proved susceptible to basic cleavage of Boc groups, for which selective (re)protection of the phenolic hydroxyls provided an alternative route. Preparation of the polybasic adhesive proved straightforward. However, preparation of the polyacidic adhesive proved difficult, as the monomer has complex polymerisation behaviour dependent upon solution pH, and poisons copper/bipyridyl systems. The use of a protected monomer precursor for polymerisation, followed by acid cleavage, successfully gave the required polyacidic adhesive. The overall synthetic route for the calixarene adhesives is shown in Figure 2.29.

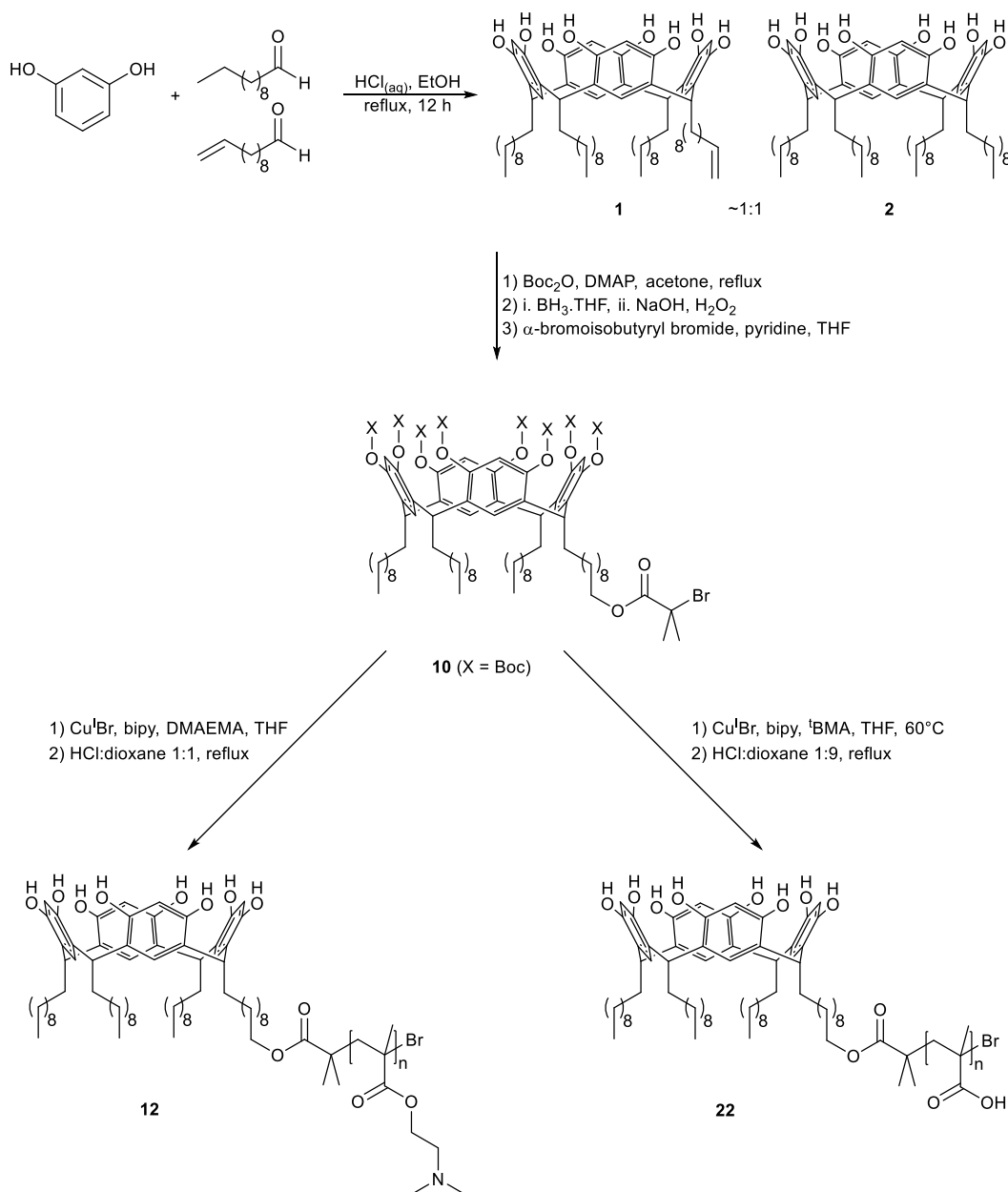


Figure 2.29: Overall synthetic route for the calix[4]resorcinarene adhesives.

In addition to the calixarene-based material, two control compounds using decane instead of calixarene were also prepared using the same methodologies. The overall synthetic route for these control compounds is shown in Figure 2.30.

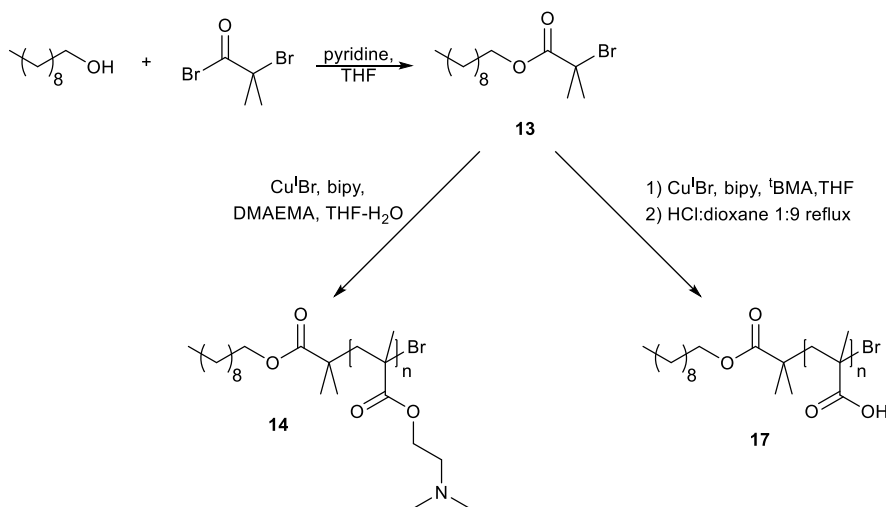


Figure 2.30: Overall synthetic route for the decyl control compounds.

3. Synthesis of Calixarene-Polyelectrolyte Adhesives using RAFT

3.1. Introduction

In addition to the polyacidic calixarene-adhesive prepared in the previous chapter via ATRP, synthesis of the adhesive via radical addition fragmentation transfer (RAFT) was also investigated contemporaneously. RAFT polymerisation was investigated as an alternative to the ATRP polymerisation of the methacrylic acid monomer, which was proving problematic due to the sensitivity of the catalyst system to the acid. RAFT polymerisation is tolerant of the methacrylic acid monomer, and provides access to the polyacid directly.^{205,206}

Although the RAFT agent prepared gave pMAA directly, the RAFT agent itself proved difficult to couple to the calix[4]resorcinarene. While this difficulty was being addressed, the use of a protected monomer (tBMA), followed by an acidic deprotection, was developed to give the polyacidic calixarene-adhesive via ATRP. As such, the material prepared by ATRP was used for the following adhesion studies. Nevertheless, with the resolution of the coupling difficulties, the calixarene-RAFT based material provides a viable alternative to material prepared by ATRP. Use of calixarene-RAFT allows the direct preparation of pMAA, removing the requirement of a protected intermediate followed by a harsh deprotection procedure. The use of calixarene-RAFT also provides access to the Boc protected calixarene-pMAA, which was previously inaccessible via ATRP.

The target calixarene-RAFT adhesive is shown in Figure 2.1, and comprises a calix[4]resorcinarene with a pMAA chain grown from the lower rim using RAFT. This chapter details the synthesis of this adhesive, as well an associated decyl control compound, and provides an alternative solution to the second half of the first objective, to synthesize a mono-functional calixarene which can be used to grow pMAA.

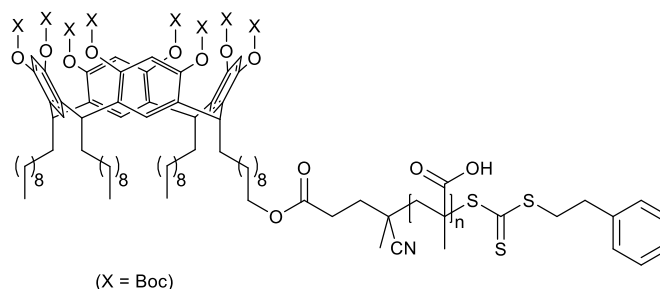


Figure 3.1: Target calix[4]resorcinarene-pMAA (RAFT).

3.2. Synthesis of the RAFT agent

The RAFT agent 4-cyano-4-[(phenethylthio)thiocarbonylthio] valerate **25** (PETTC) has been shown to be tolerant of methacrylates, including MAA.²⁰⁶ It can be prepared by a relatively simple method and contains a carboxylic acid terminal moiety, which can be used to attach the RAFT agent to the calix[4]resorcinarene framework or the decyl control. The RAFT agent PETTC **25** was prepared according to the method reported by M. Semsarilar et al.²⁰⁷ (Figure 3.2).

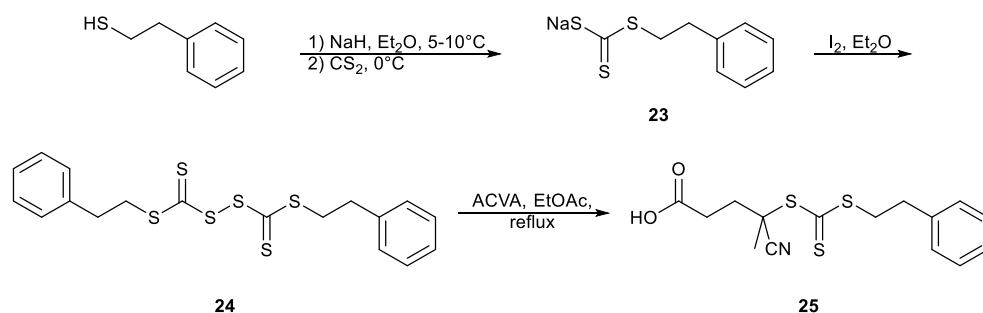


Figure 3.2: Synthesis of RAFT agent PETTC **25**. NaH – sodium hydride. Et₂O – diethyl ether. CS₂ – carbon disulfide. I₂ – solid iodine. ACVA – 4,4'-azobis(4-cyanopentanoic acid). EtOAc – ethyl acetate.

The polymerisation of MAA using PETTC **25** was performed to test the RAFT process and polymerisation conditions before it was attached to the molecules of interest. This polymerisation successfully gave pMAA **26** (Figure 3.3).²⁰⁵ Analysis of the polymer **26** by ¹H NMR integration with the RAFT aromatic end group signals showed a degree of polymerisation of 23, out of 30 equivalents of added methacrylic acid. This showed that the RAFT process was suitable for polymerising the acidic monomer.

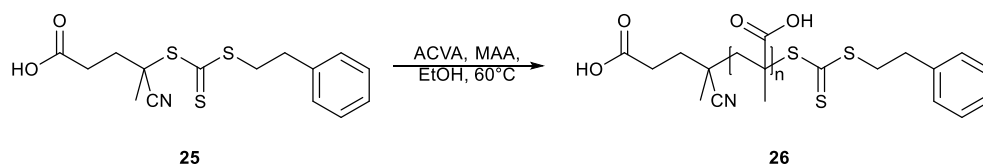


Figure 3.3: RAFT polymerisation of methacrylic acid to give pMAA **26**.

3.2.1. Coupling of PETTC using acyl chloride intermediates

The RAFT agent PETTC **25** is susceptible to decomposition upon reaction with chlorinating reagents, so the diacid precursor ACVA was used instead, as this has a greater stability. Formation of this acyl halide would provide a molecule which could be coupled to the alcohol in the same manner as the ATRP initiator, and then cleaved with the disulfide **24** to form the RAFT agent functionalised molecule. The couplings were initially performed using decanol to give decyl-PETTC. As well as an appropriate test of the coupling conditions, decyl-PETTC also acted as a control analogue in a similar manner to the ATRP decyl-initiator **13**.

A variety of conditions for forming the acyl chloride were investigated based upon conditions reported in the literature^{208–213} (Table 3.1). Many of these required long reaction times or harsh conditions which resulted in decomposition of the azo group (Entries 1-5). Refluxing ACVA in neat thionyl chloride for 10 min, and rapidly quenching the reaction by cooling in an ice bath, gives the required acyl chloride quantitatively after evaporation of excess thionyl chloride (Entry 6). By only heating the reaction mixture for short period of time, the required acyl chloride **27** was formed without degradation (Figure 3.4).

Table 3.1: Summary of conditions for formation of acyl chloride. SOCl₂ – thionyl chloride, (COCl)₂ – oxalyl chloride, DMF – dimethylformamide, RT – room temperature.

Entry	Acid	Conditions
1	ACVA	SOCl ₂ , 30°C, 6 h
2	ACVA	SOCl ₂ , DMF, 60°C, 1.5 h
3	ACVA	(COCl) ₂ , DMF, THF, 0°C then RT overnight
4	ACVA	(COCl) ₂ , DMF, THF, RT, 3 h
5	ACVA	SOCl ₂ , DMF, DCM, RT, 2 days
6	ACVA	SOCl ₂ , 100°C, 10 min

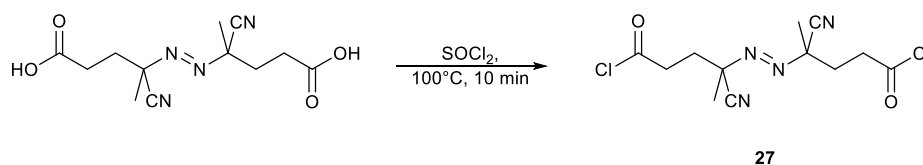


Figure 3.4: Synthesis of 4,4'-azobis(4-cyano-valeroyl chloride) **27**.

The acyl chloride **27** was reacted with decanol in THF with pyridine to give the diester **28** (Figure 3.5). Initially an excess of alcohol was used to ensure complete conversion of the diacyl chloride, however the excess decanol could not be separated from the diester by chromatography. Instead, the diacyl chloride was reacted with 1.8 eq. of alcohol and an additional 0.25 eq. of acyl chloride **27** added at the end of the reaction time. This ensured reaction with all the alcohol and allowed separation of the products, as the monoacid and diacid (ACVA) side products can be readily separated from the diester by chromatography.

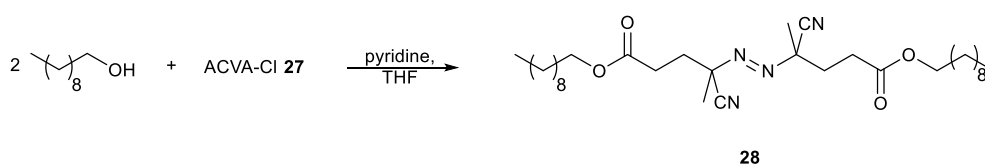


Figure 3.5: Synthesis of diester **28**.

Radical cleavage of the diester **28** with the disulfide **24** gave decyl-PETTC **29** (Figure 3.6). However, this could not be separated from the radical decay product of diester **28** (Figure 3.7). Use of an excess of disulfide cannot avoid this decay product, as there is always ~15% recombination of these radicals within the solvent sphere in which they are formed.²¹⁴ Therefore, coupling of PETTC **25** via an active ester intermediate was also investigated.

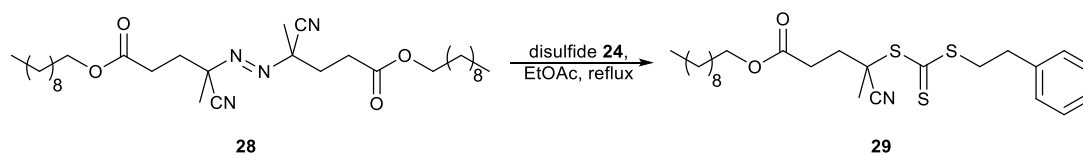


Figure 3.6: Radical cleavage of diester **28** to give decyl-PETTC **29**.

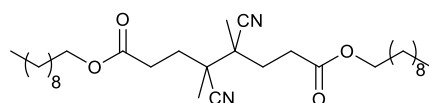


Figure 3.7: Radical decay product of diester **28**.

3.3. Coupling of PETTC using activating reagents

An alternative to the use of the harsh conditions required to form the acyl chloride is the use of reagents which activate the carboxylic acid through the formation of an active ester intermediate. Cyanuric chloride (CC) can be used to form an active ester, which can either react directly with the alcohol of interest or proceed to the acyl chloride with loss of dichlorohydroxy-*s*-triazine (Figure 3.8).^{215–217}

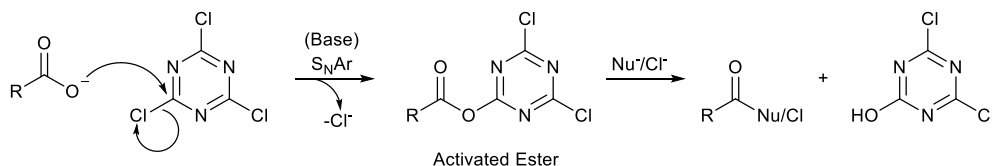


Figure 3.8: Formation of ester/acyl chloride using cyanuric chloride.

The use of cyanuric chloride as a coupling agent was investigated using hexanoic acid and decanol as these were representative of the alcohol and carboxylic acid present in the target system. The ^1H NMR spectrum of the starting materials and product were also much simpler and more straightforward to interpret. The model reaction for the formation of decyl hexanoate **30** is shown in Figure 3.9.

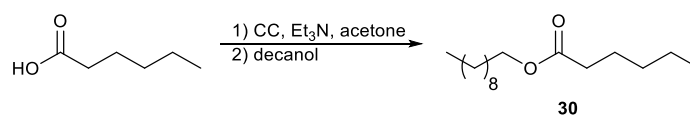


Figure 3.9: Formation of decyl hexanoate **30** using cyanuric chloride.

Reaction parameters such as reaction times, reagent equivalents, and non-anhydrous/anhydrous conditions were varied (Table 3.2). This showed that decyl hexanoate **30** can be successfully formed under a variety of conditions with consistent results (Entries 1-4). The use of anhydrous solvent improved the yield (Entry 5), which was attributed to water in the solvent competing for the activated ester. However, use of less than an equivalent of cyanuric chloride reduced the yield (Entries 6-8). This was attributed to the dichlorohydroxy-*s*-triazine by-product precipitating out of solution before it could react further.

Further experiments on the decyl hexanoate **30** system (Table 3.3) showed that the reaction stages are complete within the literature times of 3 h and 2 h (Entries 9-11).²¹⁵ The addition of an excess of cyanuric chloride to non-anhydrous solvent gave similar results as one equivalent in anhydrous conditions (Entry 12). The addition of a catalytic amount of DMAP with the alcohol has been suggested to improve the coupling reaction when forming esters,²¹⁸ however it did not improve the yield compared to the established system (Entries 13 and 14).

Table 3.2: Summary of conditions for formation of decyl hexanoate **30** using cyanuric chloride. (a) Reaction time for hexanoic acid and cyanuric chloride in presence of base. (b) Reaction time for activated hexanoic ester and decanol.

Entry	Conditions	Reaction time (h)		
		Activation ^a	Coupling ^b	Yield (%)
1	1 eq. CC, Et ₃ N, 8 ml acetone	3	2	46
2	1 eq. CC, Et ₃ N, 8 ml acetone	0.5	2	45
3	1 eq. CC, Et ₃ N, 8 ml acetone	3	0.5	46
4	1 eq. CC, Et ₃ N, 8 ml acetone	0.5	0.5	48
5	1 eq. CC, Et ₃ N, 8 ml dry acetone	3	2	77
6	0.5 eq. CC, Et ₃ N, 4 ml dry acetone	3	2	53
7	0.5 eq. CC, Et ₃ N, 2 ml dry acetone	3	2	63
8	0.3 eq. CC, Et ₃ N, 1 ml dry acetone	3	2	32

Table 3.3: Summary of conditions for formation of decyl hexanoate **30** using cyanuric chloride with varying reaction times. (a) Reaction time for hexanoic acid and cyanuric chloride in presence of base. (b) Reaction time for activated hexanoic ester and decanol.

Entry	Conditions	Reaction time (h)		
		Activation ^a	Coupling ^b	Yield (%)
9	1 eq. CC, Et ₃ N, 3 ml dry acetone	12	2	75
10	1 eq. CC, Et ₃ N, 3 ml dry acetone	3	12	75
11	1 eq. CC, Et ₃ N, 3 ml dry acetone	12	12	75
12	2 eq. CC, Et ₃ N, 3 ml acetone	3	2	67
13	1 eq. CC, Et ₃ N, DMAP, 3 ml dry acetone	3	2	67
14	1 eq. CC, Et ₃ N, 3 ml dry acetonitrile	3	2	76

Once the use of the cyanuric chloride system was shown to be a successful and repeatable method, it was applied to ACVA and decanol to give decyl-ACVA **28**. The yield was lower than that recovered in the decyl hexanoate control experiments (Table 3.4, Entry 1), but still gave a useful quantity of material. The coupling was then applied to PETTC **25** and decanol to give decyl-PETTC **29**, which resulted in a drop in the isolated yield for decyl-PETTC **29** compared to decyl-ACVA **28** (Entry 2).

Mono-hydroxyl calix[4]resorcinarene **5** was then coupled to PETTC **25** to give calix[4]resorcinarene-PETTC **31** (Figure 3.10). This resulted in a low yield of material (Table 3.4, Entry 3). However, when the quantity of cyanuric chloride was increased to two equivalents, there was an increase in the yield (Entry 4). The yield was comparable to that obtained for decyl-PETTC **29** using one equivalent of cyanuric chloride. However, it is still much lower than decyl-ACVA **28** and the decyl hexanoate system.

Table 3.4: Summary of conditions for formation of RAFT esters using cyanuric chloride. (a) All reactions were conducted in anhydrous acetone using triethylamine as a base. (b) Reaction time for acid and cyanuric chloride in presence of base. (c) Reaction time for activated ester and alcohol.

Entry	Conditions ^a	Reaction time (h)		Yield (%)
		Activation ^b	Coupling ^b	
1	ACVA, decanol, 1 eq. CC	3	2	56
2	PETTC 25 , decanol, 1 eq. CC	3	2	11
3	PETTC 25 , Calix 5 , 1 eq. CC	3	2	3
4	PETTC 25 , Calix 5 , 2 eq. CC	3	2	17

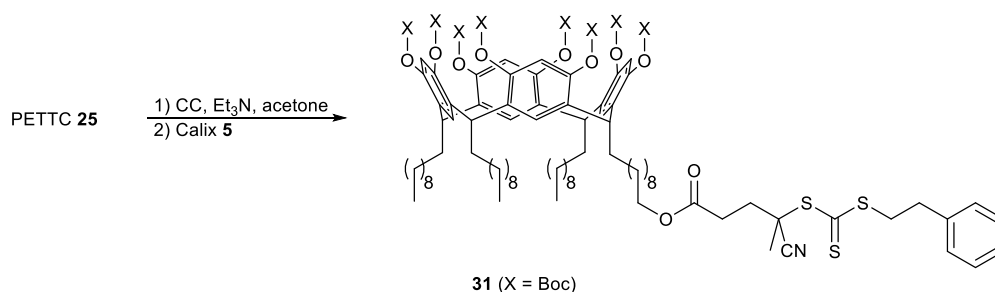


Figure 3.10: Synthesis of calix[4]resorcinarene-PETTC **31** using CC.

In addition to forming the ester of PETTC **25**, an amide was also investigated as an alternative linker. The increased nucleophilicity of amines was expected to improve coupling with the activated ester formed from cyanuric chloride, and the resulting amide would be a stronger linking group. As amines can react with acetone, the reaction was conducted in acetonitrile (MeCN). Octylamine was coupled to PETTC **25** using cyanuric chloride to give octyl-PETTC **32** (Figure 3.11). The amide was isolated in a low yield (10%). This yield is comparable to the decyl-PETTC **29** ester and shows no benefit to using an amine instead of an alcohol, suggesting that activation of the carboxylic acid is the limiting factor.

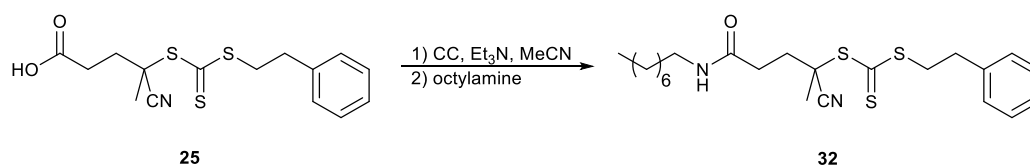


Figure 3.11: Synthesis of octyl-PETTC **32**.

The conditions to form the activated ester were studied by varying the reagent quantities and monitoring the development of the activated ester by thin-layer chromatography (TLC) (Table 3.5, Figure 3.12). Initially, the reaction was studied at equivalent amounts of reagents at different concentrations over time (Entries 1 and 2). The activated ester developed slowly, mostly as a di- or tri- substituted triazine, and did not achieve a high conversion. The quantities of cyanuric chloride and base were then increased progressively up to 3 eq. cyanuric chloride and excess base (Entries 3-5).

Upon addition of the excess base a large exotherm was observed and a precipitate formed, indicating rapid formation of the triethylamine salt. TLC showed a higher degree of conversion, mostly to the mono-substituted triazine, over a shorter period of time. However, full conversion could not be achieved, even with the use of stronger bases (Table 3.5, Entries 6 and 7). This suggests that the incomplete activation of the PETTC **25** carboxylic acid is having an effect upon the coupling reactions, and resulted in the reduced yields observed compared to the other acids studied.

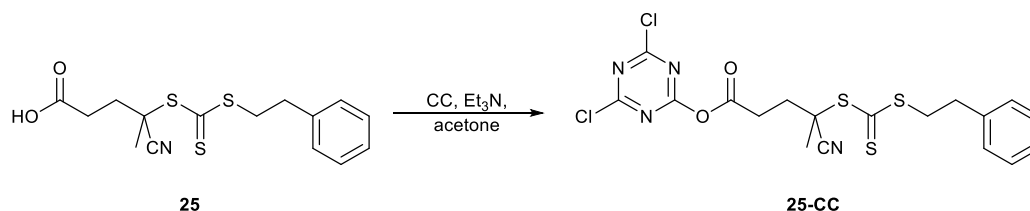


Figure 3.12: Activation of PETTC **25** with cyanuric chloride.

Table 3.5: Summary of conditions for formation of activated PETTC **25-CC** using cyanuric chloride. (a) Concentration of PETTC **25** in solution. (b) Concentration reduced due to increased volume of added base. (c) Base used is triethylamine. (d) Base used is sodium hydroxide. (e) Base used is sodium hydride.

Entry	[PETTC 25] (mol L ⁻¹) ^a	Equivalentents used		
		PETTC 25	CC	Base
1	0.04	1	1	1 ^c
2	0.3	1	1	1 ^c
3	0.3	1	2	2.5 ^c
4	0.3	1	3	3.5 ^c
5	0.2 ^b	1	3	25 ^c
6	0.3	1	1	1 ^d
7	0.3	1	1	1 ^e

More reactive coupling agents were then investigated, many of these reagents are well established for peptide coupling reaction, and have also been used for the formation of esters. PETTC **25** was activated using 1,1'-carbonyldiimidazole (CDI) and reacted with deanol to give decyl-PETTC **29** (Figure 3.13).²¹⁹ The isolated yield of the coupling was 10%, this was lower than expected for these coupling conditions, and similar to those obtained using cyanuric chloride (Table 3.4).

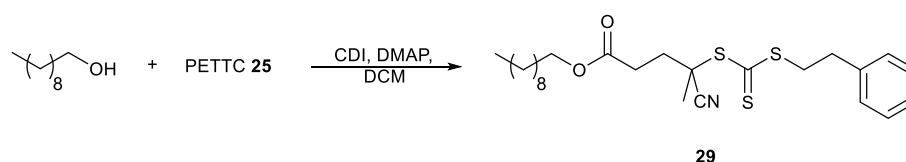


Figure 3.13: Synthesis of decyl-PETTC **29** using CDI.

The coupling conditions used for decyl-PETTC **29** were then used to couple mono-hydroxyl calix[4]resorcinarene **5** to PETTC **25** using CDI. Analysis by ¹H NMR showed that while PETTC **25** had formed some of the activated ester, it had not reacted with the calix[4]resorcinarene alcohol.

The coupling reaction was then investigated using the decanol system (decyl-PETTC **29**). First, the quantity of base was increased to an equivalent amount, however this yielded no conversion (Table 3.6, Entry 1). The coupling reagent was then switched from 1,1'-carbonyldiimidazole (CDI) to 1-ethyl-3-(3-dimethylaminopropyl)carbodiimide (EDC), and an excess of a stronger base (triethylamine (Et₃N)) was used. The solvent was also changed to THF to improve the solubility of calix[4]resorcinarene **5**. These changes also failed to produce a substantial increase in the coupling yield (Entry 2).

To investigate what may be causing the reaction to fail, a series of control experiments were performed, which included varying the alcohol and the acid used in the coupling to identify the limiting factor (Table 3.6, Entries 3-7). Of these, only the reactions with ACVA produced a small amount of coupling in ~11-12% yield (Entries 6 and 7). Use of *N,N*-dicyclohexylcarbodiimide (DCC) and mixture of DCM and THF afforded a slight improvement in yield (Entries 8 and 9) for decyl-ACVA **28** (Figure 3.14) and decyl-PETTC **29** coupling, but gave a low yield (Entry 10) when decanol was replaced by mono-hydroxyl calix[4]resorcinarene **5** (Figure 3.15). Use of more reactive activating agents HATU²²⁰ and trifluoromethanesulfonyl chloride (TfCl) (Entries 11 and 12) afford no improvement in yield for the formation of decyl-PETTC **29**.

Table 3.6: Summary of coupling conditions between varying alcohols and acids. DIPEA – *N,N*-Diisopropylethylamine, (a) All reactions were conducted under anhydrous conditions.

Entry	Alcohol	Acid	Conditions ^a	Yield (%)
1	Decanol	PETTC 25	CDI, DMAP, DCM	<1
2	Decanol	PETTC 25	EDC, Et ₃ N, THF	<1
3	Decanol	Hexanoic acid	EDC, Et ₃ N, THF	<1
4	Ethanol	PETTC 25	EDC, Et ₃ N, THF	<1
5	Ethanol	Hexanoic acid	EDC, Et ₃ N, THF	<1
6	Decanol	ACVA	EDC, Et ₃ N, THF	11
7	Ethanol	ACVA	EDC, Et ₃ N, THF	12
8	Decanol	ACVA	DCC, DMAP, DCM:THF	19
9	Decanol	PETTC 25	DCC, DMAP, DCM:THF	15
10	Calix 5	ACVA	DCC, DMAP, DCM:THF	4
11	Decanol	PETTC 25	HATU, Et ₃ N, MeCN	19
12	Decanol	PETTC 25	TfCl, DIPEA, Et ₂ O	18

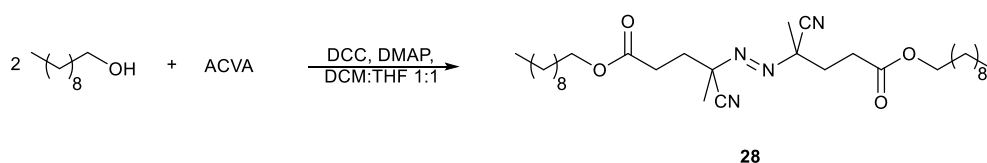


Figure 3.14: Synthesis of decyl-ACVA **28** using DCC.

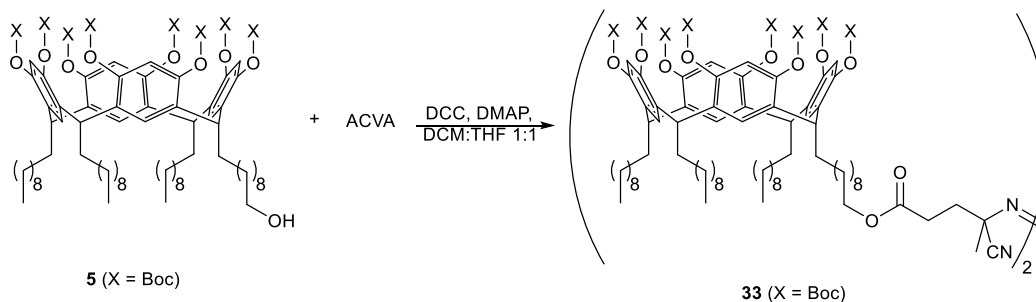


Figure 3.15: Synthesis of calix[4]resorcinarene-ACVA **33**.

Investigation of the RAFT agent PETTC **25** showed that the nitrile was prone to decomposition to the primary amide in the presence of water or an acid catalyst (Figure 3.16). This can be seen from the ^1H NMR, where singlet for the methyl adjacent to the nitrile shifts from $\delta = 1.91$ to $\delta = 1.67$. It has also been shown²²¹ that the molecule can self-catalyse this decomposition through interaction with the terminal carboxylic acid. This decomposition occurs even when stored under anhydrous conditions in the freezer. It was observed that the material would change from an oil to a solid upon decomposition, and if not properly stored this phase change would occur within two days. This decomposition is not observed for the diazo precursor (ACVA), suggesting that the formation of the active centre of the RAFT agent activates the nitrile to decomposition.

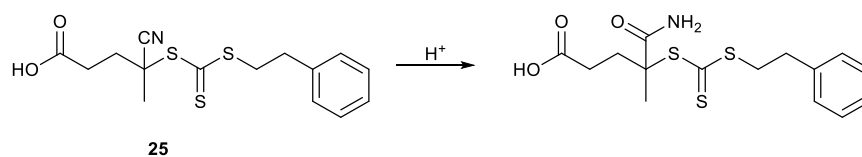


Figure 3.16: Decomposition of PETTC **25**.

The primary amide formed from the decomposition can compete with the other nucleophiles in the coupling reaction, resulting in the observed drop in the yield for many of the recorded reactions. Based upon these findings, PETTC **25** was prepared in small quantities and used for coupling within one day to prevent decomposition.

PETTC **25** was coupled to decanol using DCC and a catalytic quantity of DMAP in DCM,²²² and successfully gave decyl-PETTC **29** in 52% yield (Figure 3.17). Based upon this success, PETTC **25** was then coupled to mono-hydroxyl calix[4]resorcinarene **5** using the same conditions, which gave Boc mono-PETTC calix[4]resorcinarene **31** in 38% yield (Figure 3.18).

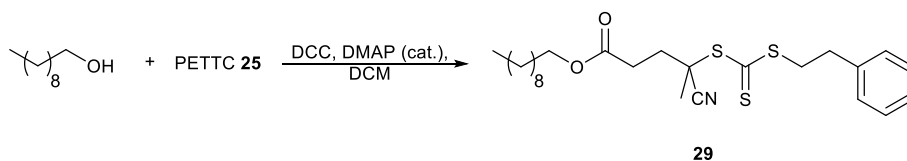


Figure 3.17: Synthesis of decyl-PETTC **29**.

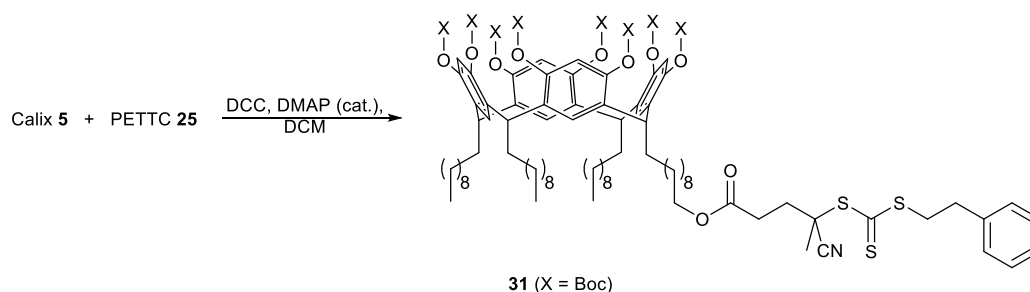


Figure 3.18: Synthesis of calix[4]resorcinarene-PETTC **31**.

3.4. RAFT polymerisation

Decyl-PETTC **29** was used to polymerise MAA following the same conditions used for pMAA **26** to give decyl-pMAA **34** (Figure 3.19).²⁰⁵ The successful polymerisation showed that PETTC **25** is still effective when attached to a molecule.

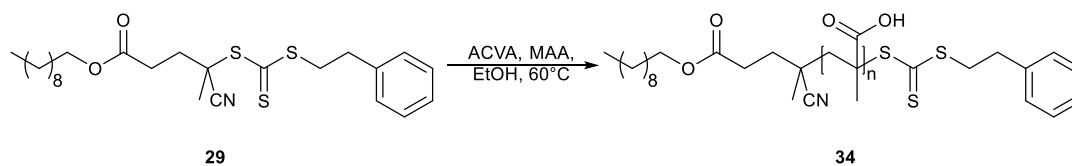


Figure 3.19: RAFT polymerisation of methacrylic acid using decyl-PETTC **29** to give decyl-pMAA **34**.

Boc mono-PETTC calix[4]resorcinarene **31** was then used to polymerise MAA to give Boc-calix[4]resorcinarene-pMAA **35** (Figure 3.20). Analysis by ^1H NMR showed the expected appearance of the backbone signals and disappearance of the monomer alkene signals. The target degree of polymerisation (DP) was 60 units, and analysis by GPC showed a measured DP of 86 units with a dispersity index (\mathcal{D}) of 1.39. This is similar to that obtained from the polymerisation of t BMA by ATRP using calixarene **10**, which had a DP of 85 and $\mathcal{D} = 1.49$, but does not require deprotection of the monomer.

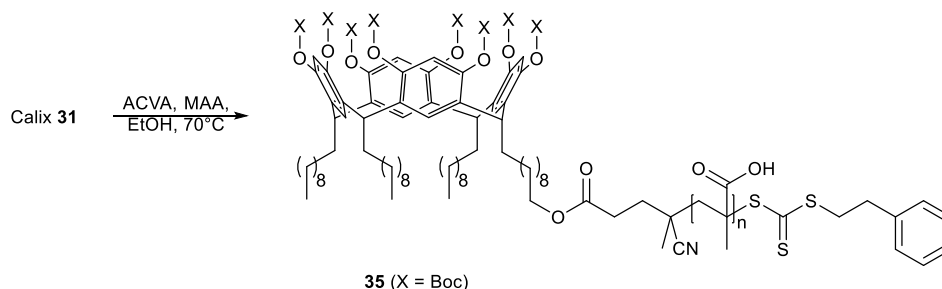


Figure 3.20: RAFT polymerisation of methacrylic acid using Boc-calix[4]resorcinarene-PETTC **31** to give Boc-calix[4]resorcinarene-pMAA **35**.

3.5. Summary

In this chapter, the polyacidic calixarene-based adhesive was prepared directly via RAFT polymerisation, and provides an alternative solution to the second half of the first objective, to synthesize a mono-functional calixarene which can be used to grow pMAA.

The RAFT agent PETTC was prepared and showed to polymerise MAA directly, without the need for an intermediate protected monomer. However, coupling of PETTC, or the diazo precursor, proved problematic. Although the diazo could be coupled to decanol via the acyl halide, the radical cleavage product of this could not be separated from the major side product.

Use of activating agents to form an active ester gave low yields over a variety of conditions. It was found that the RAFT agent PETTC is prone to decomposition even upon cold storage. Use of freshly prepared PETTC with appropriate carbodiimide coupling conditions, gave both the decyl- and calixarene-PETTC functionalised molecules. MAA was then successfully polymerised from these molecules, and shown to give a similar degree of polymerisation and dispersity as pMAA grown from calixarene by ATRP, but without the requirement for a protected monomer. The overall synthetic routes for Boc-calixarene-pMAA and decyl-pMAA prepared by RAFT are shown in Figure 3.21 and Figure 3.22.

With the resolution of the coupling difficulties, the calixarene-RAFT based material provides a viable alternative to material prepared by ATRP. Use of calixarene-RAFT allows the direct preparation of pMAA, removing the requirement of a protected intermediate followed by a harsh deprotection procedure. The use of calixarene-RAFT also provides access to the Boc protected calixarene-pMAA, which was previously inaccessible via ATRP, and may improve the surface adhesion of this material to more hydrophobic surfaces.

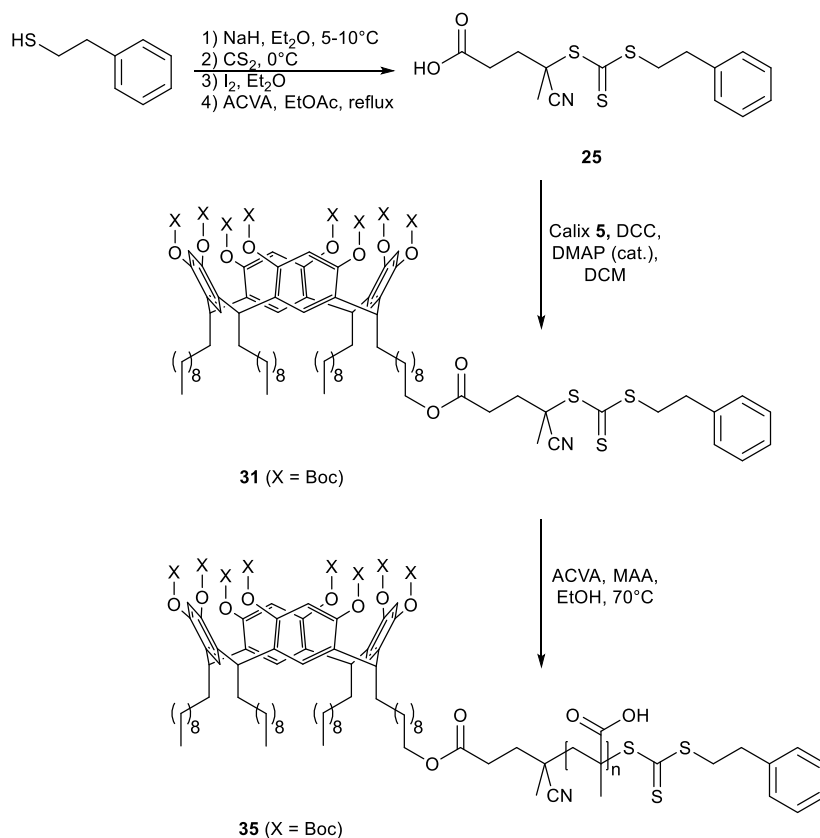


Figure 3.21: Overall synthetic route for the Boc-calix[4]resorcinarene-pMAA **35**.

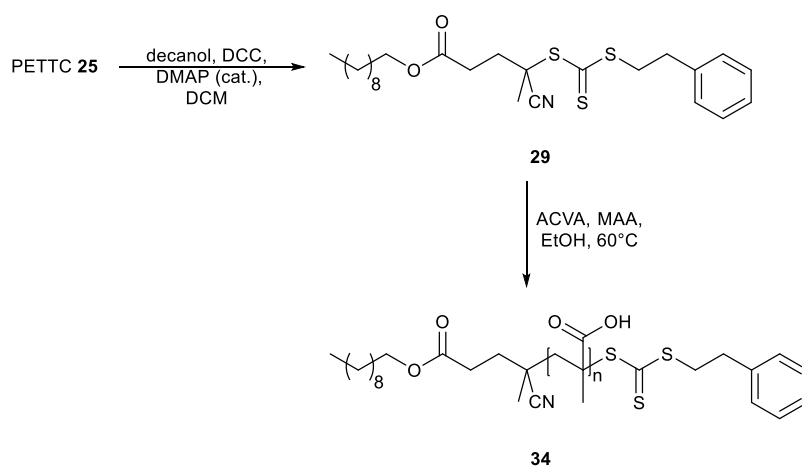


Figure 3.22: Overall synthetic route for decyl-pMAA **34**.

4. Deposition of Calixarene-Polyelectrolyte Adhesives

4.1. Introduction

The calixarene based adhesives have been designed to allow for the deposition of the polyelectrolyte adhesive to a surface of interest via the grafting-to method. The intention of this is to provide a one-pot route to the formation of a single monolayer of adhesive without the use of synthetically intensive methods.

This chapter covers the deposition of the calixarene adhesives and the decyl controls (Figure 4.1). These fulfil the second objective, to deposit the adhesives to form an ordered brush monolayer using a physical bond, and allows the first thesis question to be answered:

- c) *Can a calix[4]resorcinarene be used as a surface active head group for the direct attachment of polyelectrolyte adhesives to surfaces?*

The adhesives were initially deposited by spontaneous assembly from solution, but the use of Langmuir-Schaefer deposition proved more efficient at transferring material.

Poly(vinyl acetate) (PVAc) films were spin-coated to provide thin films of similar thickness to the deposited calixarene adhesives. These PVAc films were prepared to provide a comparison between the deposited polyelectrolyte brush, and a traditional adhesive under the same test conditions, i.e., the use of a charged hydrogel in an aqueous system.

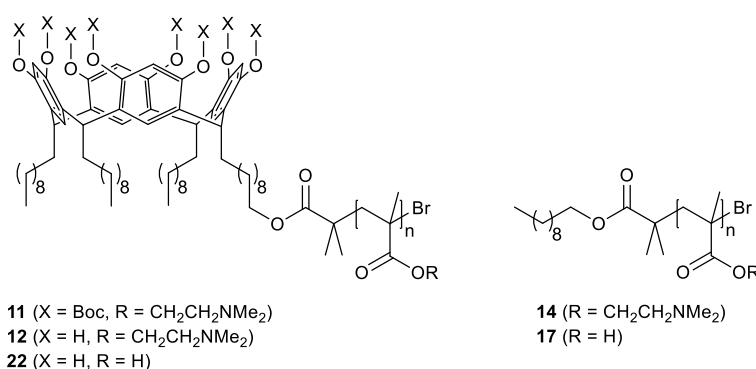


Figure 4.1: Calixarene adhesives **11**, **12**, and **22**, and decyl controls **14** and **17**.

4.2. Deposition of calixarene-polyelectrolyte adhesives from solution

The two calixarene-polyelectrolyte adhesives **12** and **22** were dissolved in DCM and methanol respectively, at a concentration of 2 mg ml⁻¹. Piranha cleaned silicon wafers were immersed in these solutions for a period of two weeks. The wafers were then removed, rinsed with fresh solvent, and dried with a stream of nitrogen.

The thickness of the deposited materials was determined using spectroscopic ellipsometry (M-2000V Rotating Compensator Ellipsometer, J. A. Woollam Co.). The data were fitted using a B-Spline model for the polymer with a silicon substrate (CompleteEASE software). The thickness of the native oxide layer was 1.39 ± 0.03 nm. The grafting density (σ) was determined using²²³

$$\sigma = \frac{l\rho_{\text{pol}}N_{\text{A}}}{M_{\text{n}}} \quad (4.1)$$

where l is the thickness of the brush, ρ_{pol} is the density of the polymer, N_{A} is Avogadro's number, and M_{n} is the number average molecular weight. The densities used were $\rho_{\text{pol}} = 1.318 \text{ gcm}^{-3}$ for pDMAEMA²²³ and $\rho_{\text{pol}} = 1.12 \text{ gcm}^{-3}$ for pMAA.²²⁴

The grafting density is, in part, limited by the conformation the polymer adopts in solution. The radius of gyration (R_{g}) describes the dimensions of a polymer chain and can be calculated from^{225,226}

$$R_{\text{g}} = \sqrt{Nb^2/6} \quad (4.2)$$

where b is the segment length and N is the number of methacrylate monomer units. The segment lengths used were $b = 0.54 \text{ nm}$ for pDMAEMA²²⁷ and $b = 0.252 \text{ nm}$ for pMAA.²²⁸

The interchain distance (D) was determined using²²⁹

$$D = \frac{1}{\sqrt{\sigma}} \quad (4.3)$$

If the interchain distance is less than the radius of gyration then the grafted polymers adopt a brush, or brush-like, regime.

The transition from a single grafted chain regime (mushroom) to a brush regime can be characterised using the reduced tether density (Σ), as determined by²³⁰

$$\Sigma = \sigma\pi R_{\text{g}}^2 \quad (4.4)$$

The polymer film can be characterised by three conformational regimes based upon grafting density: the ‘mushroom’ or weakly interacting regime at $\Sigma < 1$; the mushroom-to-brush transition regime at $1 < \Sigma < 5$; and the brush regime at $\Sigma > 5$.²³⁰

The thicknesses and characterisation parameters for the two adhesives **12** and **22** deposited from solution are listed in Table 4.1. Both polymers show a low grafting density, with the interchain distance larger than the radius of gyration of the polymer in solution. This results in a small reduced tether density, and therefore less brush-like character. The reduced tether density shows that calixarene-pMAA **22** is in the weakly interacting ‘mushroom’ regime. Calixarene-pDMAEMA **12** is in the mushroom-to-brush transition regime, but is not a ‘true’ brush as $\Sigma < 5$. The interchain distance is also greater than the radius of gyration of the free polymer, as is the case for calixarene-pMAA **22**. This shows that both the polymers are sparsely deposited across the silicon surface.

Table 4.1: Compounds deposited from solution showing thickness, number of chain units (N), radius of gyration (R_g), grafting density (σ), interchain distance (D), and reduced tether density (Σ).

Compound	Thickness (nm)	N	R_g (nm)	σ (nm ⁻²)	D (nm)	Σ
Calix-pDMAEMA 12	3 ± 1	82	2	0.19 ± 0.06	2.3 ± 0.2	2.4 ± 0.8
Calix-pMAA 22	0.5 ± 0.3	85	1	0.05 ± 0.03	4.5 ± 0.3	0.14 ± 0.09

The material was tested for adhesion using a mechanical tester (Texture Analyser TA.XT*plus*, Stable Microsystems), which brought a hemispherical hydrogel of the opposite charge into contact with the sample surface using a standard protocol. A pMAA hydrogel was used for calixarene-pDMAEMA **12** and a poly(2-(diethylamino)ethyl methacrylate) pDEAEMA hydrogel was used for calixarene-pMAA **22**.

The adhesion and work done for the deposited calixarene-adhesives are shown in Table 4.2. The plain silicon wafer showed no adhesive response to either hydrogel. Calixarene-pDMAEMA **12** showed a low adhesive response and calixarene-pMAA **22** showed no adhesive response, both of which can be explained by the low grafting densities and deposited film thicknesses leading to a lack of material to adhere to. Previous work³⁴ measuring the adhesion of ‘grafted-from’ polyelectrolyte brushes using the same experimental conditions reported adhesions of 0.12 ± 0.02 N for a pMAA gel-pDEAEMA brush system and 0.30 ± 0.02 N for a pDEAEMA gel-pMAA brush system. These values are much greater than those measured for the material deposited from solution. The brushes ‘grafted-from’ were much thicker than those deposited from solution, with thicknesses of 27.8 ± 0.1 nm for pDEAEMA brushes and 32.2 ± 0.2 nm for pMAA brushes, so there was a greater quantity of adhesive material for the hydrogel to interact with and give an adhesive response.

Table 4.2: Adhesion and Work done of calixarene adhesives deposited from solution.

Compound	Adhesion (N)	Work done ($\times 10^{-3}$ mJ)
<i>Silicon wafer</i>	0.00 ± 0.00	00 ± 0
Calix-pDMAEMA 12	0.03 ± 0.01	25 ± 5
Calix-pMAA 22	0.00 ± 0.00	00 ± 0

Deposition of the two calixarene adhesives **12** and **22** from solution gave a low grafting density and resulting thickness of material, with material remaining in the coiled ‘mushroom’ regime. The low transfer of material resulted in little to no adhesion. To improve the potential for adhesive behaviour, a greater amount of material needed to be transferred to the sample surface. To do this, and to promote a more brush-like regime, a Langmuir trough was used to compress a monolayer of material and ‘pre-order’ a surface for deposition.

4.3. Langmuir-Schaefer deposition of adhesives

Isotherms of the three calixarene adhesives **11**, **12**, and **22** and the corresponding decyl control compounds **13** and **17** were recorded using a Langmuir trough (Langmuir Film Balance for Brewster Angle Microscope, Type: 601BAM, NIMA Technology). The Boc-calixarene adhesive **11** was included to examine the effect of the calixarene bowl head-group. The increased hydrophobicity of the Boc group increases will increase the strength of the binding to hydrophobic surfaces.

The isotherms were recorded using a 1 mg ml^{-1} solution of the adhesive or control compound in either chloroform for **14**, **11**, and **12**, or 5% MeOH:CHCl₃ for **17** and **22**. 100 μl of the polymer solution was added dropwise to the surface of the sub-phase using a Hamilton syringe. Five different sub-phases were used to record the isotherms: pH2 HCl_(aq), pH4 HCl_(aq), pH6 H₂O, pH8 NaOH_(aq), and pH10 NaOH_(aq). All sub-phase solutions were made using Milli-Q water, and the pH value checked using a pH probe. The isotherms of all the compounds were recorded at pH6, the isotherms of **14**, **11**, and **12** were also recorded at pH2 and pH4, and the isotherms of **17** and **22** were also recorded at pH8 and pH10. The isotherms at high and low pH were recorded to observe the effect the sub-phase pH had upon the polyelectrolytes.

The isotherms for the calixarene adhesive **12** are shown in Figure 4.2. The isotherms all display a steady rise in pressure with decreasing surface area, with a change in the rate of pressure increase indicating a phase change from a 2D liquid to a 2D quasi-solid regime. With decreasing pH, the onset of the quasi-solid regime is depressed to lower surface areas. This is attributed to the increasing protonation state of the pDMAEMA polyelectrolyte promoting greater dissolution into the aqueous sub-phase as the hydrophobic fraction of the polymer decreases. This change is most pronounced between pH6 and pH4. The pH6 isotherm is close to the pK_a of pDMAEMA (7.5),¹¹⁸ so a greater proportion of the polymer will be uncharged and have a more hydrophobic nature. At pH4 the majority of the polymer will be charged and be more hydrophilic. The difference between pH4 and pH2 is not as great as between pH4 and pH6, as there is less difference in the charge state of the polymer. All the isotherms reach the same maximum pressure at the same surface area. This area of maximum pressure is dominated by the effects of the calixarene, which acts as a hydrophobic head group. At these high pressures, the film is organised with the polyelectrolyte dissolved in the sub-phase and an organised surface of calixarenes.

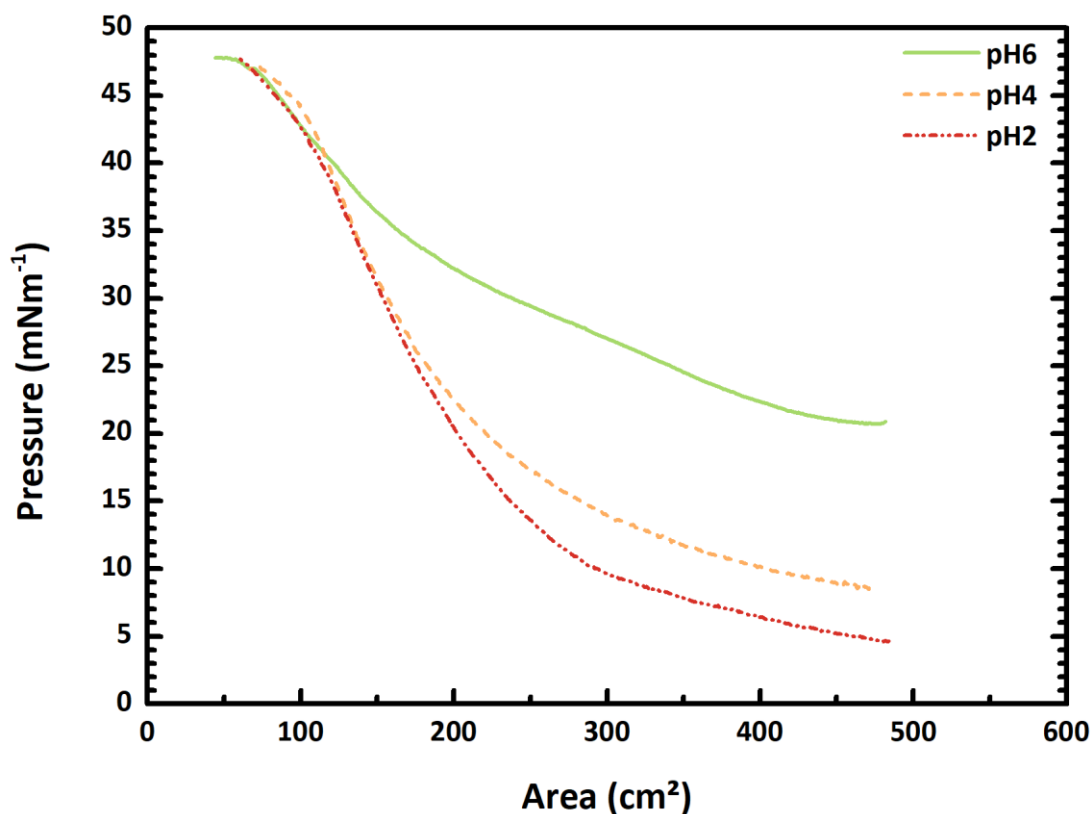


Figure 4.2: Pressure-area isotherms of calixarene-pDMAEMA adhesive **12**. The solution added was 100 μl of a 1 mg ml^{-1} solution of **12** in CHCl_3 for each isotherm. The sub-phase was pH2 $\text{HCl}_{(\text{aq})}$, pH4 $\text{HCl}_{(\text{aq})}$, or pH6 H_2O , all of which were made using Milli-Q water.

The isotherms for the Boc-calixarene adhesive **11** are shown in Figure 4.3. These isotherms also show a change between pH6, where the polymer still has uncharged regions, and pH4 where the polymer is predominately charged. These isotherms have a lower maximum pressure than the calixarene adhesive **12** due to the effects of the Boc group. The Boc groups around the upper rim of the calixarene increase the hydrophobicity of the calixarene, removing its hydrogen bonding ability. As the pH of the sub-phase is lowered the calixarene is repelled from the sub-phase and is more likely to adopt an upright conformation to reduce its contact with the surface, resulting in an increasing dominance of the polymer affecting the isotherms at higher pressures with increasing pH, and a reduction of calixarene-calixarene and calixarene orientation effects.

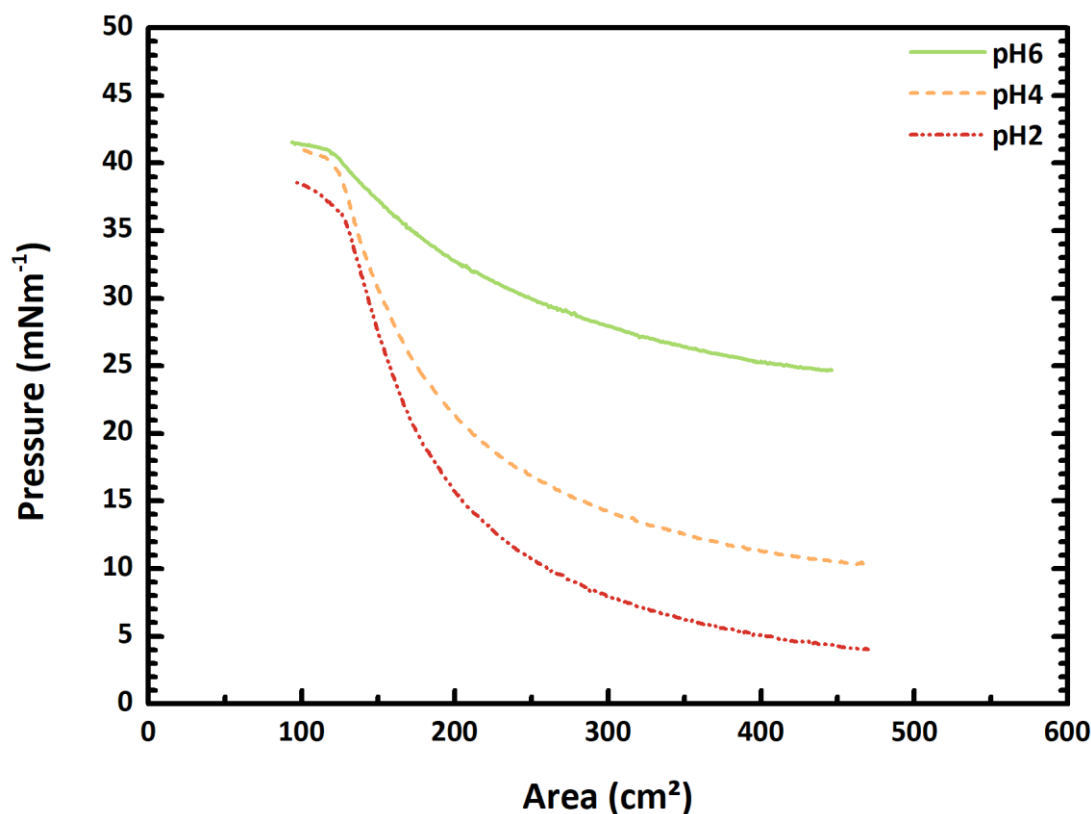


Figure 4.3: Pressure-area isotherms of Boc-calixarene-pDMAEMA adhesive **11**. The solution added was 100 μl of a 1 mg ml^{-1} solution of **11** in CHCl_3 for each isotherm. The sub-phase was pH2 $\text{HCl}_{(\text{aq})}$, pH4 $\text{HCl}_{(\text{aq})}$, or pH6 H_2O , all of which were made using Milli-Q water.

The isotherms for the decyl control **14** are shown in Figure 4.4. These isotherms also show a change between pH6, where the polymer has uncharged regions, and pH4 where the polymer is predominately charged. There is less consistency between pH4 and pH2. The decyl group is much smaller than calixarene, and so will have a much lower impact upon the organisation of the film into an ordered monolayer, resulting in the film behaviour being dominated by the polymer effects. At high pressures, the films begin to buckle and force material above the surface or into the sub-phase due to the lack of a strong hydrophobic group to promote amphiphilic behaviour.

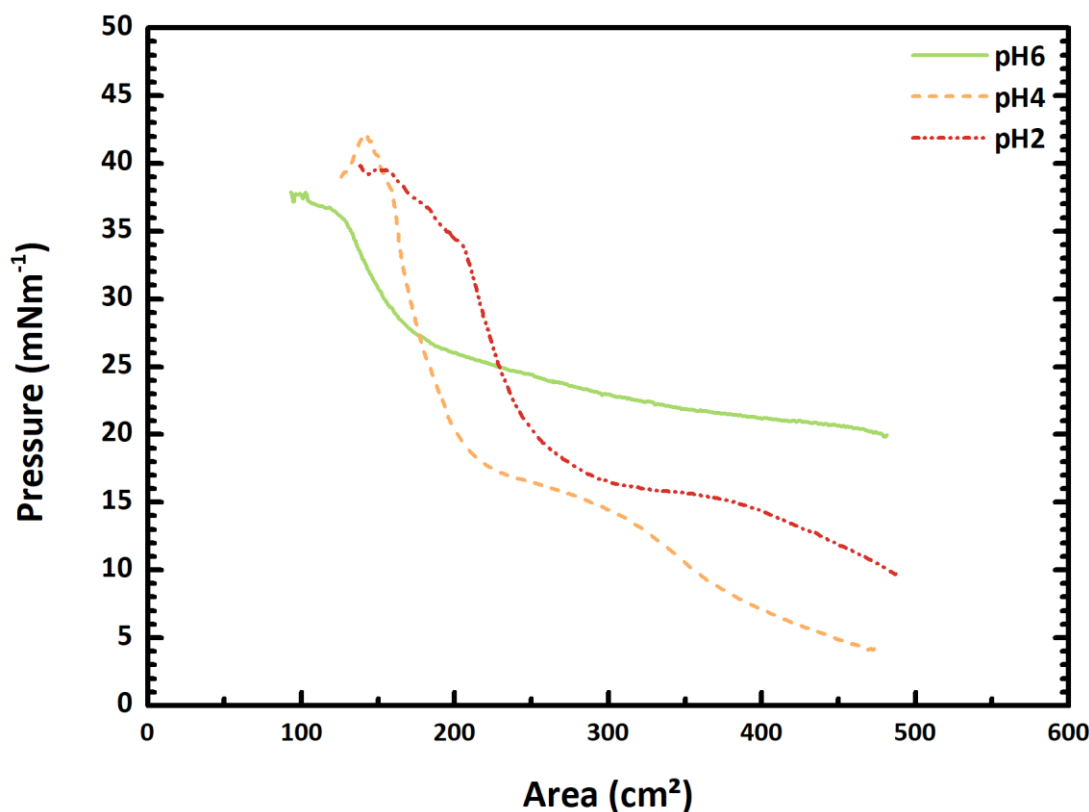


Figure 4.4: Pressure-area isotherms of decyl-pDMAEMA control **14**. The solution added was 100 μl of a 1 mg ml^{-1} solution of **14** in CHCl_3 for each isotherm. The sub-phase was pH2 $\text{HCl}_{(\text{aq})}$, pH4 $\text{HCl}_{(\text{aq})}$, or pH6 H_2O , all of which were made using Milli-Q water.

Polymers can be subject to conformational changes with increasing pressure. Without the calixarene to ‘anchor’ the polymer to the surface, it can adopt a greater number of conformations, including adsorption of loops into the sub-phase, which can lead to a number of different transitions in the pressure-area isotherm.

During compression, monolayers of polymers can sustain long-lasting pressure gradients across the film which can produce inhomogeneous films, resulting in differences in the observed pressure-area isotherms for the same material.^{231,232} The discrepancy between pH4 and pH2 is probably due to the film buckling as a result of pressure fractures across the polymer film. This results in a different amount of material being compressed within the 2D plane, causing an offset of the phase transitions.

The isotherms for the calixarene-pMAA adhesive **22** are shown in Figure 4.5. The isotherms for the calixarene-pMAA adhesive **22** display the same trends shown by the calixarene-pDMAEMA adhesive **12**. With increasing pH, the onset of the more solid regime is depressed to lower surface areas, due to the increasing deprotonation of the pMAA polyelectrolyte. Again, the pH6 isotherm is close to the pK_a of pMAA (5.7),¹¹⁹ so a proportion of the polymer will be uncharged and have a more hydrophobic nature. At pH8 and pH10 the majority of the polymer is heavily ionised and will therefore be more hydrophilic.

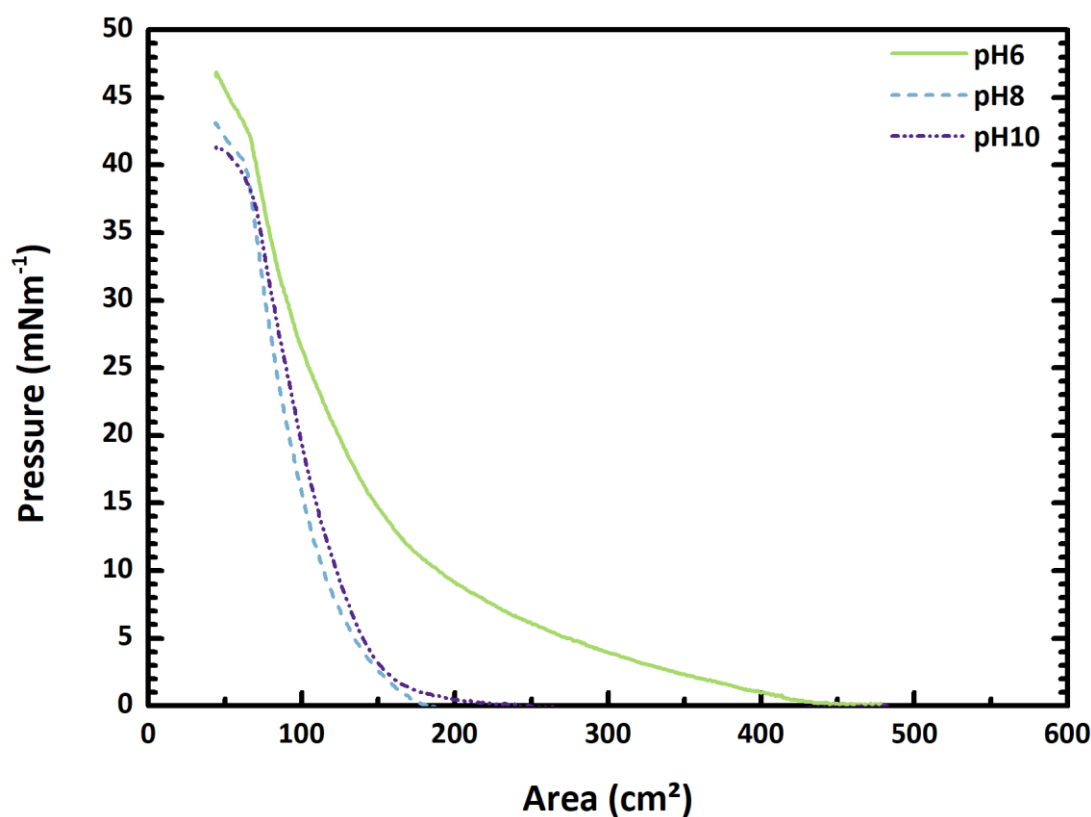


Figure 4.5: Pressure-area isotherms of calixarene-pMAA adhesive **22**. The solution added was 100 μl of a 1 mg ml^{-1} solution of **22** in 5% MeOH:CHCl₃ for each isotherm. The sub-phase was pH6 H₂O, pH8 NaOH_(aq), and pH10 NaOH_(aq), all of which were made using Milli-Q water.

The isotherms for the decyl-pMAA control **17** are shown in Figure 4.6. The isotherms display the same trends as shown by the calixarene adhesive **22**. They also show a change between pH6, where the polymer still has uncharged regions, and pH8 and pH10 where the majority of the polymer is charged.

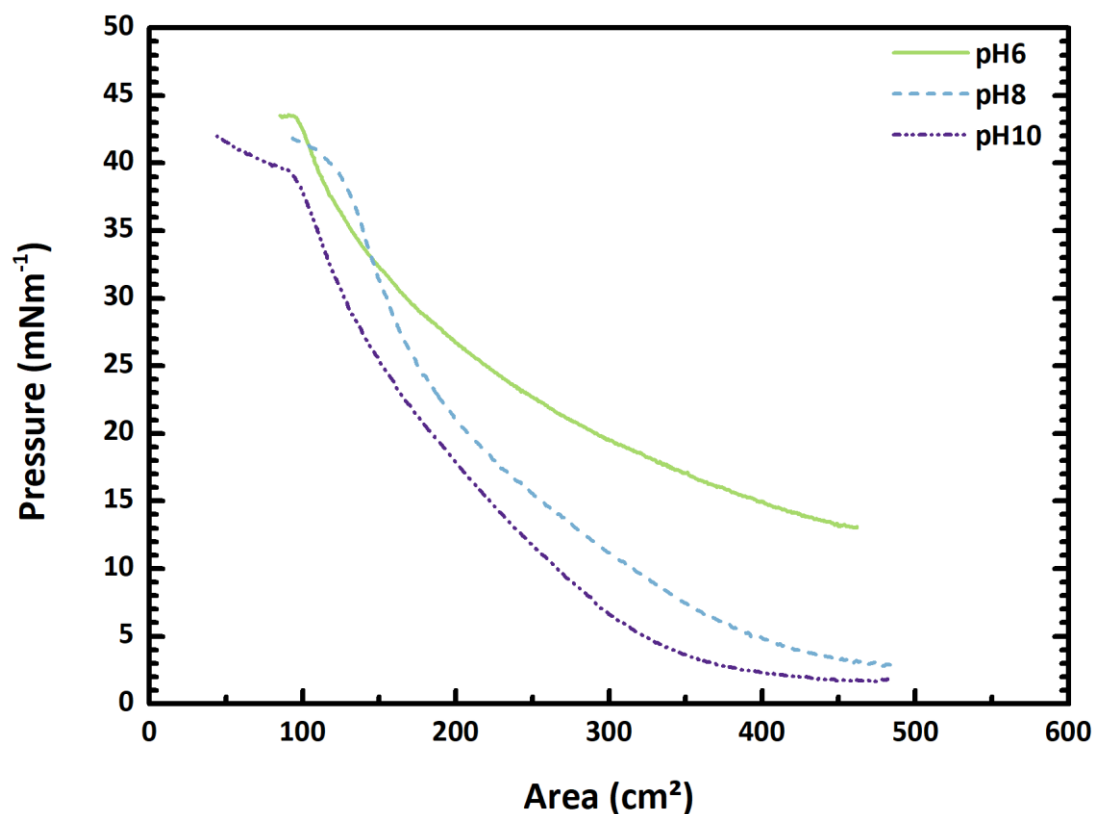


Figure 4.6: Pressure-area isotherms of decyl-pMAA control **17**. The solution added was 100 μl of a 1 mg ml^{-1} solution of **17** in 5% MeOH:CHCl₃ for each isotherm. The sub-phase was pH6 H₂O, pH8 NaOH_(aq), and pH10 NaOH_(aq), all of which were made using Milli-Q water.

Using the information from these isotherms, samples were taken using Langmuir-Schaefer deposition. All samples were taken using a pH6 Milli-Q water sub-phase. Pressure control was set to either 40 mN m^{-1} for calixarene adhesives **11**, **12**, and **22**, or 35 mN m^{-1} for decyl control compounds **14** and **17**. Silicon wafers, rendered hydrophobic by exposure to a hexamethyldisilazane (HMDS) atmosphere at 80 °C for 15 min, were used for all depositions. Hydrophobic wafers were brought into contact with the trough surface using a dipper arm (Dipper Mechanism, Type: D1L, NIMA Technology) with a speed of 35 mm min^{-1} and withdrawn with the same speed. The samples were dried using a stream of compressed air. Additional samples were also either post-baked in an oven at 100 °C for 15 min or sonicated in Milli-Q water for 15 min and dried using a stream of compressed air.

The thickness of the deposited materials was determined using spectroscopic ellipsometry (M-2000V Rotating Compensator Ellipsometer, J. A. Woollam Co.). The data were fitted using a B-Spline model for the polymer with a silicon substrate (CompleteEASE software). The total thickness of the native oxide + HMDS coating was 1.5 ± 0.1 nm. The results are summarised in Figure 4.7.

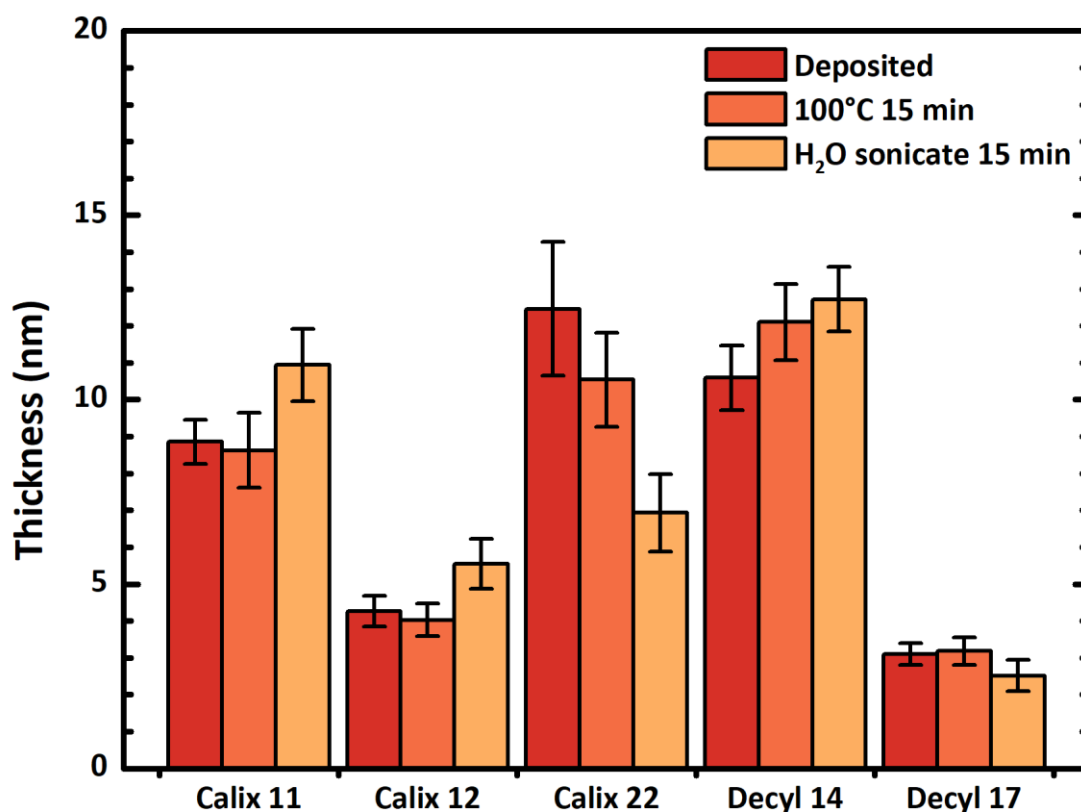


Figure 4.7: Thicknesses of material deposited by Langmuir-Schaefer. All samples were taken using a pH6 Milli-Q water sub-phase. Pressure control was set to either 40 mN m^{-1} for calixarene adhesives **11**, **12**, and **22**, or 35 mN m^{-1} for decyl control compounds **14** and **17**. All samples were deposited onto hydrophobic silicon wafers. Samples were measured as deposited, after being post-baked at 100°C for 15 min, or after being sonicated in Milli-Q water for 15 min.

Figure 4.7 shows greater thicknesses of material deposited compared to material deposited from solution, with thicknesses $\sim 10 \text{ nm}$ for calixarene adhesives **11** and **22**, and decyl control **14**. The calixarene adhesive **12** has a lower thickness at the same pressure as **11**, as the pressure relates to the compression and orientation of the calixarene in addition to the compression of the polymer, rather than just the compression of the polymer as for **11** and **14**. Similarly, calixarene adhesive **22** has a similar thickness to **11** as, while the pressure is related to the compression of the calixarene, the polymer has a lower radius of gyration (1 nm compared with 2 nm) and so will require less pressure to compress to the same density. The decyl control **17** has a lower thickness than **14** as although the surface has been rendered hydrophobic using HMDS, some surface oxide will remain exposed; which will repel the negative polymer and attract the positive polymer.

Calixarene adhesives **11** and **12**, and decyl-pDMAEMA control **14** showed resistance to the deposition post-treatments. The post-bake had no significant effect upon the thickness, showing that there was no contribution from absorbed water swelling the polymer film, and the water sonication showed the films were resistant to desorption, with the small increase in thickness attributable to swelling from absorbed water. Calixarene-pMAA adhesive **22** showed a greater change with post-treatment. The water sonication showed a reduction in film thickness, indicating a loss of material from the surface. As the polymer has a repulsive interaction with the surface, only the calixarene is anchoring the polymer to the surface. This means the material will be more susceptible to desorption.

The thicknesses and characterisation parameters for the calixarene adhesives **11**, **12**, and **22**, and decyl controls **14** and **17** deposited are listed in Table 4.3. All deposited materials apart from decyl-pMAA **17** have an interchain distance either equal to or less than the radius of gyration of the polymer in solution, and consequently are in a brush or brush-like regime. The reduced tether densities for **12** and **22** indicate that they are in the mushroom to brush transition regime, and the reduced tether densities for **11** and **14** indicate that they are in the ‘true’ brush regime.

A calixarene bowl has a diameter between 1-1.32 nm,¹⁴⁹ and therefore an area of 0.79-1.37 nm², giving a maximum grafting density of 0.73-1.27 nm⁻². Calixarene-pMAA **22** has a grafting density within this maximum grafting density of calixarene, indicating that the calixarene is the limiting factor for this polymer film, rather than the polymer.

Table 4.3: Compounds deposited from solution showing thickness, number of chain units (N), radius of gyration (R_g), grafting density (σ), interchain distance (D), and reduced tether density (Σ). (a) Material as deposited. (b) Deposition pressure of 40 mN m⁻¹. (c) Deposition pressure of 35 mN m⁻¹.

Compound	Thickness (nm) ^a	N	R_g (nm)	σ (nm ⁻²)	D (nm)	Σ
Boc-calix-pDMAEMA 11 ^b	8.9 ± 0.6	82	2	0.55 ± 0.04	1.35 ± 0.03	6.9 ± 0.5
Calix-pDMAEMA 12 ^b	4.3 ± 0.4	82	2	0.27 ± 0.03	1.92 ± 0.05	3.4 ± 0.3
Calix-pMAA 22 ^b	12 ± 2	85	1	1.1 ± 0.2	0.95 ± 0.07	3.1 ± 0.5
Decyl-pDMAEMA 14 ^c	10.6 ± 0.9	82	2	0.64 ± 0.05	1.25 ± 0.04	8.0 ± 0.7
Decyl-pMAA 17 ^c	3.0 ± 0.3	85	1	0.28 ± 0.03	1.89 ± 0.05	0.79 ± 0.07

To investigate the effect of increasing the pressure for calixarene adhesive **12** closer to the maximum pressure plateau region shown in the isotherm, samples were taken at pH6 and a pressure of 45 mN m^{-1} . The results are summarised in Table 4.4. The increase in pressure resulted in an increase to a thickness similar to calixarene adhesives **11** and **22**. The reduced tether density also increased, showing a shift from the mushroom-to-brush transition regime to the ‘true’ brush regime.

Table 4.4: Compounds deposited from solution showing thickness, number of chain units (N), radius of gyration (R_g), grafting density (σ), interchain distance (D), and reduced tether density (Σ). (a) Material as deposited. (b) Deposition pressure of 40 mN m^{-1} . (c) Deposition pressure of 45 mN m^{-1} .

Compound	Thickness (nm) ^a	N	R_g (nm)	σ (nm ⁻²)	D (nm)	Σ
Calix-pDMAEMA 12 ^b	4.3 ± 0.4	82	2	0.27 ± 0.03	1.92 ± 0.05	3.4 ± 0.3
Calix-pDMAEMA 12 ^c	9.7 ± 0.5	82	2	0.60 ± 0.03	1.29 ± 0.03	7.5 ± 0.4

Use of a Langmuir trough to deposit calixarene adhesives **11**, **12**, and **22**, and the decyl controls **14** and **17** resulted in polymer films with high grafting densities and films in the mushroom to brush transition or ‘true’ brush regimes. Decyl-pMAA **17** was the only material in the ‘mushroom’ weakly interacting regime. The deposited films were resistant to post-treatment with only calixarene-pMAA **22** showing a decrease in film thickness with sonication in water.

4.4. AFM imaging of deposited brushes

The surface roughness and topography of the deposited materials were determined using Atomic Force Microscopy (Asylum MFP-3D AFM, Bruker). Images were taken in contact mode over a $5 \mu\text{m}$ square area with a resolution of 256×256 points.

The images for the HMDS treated wafers are shown in Figure 4.8. The surface has numerous regular features, rather than a smooth continuum. These features have an average diameter of $190 \pm 10 \text{ nm}$, and an average height of $4.6 \pm 0.8 \text{ nm}$. This leads to the observed surface roughness of $R_a = 0.88 \pm 0.05 \text{ nm}$. These features are attributed to a build-up of the HMDS silanizing agent on the surface, potentially leaving areas of relatively exposed silicon between them. However, the overall effect of the HMDS treatment rendered the wafers hydrophobic, as determined by contact angle goniometry ($\theta \geq 90^\circ$).

The formation of these features could be due to the method used to treat the wafers: the wafers are placed in a sealed vessel with HMDS at atmospheric pressure and heated. Other techniques for the deposition of HMDS involve introduction of a HMDS vapour to the heated sample at reduced pressure, leading to greater control over the deposition. This method was not available, so deposition under atmospheric conditions was used instead.

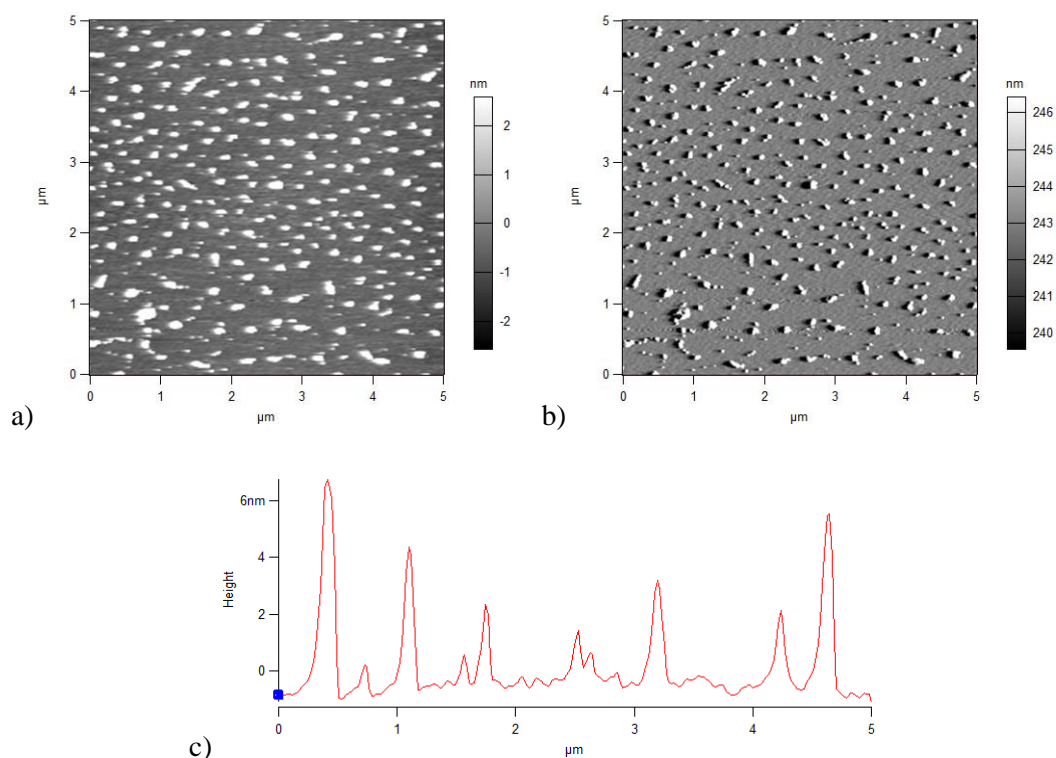


Figure 4.8: AFM images of HMDS treated wafers. a) Height retrace, b) Deflection retrace, c) Cross-section showing feature heights.

The images for the Boc-calix-pDMAEMA **11** surfaces are shown in Figure 4.9, Figure 4.10, and Figure 4.11. The numerous features from the HMDS coating have been almost completely masked by the deposited brush. The upper annulus of the calixarene is capped with *tert*-butoxycarbonyl, increasing the hydrophobicity of the head group, allowing the calixarene to adhere to the HMDS features in addition to the wafer surface. This is shown across all three surface post treatments, and is reflected in the low surface roughness for the films (Table 4.5). The two post-treated films show a slight increase in the surface roughness, indicating that there may be some small degree of reorganisation under these conditions, or that the increased handling has led to a small increase in surface contamination.

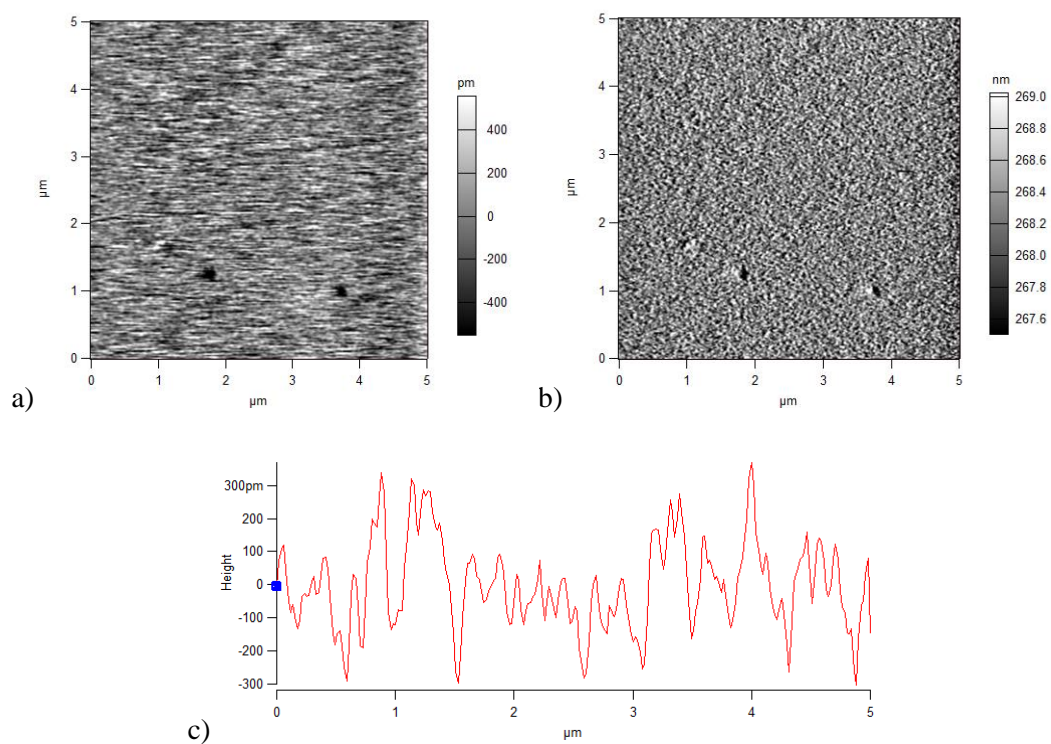


Figure 4.9: AFM images of deposited Boc-calix-pDMAEMA **11**. a) Height retrace, b) Deflection retrace, c) Cross-section showing surface roughness.

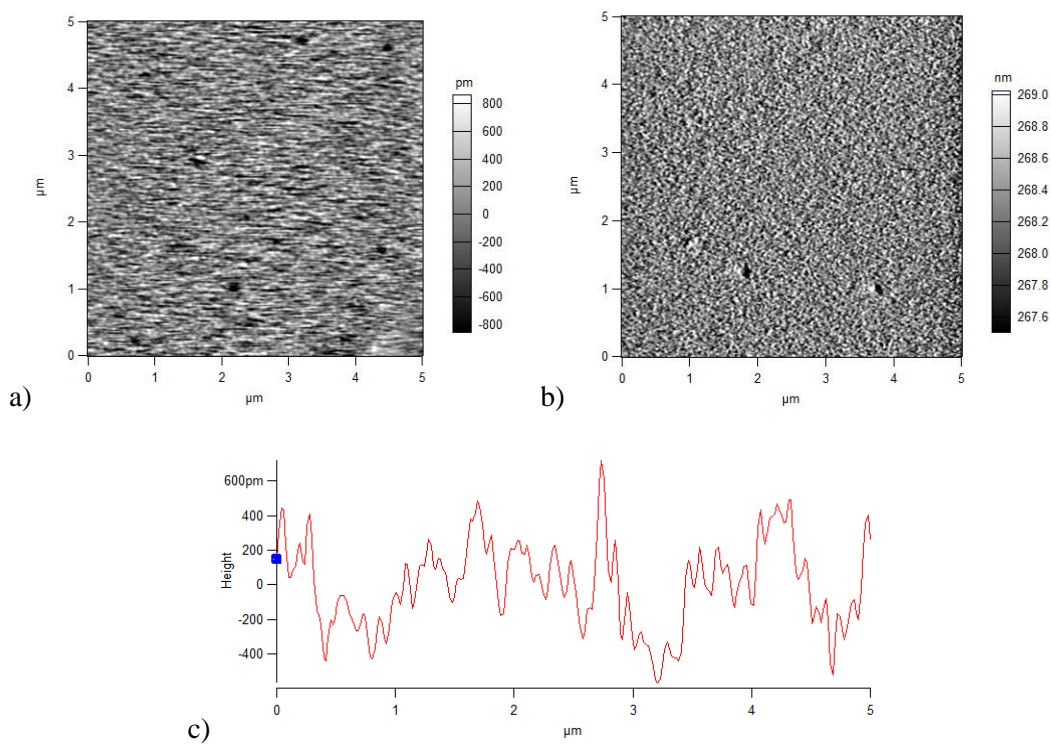


Figure 4.10: AFM images of post-baked Boc-calix-pDMAEMA **11**. a) Height retrace, b) Deflection retrace, c) Cross-section showing surface roughness.

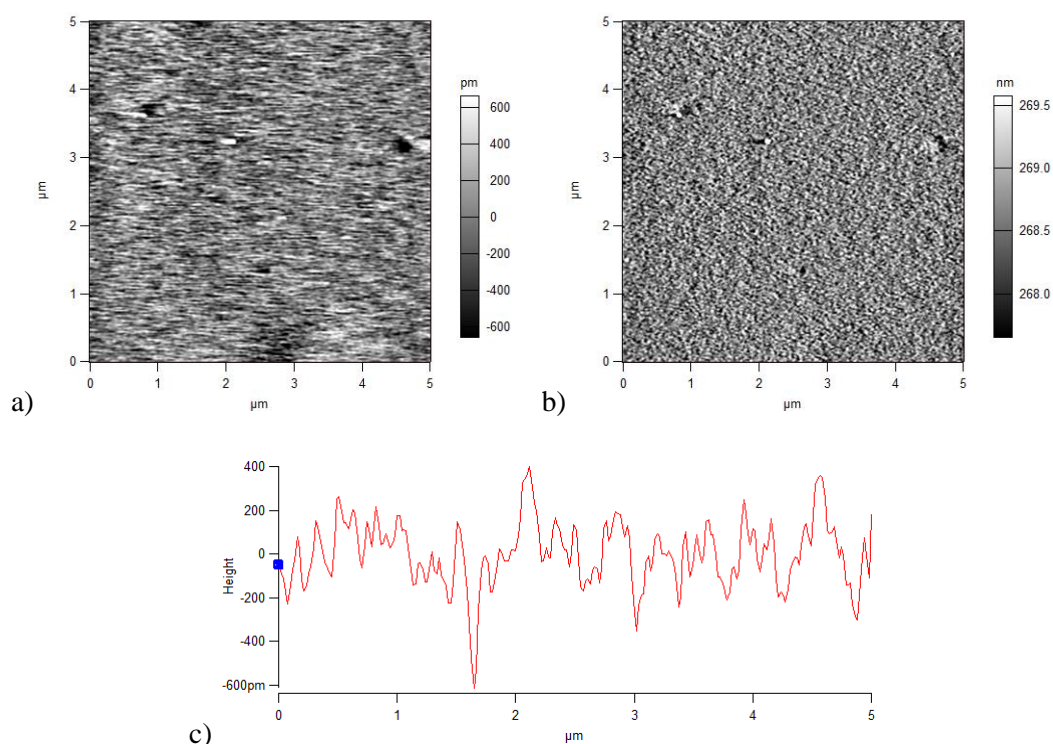


Figure 4.11: AFM images of water sonicated Boc-calix-pDMAEMA **11**. a) Height retrace, b) Deflection retrace, c) Cross-section showing surface roughness.

Table 4.5: Surface roughness of Boc-calix-pDMAEMA **11** films.

Compound	Post-treatment	R_a (nm)
Boc-calix-pDMAEMA 11	Deposited	0.26 ± 0.03
	100°C	0.31 ± 0.01
	H ₂ O	0.38 ± 0.07

The images for the calix-pDMAEMA **12** surfaces are shown in Figure 4.12, Figure 4.13, and Figure 4.14. The numerous features from the HMDS coating are translated to the brush surface as a series of ‘holes’ in the surface topography. This is supported by the similarity in the diameter of these features in the brush layer to those of the HMDS features (Table 4.6).

The upper annulus of the calixarene has free phenolic residues, making the head group more hydrophilic. This increased hydrophilicity would reduce the ability of the head group to adhere to the HMDS features, and promote adhesion to the wafer surface, leading to the brush preferentially ‘back-filling’ the area between the HMDS features. As the brush height is much smaller than the feature size (4.3 ± 0.4 vs 190 ± 10 nm), the features appear as voids in the brush layer, as the conformation of the brushes cannot sufficiently adjust to accommodate the features, and this is reflected in the overall surface roughness (Table 4.6).

The post-bake treatment (Figure 4.13) resulted in an increase in height around the voids, leading to a ring-like build up around each void. This is also accompanied by an increase in the average void diameter and surface roughness (Table 4.6). This may be the result of the brush material re-organising, and shifting away from the more hydrophobic regions, resulting in a build-up of material around these features.

The water sonication (Figure 4.14) resulted in an overall reduction in surface roughness and void depth, and an increase in the average void diameter (Table 4.6). This may also be the result of brush re-organisation, but under these conditions the brush re-organises to partially fill the voids.

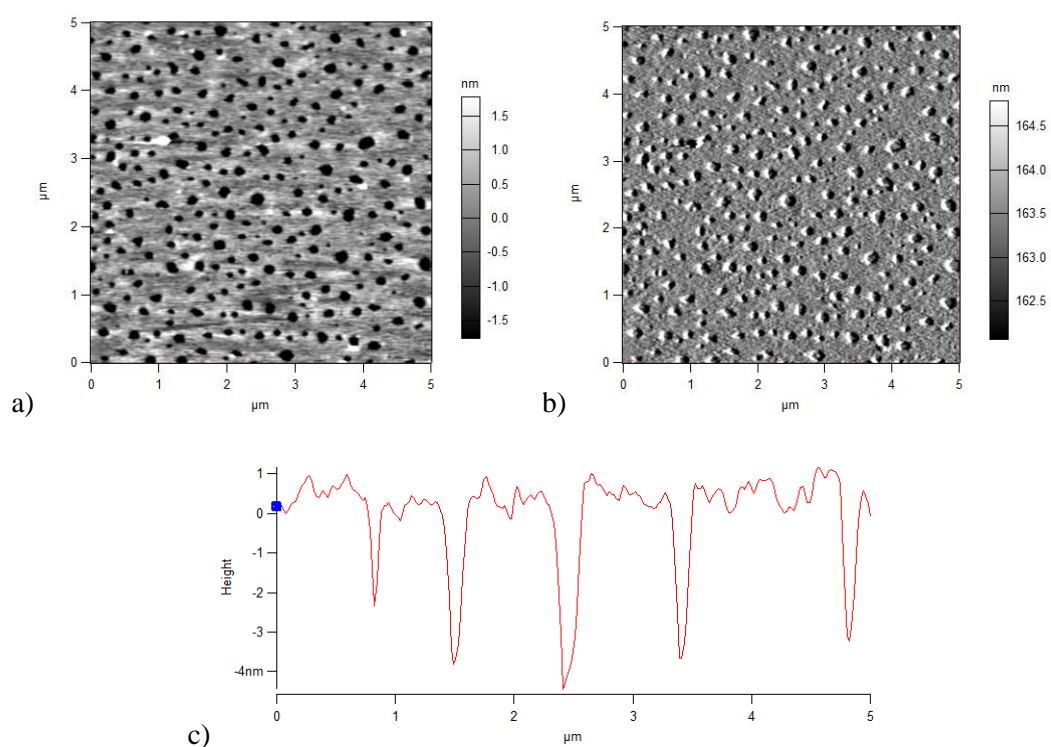


Figure 4.12: AFM images of deposited calix-pDMAEMA **12**. a) Height retrace, b) Deflection retrace, c) Cross-section showing surface roughness and feature depth.

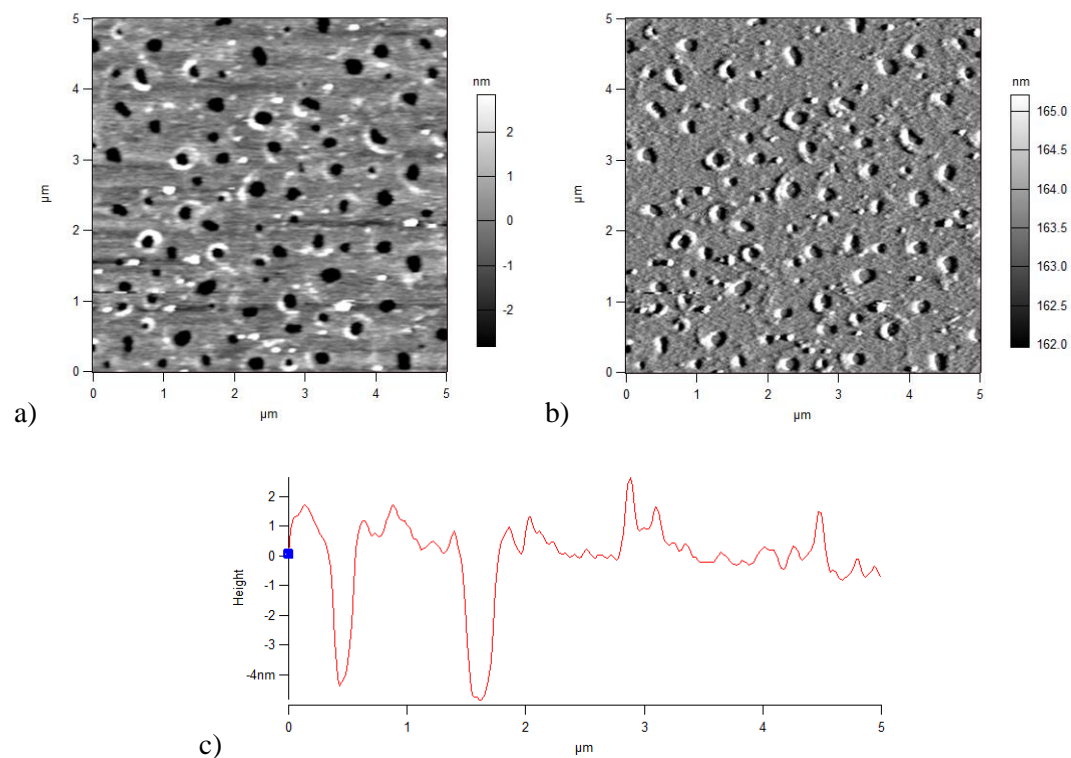


Figure 4.13: AFM images of post-baked calix-pDMAEMA **12**. a) Height retrace, b) Deflection retrace, c) Cross-section showing surface roughness and feature depth.

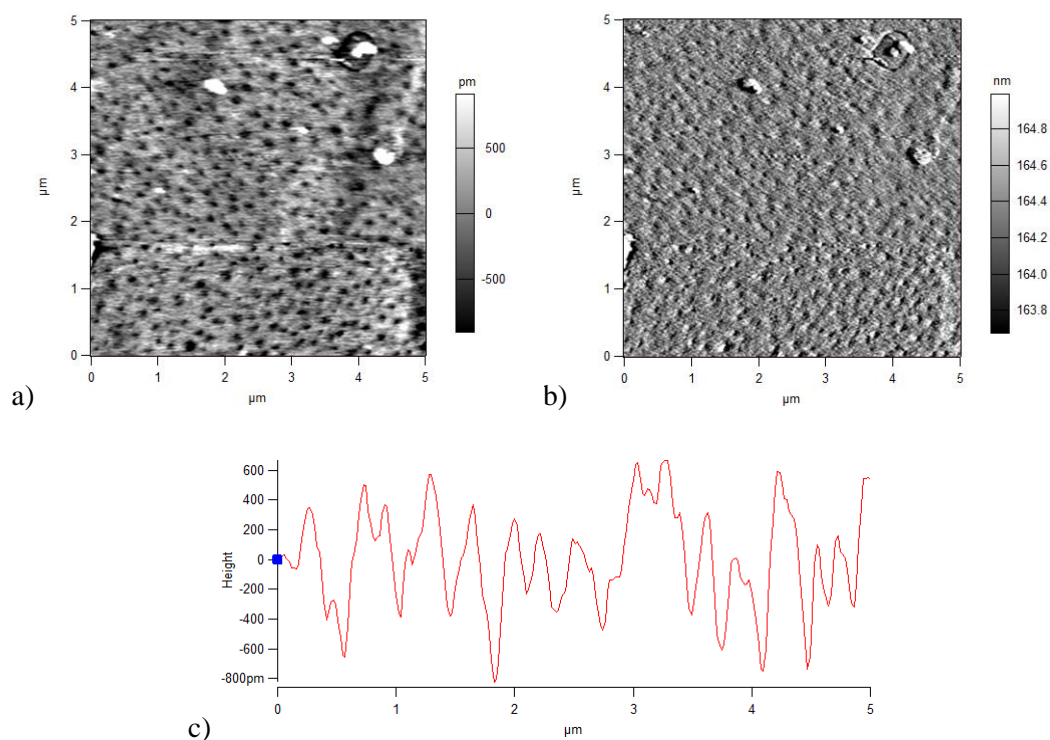


Figure 4.14: AFM images of water sonicated calix-pDMAEMA **12**. a) Height retrace, b) Deflection retrace, c) Cross-section showing surface roughness and feature depth.

Table 4.6: Surface roughness and feature dimensions of calix-pDMAEMA **12** films.

Compound	Post-treatment	R_a (nm)	Features	
			Diameter (nm)	Depth (nm)
calix-pDMAEMA 12	Deposited	0.72 ± 0.07	210 ± 20	4.0 ± 0.5
	100 °C	0.77 ± 0.02	300 ± 30	4.8 ± 0.3
	H ₂ O	0.41 ± 0.05	270 ± 40	0.8 ± 0.1

The images for the decyl-pDMAEMA **14** surfaces are shown in Figure 4.15, Figure 4.16, and Figure 4.17. There are a number of large voids in the brush layer. The size of these voids (550 ± 70 nm, Table 4.7) are much larger than the HMDS features, indicating that they are not caused by the HMDS features. They are most likely caused by film defects formed during the Langmuir compression, which is reflected in the irregular shape of the Langmuir isotherm at high compression (Figure 4.4). The smaller voids are more likely to be the result of the HMDS features.

The post-bake treatment (Figure 4.16) resulted in an overall reduction in the size of the larger voids. There was also a large build-up of material around these voids (Figure 4.16c), similar to calix-pDMAEMA **12**, but to a much larger extent (Table 4.7). This may be the result of the brush material re-organising, partially filling a film defect, but not filling it completely due to the presence of HMDS features. There is also a reduction in the overall surface roughness (Table 4.7).

The water sonication (Figure 4.17) also resulted in a reduction in the size of the larger voids (Table 4.7), but this reduction is much less than that observed for the post-bake treatment, with a number of large voids remaining. This is also reflected in the larger surface roughness (Table 4.7).

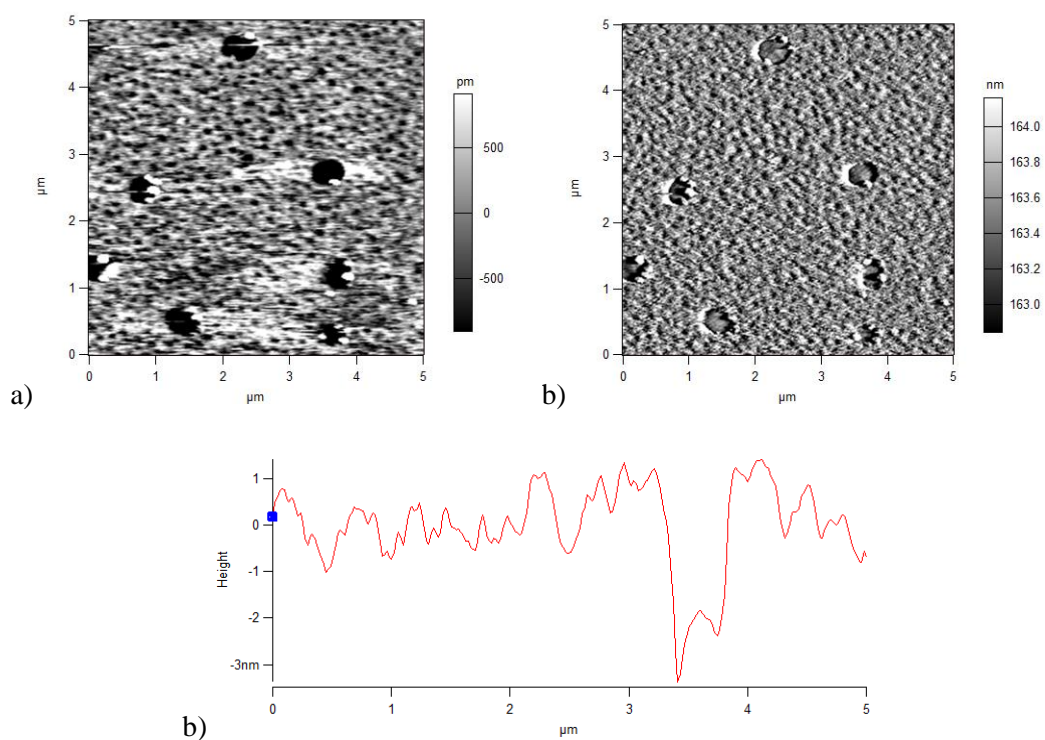


Figure 4.15: AFM images of deposited decyl-pDMAEMA **14**. a) Height retrace, b) Deflection retrace, c) Cross-section showing surface roughness and feature depth.

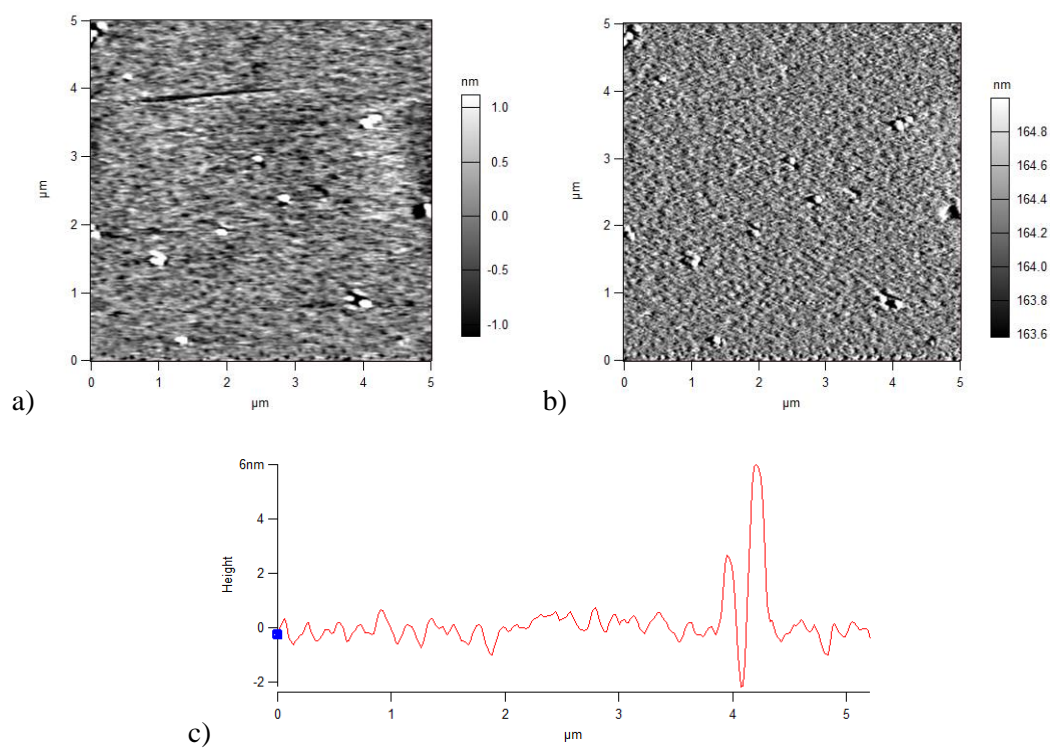


Figure 4.16: AFM images of post-baked decyl-pDMAEMA **14**. a) Height retrace, b) Deflection retrace, c) Cross-section showing surface roughness and feature size.

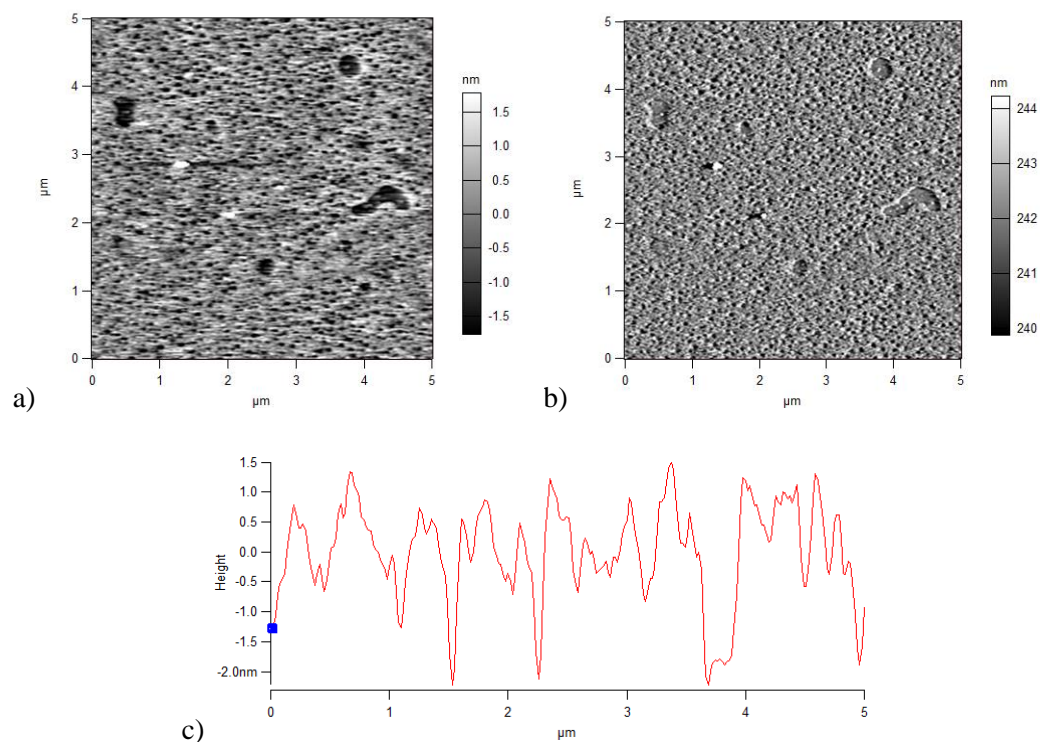


Figure 4.17: AFM images of water sonicated decyl-pDMAEMA **14**. a) Height retrace, b) Deflection retrace, c) Cross-section showing surface roughness and feature depth.

Table 4.7: Surface roughness and feature dimensions of decyl-pDMAEMA **14** films.

Compound	Post-treatment	R_a (nm)	Features		
			Diameter (nm)	Depth (nm)	Height (nm)
decyl-pDMAEMA 14	Deposited	0.49 ± 0.01	550 ± 70	2.8 ± 0.5	-
	100 °C	0.36 ± 0.01	210 ± 10	-	4.0 ± 0.8
	H ₂ O	0.64 ± 0.02	190 ± 20	2.0 ± 0.2	-

The images for the calix-pMAA **22** surfaces are shown in Figure 4.18, Figure 4.19, and Figure 4.20. In addition to the small voids related to the HMDS features, there are a number of larger irregular voids, similar to those observed for decyl-pDMAEMA **14**. These also show a build-up of material around the edge of these larger voids, and may also be due to film defects formed during the Langmuir compression, or defects formed upon deposition, as the Langmuir isotherm was relatively stable at high compression (Figure 4.5).

The post-bake treatment (Figure 4.19) resulted in a large increase in the surface roughness (Table 4.8), and the number of larger voids observed. This could be due to the brush film collapsing away from the voids, both from HMDS and film defects, resulting in the observed thickness decrease (Figure 4.7). However, the water sonication (Figure 4.20) resulted in an overall reduction in surface roughness (Table 4.8), and the disappearance of the voids. This may also be the result of brush re-organisation, but under these conditions the brush re-organises to partially fill the voids in a similar fashion to calix-pDMAEMA **12** (Figure 4.14), also resulting in an observed thickness decrease (Figure 4.7).

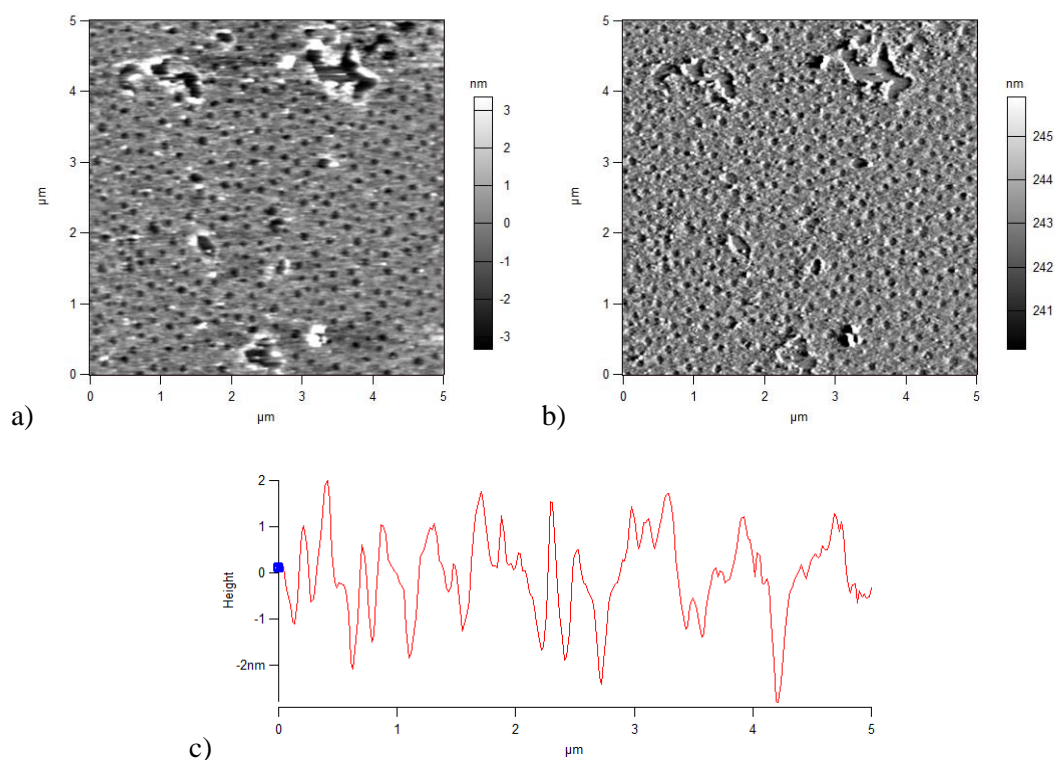


Figure 4.18: AFM images of deposited calix-pMAA **22**. a) Height retrace, b) Deflection retrace, c) Cross-section showing surface roughness and feature depth.

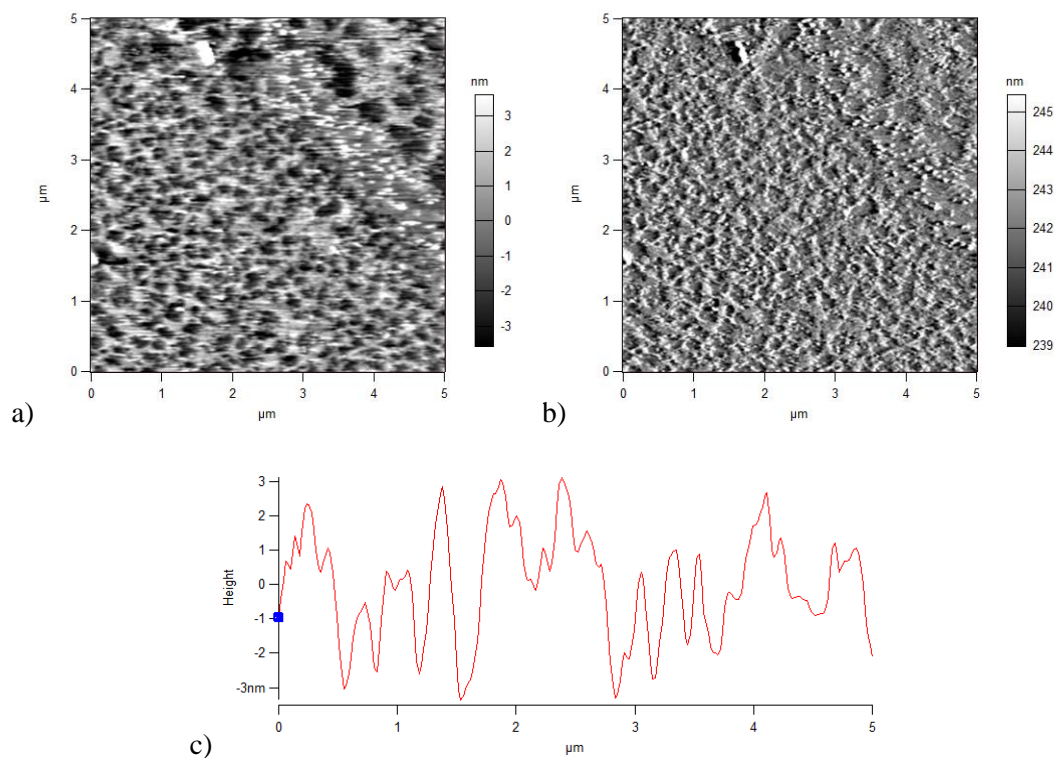


Figure 4.19: AFM images of post-baked calix-pMAA **22**. a) Height retrace, b) Deflection retrace, c) Cross-section showing surface roughness and feature depth.

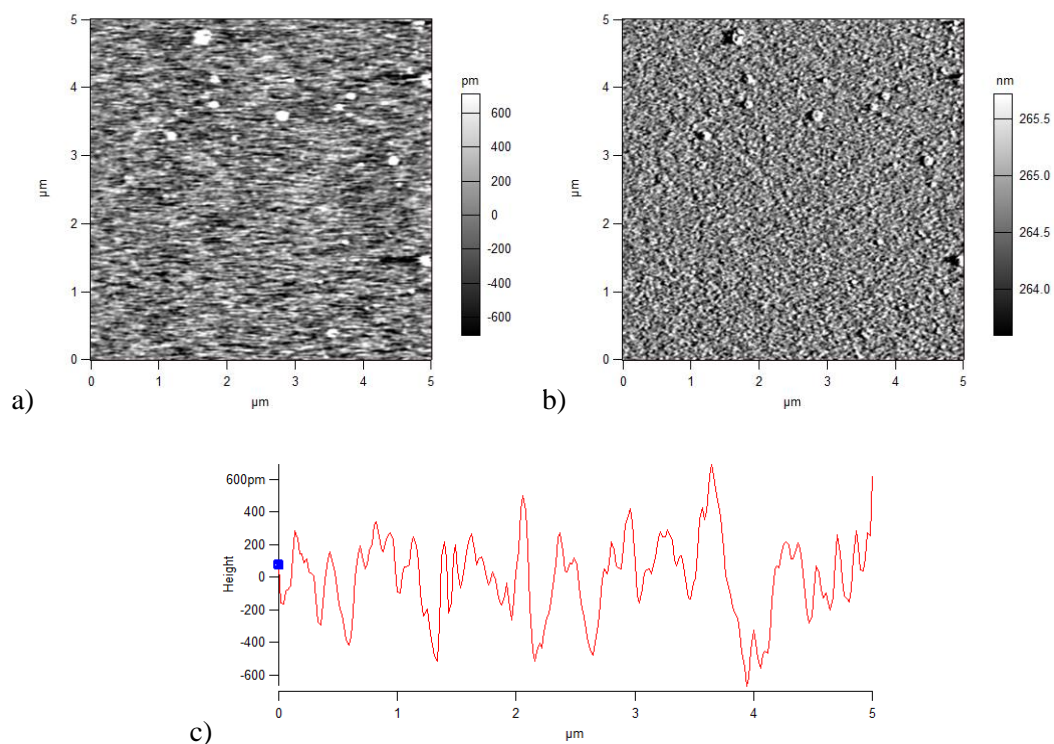


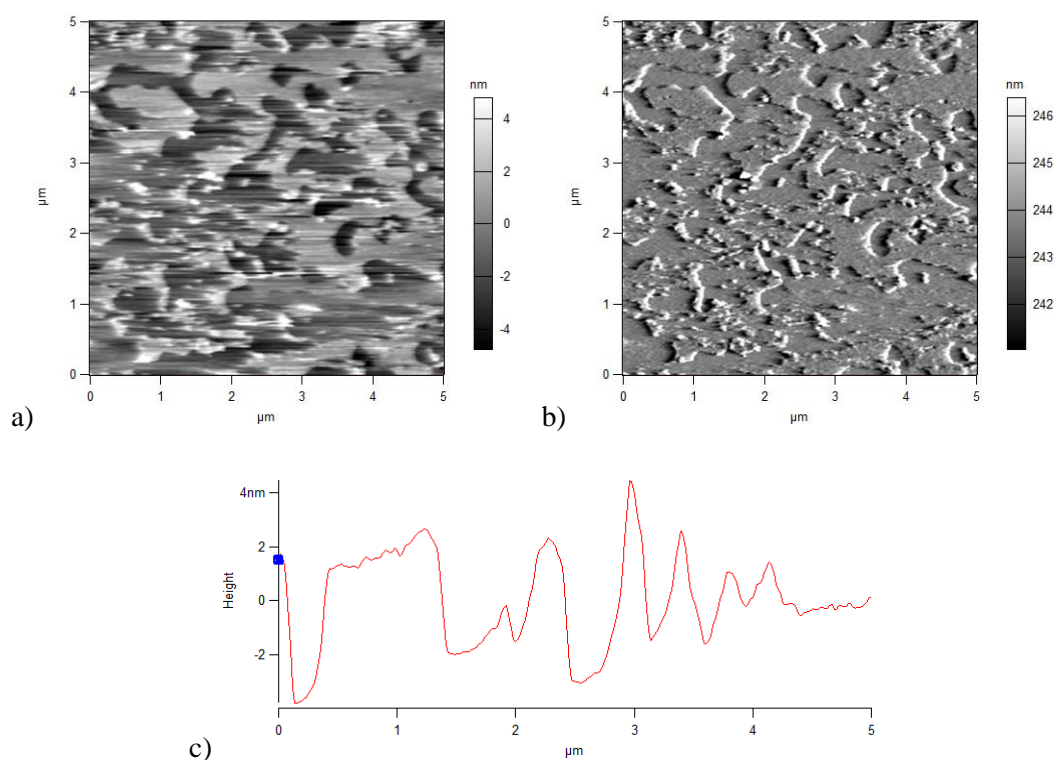
Figure 4.20: AFM images of water sonicated calix-pMAA **22**. a) Height retrace, b) Deflection retrace, c) Cross-section showing surface roughness.

Table 4.8: Surface roughness and feature dimensions of calix-pMAA **22** films.

Compound	Post-treatment	R_a (nm)	Features	
			Diameter (nm)	Depth (nm)
calix-pMAA 22	Deposited	0.6 ± 0.1	165 ± 5	4.0 ± 0.5
	100 °C	1.2 ± 0.1	280 ± 50	4.8 ± 0.3
	H ₂ O	0.40 ± 0.07	-	-

The images for the decyl-pMAA **17** surfaces are shown in Figure 4.21, Figure 4.22, and Figure 4.23. The overall coverage of these films is low, with large areas left uncovered, resulting in the large surface roughness (Table 4.9). This is reflected in the reduced tether density (Table 4.3) and overall film thickness (Figure 4.7). This is most likely caused by film defects formed during the Langmuir compression.

Although both post treatments result in changes to the film topography (Figure 4.22 and Figure 4.23), the surface roughness remains high, with the post-baked treatment yielding the largest reduction in surface roughness. This is most likely due to re-organisation of the film under these conditions.

**Figure 4.21:** AFM images of deposited decyl-pMAA **17**. a) Height retrace, b) Deflection retrace, c) Cross-section showing surface roughness and feature depth.

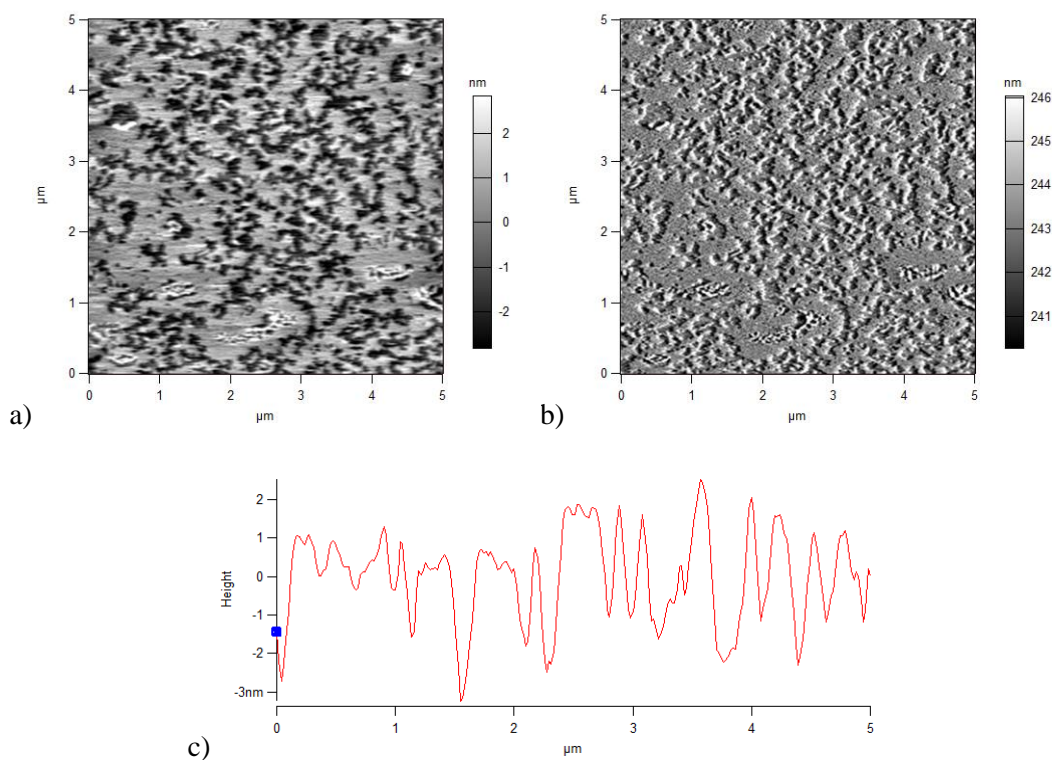


Figure 4.22: AFM images of post-baked decyl-pMAA **17**. a) Height retrace, b) Deflection retrace, c) Cross-section showing surface roughness.

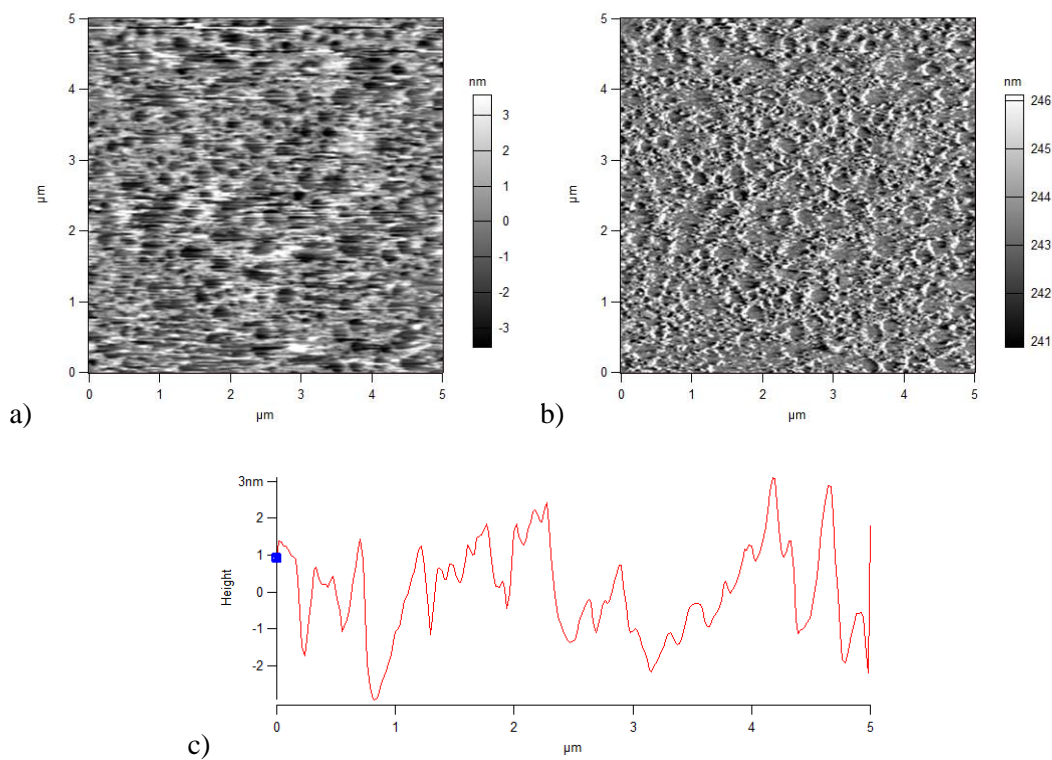


Figure 4.23: AFM images of water sonicated decyl-pMAA **17**. a) Height retrace, b) Deflection retrace, c) Cross-section showing surface roughness.

Table 4.9: Surface roughness and feature dimensions of decyl-pMAA **17** films.

Compound	Post-treatment	R_a (nm)	Features	
			Diameter (nm)	Depth (nm)
decyl-pMAA 17	Deposited	1.64 ± 0.07	-	-
	100 °C	1.15 ± 0.02	230 ± 40	2.9 ± 0.3
	H ₂ O	1.34 ± 0.06	320 ± 30	2.9 ± 0.4

4.5. Spin-coating of PVAc films

In addition to the two decyl control polymers, thin films of poly(vinyl acetate) (PVAc) were prepared by spin coating from toluene to provide films of similar thickness to the deposited calixarene adhesives. This allows a comparison between the effect of the polyelectrolyte brush on adhesion, and that of a more traditional adhesive. Films were spin coated at low (1750 rpm) and high (4500 rpm) speeds to provide two different film thickness using the same stock solution.

The final spin coated film thickness (h_f) can be predicted using²³³

$$h_f = (1 - x_1^0)h_w \quad (4.5)$$

where x_1^0 is the initial solvent mass fraction in the coating solution, and h_w is the wet film thickness. The wet film thickness (h_w) can be calculated using²³³

$$h_w = \left[\left(\frac{3\eta_0}{2\rho\omega^2} \right) k_m (x_1^0 - x_{1\infty}) \right]^{1/3} \quad (4.6)$$

where η_0 is the initial solution viscosity, ρ is the liquid density, ω is the spin speed, k_m is the mass transfer coefficient, and $x_{1\infty}$ is the solvent mass fraction that would be in equilibrium with the solvent mass fraction in the gas phase. The mass transfer coefficient (k_m) is given by²³³

$$k_m = \left(\frac{cD_g}{v_g^{1/2}\rho} \right) \left(\frac{p_1^0 M_1}{RT} \right) \omega^{1/2} \quad (4.7)$$

where c is a constant that depends on the Schmidt number of the overhead gas phase, D_g is the binary diffusivity of the solvent in the overhead gas phase, v_g is the kinematic viscosity of the overhead gas phase, p_1^0 is the vapour pressure of the pure solvent at temperature T , M_1 is the solvent molecular weight, and R is the ideal gas constant.

The values used for the PVAc-toluene system were:²³³ $T = 298$ K, $x_{1\infty} = 0$, $R = 82.06$ atm cm³ mol⁻¹ K⁻¹, $v_g = 0.1553$ cm² s⁻¹, $c = 0.5474$ ²³⁴, $\rho = 0.87$ g cm⁻³, $M_1 = 92$ g mol⁻¹, and $D_g = 0.086$ cm² s⁻¹. The vapour pressure of the pure solvent at 298 K (p_1^0) was determined using a fit of the data recorded by Besley and Bottomley²³⁵, which gave $p_1^0 = 0.0377$ atm. The spin speed (ω) was either $\omega = 183$ rad s⁻¹ (1750 rpm), or $\omega = 471$ rad s⁻¹ (4500 rpm).

The initial solution viscosity (η_0) can be calculated using^{236,237}

$$\eta_0 = (2\pi RT/V_1^2)^{1/2} M_1^{x_{m1}/2} M_2^{x_{m2}/2} \exp[(a_m + b_m T)/RT] \quad (4.8)$$

where M_2 is the molecular weight of the polymer, x_{m1} is the mole fraction of solvent, x_{m2} is the mole fraction of polymer, V_1 is the molar volume of the solvent, and a_m and b_m are parameters of the mixture. The values used for the PVAc-toluene system were: $M_2 = 50,000$ g mol⁻¹, and $V_1 = 106.3$ ml mol⁻¹. The parameters a_m and b_m can be expressed in terms of the initial polymer concentration (c_0) using²³⁶

$$a_m = a_0 + a_c c_0 \quad (4.9)$$

$$b_m = b_0 + b_c c_0 \quad (4.10)$$

where a_0 and b_0 are parameters for infinite dilution of the polymer in the solvent, and a_c and b_c are the parameters for the initial polymer concentration (c_0). The parameters used for the PVAc-toluene system were:²³⁶ $a_0 = 5,856.70$, $a_c = 10,714.30$, $b_0 = -159.65$, and $b_c = 148.76$.

Using the above equations, it was predicted that an initial polymer concentration of $c_0 = 4.35 \times 10^{-3}$ g ml⁻¹ (87 μ M) would give film thicknesses of $h_f = 19$ nm (1750 rpm) and $h_f = 12$ nm (4500 rpm). A comparison of the predicted vs actual film thickness, as measured by ellipsometry, for these two spin speeds is shown in Figure 4.24. This shows good correlation between the predicted and actual film thickness, and shows that the above models adequately predict the final film thicknesses.

The AFM images for the spin-coated films surfaces are shown in Figure 4.25 and Figure 4.26. The film spin-coated at 1750 rpm is uniform, and the thinner film spin-coated at 4500 rpm shows a degree of pin-holing. This is reflected in the surface roughness of the two films, $R_a = 0.25 \pm 0.01$ nm (1750 rpm) and $R_a = 0.40 \pm 0.01$ nm (4500 rpm).

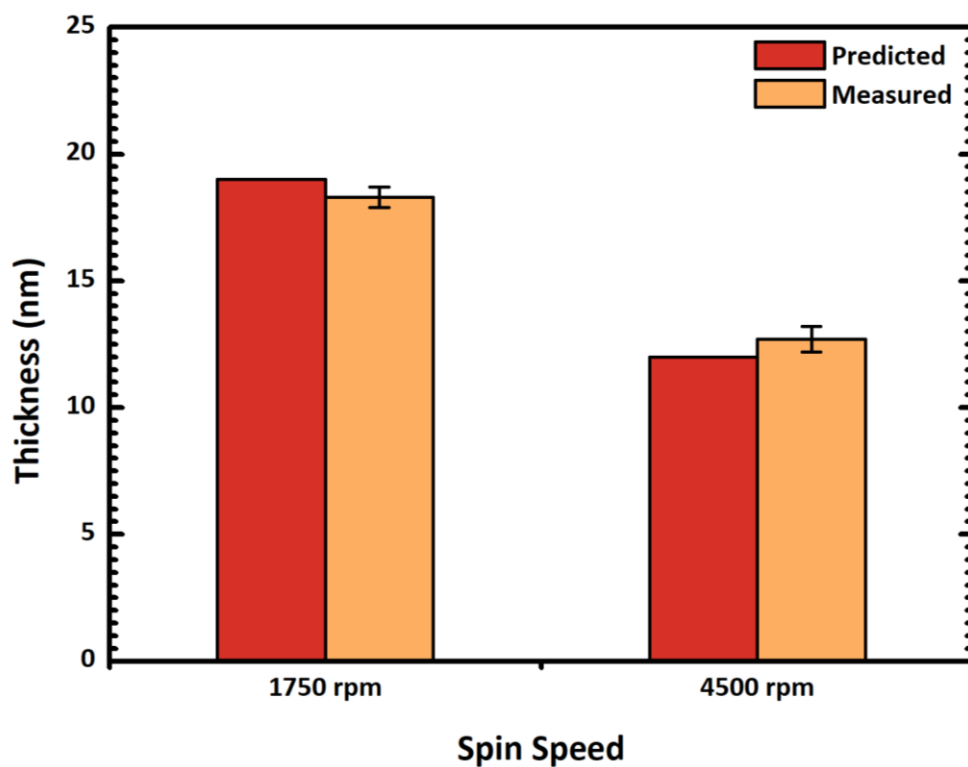


Figure 4.24: Predicted vs measured film thickness at 1750 rpm and 4500 rpm.

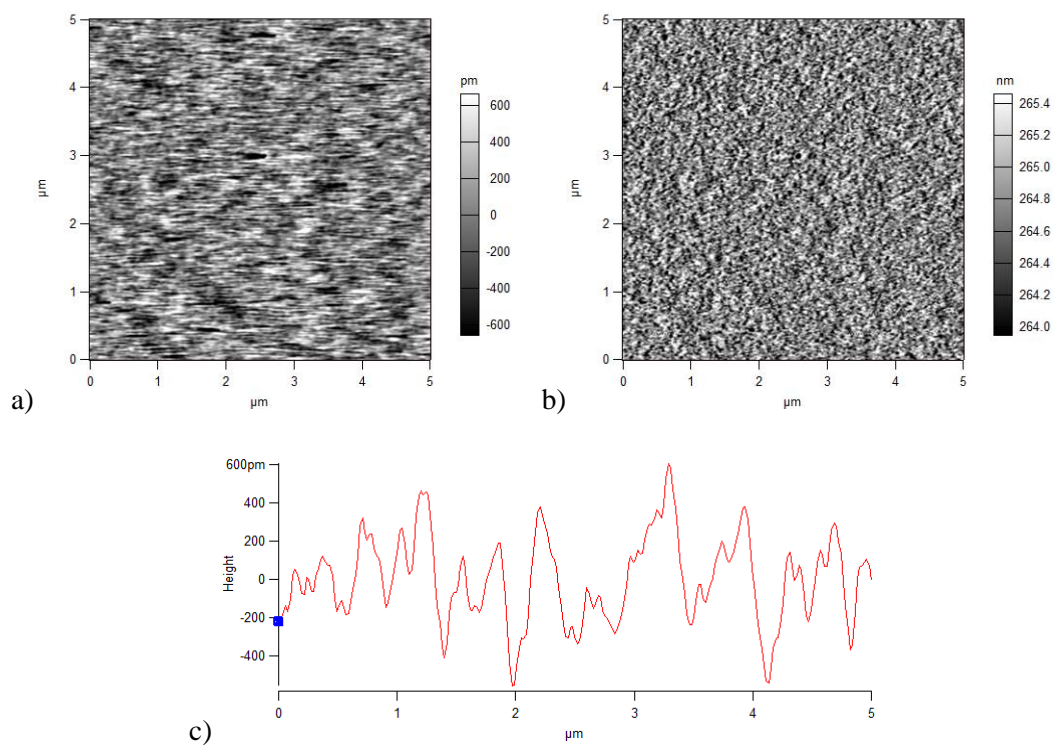


Figure 4.25: AFM images of spin coated films of PVAc at 1750 rpm. a) Height retrace, b) Deflection retrace, c) Cross-section showing surface roughness.

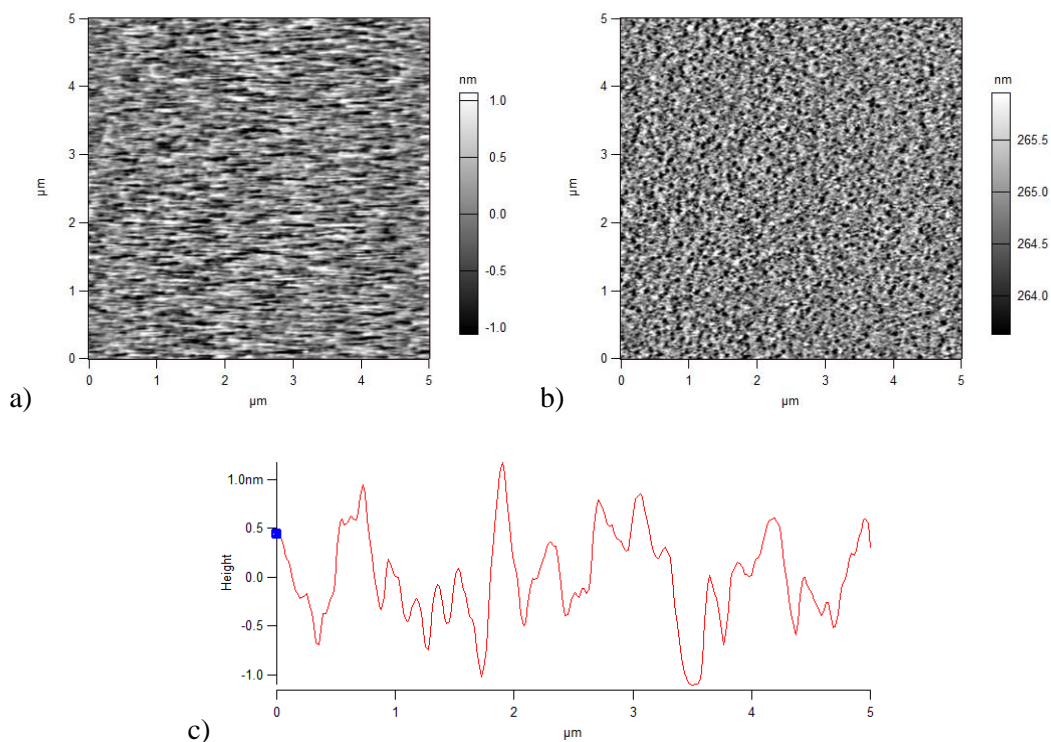


Figure 4.26: AFM images of spin coated films of PVAc at 4500 rpm. a) Height retrace, b) Deflection retrace, c) Cross-section showing surface roughness.

4.6. Summary

In this chapter, monolayers of the calixarene-based adhesives, and the associated control compounds, were prepared using grafting-to methodologies. It was found that self-assembly from solution did not give an adequate grafting density for the required brush or brush-like structures desired. Instead, Langmuir-Schaefer deposition was used to generate films with high grafting densities, generating brush or brush-like films. This overcomes the limitation on the grafting density due to the kinetic and thermodynamic barriers for grafting-to from solution. This deposited brush layer fulfils the second objective, to deposit the adhesives to form an ordered brush monolayer using a physical bond, and successfully answers the first thesis question:

- a) *A calix[4]resorcinarene can be used as a surface active head group for the direct attachment of polyelectrolyte adhesives to surfaces.*

The brushes thus generated were further characterised using AFM, where it was shown that the calixarene functionalised material had a more ordered surface conformation than the decyl functionalised control material. By generating a brush of deposited material, the polyelectrolyte is in a more ordered regime, and will be comparable with the literature ‘grafted-from’ brushes, allowing a more direct comparison of the adhesive behaviours of the two materials. These polymer brushes, or brush-like material, can be assessed for adhesive properties using a mechanical tester equipped with hemispherical hydrogels of the opposite charge.

In addition to the calixarene based material, PVAc films of similar thicknesses were prepared by spin-coating. These were prepared to provide a comparison between the effect of the polyelectrolyte brush on adhesion, and that of a more traditional adhesive under the same test conditions.

5. Adhesion Measurements

5.1. Introduction

This chapter covers the assessment of the adhesive properties of the deposited films and PVAc spin-coated surfaces prepared in the previous chapter using the compounds shown in Figure 4.1. This fulfils the third objective, to evaluate the adhesive strength of the deposited brushes, and compare the strength of the physical bond to the chemical bond used in ‘grafted-from’ brushes. It also allows the second thesis question to be answered:

b) Is the deposited material adhesive? If so, how does it compare to polyelectrolyte adhesives generated using ‘grafted-from’ techniques?

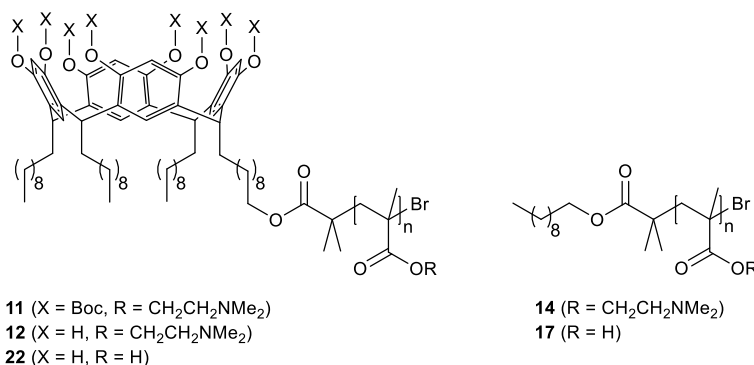


Figure 5.1: Calixarene adhesives **11**, **12**, and **22**, and decyl controls **14** and **17**.

The material was tested for adhesion using a mechanical tester (Texture Analyser TA.XTplus, Stable Microsystems), which brought a hemispherical hydrogel of the opposite charge into contact with the sample surface using a standard protocol. A double network (DN) poly(methacrylic acid)-poly(oligo(ethylene glycol) methyl ether methacrylate) (pMAA-pOEGMA) hydrogel was used for calix[4]resorcinarene adhesives **11** and **12**, and decyl control **14**. A pDEAEMA hydrogel was used for calix[4]resorcinarene adhesive **22** and decyl control **17**. Both hydrogels were used for the PVAc surfaces. The background adhesive properties of the HMDS treated silicon wafers are summarised in Table 5.1.

Table 5.1: Adhesion properties of HMDS treated silicon wafers, where -ve is the DN pMAA-pOEGMA gel, +ve is the pDEAEMA gel, F_a is adhesion force, W is work done, σ_{\max} is stress (max), ε_{\max} is strain (max), W_{deb} is work of debonding, and λ is elastic modulus.

Gel	F_a (N)	W ($\times 10^{-3}$ mJ)	σ_{\max} (kPa)	ε_{\max} (%)	λ (MPa)	W_{deb} (J m $^{-2}$)
-ve	0.04 ± 0.01	1 ± 1	1.9 ± 0.4	1.6 ± 0.2	0.12 ± 0.03	0.05 ± 0.01
+ve	0.06 ± 0.01	1 ± 1	1.6 ± 0.6	1.05 ± 0.04	0.15 ± 0.06	0.04 ± 0.01

5.2. Adhesion force and work done

The adhesion and work done (the energy transferred when the hydrogel is displaced by the adhesive force) for Boc-calixarene-pDMAEMA **11** is shown in Figure 5.2. The Boc-calixarene-pDMAEMA **11** brush shows a strong adhesive response across all samples, with only the water sonication showing a decrease in the measured adhesion force and work done. The adhesion measurements were repeated using the same hydrogel on a different area of the sample, to determine if the adhesion measured was adhesive failure at the gel-brush interface, or failure at the brush-wafer interface. Although there is a small decrease in measured adhesion force, in general the adhesion is repeatable. This indicates that the adhesion force measured is predominately adhesive failure at the gel-brush interface.

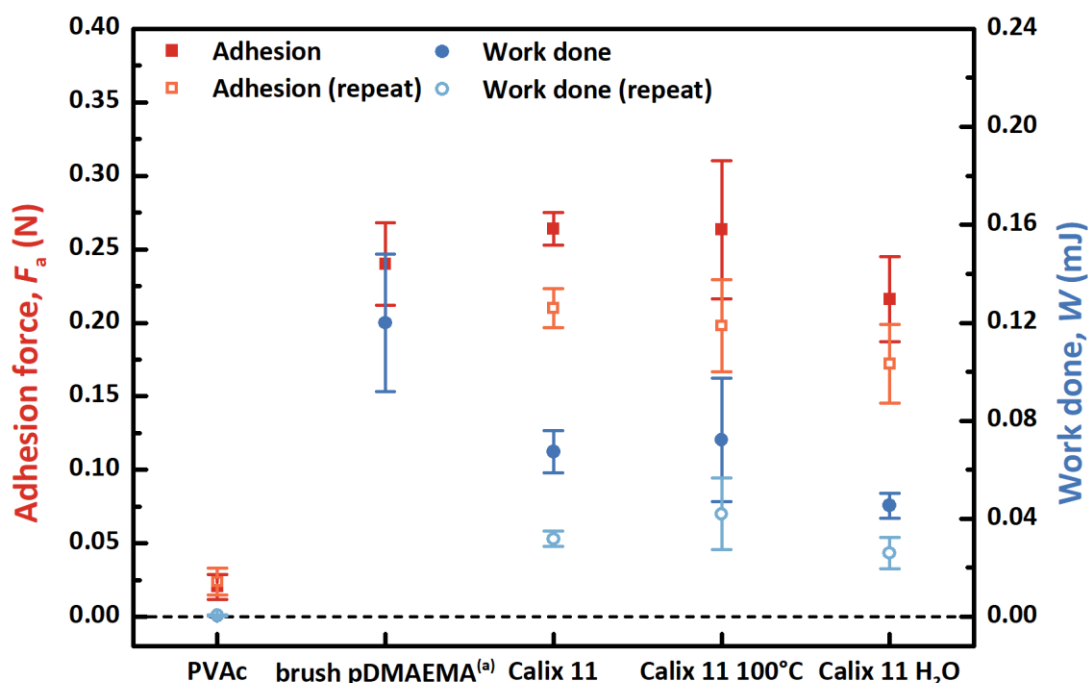


Figure 5.2: Adhesion and work done of Boc-calixarene-pDMAEMA **11**. Material was deposited at 40 mN m^{-1} , and measurements were conducted in pH6 Milli-Q water using DN pMAA-pOEGMA hydrogel. Applied load = 0.5 N, contact time = 2 min, pre- and post-test speed = 50 mm min^{-1} . a) Data for grafted-from pDMAEMA brush from Alfhaid et al.³³

The adhesion of the brush compares favourably with the previously reported grafted-from brush under the same experimental conditions for measuring adhesion, with all three surfaces giving a similar value for adhesion within the reported margin of error.³³ However, the work done is lower than for the grafted-from brush, so the adhesion acts over a shorter distance, and less energy is required to separate the gel from the brush. This, in part, may be due to the shorter length of the deposited brushes (Calix **11** = 8.9 ± 0.6 nm, grafted-from brush = 70-80 nm³³), as this affects the degree of interdigitation into the hydrogel, and the overall strength of the adhesive bond.³⁴

The adhesive force and work done for Boc-calixarene-pDMAEMA **11** is also much larger than those of the spin-coated PVAc surface under the same test conditions. This shows that it is the presence of the polyelectrolyte brush, and the electrostatic interactions with the polyelectrolyte gel, that is causing the adhesion, rather than the presence of a polymer film.

The adhesion and work done for calixarene-pDMAEMA **12** is shown in Figure 5.3. Calixarene-pDMAEMA **12** also shows a strong adhesive response, with an adhesion force for the deposited material similar to that for Boc-calixarene-pDMAEMA **11**, yet the post-baked and sonicated samples both show a decrease in measured adhesion force and work done, which is smaller than both of the values for Boc-calixarene-pDMAEMA **11**. Despite showing a similar adhesion force for the deposited material, the work done for calixarene-pDMAEMA **12** deposited material is noticeably smaller than for the Boc-calixarene-pDMAEMA **11** deposited material. This trend is continued with both of the post-treatment surfaces as well.

The reduction in performance for calixarene-pDMAEMA **12** is probably due to the thinner film thickness for the calixarene-pDMAEMA **12** surfaces, as well as the lack of binding to the HMDS surface features, as observed by AFM. The observed change in the surface topography in the post-treated samples may also be contributing to the reduced adhesion for these surfaces, potentially due to the re-organisation of the brush.

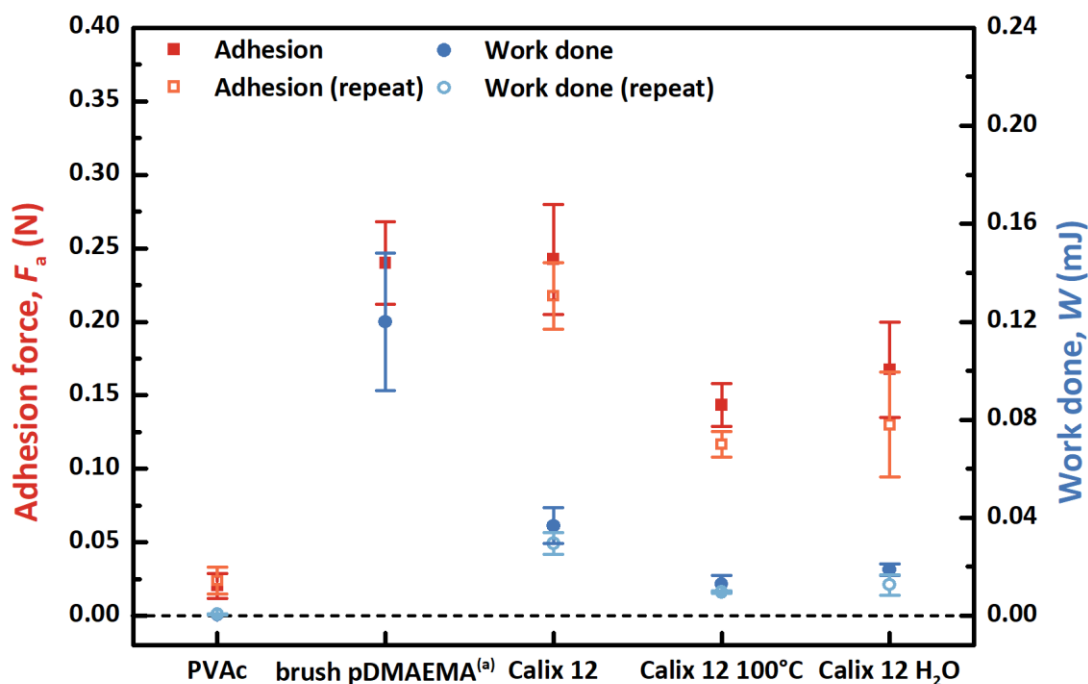


Figure 5.3: Adhesion and work done of calixarene-pDMAEMA **12**. Material was deposited at 40 mN m^{-1} , and measurements were conducted in pH6 Milli-Q water using DN pMAA-pOEGMA hydrogel. Applied load = 0.5 N, contact time = 2 min, pre- and post-test speed = 50 mm min^{-1} . a) Data for grafted-from pDMAEMA brush from Alfahid et al.³³

In the repeat adhesion measurements calixarene-pDMAEMA **12** also shows a small decrease in the repeat adhesion measured using the same hydrogel, as shown for Boc-calixarene-pDMAEMA **11**, thereby also showing that the adhesion measured is predominately adhesive failure at the gel-brush interface. The adhesion of the deposited material compares favourably with the previously reported grafted-from brush, however, the two post-treated surfaces do not. Despite the overall reduction in performance compared to Boc-calixarene-pDMAEMA **11**, and by extension the literature brushes, all three deposited surfaces still had a higher adhesive force and work done than the PVAc surface, showing that the adhesion is also the result of the polyelectrolyte brush in this case as well.

The adhesion force and work done for decyl-pDMAEMA **14** is shown in Figure 5.4. Decyl-pDMAEMA **14** shows a much smaller adhesion force and work done than both of the calixarene adhesives **11** and **12**, despite having a similar thickness. This indicates that the polymer is not strongly adhered to the surface and is more likely to be removed by the hydrogel, or perhaps pushed away from the adhesion site. The presence of the large film defects observed by AFM are also likely to be contributing to the reduced adhesion, as there is less material to interact with per unit area.

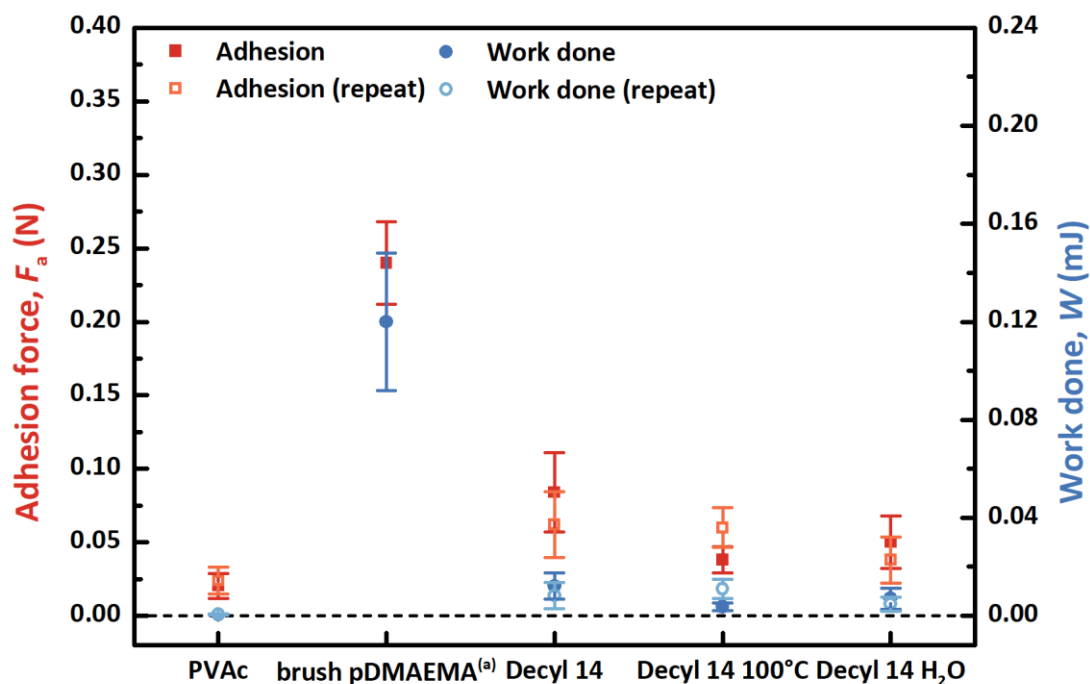


Figure 5.4: Adhesion and work done of decyl-pDMAEMA **14**. Material was deposited at 35 mN m^{-1} , and measurements were conducted in pH6 Milli-Q water using DN pMAA-pOEGMA hydrogel. Applied load = 0.5 N, contact time = 2 min, pre- and post-test speed = 50 mm min^{-1} . a) Data for grafted-from pDMAEMA brush from Alfhaid et al.³³

Despite the low adhesion values recorded for the initial measurements for decyl-pDMAEMA **14**, the repeat adhesion measurements have a similar value, indicating that the low measured adhesion is not completely due to failure at the brush-wafer interface, as this would coat the hydrogel with a layer of positive polymer, which would not adhere strongly to the fresh positive brush. Although the adhesion for this control compound is small when compared to the calixarene-adhesives **11** and **12**, it is still larger than for PVAc,

The adhesion and work done for calixarene-pMAA **22** is shown in Figure 5.5. While calixarene-pMAA **22** shows an adhesive response, the adhesion force is smaller than for calixarene-pDMAEMA **12**. This could indicate that the pMAA polymer film is less adhesive at these thicknesses than the pDMAEMA film, or that the pDMAEMA polymer contributes to the surface adhesion of compounds **11**, **12**, and **22**. The pDMAEMA would be attracted to any remaining native oxide on the wafer surface, which may be present as the areas between the HMDS features observed by AFM, whereas the pMAA is not attracted to this oxide.

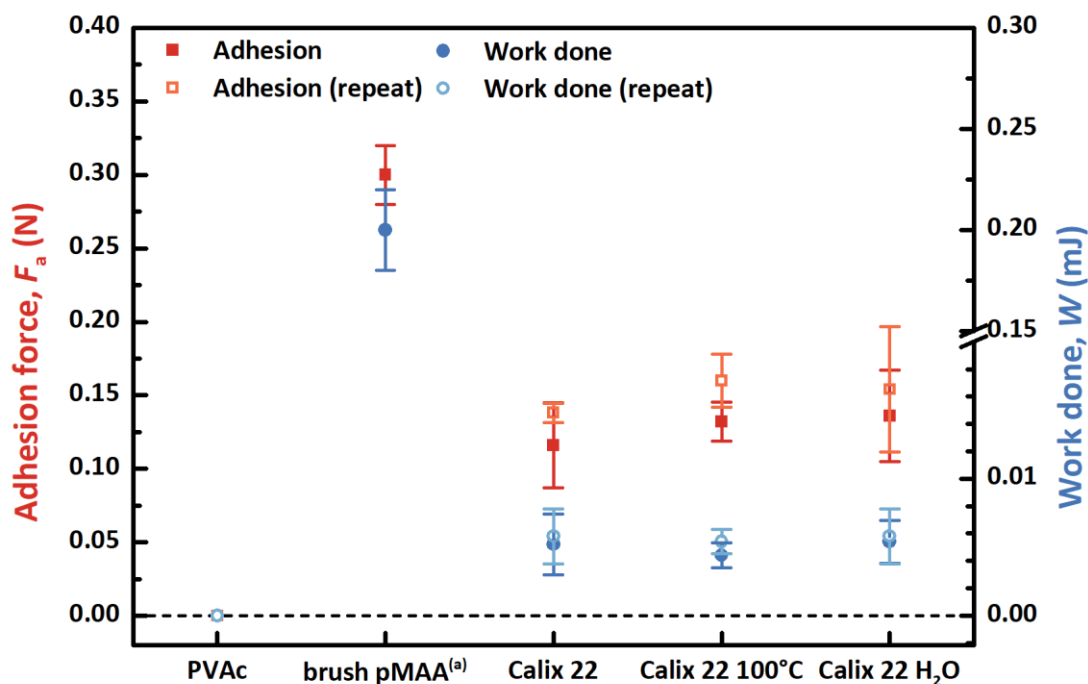


Figure 5.5: Adhesion and work done of calixarene-pMAA **22**. Material was deposited at 40 mN m^{-1} , and measurements were conducted in pH6 Milli-Q water using pDEAEMA hydrogel. Applied load = 0.5 N, contact time = 2 min, pre- and post-test speed = 50 mm min^{-1} . a) Data for grafted-from pMAA brush from Alfahid et al.³⁴

The calixarene-pMAA **22** brush shows a similar adhesive response across all samples, indicating that the post-treatment does not have an effect on the adhesion, even though it causes a change in the surface topography as observed by AFM. In the repeat adhesion measurements, calixarene-pMAA **22** does not show a decrease in the measured adhesion force or work done. This indicates that the measured adhesion is predominately adhesive failure at the gel-brush interface.

The adhesion force of the brush is much smaller than the previously reported grafted-from brush.³⁴ The work done is also much lower than for the grafted-from brush, so the adhesion acts over a shorter distance, and less energy is required to separate the gel from the brush. This, in part, may also be due to the shorter length of the deposited brushes (Calix **11** = $12 \pm 2 \text{ nm}$, grafted-from brush = $32.2\text{-}0.2 \text{ nm}$ ³⁴), as this effects the degree of interdigitation into the hydrogel, and the overall strength of the adhesive bond.³⁴ However, all three surfaces still had a higher adhesive force and work done than the PVAc surface, which showed no adhesive response under the test conditions.

The adhesion and work done for decyl-pMAA **17** is shown in Figure 5.6. Decyl-pMAA **17** shows no adhesive response across all samples. This indicates that the polymer is not strongly adhered to the surface and is more likely to be removed by the hydrogel, or perhaps pushed away from the adhesion site. The presence of the large film defects observed by AFM and the reduced film thickness are also probably contributing to the reduced adhesion, as there is less material to interact with per unit area. This shows that the calixarene contributes to the film thickness and surface adhesion of calixarene-pMAA **22**.

The repeat adhesion measurements for decyl-pMAA **17** also show no adhesion, which indicates that the polymer is likely to be behaving in the same way for both the initial and repeat measurements. However, it was not possible to tell if there was a build-up of material on the gel based upon these adhesion measurements.

The adhesion and work done for the PVAc surfaces is shown in Figure 5.7. As shown previously, the adhesion force and work done is smaller than for the deposited polyelectrolyte brushes. In the repeat adhesion measurements PVAc does not show a decrease in the measured adhesion force or work done. This indicates that the measured adhesion is predominately adhesive failure at the gel-film interface. Only the negative DN pMAA-pOEGMA hydrogel showed an adhesive response with the PVAc film, which is probably due to the higher affinity to negative charge of the acetate side chain.

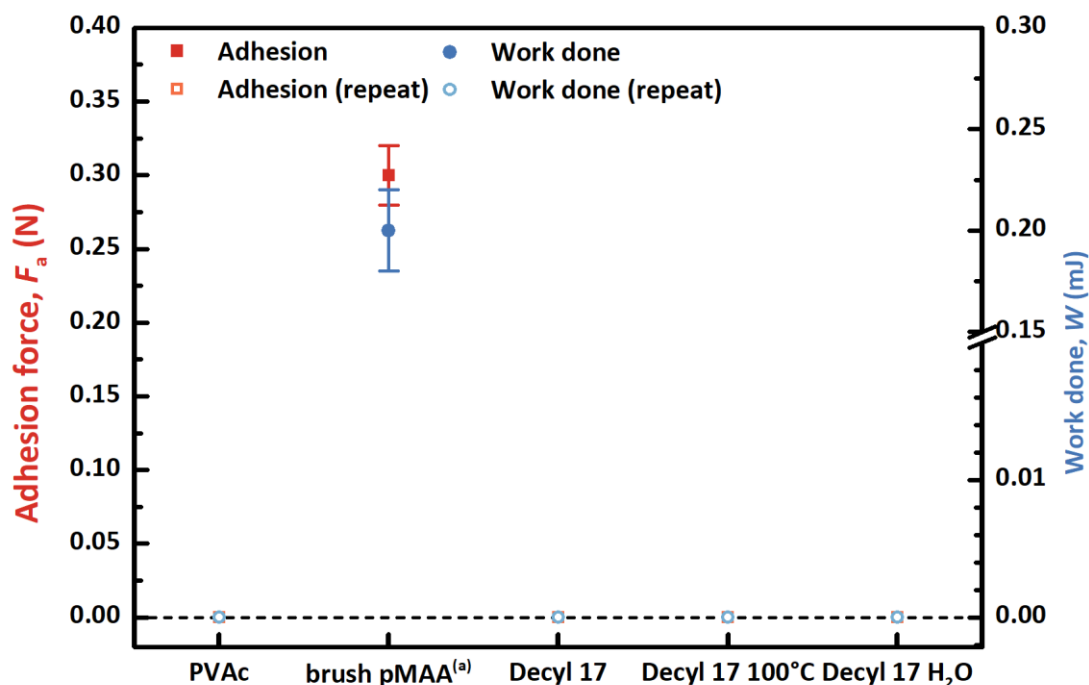


Figure 5.6: Adhesion and work done of decyl-pMAA **17**. Material was deposited at 35 mN m^{-1} , and measurements were conducted in pH6 Milli-Q water using pDEAEMA hydrogel. Applied load = 0.5 N, contact time = 2 min, pre- and post-test speed = 50 mm min^{-1} . a) Data for grafted-from pMAA brush from Alfheid et al.³⁴

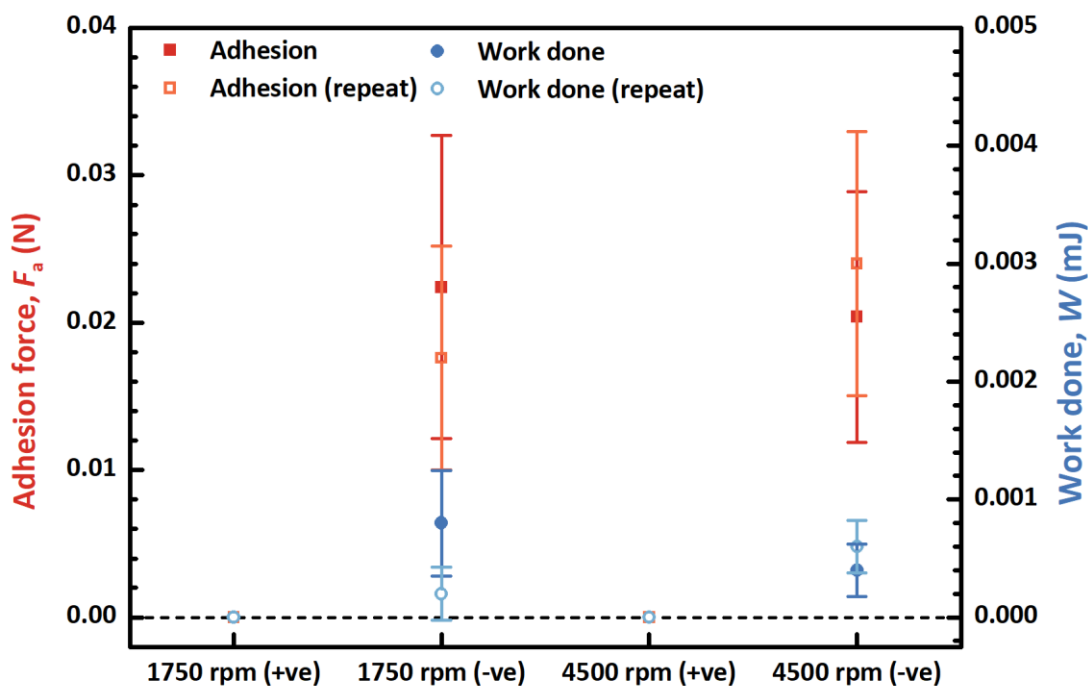


Figure 5.7: Adhesion and work done of PVAc. Measurements were conducted in pH6 Milli-Q water using pDEAEMA and DN pMAA-pOEGMA hydrogels. Applied load = 0.5 N, contact time = 2 min, pre- and post-test speed = 50 mm min⁻¹.

5.3. Stress, strain, and elastic modulus

The maximum stress and maximum strain for Boc-calixarene-pDMAEMA **11** is shown in Figure 5.8, and the resultant elastic moduli are shown in Figure 5.9. The stresses and strains are fairly consistent across all three surfaces, with a trend of repeat measurements having lower values.

The stresses are not overly large, and are similar to those reported previously for these hydrogel systems.²⁷ The strains are also reasonable, and reflect the deformable nature of the hydrogel. The smaller stress-strain characteristic observed for the PVAc material can be attributed to the much smaller adhesion between the gel and the polymer film.

The elastic moduli are also fairly consistent across all three surfaces, and similar to the moduli for PVAc as well. The repeat measurements also show elastic moduli similar to the initial measurements, indicating that the adhesion is behaving in a similar way with respect to the mechanical properties of the gel. The values for elastic moduli are smaller than what would be expected for a material behaving elastically. Whilst low modulus materials can behave elastically, the smaller than expected values suggest the hydrogel is likely to be behaving plastically under these conditions. However, the data available is limited and further work would be required to fully substantiate this.

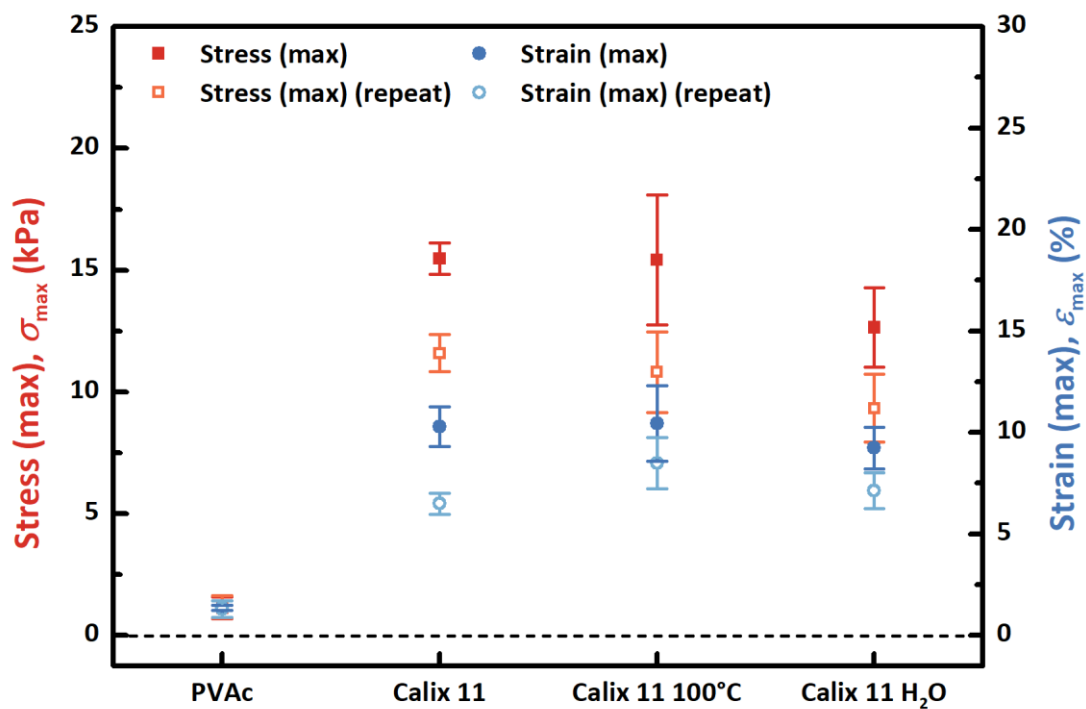


Figure 5.8: Stress (max) and strain (max) of Boc-calixarene-pDMAEMA 11. Applied load = 0.5 N.

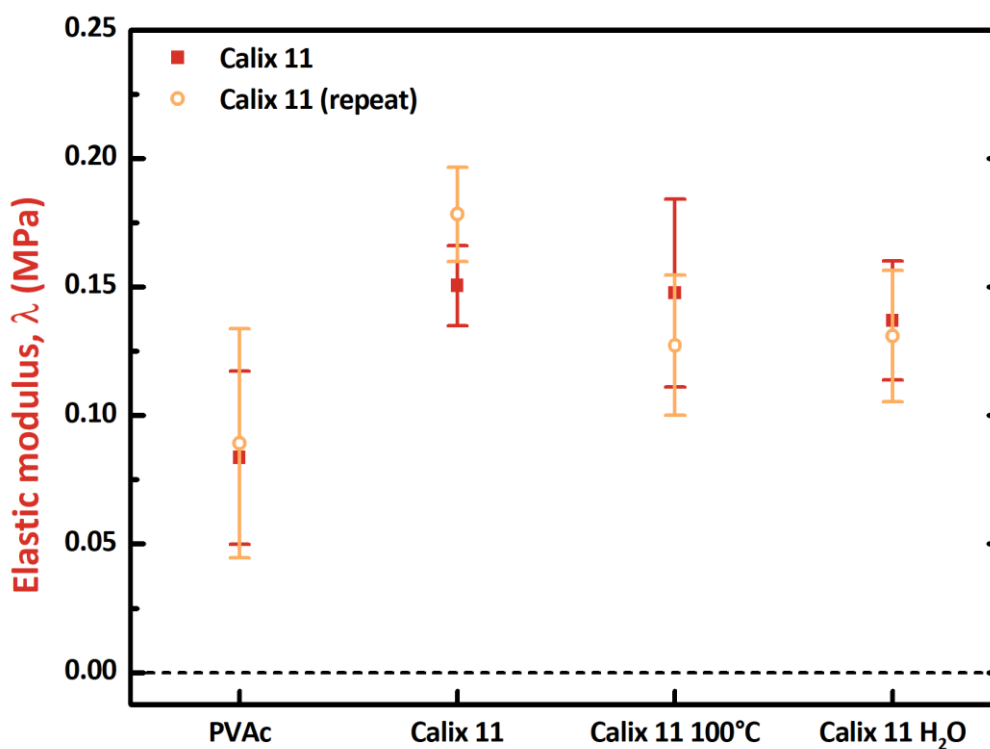


Figure 5.9: Elastic moduli of Boc-calixarene-pDMAEMA 11. Applied load = 0.5 N.

The maximum stress and maximum strain for calixarene-pDMAEMA **12** is shown in Figure 5.10, and the resultant elastic moduli are shown in Figure 5.11. The stress for the deposited surface is similar to that of Boc-calixarene-pDMAEMA **11**, but is lower for both the post-treatment surfaces, although these are similar, and reflects the reduced adhesion for these surfaces. The strains are fairly consistent across all three surfaces, with the repeat measurements having lower values for both stress and strain. The strains are slightly lower than for Boc-calixarene-pDMAEMA **11**, but still reasonably reflect the deformable nature of the hydrogel.

The elastic moduli are again fairly consistent across all three surfaces and between initial and repeat measurements also indicating that the adhesion is behaving in a similar way with respect to the mechanical properties of the gel. The values for elastic moduli also suggest that the hydrogel is probably behaving plastically under these conditions as well.

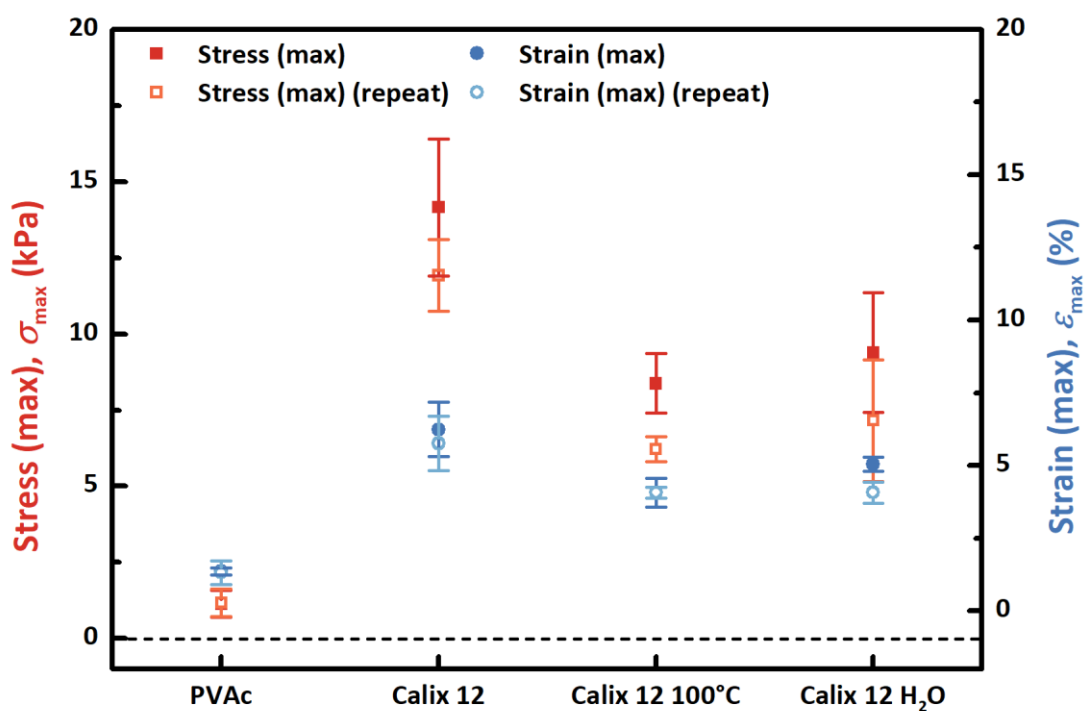


Figure 5.10: Stress (max) and strain (max) of calixarene-pDMAEMA **12**. Applied load = 0.5 N.

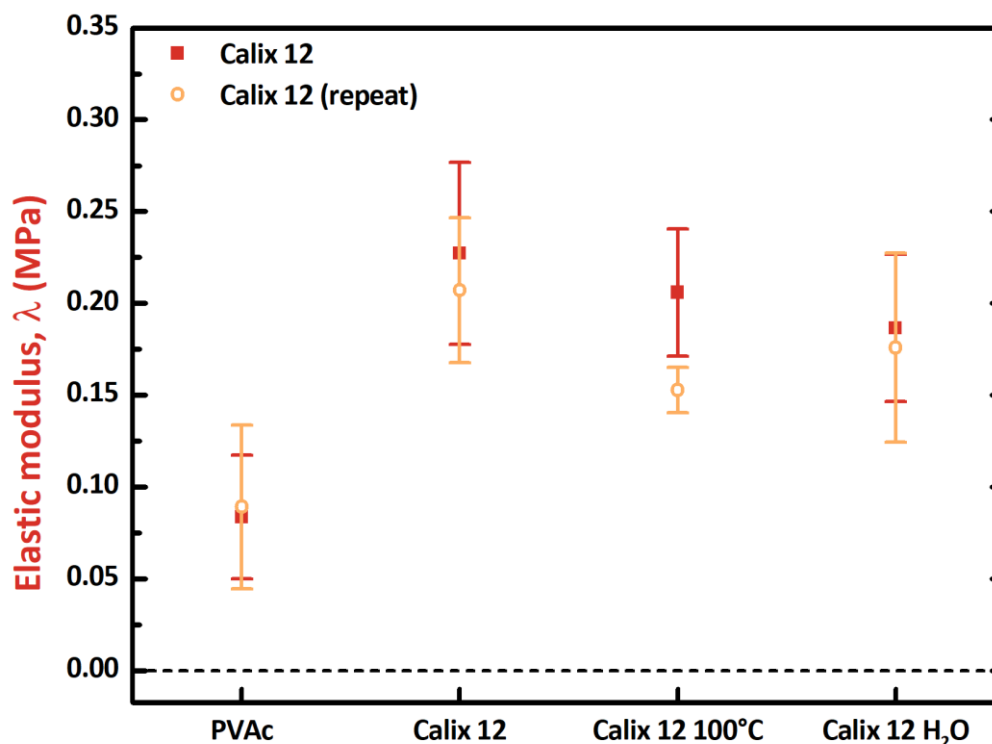


Figure 5.11: Elastic moduli of calixarene-pDMAEMA **12**. Applied load = 0.5 N.

The maximum stress and maximum strain for decyl-pDMAEMA **14** is shown in Figure 5.12, and the resultant elastic moduli are shown in Figure 5.13. The stresses for these surfaces are smaller than for the calixarene-pDMAEMA based adhesives, which can be attributed to the lower adhesive force observed for these surfaces. Similar to calixarene-pDMAEMA **12**, the stresses are lower for both the post-treatment surfaces, and reflects the reduced adhesion for these surfaces. The strains also are reasonably consistent across all three surfaces. The repeat measurements for both stress and strain show an overlap with the initial measurements, as the observed adhesion force is similar between both measurements.

The elastic moduli are again fairly consistent across all three surfaces and between initial and repeat measurements also indicating that the adhesion is behaving in a similar manner with respect to the mechanical properties of the gel. The values for elastic moduli also suggest that the hydrogel is probably behaving plastically under these conditions as well. The elastic moduli are also similar to the elastic modulus for the PVAc film, reflecting the reduced adhesion of these surfaces.

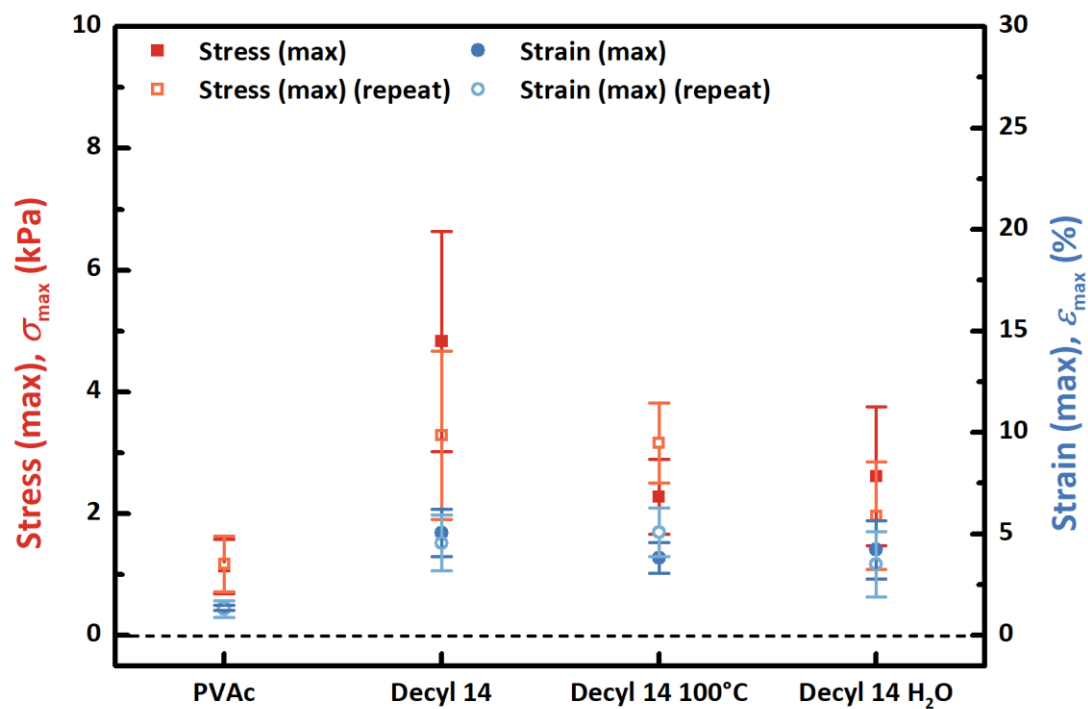


Figure 5.12: Stress (max) and strain (max) of decyl-pDMAEMA 14. Applied load = 0.5 N.

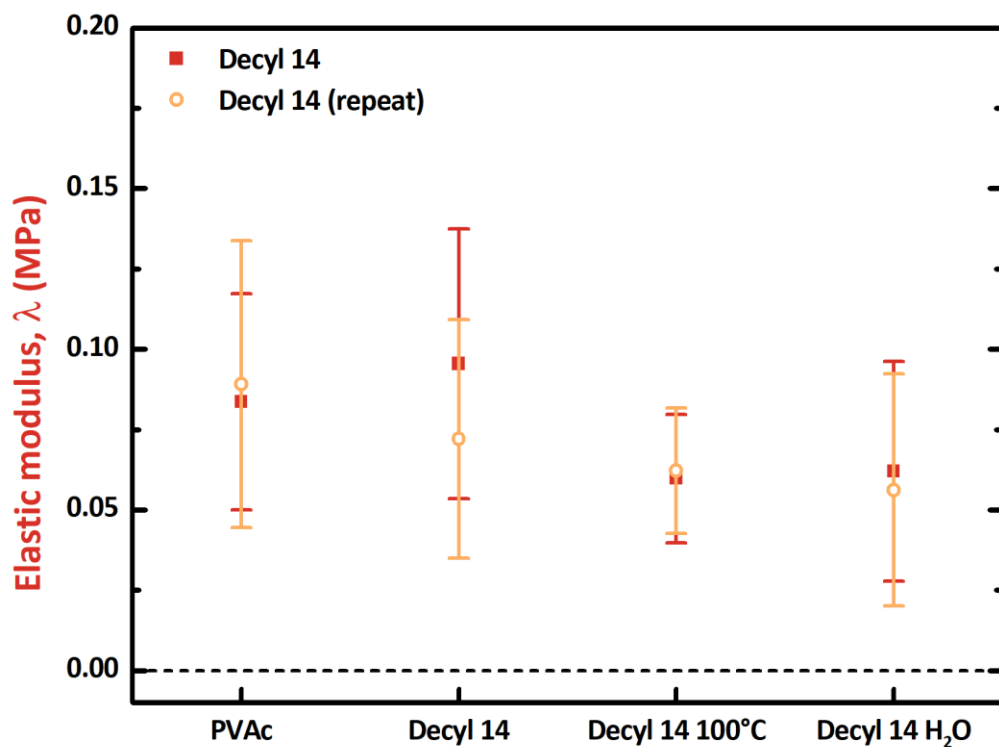


Figure 5.13: Elastic moduli of decyl-pDMAEMA 14. Applied load = 0.5 N.

The maximum stress and maximum strain for calixarene-pMAA **22** is shown in Figure 5.14, and the resultant elastic moduli are shown in Figure 5.15. The stresses and strains are fairly consistent across all three surfaces, with the repeat measurements having similar values.

The stresses are not overly large, but are smaller than those for the calixarene-pDMAEMA based adhesives, as they display a lower adhesion force. The strains are much smaller than those observed for the DN pMAA-pOEGMA hydrogel system, showing less deformation before adhesive failure for the pDEAEMA hydrogels. The PVAc material shows no stress-strain behaviour as there is no adhesion with the pDEAEMA hydrogel.

The elastic moduli are also moderately consistent across all three surfaces. The repeat measurements also show elastic moduli similar to the initial measurements, indicating that the adhesion is behaving in a similar way with respect to the mechanical properties of the gel. The values for elastic moduli are smaller than what would be expected for a material behaving elastically, so suggests that the hydrogel is probably behaving plastically under these conditions. In contrast to calixarene-pMAA **22**, as no adhesion was observed for decyl-pMAA **17**, there is also no stress or strain observed.

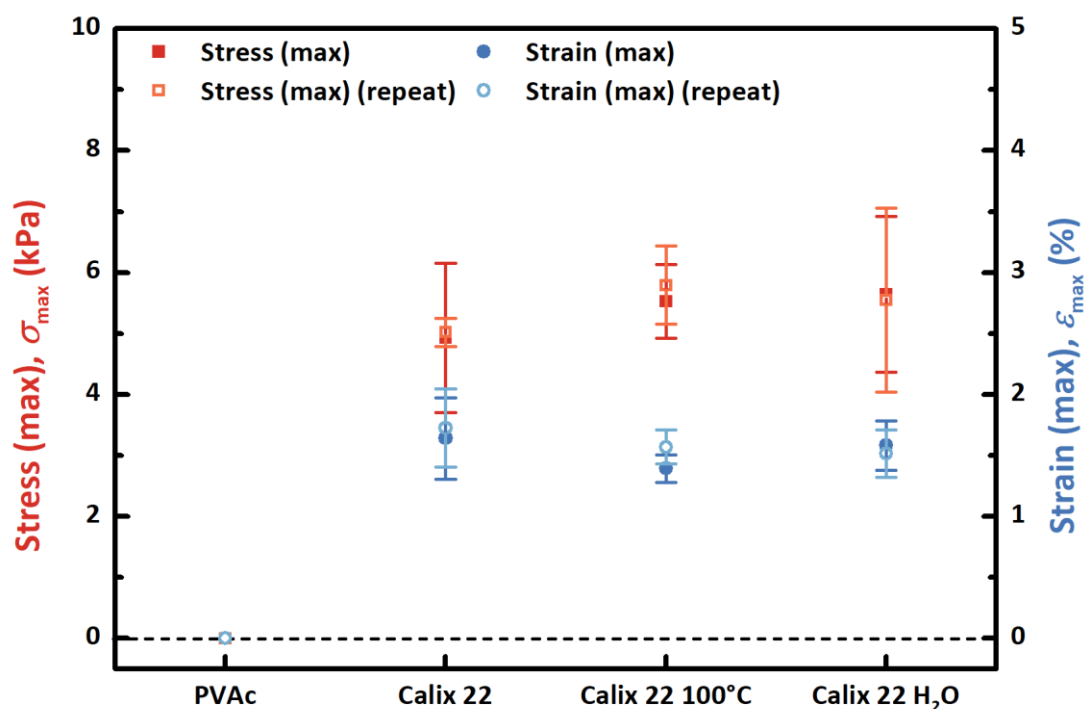


Figure 5.14: Stress (max) and strain (max) of calixarene-pMAA **22**. Applied load = 0.5 N.

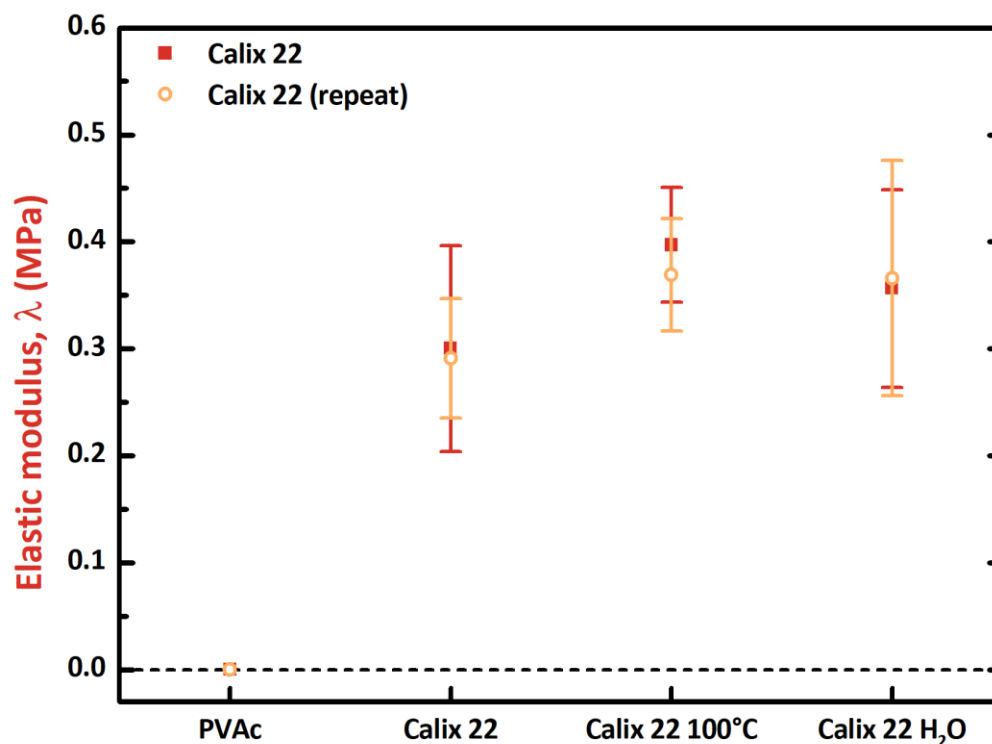


Figure 5.15: Elastic moduli of calixarene-pMAA 22. Applied load = 0.5 N.

The maximum stress and maximum strain for PVAc is shown in Figure 5.16a, and the resultant elastic moduli are shown in Figure 5.16b. The stress, strain, and elastic moduli are smaller than for the deposited polyelectrolyte brushes in most cases. In the repeat adhesion measurements PVAc does not show a decrease in the measured stress, strain, and elastic moduli. This indicates that the adhesion is behaving in a similar way with respect to the mechanical properties of the gel.

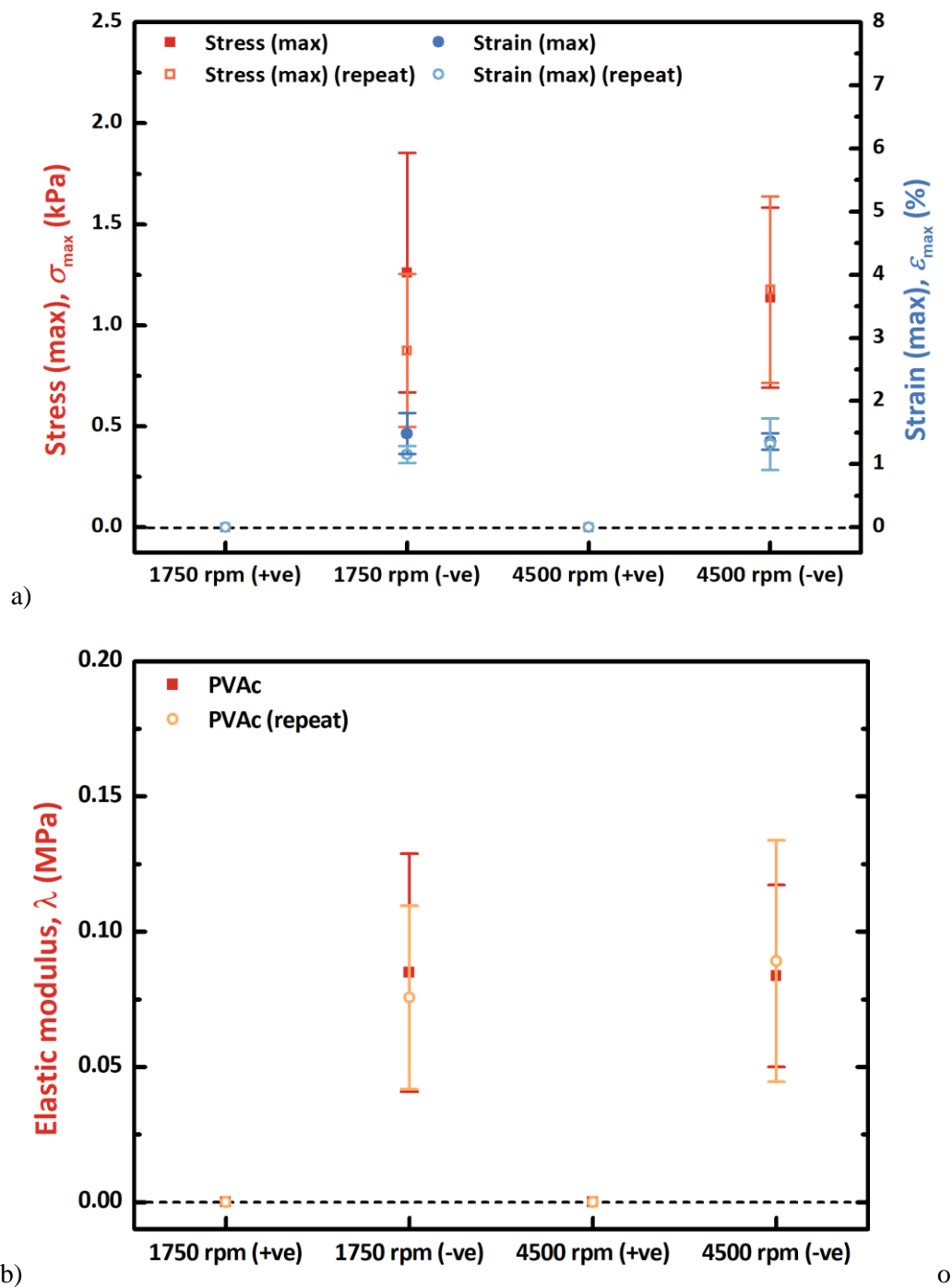


Figure 5.16: a) Stress (max) and strain (max) of PVAc. b) Elastic moduli of PVAc. Applied load = 0.5 N.

The stress measured for this system represents the force per unit area that occurs during the removal of the hydrogel, and the strain is due to the deformation caused during separation. Under this deformation, energy is stored in the system as strain energy. If the material is elastic then this energy is released when the material is returned to its original state. If the material is plastic, then a portion of the energy is dissipated causing permanent deformation of the material.

From this, if an elastic modulus of an adhesive joint suggests that the adhesion is behaving elastically, then the dissipation of energy is likely to be through interface separation, with higher elastic modulus values being stiffer. If the elastic modulus of the adhesive joint suggests that the adhesion is resulting in plastic deformation, then at least a portion of the energy dissipation will likely be through dissipation in the hydrogel, causing permanent deformation.

Although the data here is insufficient to draw a quantitative analysis for the stress-strain characterises of these adhesive joints, a qualitative analysis on the probable dissipation mechanisms can be speculated. The data suggests that for calix **11**, calix **12**, decyl **14**, and PVAc (with the pDEAEMA hydrogel) a portion of the energy dissipation was through deformation of the hydrogel, resulting in a lower stiffness joint. Conversely, the data suggests that calix **22** showed the opposite; the energy dissipation was primarily through interface separation, resulting in a higher stiffness joint.

The reason for this difference is predominately down to the differing strengths of the adhesive bond. Calix **22** had a much smaller adhesive strength, therefore the energy required to break the adhesion was smaller than the energy required to deform the hydrogel irreversibly, so the adhesive bond will break before irreversible deformation can occur.

5.4. Work of debonding

The work of debonding for Boc-calixarene-pDMAEMA **11** is shown in Figure 5.17. As the stresses for these surfaces are not particularly large, this suggests the work of debonding for these surfaces is reasonable. The initial measurement has a higher work of debonding than the repeat measurements, reflecting the stronger adhesion force observed for the initial measurements. The values are fairly consistent across all three surfaces and reflect the observed adhesion forces.

These values are greater than the values reported by La Spina et al.²⁷, but less than those reported by Alfheid et al.³⁴ However, the results reported by Alfheid et al.³⁴ were obtained at much larger stresses compared to this system, where the properties at the interface may no longer be elastic compared to the stress levels in this system. The work of debonding for all three surfaces is much larger than the value obtained for the PVAc surface, emphasising the effect of the polyelectrolyte brush on the observed adhesion.

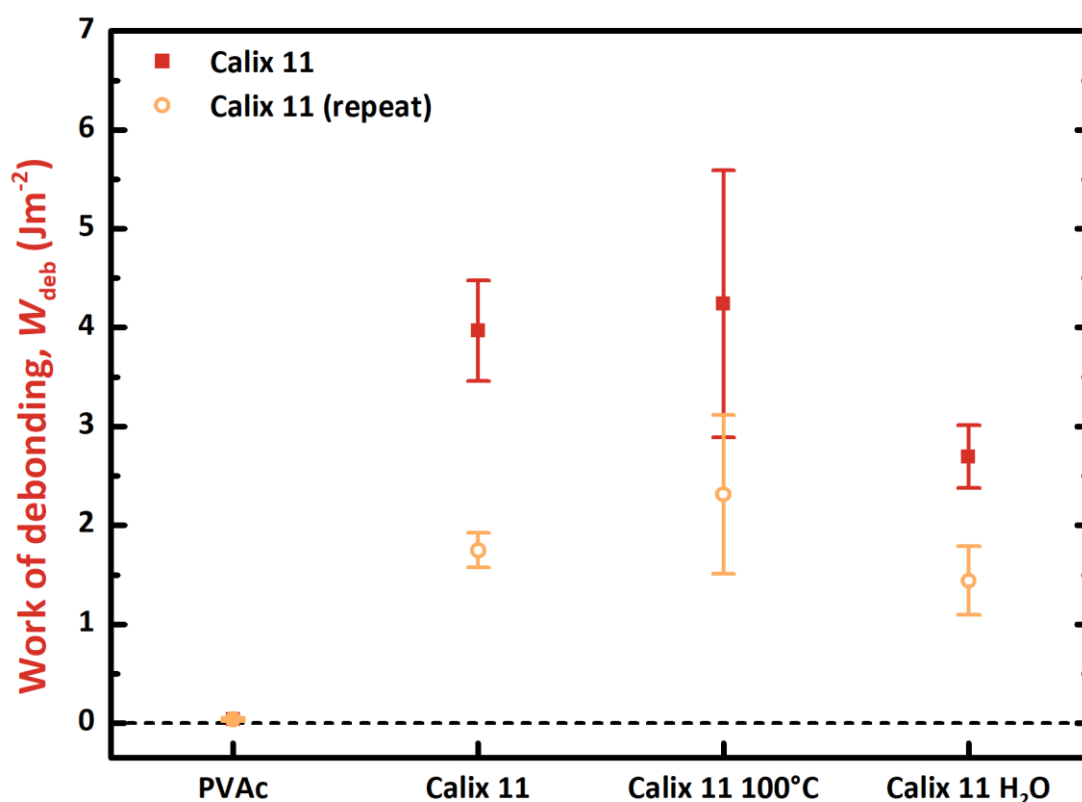


Figure 5.17: Work of debonding for Boc-calixarene-pDMAEMA **11**. Applied load = 0.5 N.

The work of debonding for calixarene-pDMAEMA **12** is shown in Figure 5.18. The work of debonding is lower than for Boc-calixarene-pDMAEMA **11**, despite having similar adhesion forces. This is due to the smaller strain observed for these surfaces, meaning the adhesion acts over a shorter distance, and less energy is required to separate the gel from the brush, similar to the work done. The work of debonding is lower for both the post-treatment surfaces, and reflects the reduced adhesion for these surfaces, but all surfaces have a larger work of debonding than the PVAc surface.

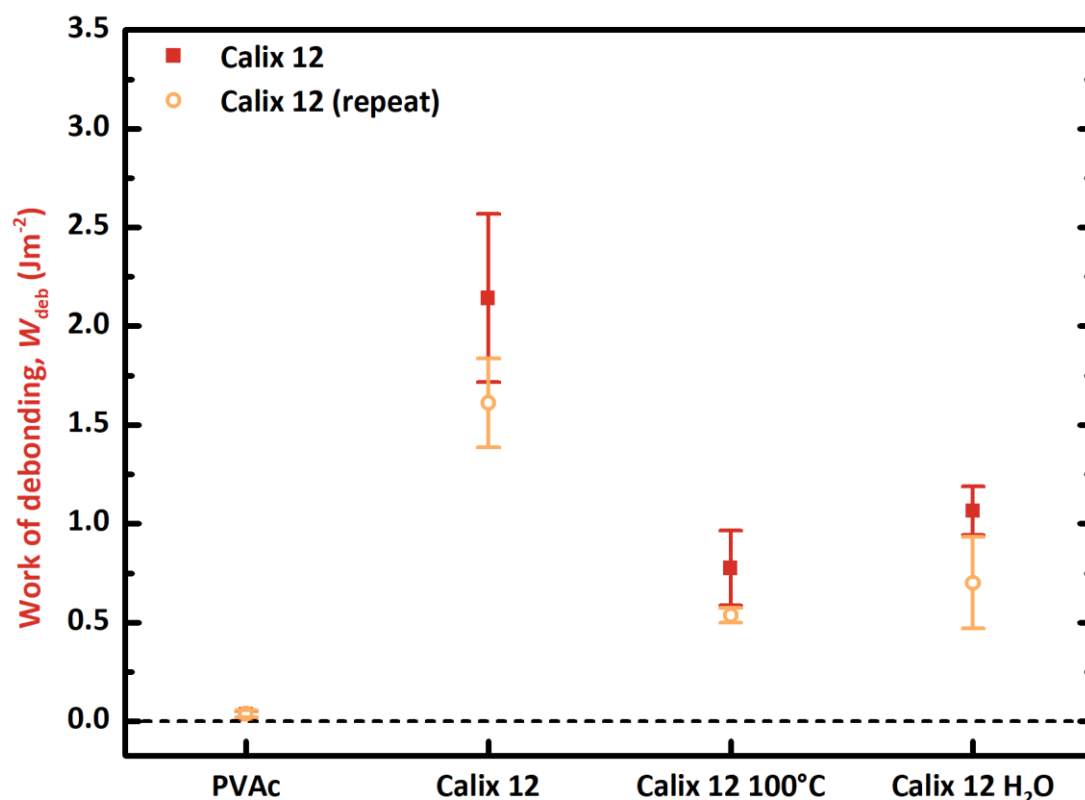


Figure 5.18: Work of debonding for calixarene-pDMAEMA **12**. Applied load = 0.5 N.

The work of debonding for decyl-pDMAEMA **14** is shown in Figure 5.19. The work of debonding for these surfaces is smaller than for the calixarene-pDMAEMA based adhesives, which can be attributed to the lower adhesive force observed for these surfaces. Similar to calixarene-pDMAEMA **12**, the work of debonding is lower for both the post-treatment surfaces, and so reflects the reduced adhesion for these surfaces. The repeat measurements for both stress and strain show an overlap with the initial measurements, as the observed adhesion force is similar between both measurements.

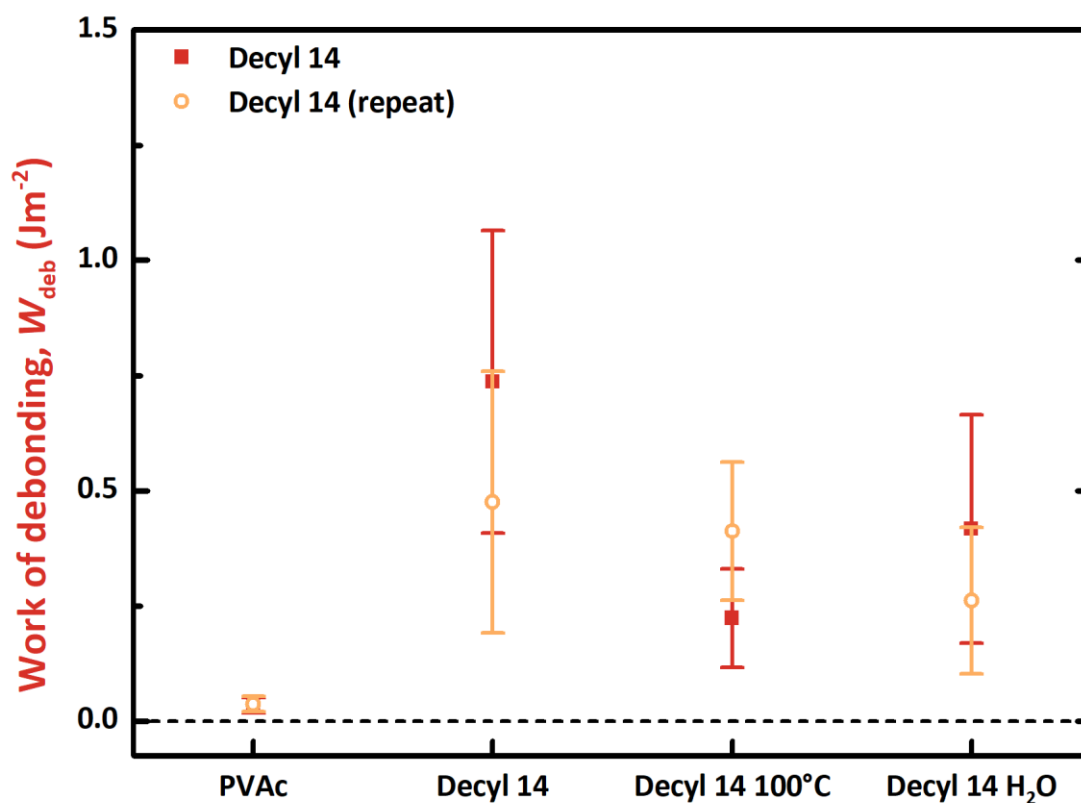


Figure 5.19: Work of debonding for decyl-pDMAEMA **14**. Applied load = 0.5 N.

The work of debonding for calixarene-pMAA **22** is shown in Figure 5.20. The work of debonding for calixarene-pMAA **22** is lower than for the calix-pDMAEMA surfaces. However, this is reasonable as the stresses are also lower for calixarene-pMAA **22**. The work of debonding is relatively consistent across all three surfaces, with the repeat measurements overlapping with the initial measurements, as the observed adhesion force is similar between both measurements. These values are similar to the values reported by La Spina et al.²⁷, but smaller than those reported by Alfahid et al.³⁴ The PVAc material shows work of debonding as there is no adhesion with the pDEAEMA hydrogel.

The work of debonding for decyl-pMAA **17** is shown in Figure 5.21. As no adhesion was observed for these surfaces, there is also no associated work of debonding.

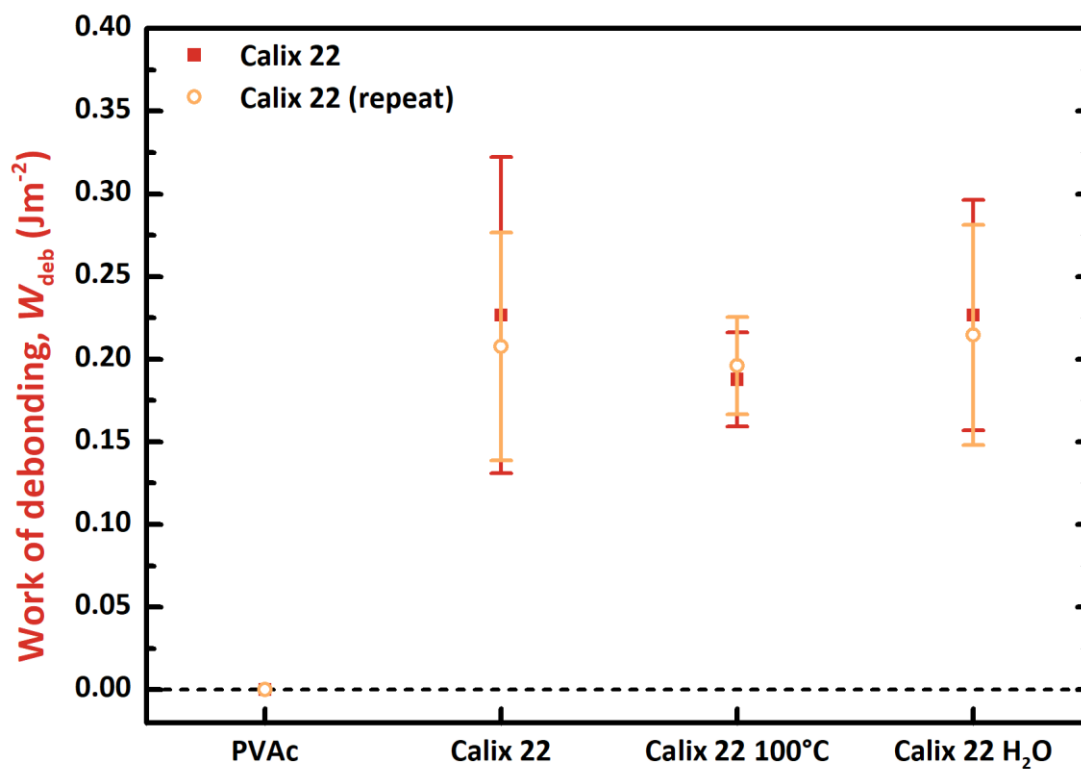


Figure 5.20: Work of debonding for calix-pMAA 22. Applied load = 0.5 N.

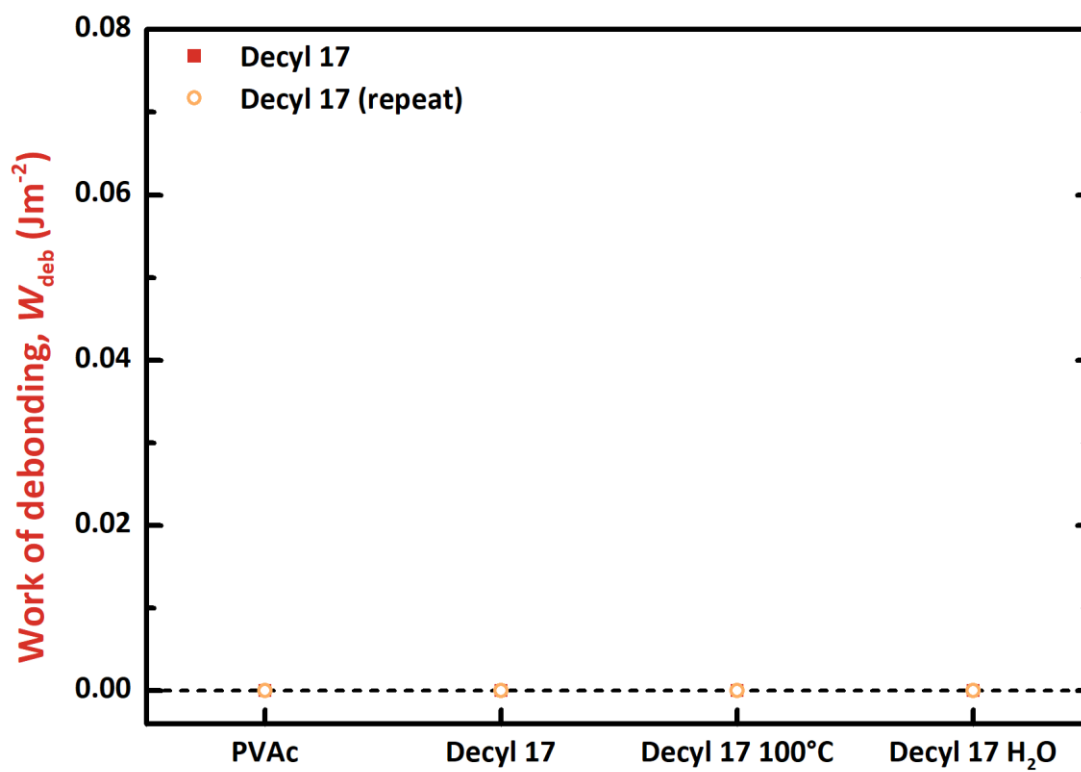


Figure 5.21: Work of debonding for decyl-pMAA 17. Applied load = 0.5 N.

The work of debonding for PVAc is shown in Figure 5.22. As shown previously, the work of debonding is smaller than for the deposited polyelectrolyte brushes. In the repeat adhesion measurements PVAc does not show a decrease in the work of debonding. This indicates that the measured adhesion is predominately adhesive failure at the gel-film interface.

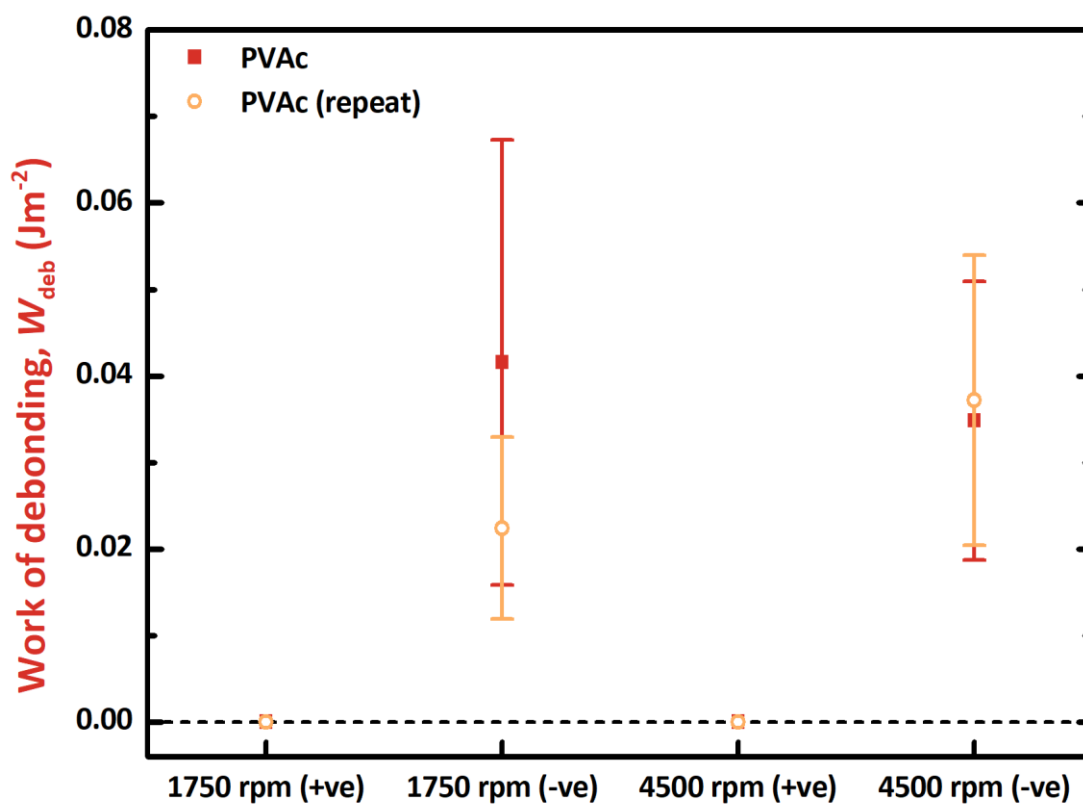


Figure 5.22: Work of debonding for PVAc. Applied load = 0.5 N.

5.5. Variation of load

The applied load was varied to determine the effect upon the adhesion characteristics of the brush-gel system. The effect of load upon the adhesion characteristics of Boc-calixarene-pDMAEMA **11** is shown in Figure 5.23.

At low loads (0.1 N), Boc-calixarene-pDMAEMA **11** shows a similar adhesion force to medium loads (0.5 N), but as this is over a smaller contact area, this results in a higher stress. The work done to remove the hydrogel is much smaller than that for medium loads, indicating that the adhesion occurs over a much smaller distance, as shown by the smaller strain. The elastic modulus during the debonding is much larger than medium loads, which might suggest that the hydrogel is behaving more elastically, or at least less plastically. Nevertheless, the data available is still limited and further work would be required to fully substantiate this. Despite the potential increased elasticity, the overall work of debonding is lower than at medium loads. This is because the adhesion is occurring over a shorter distance, which is a result of the reduced contact area of the hydrogel.

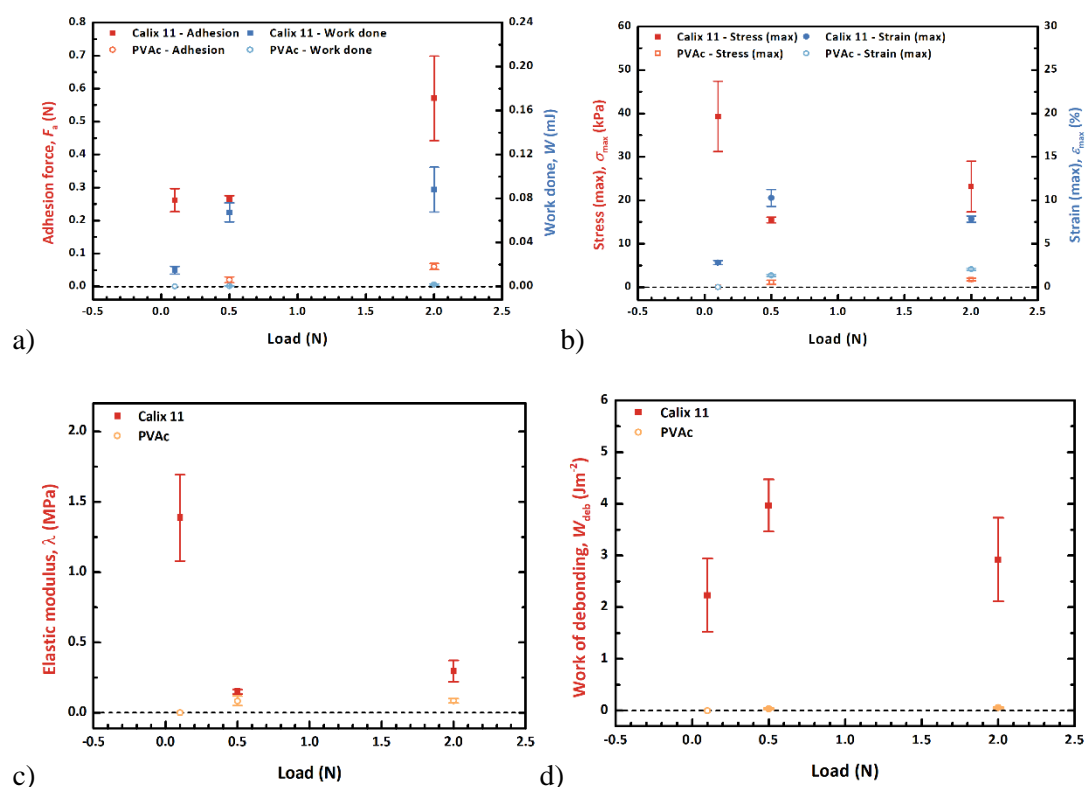


Figure 5.23: Effect of load upon the adhesion characteristics of Boc-calixarene-pDMAEMA **11**. a) Adhesion force and work done, b) Stress (max) and strain (max), c) Elastic modulus, d) Work of debonding.

At high loads (2 N), Boc-calixarene-pDMAEMA **11** shows a larger adhesion force to medium loads (0.5 N), but the increase in contact area is greater, resulting in less of an increase in the stress. The work done to remove the hydrogel is similar to that for medium loads, indicating that the adhesion occurs over a similar distance, as shown by the strain. The elastic modulus during the debonding is, similar to that of medium loads, quite small, suggesting that the hydrogel is behaving plastically. The stress-strain diagram for an elastic material is linear at low strains. However, increasing strain above a certain point causes the stress to stop rising and even decrease at the yield point before recovering somewhat as the material strain-hardens. The modulus therefore is constant at low loads, decreases dramatically at yield, and increases again as the material plastically deforms. It never recovers its original modulus. The data obtained in Figure 5.23c are consistent with this picture, which makes it tempting to identify plastic deformation in the gels at the largest loads. Despite the increased adhesion force, the overall work of debonding is similar to medium loads. This is due to the adhesion occurring over a similar distance, which is probably a result of the strain hardening of the hydrogel.

The effect of load upon the adhesion characteristics of calixarene-pDMAEMA **12** is shown in Figure 5.24. At low loads (0.1 N), calixarene-pDMAEMA **12** shows a similar adhesion force to medium loads (0.5 N), but as this is over a smaller contact area, resulting in a higher stress. The work done to remove the hydrogel is smaller than that for medium loads, indicating that the adhesion occurs over a smaller distance, as shown by the smaller strain. This difference is not as pronounced as for Boc-calixarene-pDMAEMA **11**, as the work done for calixarene-pDMAEMA **12** is lower at medium loads. The elastic modulus during the debonding is much larger than medium loads, which suggests that the hydrogel is behaving more elastically. Despite the potential increased elasticity, the overall work of debonding is similar to that at medium loads. This is due to the much smaller difference in the distance the adhesion is occurring over between the two loads, resulting in the increase in strain with load matching the decrease in strain with load.

At high loads (2 N), calixarene-pDMAEMA **12** shows a larger adhesion force compared to medium loads (0.5 N), but the increase in contact area is greater, resulting in a proportionally lower increase in the stress. The work done to remove the hydrogel is slightly larger than that for medium loads, but the strain shows that the adhesion occurs over a similar distance. The elastic modulus during the debonding is quite small, similar to medium loads, suggesting that the hydrogel may be behaving plastically. The elastic modulus is slightly higher than that for medium loads, which potentially indicates the onset of strain hardening in the hydrogel. Despite the increased adhesion force, the overall work of debonding is similar to medium loads. This is because the adhesion is occurring over a similar distance, which is probably a result of the strain hardening of the hydrogel.

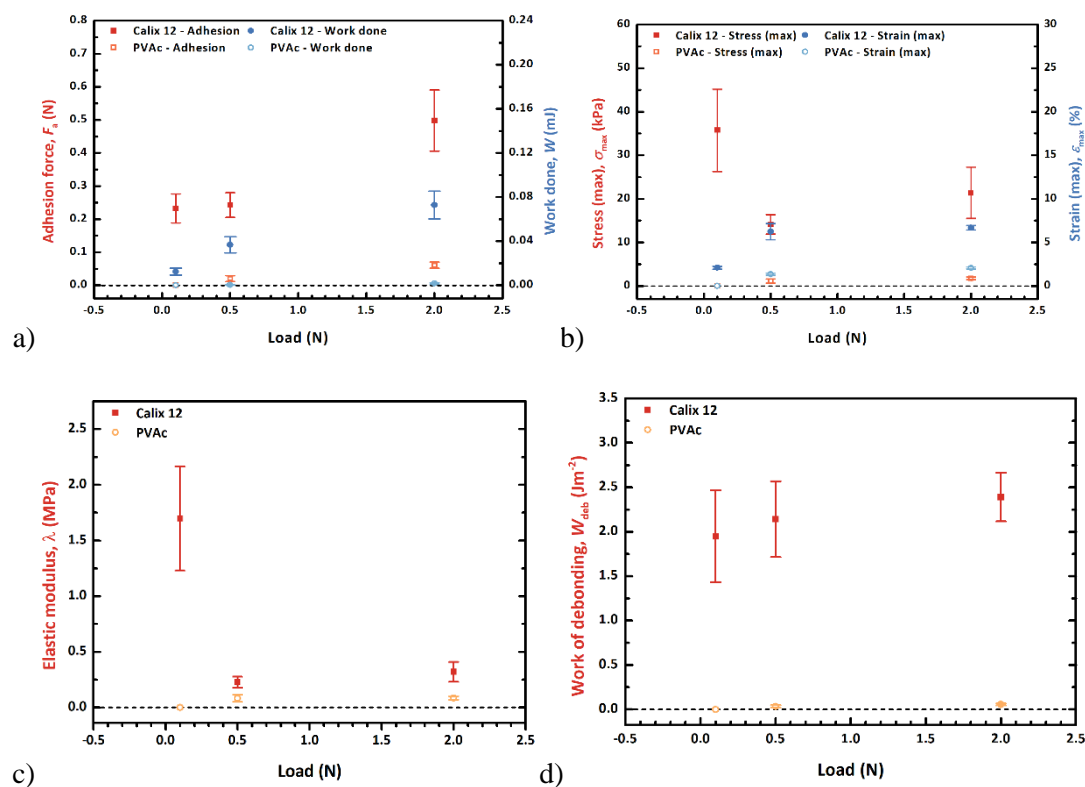


Figure 5.24: Effect of load upon the adhesion characteristics of calixarene-pDMAEMA **12**. a) Adhesion force and work done, b) Stress (max) and strain (max), c) Elastic modulus, d) Work of debonding.

The effect of load upon the adhesion characteristics of decyl-pDMAEMA **14** is shown in Figure 5.25. At low loads (0.1 N), decyl-pDMAEMA **14** shows a similar adhesion force to medium loads (0.5 N), but as this is over a smaller contact area, this results in a higher stress. The work done to remove the hydrogel is smaller than that for medium loads, indicating that the adhesion occurs over a smaller distance, as shown by the smaller strain. This difference is not as pronounced as for Boc-calixarene-pDMAEMA **11**, as the work done for decyl-pDMAEMA **14** is lower at medium loads. The elastic modulus during the debonding is fairly large, which suggests that the hydrogel may be behaving more elastically. Despite the increased elasticity, the overall work of debonding is similar to that at medium loads. This is due to the much smaller difference in the distance the adhesion is occurring over between the two loads, resulting in the increase in strain with load matching the decrease in strain with load.

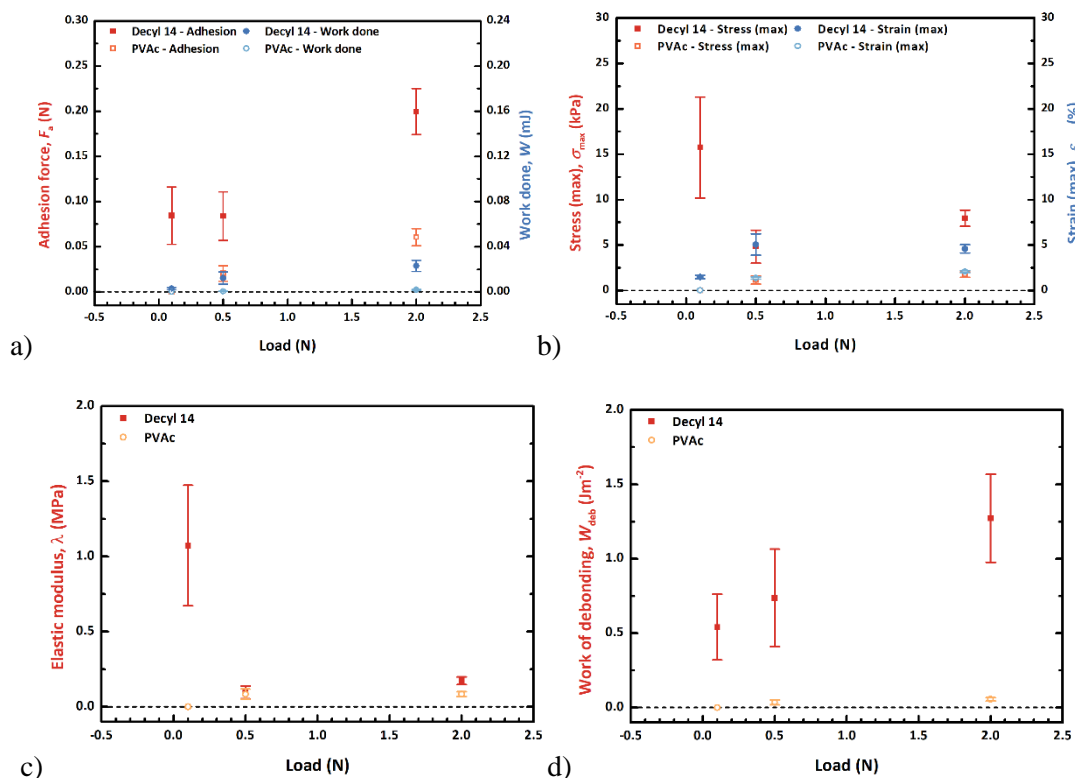


Figure 5.25: Effect of load upon the adhesion characteristics of decyl-pDMAEMA **14**. a) Adhesion force and work done, b) Stress (max) and strain (max), c) Elastic modulus, d) Work of debonding.

At high loads (2 N), decyl-pDMAEMA **14** shows a larger adhesion force to medium loads (0.5 N), but the increase in contact area is greater, resulting in a proportionally lower increase in the stress. The work done to remove the hydrogel is similar to that for medium loads, indicating that the adhesion occurs over a similar distance, as shown by the strain. The elastic modulus during the debonding is, similar to medium loads, quite small, suggesting that the hydrogel is probably behaving plastically. The elastic modulus is slightly higher than that for medium loads, which indicates the onset of strain hardening in the hydrogel. Despite the increased adhesion force, the overall work of debonding is similar to medium loads. This is because the adhesion is occurring over a similar distance, which is probably a result of the strain hardening of the hydrogel.

The effect of load upon the adhesion characteristics of calixarene-pMAA **22** is shown in Figure 5.26. At low loads (0.1 N), calixarene-pMAA **22** shows no measurable adhesive response. This probably due to the overall lower adhesiveness of these films.

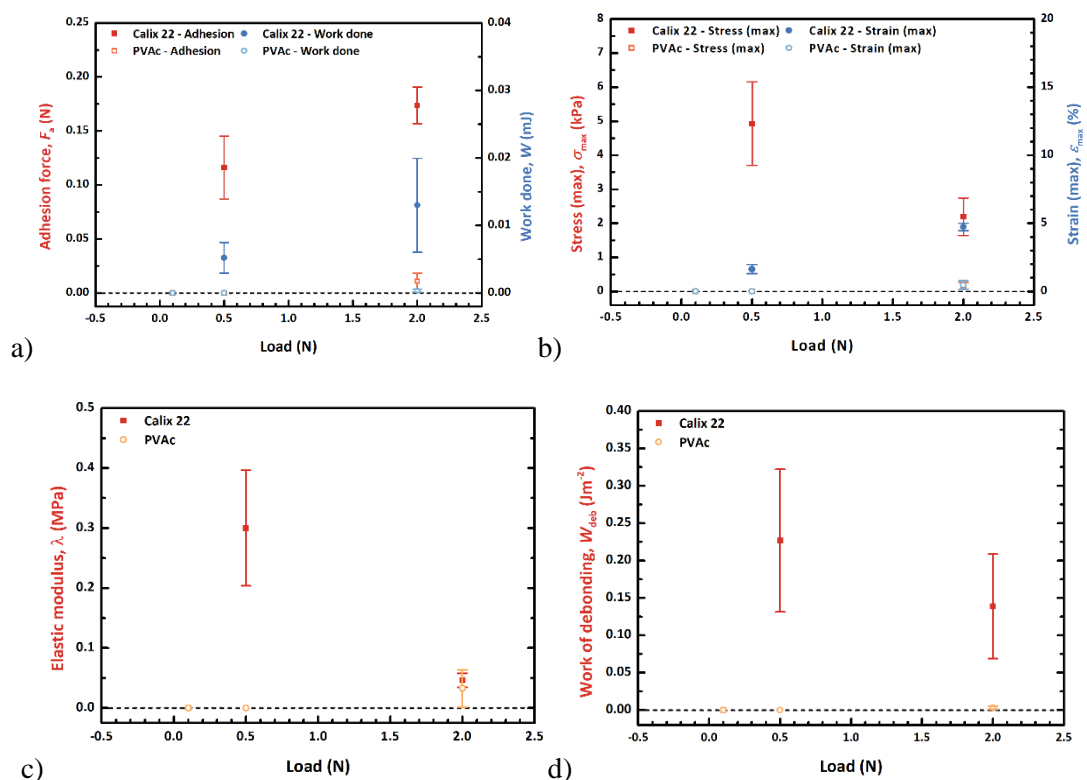


Figure 5.26: Effect of load upon the adhesion characteristics of calixarene-pMAA **22**. a) Adhesion force and work done, b) Stress (max) and strain (max), c) Elastic modulus, d) Work of debonding.

At high loads (2 N), calixarene-pMAA **22** shows a larger adhesion force to medium loads (0.5 N), but the increase in contact area is greater, resulting in a proportionally lower increase in the observed stress. The work done to remove the hydrogel is slightly larger than for medium loads, but does overlap with those values, indicating that the adhesion occurs over a larger distance, as shown by the strain. The elastic modulus during the debonding is much smaller than that for medium loads, which means that the hydrogel is probably behaving plastically. Despite the increased adhesion force, the overall work of debonding is slightly smaller than for medium loads, but still overlaps these values. This is due to the reduced stress caused by the larger contact area, which itself is a result of the increased plasticity of the hydrogel.

The effect of load upon the adhesion characteristics of decyl-pMAA **17** is shown in Figure 5.27. At low loads (0.1 N), decyl-pMAA **17** shows no measurable adhesive response, similar to medium loads (0.5 N). At high loads (2 N), decyl-pMAA **17** does show an adhesive response, with similar behaviour to calixarene-pMAA **22**. This suggests that the greater adhesive performance of calixarene-pMAA **22** is more pronounced at lower loading regimes.

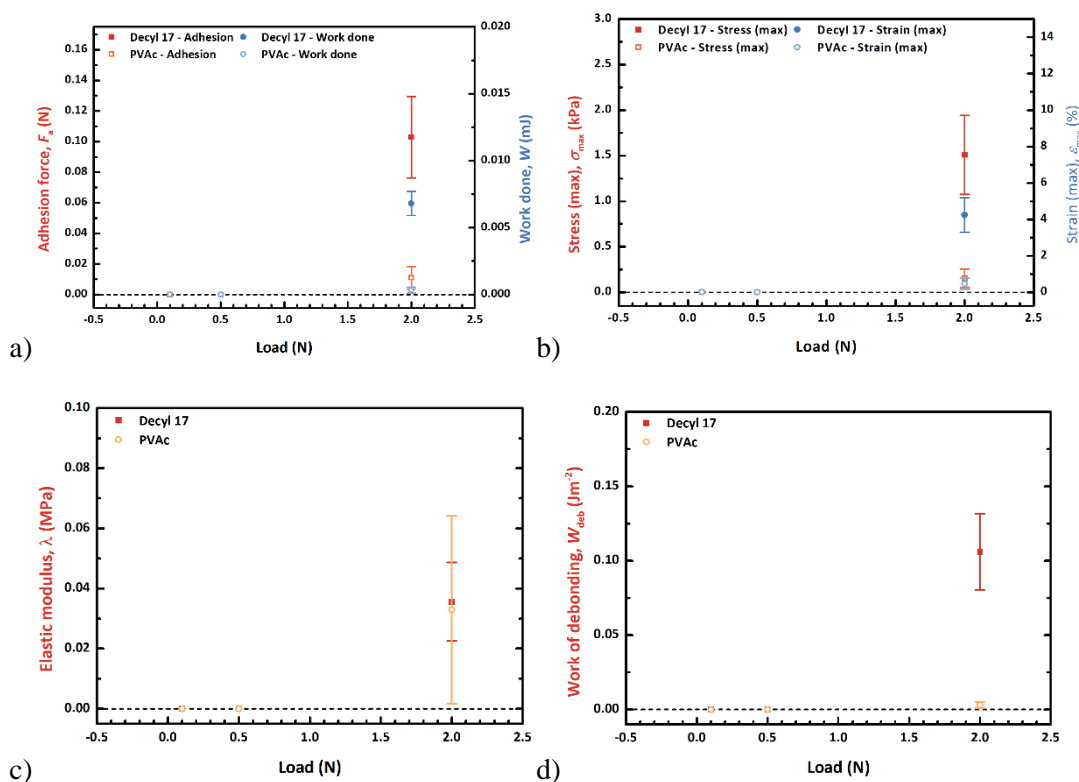


Figure 5.27: Effect of load upon the adhesion characteristics of decyl-pMAA **17**. a) Adhesion force and work done, b) Stress (max) and strain (max), c) Elastic modulus, d) Work of debonding.

The effect of load upon the adhesion characteristics of PVAc when tested with the pDEAEMA hydrogel is shown in Figure 5.28. At low loads (0.1 N), PVAc shows no measurable adhesive response to pDEAEMA hydrogels, similar to medium loads (0.5 N). At high loads (2 N), PVAc does show an adhesive response to pDEAEMA hydrogels, although the adhesion is the lowest of the tested compounds. Only the elastic modulus is similar to the other surfaces, showing that the hydrogel is behaving in a similar fashion.

The effect of load upon the adhesion characteristics of PVAc when tested with the DN pMAA-pOEGMA hydrogel is shown in Figure 5.29. At low loads (0.1 N), PVAc shows a much smaller adhesion than at medium loads (0.5 N), with all values being much smaller, except for the elastic modulus. The similar elastic modulus shows that the hydrogel is behaving in a similar fashion across all loads. At high loads (2 N), the adhesion characteristics are broadly similar to those at medium loads. However, at higher loads, the films spin-cast at 4500 rpm are more adhesive than those at 1750 rpm (4500 rpm = 0.06 ± 0.01 N vs 1750 rpm = 0.02 ± 0.01 N). This may show that at higher film thicknesses, cohesive failure of the film is more likely to occur, reducing the observed adhesion.

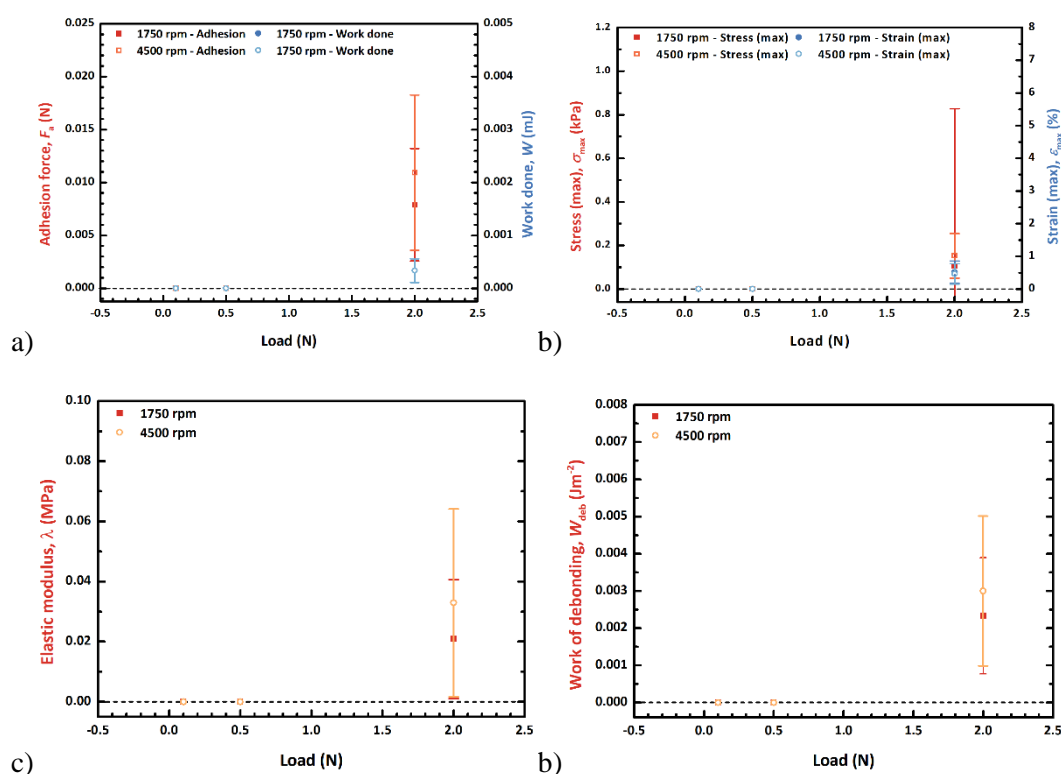


Figure 5.28: Effect of load upon the adhesion characteristics of PVAc tested with pDEAEMA hydrogel. a) Adhesion force and work done, b) Stress (max) and strain (max), c) Elastic modulus, d) Work of debonding.

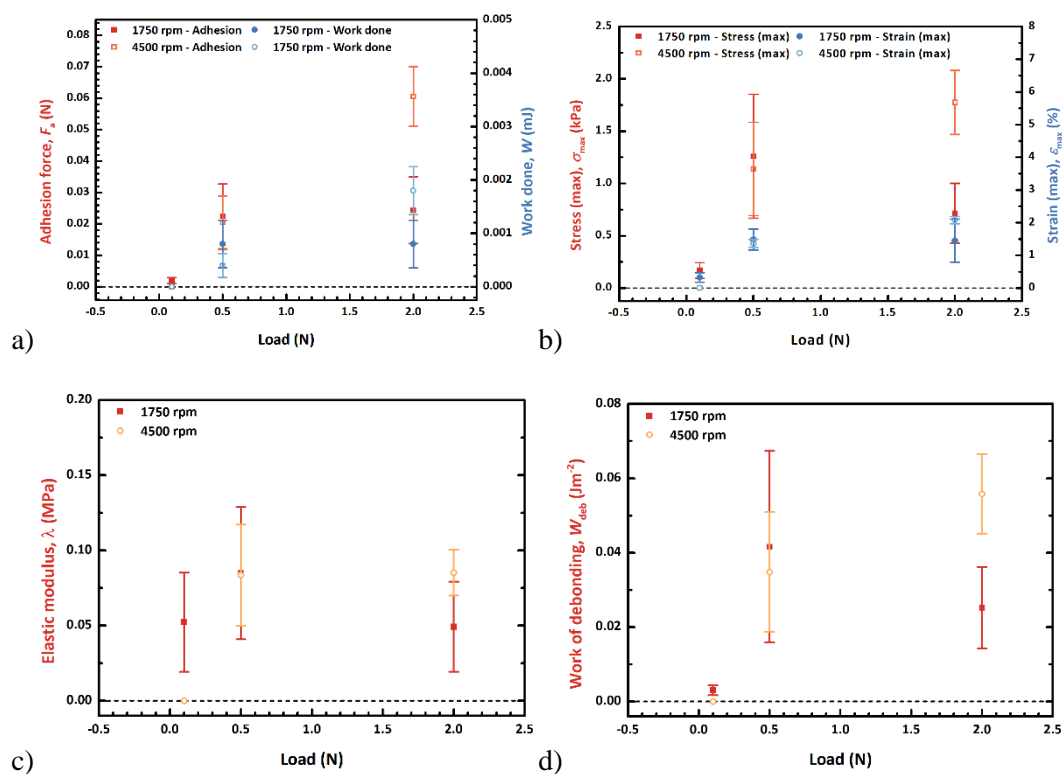


Figure 5.29: Effect of load upon the adhesion characteristics of PVAc tested with DN pMAA-pOEGMA hydrogel. a) Adhesion force and work done, b) Stress (max) and strain (max), c) Elastic modulus, d) Work of debonding.

5.5.1. Stress-strain characteristic of the hydrogel under compression

The effect of the load on the hydrogel during the contact was examined by determining the compressive stress and strain characteristics of the two hydrogels. The elastic moduli for these hydrogels have been previously determined^{33,34} (Table 5.2), and comparison to these moduli suggests how these hydrogels are behaving.

Table 5.2: Elastic moduli of hydrogels.

Hydrogel	Elastic modulus, λ (MPa)
DN pMAA-pOEGMA ³³	1.09 ± 0.01
pDEAEMA ³⁴	0.48 ± 0.03

The stress-strain relation of the DN pMAA-pOEGMA hydrogel is shown in Figure 5.30, where the grey line indicates the previously measured modulus of the hydrogel.³³ Whilst inter-sample variation is possible, the same method was used for both samples. At low loads (0.1 N), the measured elastic modulus overlaps with the recorded elastic modulus of the hydrogel. Therefore, the hydrogel is within the proportionality limit; where stress is proportional to strain, and is behaving elastically.

At medium loads (0.5 N), the measured elastic moduli are much smaller than the recorded elastic modulus of the hydrogel. Therefore, the hydrogel is no longer behaving elastically, and is in a plastic regime.

At high loads (2 N), the measured elastic moduli increase slightly, but are still lower than the recorded elastic modulus of the hydrogel. Therefore, the hydrogel is still in a plastic regime, but is likely undergoing strain hardening. These results mirror those obtained for the hydrogels during debonding (tensile stress-strain) and suggest that the initial loading conditions are causing the observed mechanical properties during debonding.

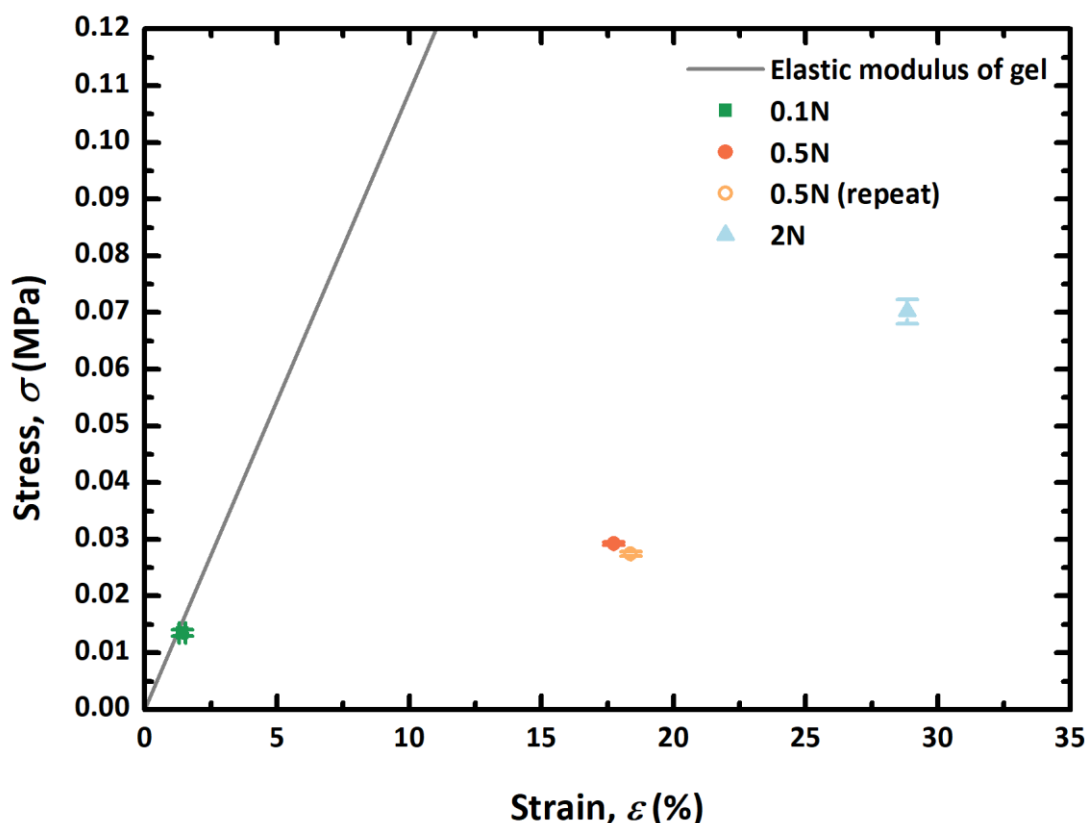


Figure 5.30: Stress-strain characteristics of DN pMAA-pOEGMA hydrogel under varying load.

The stress-strain relation of the pDEAEMA hydrogel is shown in Figure 5.31, where the grey line represents the previously measured modulus³⁴ of the hydrogel. At all three loads, the measured elastic moduli are lower than the recorded elastic modulus of the hydrogel. Therefore, the hydrogel is not behaving elastically at any load, and is in the plastic regime under all loads.

As the load is increased, the measured elastic moduli increase slightly, but are still smaller than the recorded elastic modulus of the hydrogel. This is indicative of the hydrogel undergoing strain hardening. These results do not match those obtained for the hydrogels during debonding (tensile stress-strain) and suggest that the observed mechanical properties during debonding are more effected by the adhesive strength of the bond to the surface.

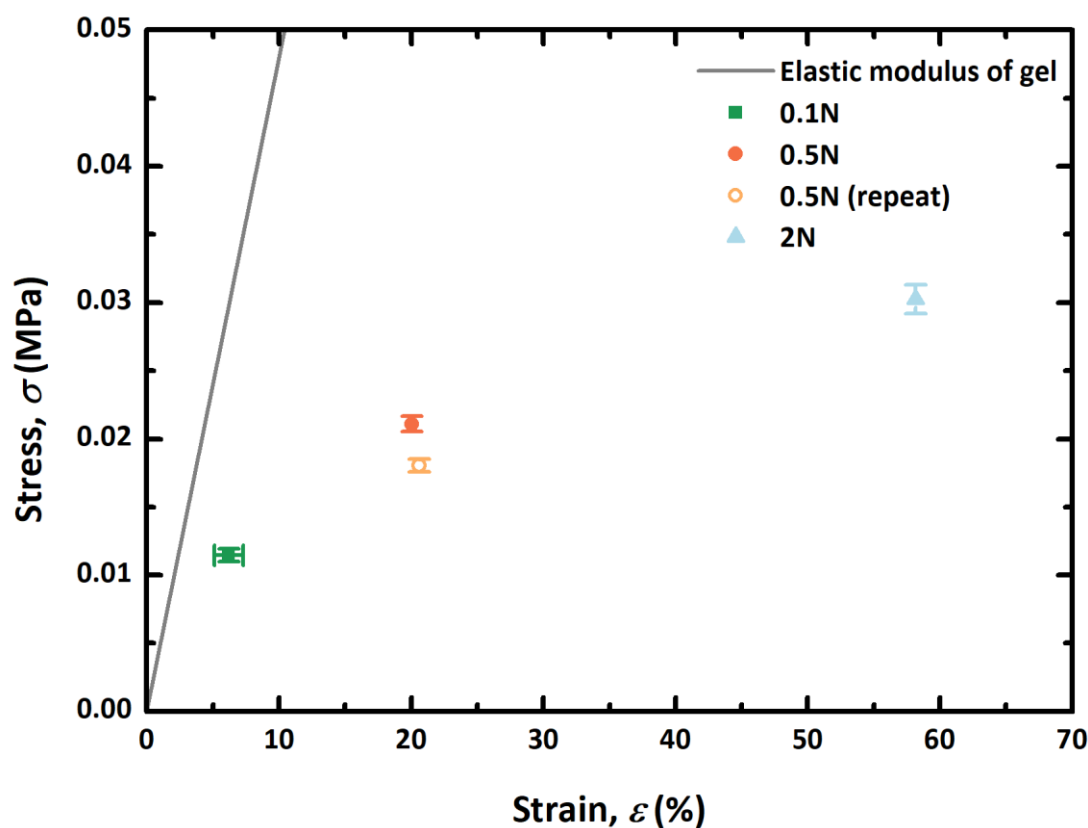


Figure 5.31: Stress-strain characteristics of pDEAEMA hydrogels under varying load.

5.6. Comparison to previous studies

The values obtained for the work of debonding and the maximum stress were plotted against the data reported by La Spina et al.²⁷ and Alfheid et al.³⁴ and is shown in Figure 5.32.

The stresses measured are not overly large, and are similar to those reported by La Spina et al.²⁷ The values for the Work of debonding are greater than those obtained by La Spina et al.²⁷ but less than those reported by Alfheid et al.³⁴ However, the results reported by Alfheid et al.³⁴ were obtained at much larger stresses.

This shows that the data obtained is reasonable within the context of these polyelectrolyte brush systems. These polyelectrolyte brush systems will not give the strongest adhesive bonds, but the data obtained using these calixarene-polyelectrolyte brushes is similar to that for brushes attached to the surface using a chemical bond. This shows that the calixarene is anchoring the brush to the surface as sufficiently as a chemical bond.

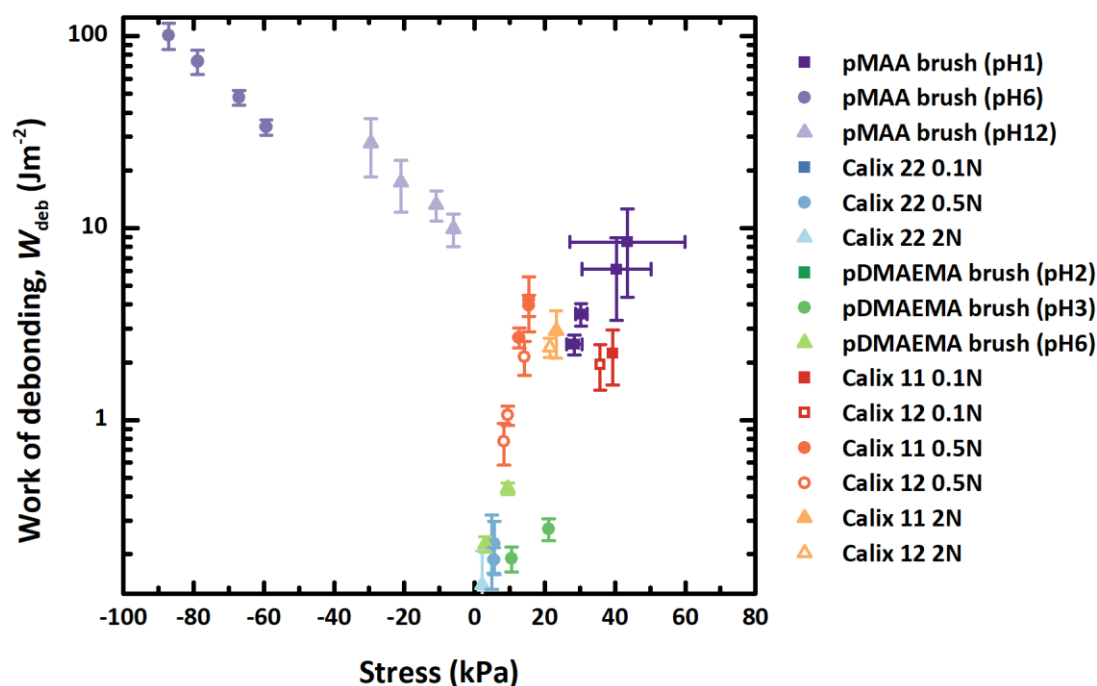


Figure 5.32: Comparison of Work of debonding and stress. pMAA data from Alfheid et al.³⁴, pDMAEMA data from La Spina et al.²⁷

5.7. Summary and conclusions

In this chapter, the monolayers of the calixarene based adhesives, and the associated control compounds, were tested for adhesiveness using a mechanical tester. It was found that the calixarene based adhesives showed a stronger adhesive response compared to the control compounds. This shows that the calixarene anchors the adhesive to the surface, therefore showing that it is the presence of the surface-active group, rather than the formation of an ordered monolayer, which is adhering the polyelectrolyte adhesive to the surface.

Although there was a decrease in the adhesion observed when the measurements were repeated using the same hydrogel on a different part of the surface for most samples, this decrease was relatively small. This shows that the majority of the measured adhesion was due to adhesive failure at the gel-brush interface, rather than the brush-wafer interface. This means that the limiting factor in this system is the polyelectrolyte adhesion, and not the method of attachment of the polymer to the surface. Therefore, the adhesion has not been adversely impacted by transitioning from a chemically tethered brush, which is hard to produce, to a physically tethered brush, which is comparatively easier to deposit.

As the applied load was varied, it was found that the surfaces generally showed a lower adhesive response at low loads, but a predominantly similar adhesive response at high loads. This was attributed to the changing mechanical properties of the hydrogel system for the pDMAEMA surfaces, and the adhesive strength of the bond to the surface for the pMAA surfaces. This shows that the loading conditions impact the observed adhesion of these systems. This could potentially mean that when these materials are further developed for use, substrates would only bond strongly upon a certain pressure, allowing a degree of removability from a loose 'test-fit' before final application of pressure to bond the joint.

The values obtained for work of debonding were shown to be similar to the values obtained by La Spina et al.²⁷ and Alfheid et al.³⁴ This shows that the data obtained is realistic within the context of these polyelectrolyte brush systems. This shows that the calixarene is anchoring the brush to the surface as sufficiently as a chemical bond, again showing that the adhesion has not been adversely impacted by transitioning from a chemically tethered brush.

This fulfils the third objective, to evaluate the adhesive strength of the deposited brushes, and compare the strength of the physical bond to the chemical bond used in 'grafted-from' brushes. It also allows the second thesis question to be answered:

- b) The deposited material is adhesive, and has a similar adhesion to polyelectrolyte adhesives generated using 'grafted-from' techniques.*

6. Polyelectrolyte Multilayers and AFM Force Measurements

6.1. Introduction

This chapter covers the formation of polyelectrolyte films by layer-by-layer (LbL) deposition and the adhesive properties of these films. These films were prepared to investigate a different deposition method, and compare these films to the brushes prepared. This presents a follow-up to the second objective by investigating alternative methods to deposit polymers upon surfaces, and how this compares to the calixarene-adhesives. It also covers an initial investigation of the binding strength of the calixarene to silicon surfaces to expanded upon the observed strength of the calixarene surface tether.

6.2. Formation of polyelectrolyte films by layer-by-layer deposition

To determine the best conditions to prepare the required films, a variety of deposition conditions were tested based upon those reported in the literature.^{238,239} The deposition solution and the deposition time were varied to determine which gave the thickest films. Two types of alternating surfaces were investigated: one where depositions were made onto a silicon wafer (silicon/pDMAEMA/pMAA/pDMAEMA (Si/+/-/+)); and another where depositions were made onto a (3-aminopropyl)triethoxysilane (APTES) functionalised wafer (silicon-APTES/pMAA/pDMAEMA/pMAA (Si-APTES/-/+/-)). This gave both a polycation and a polyanion surface for each layer count. This allowed any effects on adhesion due to the order of film build-up to be studied. For these studies, decyl-pDMAEMA **14** and decyl-pMAA **17** were used for the polyelectrolytes.

The initial deposition solutions were: Milli-Q water, 0.5 M aqueous sodium chloride ($\text{NaCl}_{(\text{aq})}$), and pH 3 (HCl) water. In addition to these solutions, silicon-based depositions also included an alternating deposition between pH 1 (HCl) water (pDMAEMA) and 0.5 M aqueous sodium chloride (pMAA). These solutions were chosen to provide either: a solution in which the polymer was well dissolved (Milli-Q water); a solution where the negative charge of the pMAA carboxylates was partially screened to give the polyanion a more coiled conformation, and therefore a potentially thicker film²³⁸ (0.5 M aqueous sodium chloride); and a solution where the amine residues of the pDMAEMA would have a higher degree of protonation, and increase the number of charge sites to adhere to the native oxide of the silicon wafer or pMAA²³⁹ (pH 1 and 3 (HCl) water).

The thicknesses of the three alternating layers on silicon substrates using these deposition solutions were recorded using ellipsometry (M-2000V Rotating Compensator Ellipsometer, J. A. Woollam Co.), and are shown in Figure 6.1. From this it can be seen that the deposition of pMAA gave the greatest increase in film thickness across all deposition conditions, with the pMAA deposited from 0.5 M NaCl_(aq) giving the largest film thickness. This agrees with the prediction that the electrolyte partially screens the charge on the carboxylate, causing the chain to be deposited in a more coiled conformation, rather than stretched out across the surface.

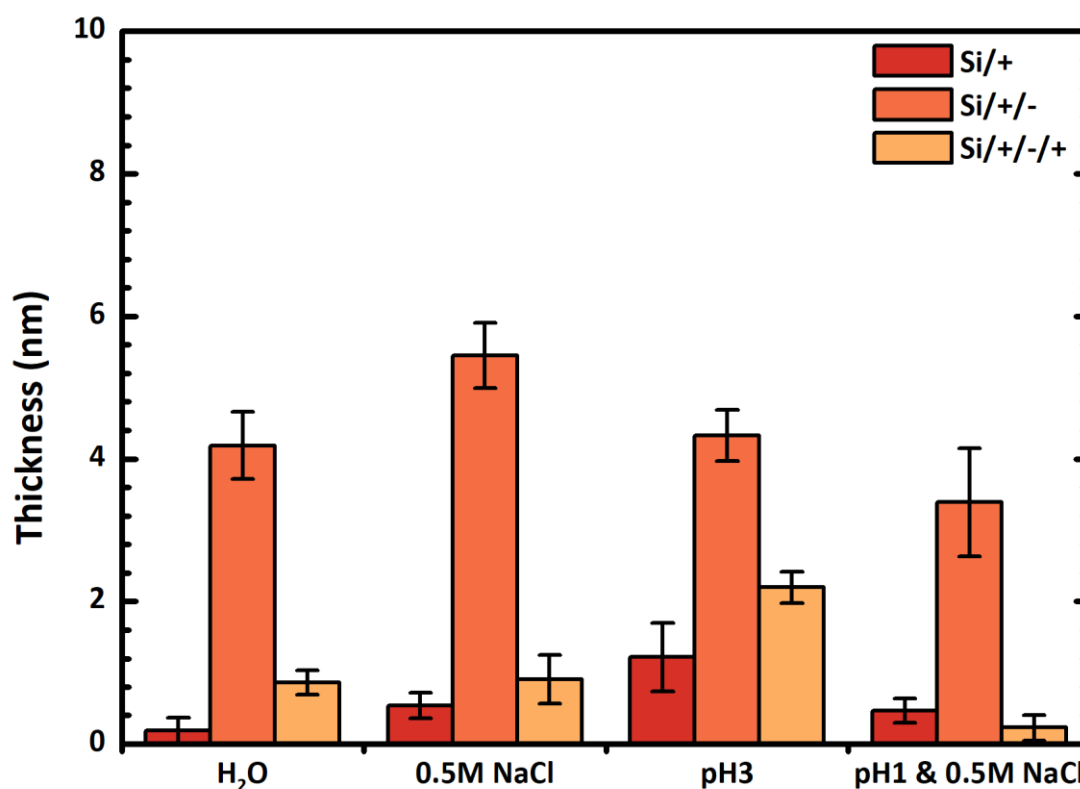


Figure 6.1: Total thickness of layer-by-layer films on silicon, arranged by deposition solution.

Similarly, the pDMAEMA deposited from pH 3, rather than pH 1, water gave the largest film thickness. This is due to the increase in charged residues increasing the adhesion to the native oxide and pMAA at pH 3, but at pH 1 the increased protonation causes the polyelectrolyte to adopt a highly extended conformation, with the pDMAEMA stretched out across the surface.

The overall film thickness dropped between the second and third depositions across all conditions. This is probably due to the weak electrolytic nature of these polyelectrolytes resulting in the desorption of some of the previous layer. When one polyelectrolyte layer binds to the previous layer of opposing charge, there is a degree of charge quenching between the two polyelectrolytes.^{111,112,117} This will reduce the overall charge density at the interface, and results in a weakened interface between the two layers, causing the third treatment to remove the previous layer.

The deposition time was then investigated to determine if a prolonged duration in the deposition solution would result in an increase in the measured film thickness. In addition to the conditions used previously, pDMAEMA was also deposited from dichloromethane. The results are shown in Figure 6.2. From this it can be seen that an increased deposition time does not result in an increase of the observed film thickness.

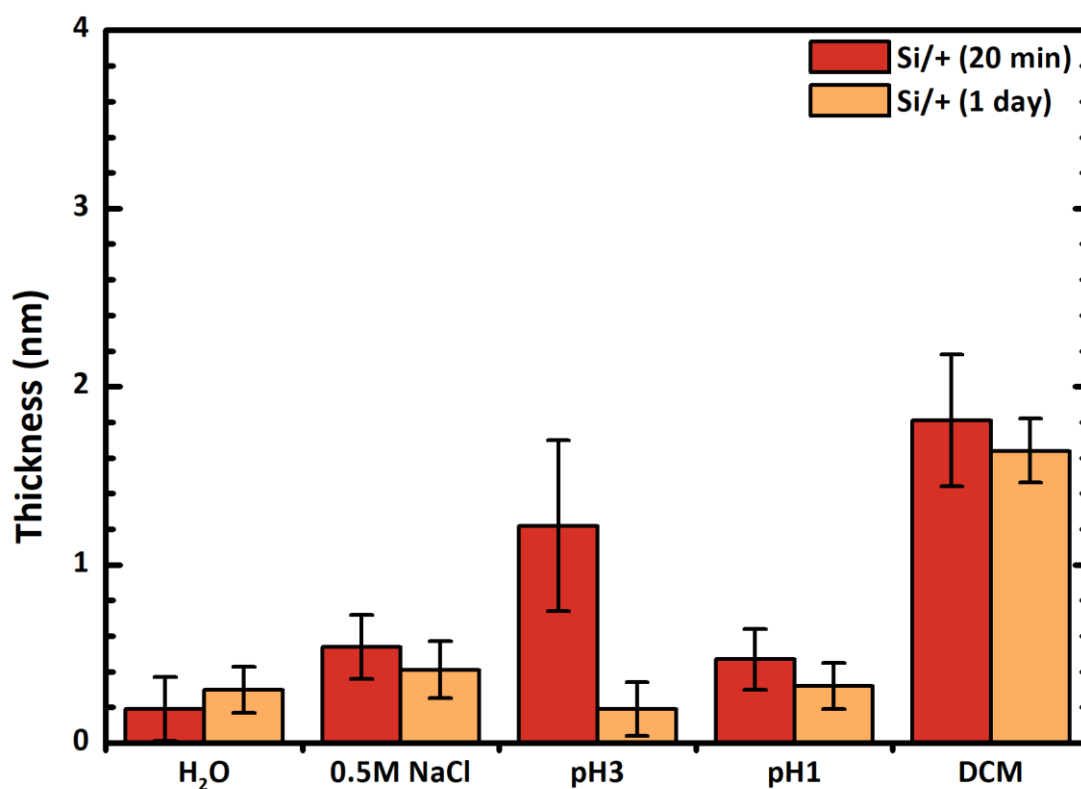


Figure 6.2: Thickness of pDMAEMA deposited on silicon at different deposition times.

The majority of the conditions showed no significant change in the film thickness between the time intervals. Deposition from pH 3 water showed a significant decrease in the observed thickness for the longer time interval, which suggests that the initial film thickness was the kinetic product of deposition, and the film thickness after a longer time interval was a more thermodynamic film thickness. This decrease in film thickness was not observed for pH 1 water, so the transition between film thicknesses at pH 3 may be due to a reorganisation of the polymer from a coiled to an extended conformation on the surface. The reason that this decrease in film thickness was not observed for pH 1 water is that the polymer was already in an extended conformation upon initial deposition due to the increased charge density along the polymer.

Deposition from dichloromethane gave the largest film thickness for pDMAEMA of all the conditions used. As dichloromethane is a good solvent for the neutral pDMAEMA polymer, the chains adopted an expanded self-avoiding walk conformation.¹¹⁵ This resulted in a relatively large radius of gyration, rather than in the more extended directed random walk conformation that occurs when ionised in solution.¹¹⁵

The deposition of pMAA onto APTES was also investigated, with a deposition solution of pMAA in ethanol replacing pDMAEMA in dichloromethane. The results are shown in Figure 6.3. Again, from this it can be seen that an increased deposition time did not result in an increase of the observed film thickness. The majority of the conditions showed no significant change in the film thickness between each of the time intervals, and the three aqueous depositions gave similar film thickness. Deposition from ethanol showed a decrease in the observed thickness for the later time interval, which is likely to have been caused by a collapse of the film due to charge quenching.

Based upon these experiments, films were prepared on both substrates by alternating between pDMAEMA dissolved in dichloromethane and pMAA dissolved in 0.5 M NaCl_(aq) as appropriate. The results for depositions onto silicon substrates are shown in Figure 6.4a, and the results for depositions onto silicon-APTES substrates are shown in Figure 6.4b. These show that the film thickness consistently increased with deposition number, and provided the multilayers desired.

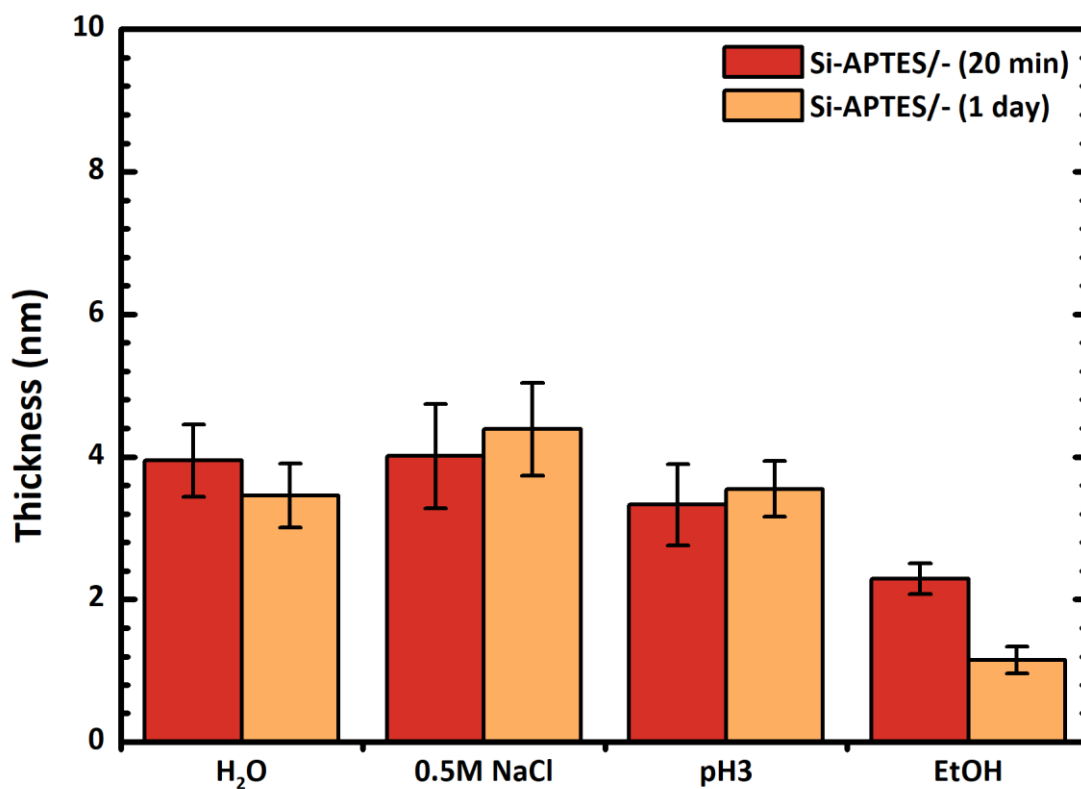


Figure 6.3: Thickness of pMAA deposited on silicon-APTES at different deposition times.

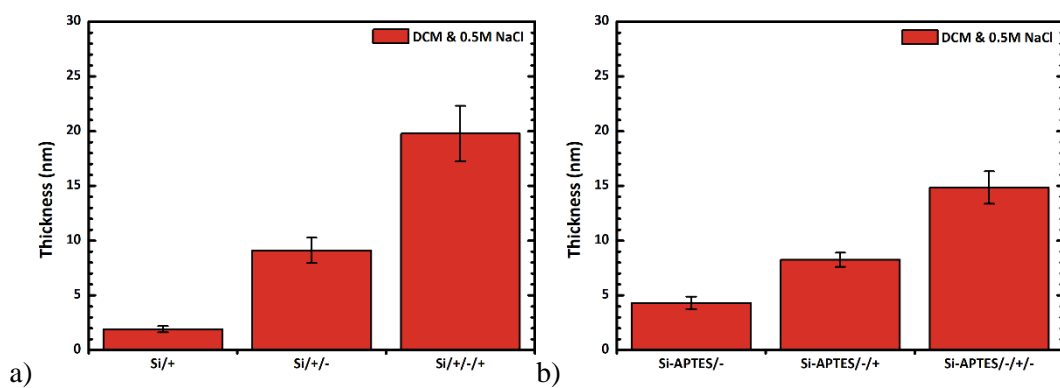


Figure 6.4: Thickness of depositions from dichloromethane and 0.5 M NaCl_(aq). a) Depositions onto silicon, b) Depositions onto silicon-APTES.

6.3. AFM imaging of the deposited polyelectrolyte films

The surface roughness and topography of the deposited materials were determined using Atomic Force Microscopy (Asylum MFP-3D AFM, Bruker). Images were taken in contact mode over a 5 μm square area with a resolution of 256 x 256 points.

The images for the depositions onto silicon substrates are shown in Figure 6.5, Figure 6.6, and Figure 6.7. It can be seen from these images that the depositions gave good surface coverage, without any of the ‘voids’ observed in the calixarene brush layers due to HMDS pre-treatment. Despite the slightly globular appearance of some areas of the depositions, the overall surface roughness was relatively low (Table 6.1). This means the films deposited were even and had a high degree of surface coverage.

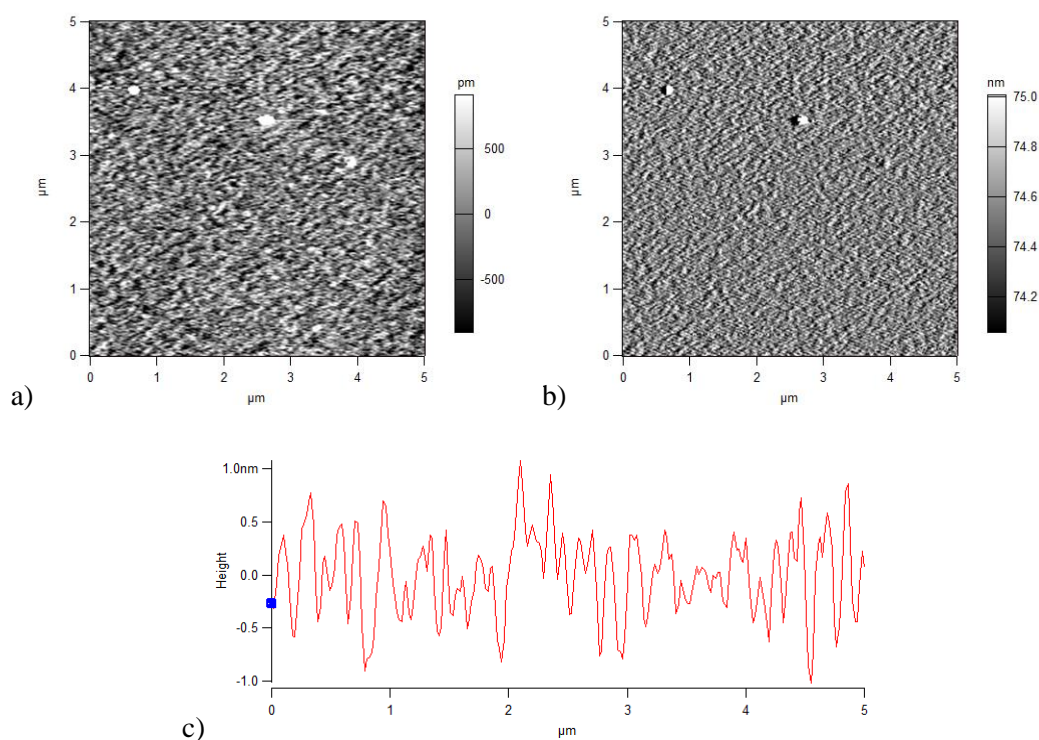


Figure 6.5: AFM images of the first deposited layer onto silicon (Si/+). a) Height retrace, b) Deflection retrace, c) Cross-section showing surface roughness.

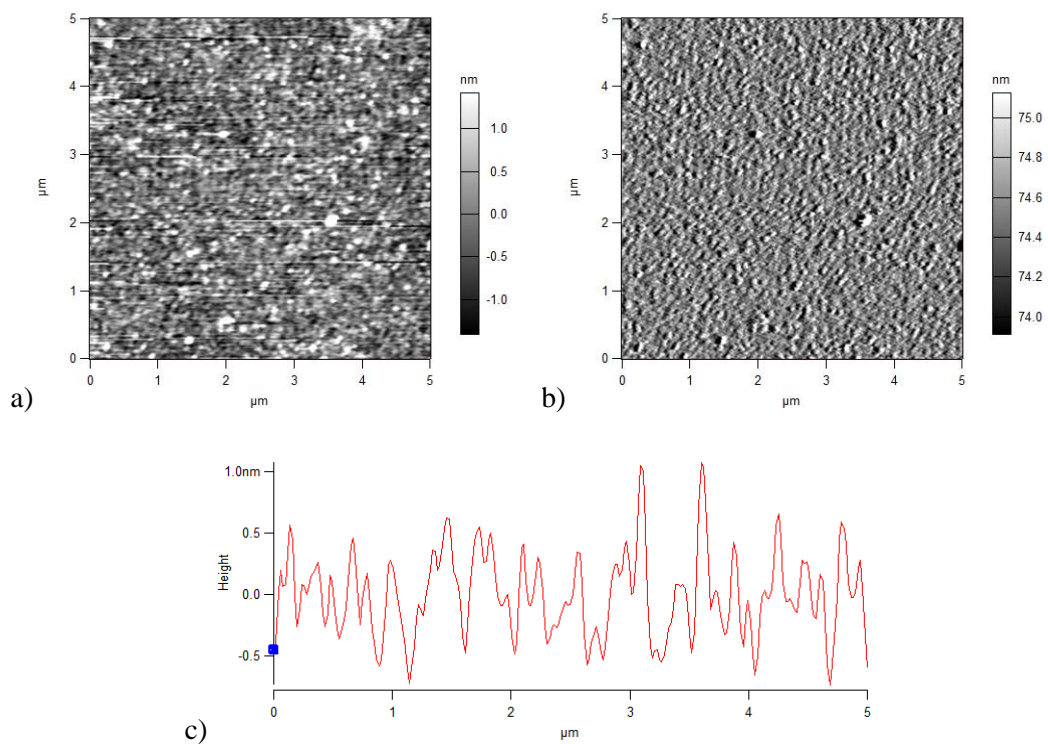


Figure 6.6: AFM images of the second deposited layer onto silicon (Si/+/-). a) Height retrace, b) Deflection retrace, c) Cross-section showing surface roughness.

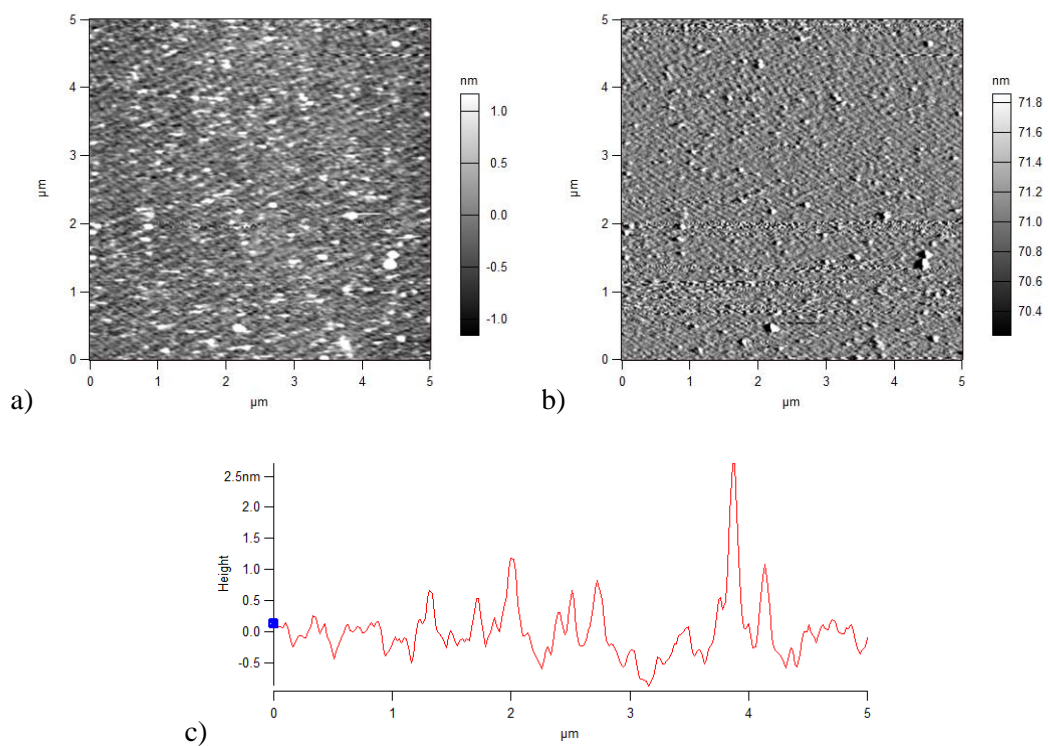


Figure 6.7: AFM images of the third deposited layer onto silicon (Si/+/-/+). a) Height retrace, b) Deflection retrace, c) Cross-section showing surface roughness.

Table 6.1: Surface roughness of layer-by-layer depositions onto silicon.

Deposition	R_a (nm)
silicon/pDMAEMA	0.41 ± 0.01
silicon/pDMAEMA/pMAA	0.39 ± 0.05
silicon/pDMAEMA/pMAA/pDMAEMA	0.36 ± 0.04

The images for the depositions onto silicon substrates are shown in Figure 6.8, Figure 6.9, and Figure 6.10. It can be seen from these images that the depositions gave good surface coverage, again without any of the ‘voids’ observed in the calixarene brush layers. The initial deposition gave a relatively even surface (Table 6.2). However, the second deposition gave a uniformly rough surface comprising of densely packed regular globules. This would appear to show that where a polymer came in the deposition sequence affected the resultant topography of the deposited surface. After deposition of the polycation, the surface roughness decreased and is observed to be smoother than the single polyanion layer by AFM. This is likely to be due to the depositing polymer back-filling the areas between globules to give a more uniform surface.

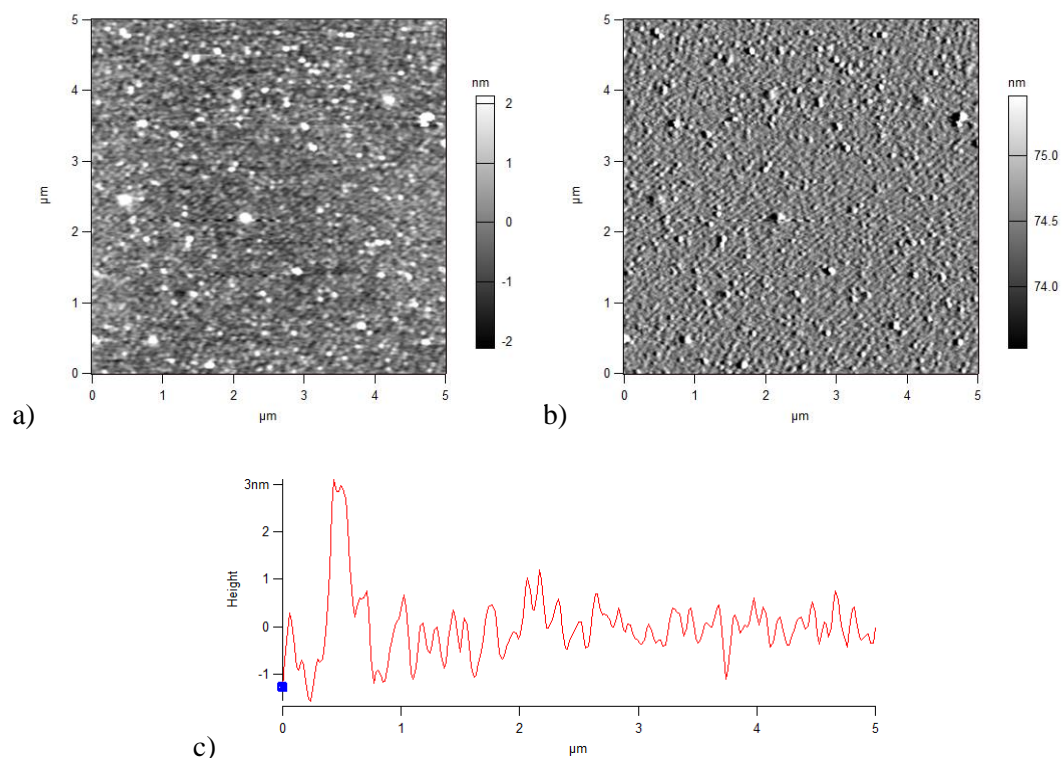


Figure 6.8: AFM images of the first deposited layer onto silicon-APTES (Si-APTES/-). a) Height retrace, b) Deflection retrace, c) Cross-section showing surface roughness.

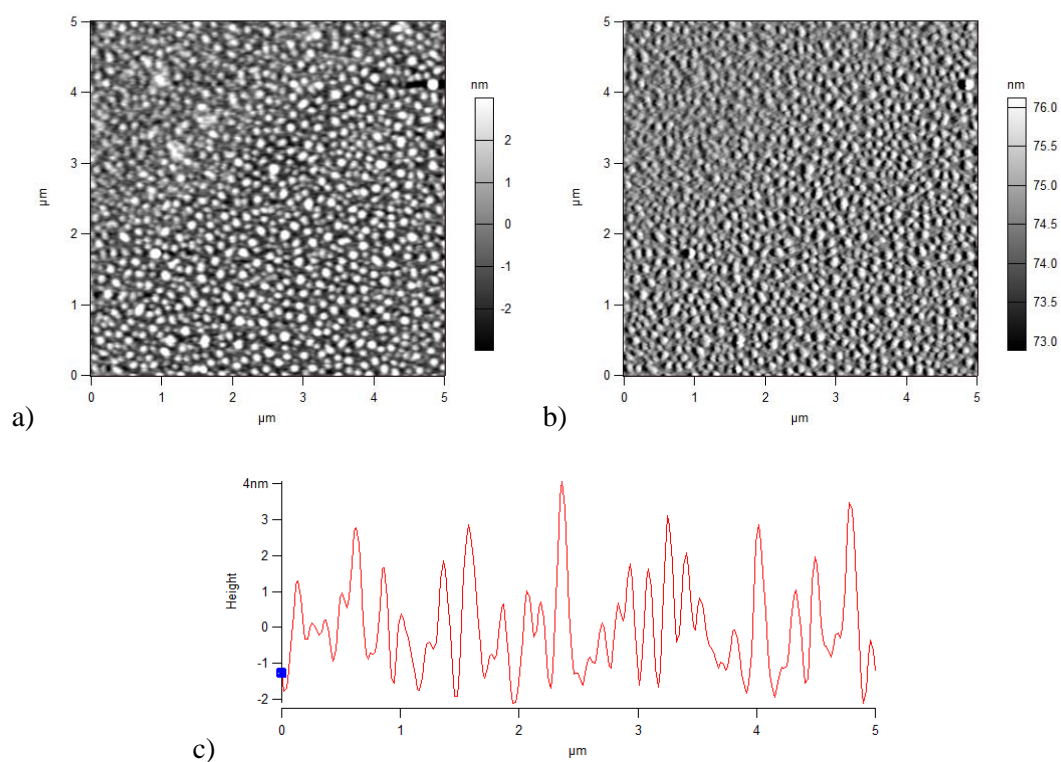


Figure 6.9: AFM images of the second deposited layer onto silicon-APTES (Si-APTES/-/+). a) Height retrace, b) Deflection retrace, c) Cross-section showing surface roughness.

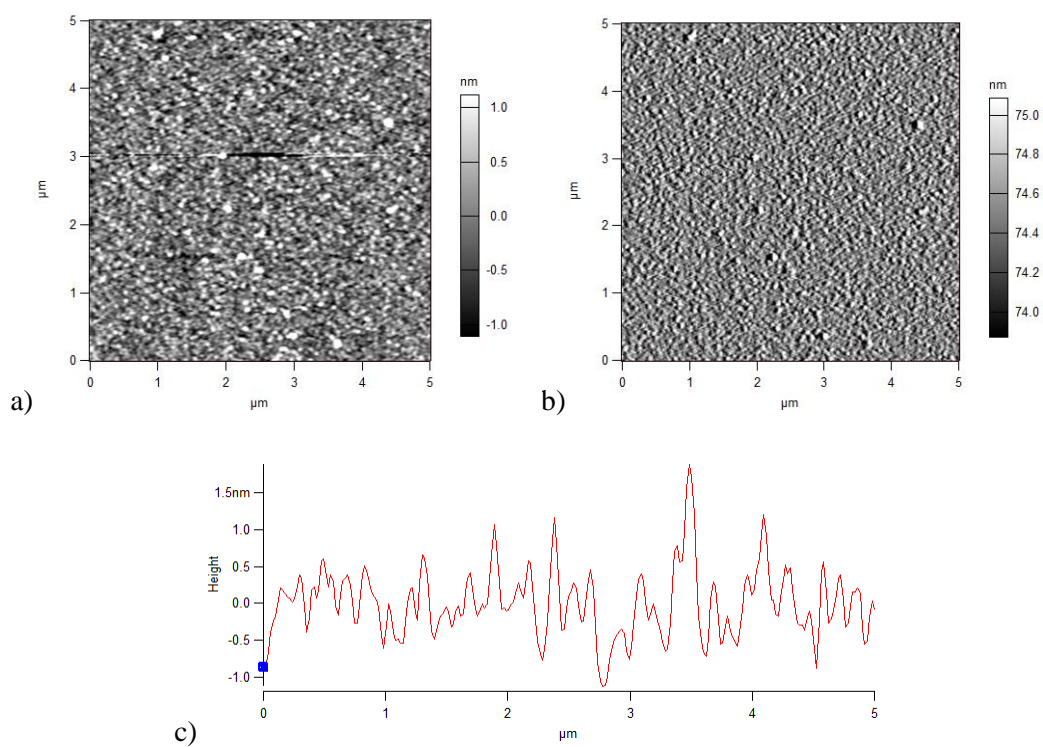


Figure 6.10: AFM images of the third deposited layer onto silicon-APTES (Si-APTES/-/+/-). a) Height retrace, b) Deflection retrace, c) Cross-section showing surface roughness.

Table 6.2: Surface roughness of layer-by-layer depositions onto silicon-APTES.

Deposition	R_a (nm)
Silicon-APTES/pMAA	0.43 ± 0.08
Silicon-APTES/pMAA/pDMAEMA	1.4 ± 0.1
Silicon-APTES/pMAA/pDMAEMA/pMAA	0.27 ± 0.05

6.4. Adhesion measurements of layer-by-layer polyelectrolyte films

The material was tested for adhesion using a mechanical tester (Texture Analyser TA.XTplus, Stable Microsystems), which brought a hemispherical hydrogel of the opposite charge into contact with the sample surface using a standard protocol. A double network (DN) poly(methacrylic acid)-poly(oligo(ethylene glycol) methyl ether methacrylate) (pMAA-pOEGMA) hydrogel and a pDEAEMA hydrogel were used for surfaces. The background adhesive properties of the APTES treated silicon wafers are summarised in Table 6.3.

Table 6.3: Adhesion properties of APTES treated silicon wafers, where -ve is the DN pMAA-pOEGMA gel, +ve is the pDEAEMA gel, F_a is adhesion force, W is work done, σ_{\max} is stress (max), ε_{\max} is strain (max), W_{deb} is work of debonding, and λ is elastic modulus.

Gel	F_a (N)	W ($\times 10^{-3}$ mJ)	σ_{\max} (kPa)	ε_{\max} (%)	λ (MPa)	W_{deb} (J m ⁻²)
-ve	0.14 ± 0.05	8 ± 5	8 ± 3	3.7 ± 0.4	0.21 ± 0.07	0.4 ± 0.3
+ve	0	0	0	0	0	0

The adhesion characteristics of the layer-by-layer depositions onto silicon substrates tested with DN pMAA-pOEGMA hydrogels are shown in Figure 6.11. These measurements showed the expected alternating adhesiveness between the polycation and polyanion surfaces, however there was some adhesive response from the polyanion layer (Si/+/-), suggesting an adhesive contribution from the previous polycation layer. The second polycation layer (Si/+/-/+) showed a lower adhesive response compared to the first (Si/+), which was not expected for a thicker film. The repeat measurements also showed a significant drop in adhesion compared to the initial measurements. These two results suggest that the deposited films were not bound strongly to the previous layer.

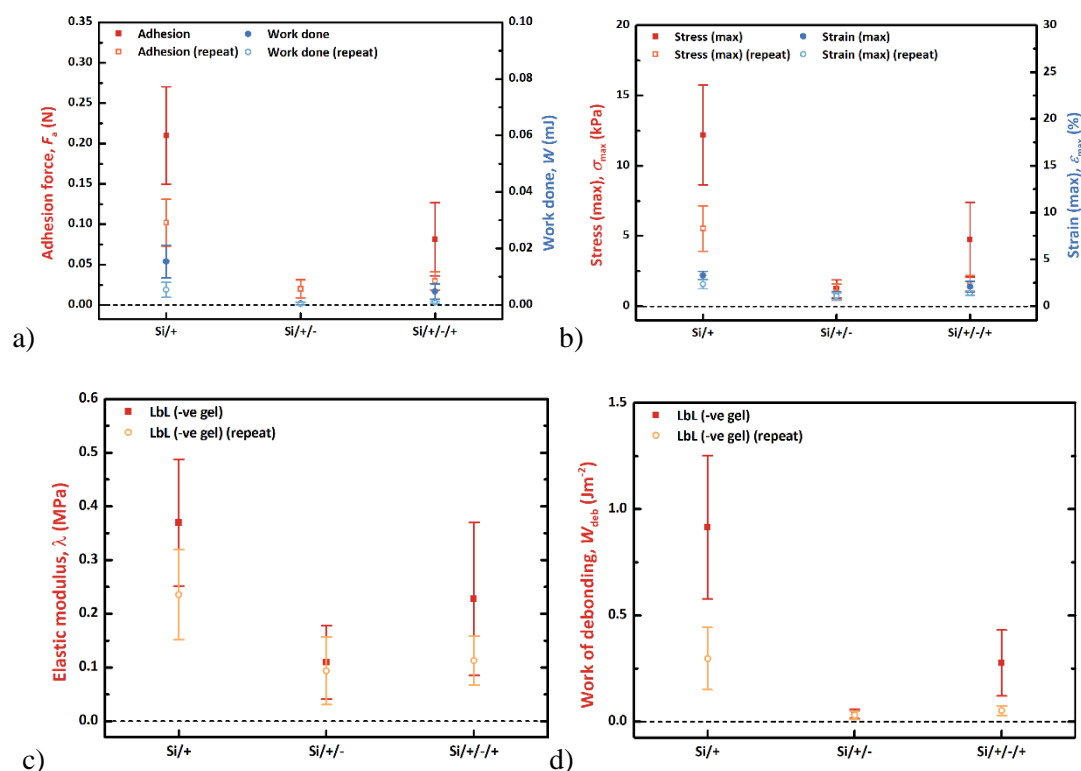


Figure 6.11: Adhesion characteristics of LbL depositions on silicon substrates tested with DN pMAA-pOEGMA hydrogels. a) Adhesion force and work done, b) Stress (max) and strain (max), c) Elastic modulus, d) Work of debonding.

To investigate how strongly the layers are bound to each other, the thicknesses of the layers were measured after the adhesion measurements had been performed. The layers had been immersed in Milli-Q water for the duration of the experiment, and had potentially been ablated by the testing process. The results of this are shown in Figure 6.12. From this it can be seen that the second and third deposited layer thicknesses decreased over the course of the measurements. The loss of material from these surfaces caused the reduction in the measured adhesion observed, both for different layers and between measurements. The thinning of the polyanion layer (Si/+/-) resulted in the small observed adhesion to this layer, as the previous polycation layer (Si/+) was contributing to the adhesion. The reduction in the binding strength of the polyelectrolyte layers to the previous layer is due to the charge quenching between the two polyelectrolytes.^{111,112,117} This reduced the overall charge density at the interface, and resulted in a weakened interface between the two layers.

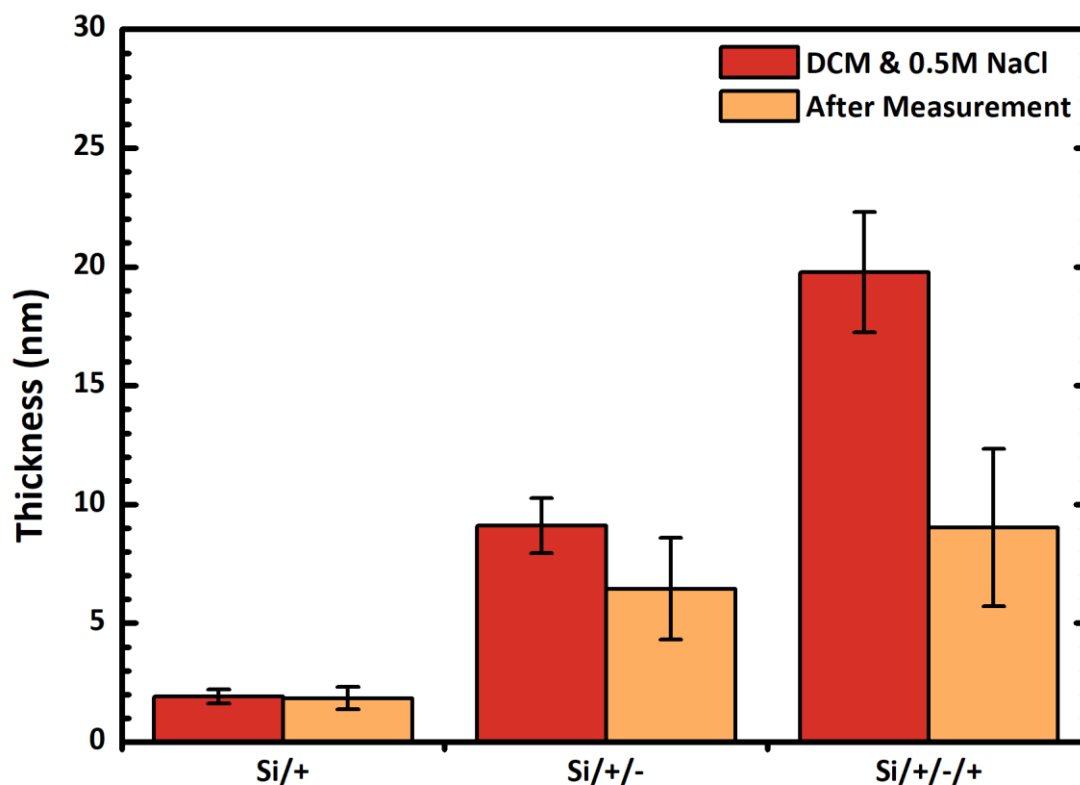


Figure 6.12: Thickness of films deposited onto silicon substrates before and after measurements.

The adhesion characteristics of the layer-by-layer depositions onto silicon substrates tested with pDEAEMA hydrogels are shown in Figure 6.13. None of the deposited layers showed an adhesive response to the pDEAEMA hydrogel. Although this was expected for the polycation layers, the polyanion layer (Si/+/-) would be expected to show an adhesive response. This lack of adhesion is possibly due to the loss of material from the surface, as shown in Figure 6.12 and by the adhesive response of this layer to the DN pMAA-pOEGMA hydrogel (Figure 6.11).

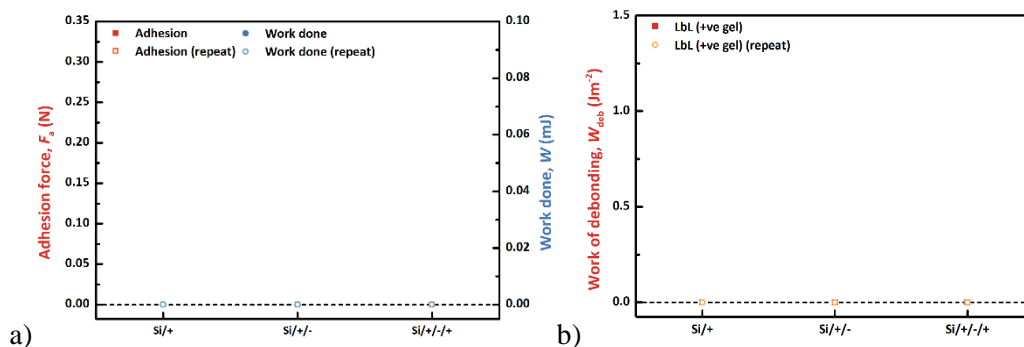


Figure 6.13: Adhesion characteristics of LbL depositions on silicon substrates tested with pDEAEMA hydrogels. a) Adhesion force and work done, b) Work of debonding.

The adhesion characteristics of the layer-by-layer depositions onto silicon-APTES substrates tested with DN pMAA-pOEGMA hydrogels are shown in Figure 6.14. These measurements showed the expected alternating adhesiveness between polyanion and polycation surfaces, however there was some adhesive response from the polyanion layers, suggesting an adhesive contribution from the previous polycation layer or APTES functionalised surface. The repeat measurements also showed a significant drop in adhesion compared to the initial measurements for the polycation surface (Si-APTES/-/+). This suggests that the deposited films were not bound strongly to the previous layer, as shown for the silicon substrate depositions.

To see if the same desorption was occurring for the silicon-APTES surfaces, the thicknesses of the layers were again measured after the adhesion measurements had been performed. The results of this are shown in Figure 6.15. This also shows that the deposited layer thicknesses decreased over the course of the measurement, and that the loss of material from these surfaces caused the reduction in the measured adhesion.

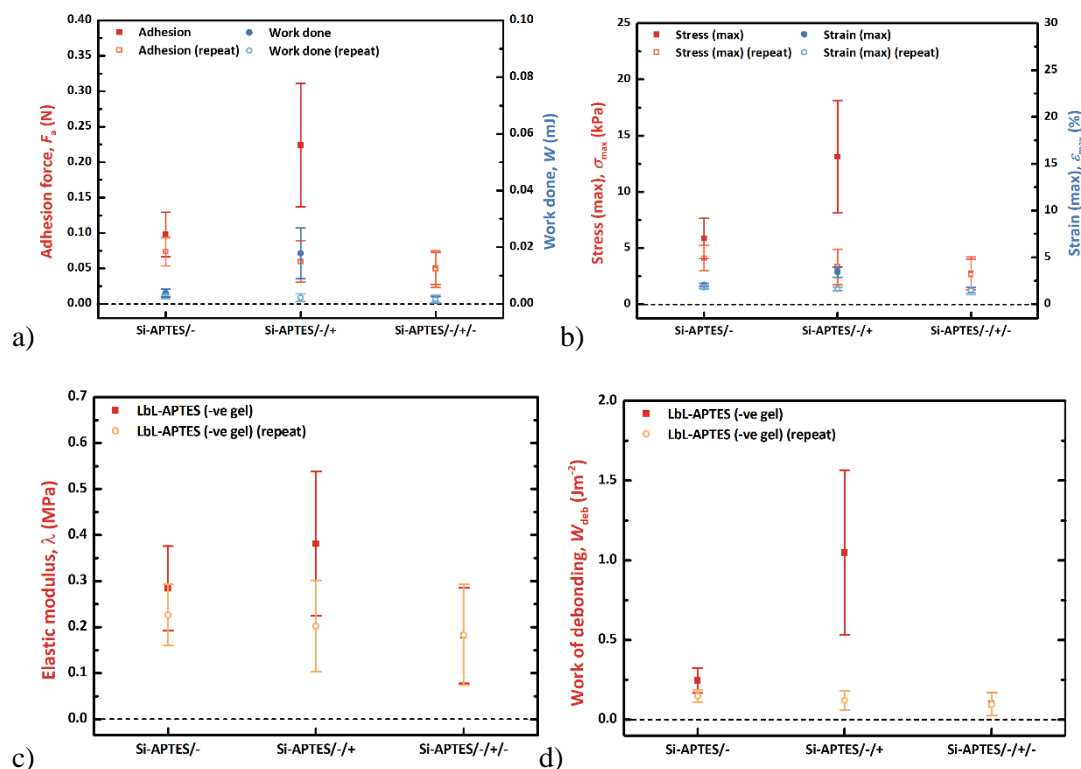


Figure 6.14: Adhesion characteristics of LbL depositions on silicon-APTES substrates tested with pDEAEMA hydrogels. a) Adhesion force and work done, b) Stress (max) and strain (max), c) Elastic modulus, d) Work of debonding.

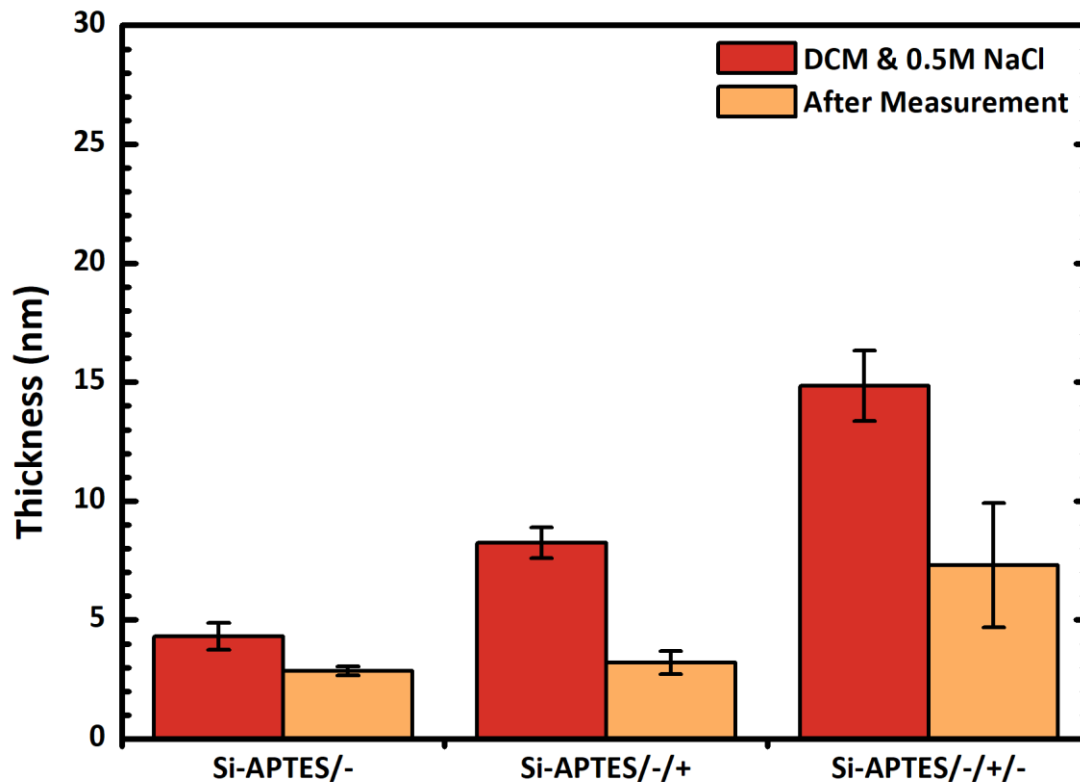


Figure 6.15: Thickness of films deposited onto silicon-APTES substrates before and after measurements.

The adhesion characteristics of the layer-by-layer depositions onto silicon-APTES substrates tested with pDEAEMA hydrogels are shown in Figure 6.16. None of the deposited layers showed an adhesive response to the pDEAEMA hydrogel. Although this was expected for the polycation layer, the polyanion layers (Si-APTES/- and Si-APTES/-/+/-) would be expected to show an adhesive response. Again, this lack of adhesion was possibly due to the loss of material from the surface, as shown in Figure 6.15 and by the adhesive response of these layers to the DN pMAA-pOEGMA hydrogel (Figure 6.14).

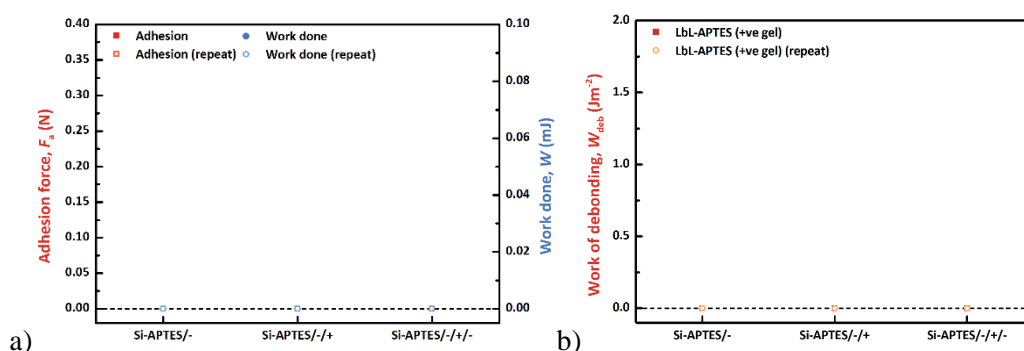


Figure 6.16: Adhesion characteristics of LbL depositions on silicon-APTES substrates tested with pDEAEMA hydrogels. a) Adhesion force and work done, b) Work of debonding.

The overall adhesive strength of these layers is not as strong as the deposited calixarene-based adhesives. The strongest work of debonding for Si-APTES/-/+, $W_{deb} = 1.0 \pm 0.5 \text{ J m}^{-2}$, is much smaller than the strongest work of debonding for Boc-calixarene-pDMAEMA **11**, $W_{deb} = 4.0 \pm 0.5 \text{ J m}^{-2}$. This further demonstrates that the calixarenes are strongly anchoring the polyelectrolytes to the substrate, and that this compensates for any reduction in surface coverage.

6.5. AFM force measurements of calixarene bonding strength

To investigate the binding strength of the calixarene to silicon surfaces the calixarene needed to be deposited on a surface ‘bowl up’, so the adhesiveness of the upper rim could be measured using AFM force measurements. To do this, a tetra-functionalised calixarene was required. This was prepared by a similar method to the monofunctional calixarene,¹⁴⁶ but only the undecenal aldehyde was used, to give the C-decenyyl calix[4]resorcinarene **36** (Figure 6.17).

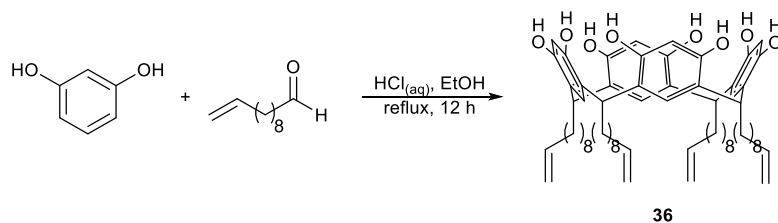


Figure 6.17: Synthesis of C-decenylyl calix[4]resorcinarene **37**.

The phenolic residues on the upper annuls were protected with *tert*-butoxycarbonyl (Boc) using the same procedure as for the monofunctionalised calixarene,¹⁷⁷ to give the Boc-C-decenylyl calix[4]resorcinarene **37** (Figure 6.18).

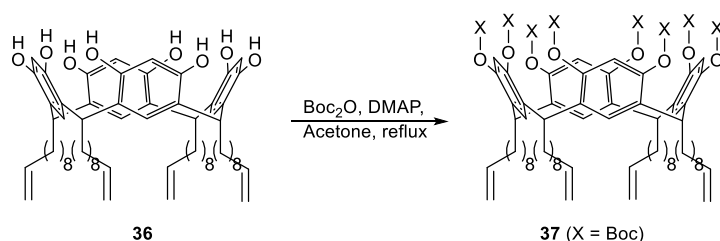


Figure 6.18: Synthesis of Boc-C-decenylyl calix[4]resorcinarene **37**.

The terminal alkenes were then converted to hydroxyl groups by hydroboration with borane-tetrahydrofuran complex ($\text{BH}_3 \cdot \text{THF}$), followed by a basic oxidative workup,¹²⁹ to give the Boc-C-hydroxydecyl calix[4]resorcinarene **38** (Figure 6.19).

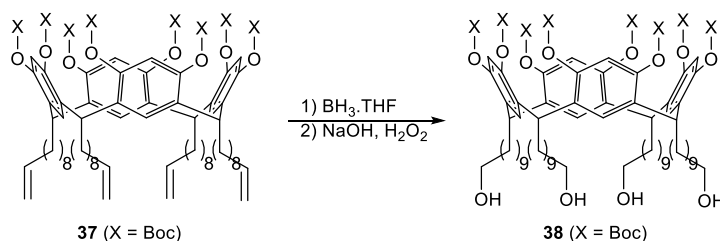


Figure 6.19: Synthesis of Boc-C-hydroxydecyl calix[4]resorcinarene **38**.

The hydroxyl groups were then functionalised using 3-(triethoxysilyl)propyl isocyanate in dichloromethane with triethylamine to give the APTES functionalised calix[4]resorcinarene **39** (Figure 6.20).

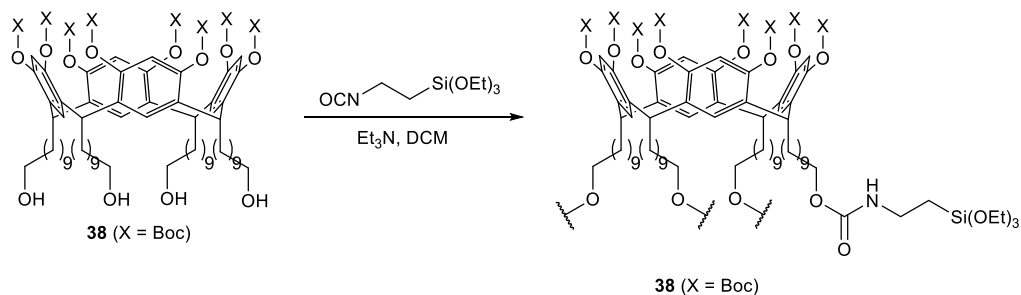


Figure 6.20: Synthesis of APTES calix[4]resorcinarene **39**.

Surfaces of APTES functionalised calix[4]resorcinarene **39** were prepared by deposition from ethanol followed by annealing at 120 °C. This annealing step insures that the silyl ethers reacted with the surface oxide and each other to chemically bind to the surface. It also insured that the Boc protecting groups were removed by thermolysis, giving the required surface of calixarenes attached to a surface ‘bowl-up’ with the phenolic residues on the upper annuls exposed.

The thickness of the deposited APTES-calixarene was measured by ellipsometry, and was 2.20 ± 0.01 nm. The surface roughness and adhesive force of the deposited materials were determined using atomic force microscopy (Asylum MFP-3D AFM, Bruker). The images are shown in Figure 6.21. It can be seen from these images that the surface had numerous irregular features, rather than a smooth continuum. These features have an average diameter of 120 ± 20 nm, and an average height of 13 ± 4 nm. This leads to the observed surface roughness of $R_a = 2.48 \pm 0.06$ nm. These features are attributed to aggregation of the APTES-calixarene. This aggregation is caused by residual water in the deposition solution causing the silyl ethers to hydrolyse. The resulting silanols can react further with other silyl ethers to cross link the material in solution or on the surface. As the APTES-calixarene contains four silyl ethers, it could readily cross link with other molecules and itself to form the observed aggregates.

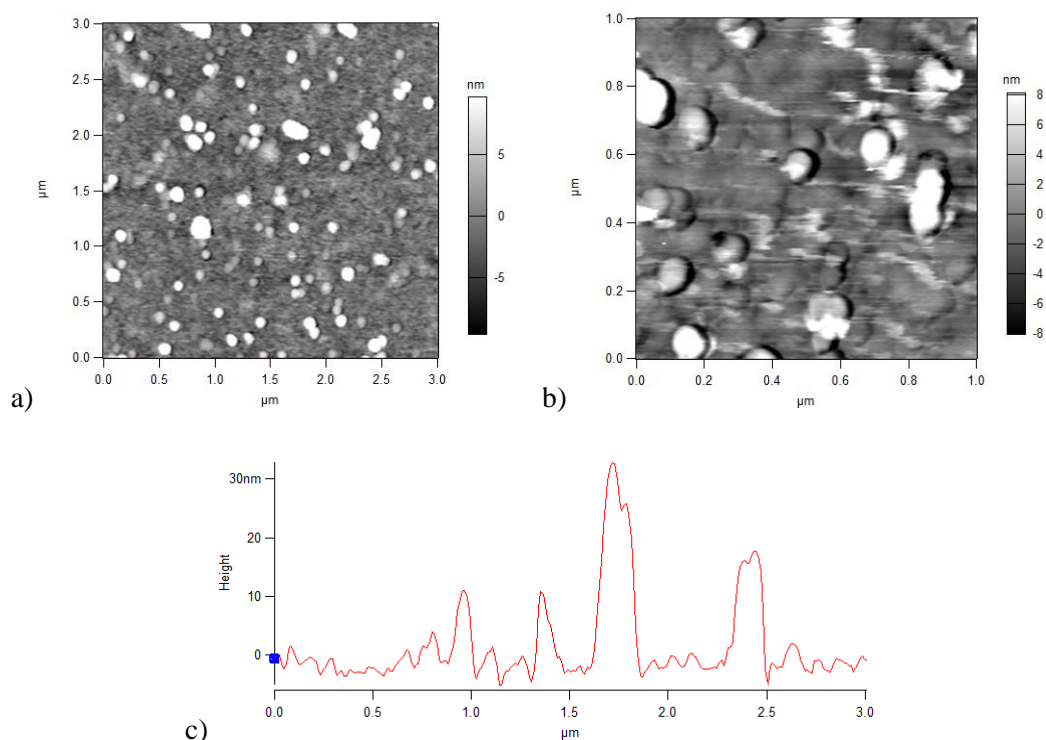


Figure 6.21: AFM images of APTES-calixarene treated wafers. a) Height retrace, 3×3 μm, b) Height retrace, 1×1 μm, c) Cross-section showing feature heights (3×3 μm).

The adhesive force of the deposited surface was measured using force mapping under aqueous conditions. The force map of a 5×5 μm area is shown in Figure 6.22a, and a histogram of the measured forces is shown in Figure 6.22b. The data were fitted using a Gaussian distribution, from which the average adhesion force was determined to be 1.67 ± 0.01 nN, with a standard deviation of 0.89 nN. The thermodynamic work of adhesion (W_a) can be calculated from JKR theory using^{173,240}

$$W_a = \frac{2F_{ad}}{3\pi R} \quad (6.1)$$

where F_{ad} is the adhesion force and R is the tip radius. Taking the tip radius to be 20 nm,²⁴¹ the thermodynamic work of adhesion was estimated to be 17.7 ± 0.1 mJ m⁻². This is similar to the work of adhesion measured for a hydrophobic interaction between an alkyl SAM and polypropylene in water (14 ± 5 mJ m⁻²).²⁴⁰ However, the surface deposited here was not uniform, so is not an accurate representation of the deposited surface. Therefore, future work could be done to determine the adhesive strength of a calixarene surface using a more uniform surface, which would better represent the deposited calixarene-adhesive. Nevertheless, the fact that these surfaces show an adhesive response under non-ideal conditions indicates that the calixarene will still be adhesive in more ‘real-world’ environments.

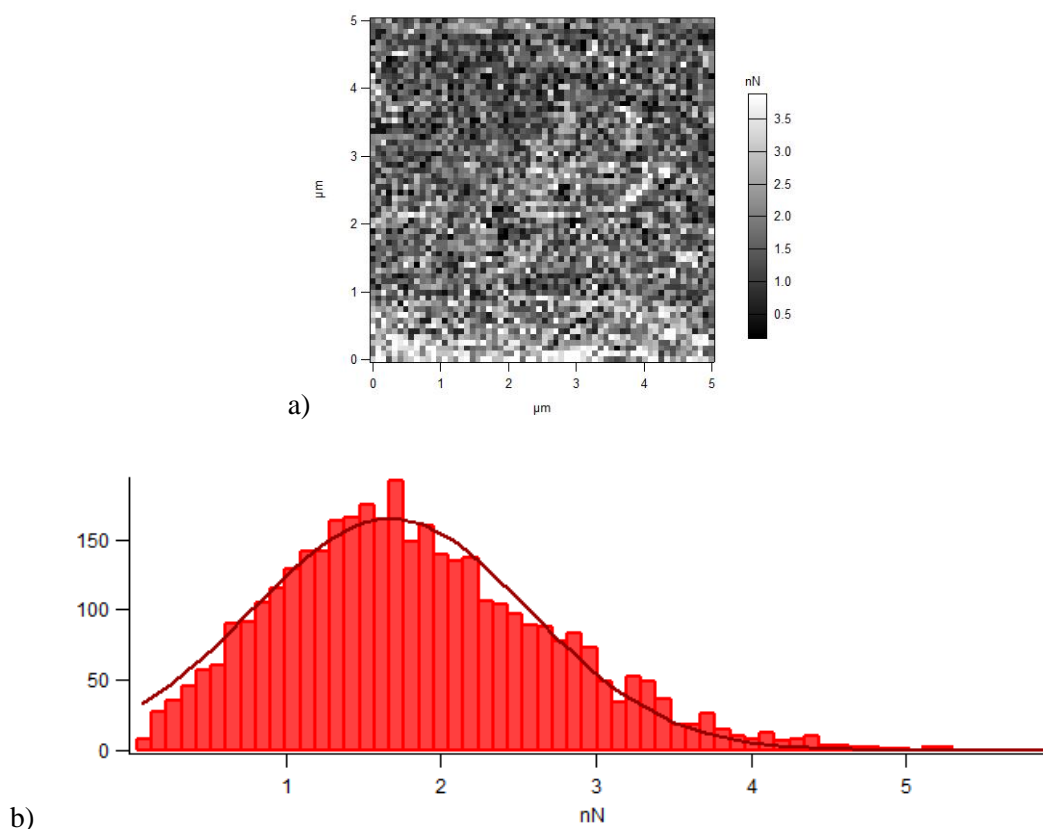


Figure 6.22: Force mapping of APTES-calixarene surfaces. a) Force map of APTES-calixarene surface (62 x 62 points), b) Histogram of pull-off forces for APTES-calixarene surfaces with Gaussian fit.

6.6. Overall comparison of adhesives

A comparison matrix for all of the systems studied in this thesis is shown in Table 6.4. Each category was ranked independently, and colour coded from worse (red) to best (green). Where a category had a measured value (thickness and adhesion), these were ranked from smallest (red) to largest (green). For categories which did not have a directly measured value (synthesis, deposition, attachment, coverage), they were ranked based upon overall performance. Synthesis was ranked based upon number of synthetic steps, deposition was ranked based upon the difficulty of the technique, attachment was ranked based upon the observed relative strength of the bond to the surface, and coverage was ranked based upon the observed number and size of any defects or voids.

The relative importance of the categories is not represented, so what is coded as ‘good’ may not be as important as what is coded as ‘bad’ in a different category. However, this matrix still gives an overall indication of the relative strengths and weakness of the materials discussed in this thesis.

Table 6.4: Comparison matrix for all adhesive systems investigated, and for the systems present in the literature.^{27,33,34} Compounds were ranked either by the measured value for each category, or qualitatively, for example based upon difficulty of deposition.

	Synthesis	Depositon	Attachment	Coverage	Thickness	Adhesion
brush-pDMAEMA	Light Green	Red	Dark Green	Dark Green	Dark Green	Dark Green
brush-pMAA	Yellow	Red	Dark Green	Dark Green	Dark Green	Dark Green
calix 11	Orange	Light Green	Light Green	Light Green	Orange	Light Green
calix 12	Orange	Light Green	Light Green	Light Green	Orange	Light Green
calix 22	Red	Light Green	Light Green	Light Green	Light Green	Orange
decyl 14	Light Green	Light Green	Orange	Red	Yellow	Yellow
decyl 17	Red	Light Green	Orange	Red	Red	Red
LbL	Light Green	Light Green	Red	Light Green	Red	Orange
PVAc	Light Green	Light Green	Red	Light Green	Light Green	Red

- Chemically tethered brushes had the strongest adhesion and attachment to the surface. However, they are the hardest to apply to a surface, as they must be prepared in situ under stringent laboratory conditions (inert/deoxygenated atmosphere, heavy metals in solution). This means they cannot be used as readily in a commercial environment, as these conditions preclude the use of large components, and would require specialist knowledge to prepare.
- The calixarene adhesives were much easier to apply to a surface, and the anchor to the surface was strong enough not to impact the observed adhesion. The adhesion for calix **11** and **12** was also similar in strength to the chemically tethered brushes in the literature. This means that although the adhesive compound used to apply to the surface was more difficult to prepare, and had a slightly reduced adhesion, this was more than compensated for by the ease of deposition when compared to preparing the brush in situ.
- The calixarene-adhesive calix **22** gave good deposited layers, but was much less adhesive than the chemically tethered brush. This was attributed to the calix **22** brushes being shorter than those of the chemically tethered brush, as this reduces the adhesion of brushes.
- Although the deposition of the calixarene adhesives was much easier than preparing the adhesive in situ, it still required the use of specialised equipment (Langmuir trough). However, this technique is fairly straightforward, and can be used to produce multiple deposited surfaces after initial set up. It would also only require a technical level of knowledge to prepare these films.

-
- Nevertheless, alternative methods exist to deposit polymers upon surfaces. One such method investigated was the use of layer-by-layer deposition. It can be seen from the comparison matrix that although this technique is one of the easiest to deposit material (deposition from solution), the overall performance was very poor. This was attributed to the weakened electrostatic interactions between layers, caused by charge quenching. This shows that while it may be easier to form the multilayers in the first instance, this is negated by the much-reduced adhesion and strength of attachment.
 - It is also worth noting that the LbL deposition also gave polyelectrolyte in a different conformation to the calixarene and literature adhesives. The LbL deposition gave films of material likely organised as polymer chains extended along the substrate surface, or as deposited ‘mushroom’ like polymers, whereas the calixarene and literature adhesives were both deposited as much more ordered brushes. It is tempting to draw the conclusion from this that it is the brush conformation that was affecting the difference in adhesion between LBL and Langmuir-Schaefer deposited material. However, the two polymers were anchored to the substrate in different ways, and to different substrates, so direct comparison of the polymer conformation should be avoided.
 - Nevertheless, the initial LBL deposition can be compared to the decyl-pDMAEMA **14** control adhesive deposited by Langmuir-Schaefer. This showed that, under these circumstances, the LbL material gave a much stronger adhesion. This implies that the decyl-pDMAEMA binds to the native oxide surface with a higher strength than it does to the HMDS treated wafer. This is reasonable considering that in the former case the interaction is electrostatic, and in the later it is hydrophobic.
 - This poor surface anchorage is further exemplified by the comparison between the decyl-adhesives and calixarene-adhesives deposited by Langmuir-Schaefer. Despite having a similar deposition, the decyl-adhesives performed considerably worse than the calixarene-adhesives. This shows that the calixarenes were anchoring the adhesives much more effectively than the decyl chains. This is further supported by, as mentioned previously, observation that the calixarene surface anchor is strong enough not to impact the adhesion.

- Spin-coated PVAc provided a comparison to a traditional neutral adhesive. It was the easiest to prepare, as it is commercially available, and once the correct conditions had been determined, spin-coating produced films of the desired thickness quickly and easily, and with a high degree of surface coverage. However, this ease of access is offset by the poor adhesive performance of the films, which was due to the fairly weak adhesion both between the film and hydrogel, and between the film and the substrate. This shows that it is the electrostatic interactions, combined with an adequate surface anchor, that generate the adhesive response measured, rather than the presence of a polymer film.
- Of all the adhesive investigated, calix **11** was deemed the best because it gave a similar adhesion to the existing chemically tethered brushes, but had a much easier deposition, meaning a very similar result can be achieved using a material which is much more accessible within a commercial context.

6.7. Summary and conclusions

Alternating layers of polyelectrolytes were prepared using layer-by-layer deposition. The best deposition conditions were determined to be a combination of deposition from organic and salt solutions, as these gave the thickest films. These films also did not lose material upon subsequent depositions, so could be used to study the adhesion of various numbers of deposited layers, to determine how the increased multilayering impact the adhesion. These depositions gave multilayer films of similar thicknesses to calixarene-adhesives, so provide a useful comparison of how the deposition conditions affect the adhesion of a polyelectrolyte film of the same thickness. The multilayers and were shown to have a better surface coverage than some of the calixarene-adhesives as determined by AFM, which means there is a higher density of potentially adhesive molecules for the hydrogel to interact with, which should yield an improved adhesion.

Although these depositions resulted in an increase in final film thickness and surface coverage, the adhesion was much smaller than that recorded for the calixarene-based adhesives. This shows that the calixarenes are strongly anchoring the polyelectrolytes to the substrate, compensating for any reduction in surface coverage. Therefore, the calixarene-adhesives provide the best cost-benefit ratio compared to the other systems examined in thesis.

Calixarenes were also deposited 'bowl up' onto silicon wafers and the adhesive strength was measured using AFM. Although the surface deposited was not uniform, future work could be done to determine the adhesive strength of a calixarene surface using a more uniform surface. These surfaces were found to be covered in aggregations of the deposited material, and had a measured work of adhesion similar to hydrophobic interactions. Nevertheless, the fact that these surfaces show an adhesive response under non-ideal conditions indicates that the calixarene will still be adhesive in more 'real-world' environments.

7. Conclusions and Future Work

7.1. Introduction

Polyelectrolyte adhesives have been shown to bind reversibly and repeatedly using pH as an external stimulus.^{33,34} However, like many current switchable adhesives,^{27–29} they require laboratory techniques for preparation at the surface, including anhydrous and inert conditions.^{27,34} In this project, a new type of adhesive with the potential for pH switching has been developed and tested for adhesive strength. Use of a calix[4]resorcinarene functionalised with a polyelectrolyte allowed adhesive material to be applied directly to a substrate in contrast to adhesives that have been synthesised in-situ previously. This new deposited material was shown to have a similar adhesive strength to material generated in-situ, demonstrating that calixarene anchors the polyelectrolyte to the surface as sufficiently as a chemical bond. Therefore, the adhesion has not been adversely impacted by transitioning from a chemically tethered brush to a physically tethered brush, which is comparatively easier to deposit.

This thesis posed the questions:

- d) Can a calix[4]resorcinarene be used as a surface active head group for the direct attachment of polyelectrolyte adhesives to surfaces?*
- e) Is the deposited material adhesive? If so, how does it compare to polyelectrolyte adhesives generated using ‘grafted-from’ techniques?*

The key objectives for this project were:

- *Synthesis of mono-functional calixarenes, which can then be used to grow pDMAEMA and pMAA.*
- *Deposition of these adhesives to form an ordered brush monolayer using a physical bond.*
- *Evaluation of the adhesive strength of the deposited brushes, and comparison of the strength of the physical bond to the chemical bond used in ‘grafted-from’ brushes.*

In addition to these objectives, a comparison to material deposited by layer-by-layer deposition, and the strength of the calixarene head group, were explored over the course of this investigation. The material deposited by layer-by-layer provided a comparison with an alternative deposition mechanism to the one used for the calixarene-adhesives, and the investigation of the strength of the calixarene head group expanded upon the observed strength of the calixarene surface tether.

7.2. Findings and Implications

A new synthetic route was developed to grow a variety of polyelectrolyte chains from a calix[4]resorcinarene, which is useful for functionalising polar surfaces, and has been shown to form self-assembled monolayers.^{153,155} Preparation of the polybasic adhesive using ATRP proved straightforward. However, preparation of the polyacidic adhesive required use of a protected monomer precursor for polymerisation. An alternative route using RAFT polymerisation was also developed, which avoided the requirement of a protected monomer. In addition to the calixarene-based material, two control compounds, using decane instead of calixarene, were also prepared using the same methodologies. This shows that:

a variety of functional polymers can be selectively grown from a calixarene to give a polyelectrolyte adhesive which can be directly deposited onto a substrate.

It was found that self-assembly from solution did not give an adequate grafting density for the required brush or brush-like structures desired. It was observed that:

calixarene-adhesives do not form brushes by spontaneous assembly from solution due to kinetic and thermodynamic barriers for grafting-to substrates from solution.

Consequently, an alternative deposition method was required. Instead, Langmuir-Schaefer deposition was used to generate films with high grafting densities, generating brush or brush-like films. This successfully answers the first research question a) by demonstrating that a calix[4]resorcinarene can be used as a surface active head group for the direct attachment of polyelectrolyte adhesives to surfaces, and shows that:

kinetic and thermodynamic barriers to deposition can be overcome using pre-ordering of the monolayer as a Langmuir film to give dense brush layers.

Therefore, a brush similar to a chemically-tethered one prepared in situ can be generated by a much simpler technique, whilst overcoming the limitations of depositing from solution. The monolayers of the calixarene-adhesives and the associated decyl control compounds were tested for adhesiveness using a mechanical tester equipped with a hydrogel of an oppositely charge polyelectrolyte. It was found that the calixarene-based adhesives showed a stronger adhesive response compared to the control compounds. This shows that:

the calixarene anchors the adhesive to the surface, and does so better than a plain alkyl chain. This is due to the increased interactions with the surface caused by the macrocyclic ordering of the functionalities around the upper annulus of a calixarene.

Films of PVAc were also spin-coated onto silicon wafers to give films of a similar thickness to the deposited polyelectrolyte brushes. These films gave a much smaller adhesive response compared to the calixarene-adhesives. This shows that:

it is the presence of the polyelectrolyte brush, and the electrostatic interactions with the polyelectrolyte gel, that is causing the adhesion, rather than the presence of a polymer film.

This is supported by the previous research on the ‘grafted-from’ polyelectrolyte brushes. This found that at short brush lengths, adhesion is dominated by electrostatic interactions, and interdigitation is negligible.³⁴ This means that the adhesion is dominated by the electrostatic interface between the two components, rather than any mechanical interlocking of polymer chains.

Repeat adhesion measures were performed using the same hydrogel on a different area of the sample to determine if the adhesive bond was failed at the gel-brush or brush-wafer interface. Only a relatively small decrease in adhesion was observed. This shows that:

the measured adhesion was due to adhesive failure at the gel-brush interface, rather than the brush-wafer interface, and was therefore not limited by the grafted-to nature of the brush.

This means that the limiting factor in this system is the polyelectrolyte adhesion, and not the method of attachment of the polymer to the surface. Variation of the applied load showed that the surfaces generally showed a lower adhesive response at low loads, but a predominantly similar adhesive response at high loads. Based upon measurement of the mechanical properties of the hydrogel this was attributed to the mechanical properties of the hydrogel for the pDMAEMA surfaces, and the adhesive strength of the bond for the pMAA surfaces. This shows that:

there is a load dependency on the observed adhesion due to the onset of plastic deformation of the hydrogel.

Therefore, the deformable medium used for these adhesive joints would need to be tailored to any future application to ensure the adhesive joint had the required mechanical properties.

AFM imaging of the deposited brush layers identified numerous small voids in the brush surface due to the presence of HMDS aggregate features. To investigate if improved surface coverage might improve adhesion, alternating layers of polyelectrolytes were built-up using layer-by-layer deposition. These depositions gave multilayer films of similar thicknesses to calixarene-adhesives, and were shown to have a better surface coverage as determined by AFM, which gave the potential for more adhesive sites on the surface for the hydrogel to interact with. However, the adhesion measured was much smaller than that recorded for the calixarene based adhesives, and the film thickness reduced over the course of the measurements due to loss of material. This shows that:

the calixarenes are strongly anchoring the polyelectrolytes to the substrate, and that this compensates for any reduction in surface coverage.

Therefore, the calixarene-adhesives provide the best cost-benefit ratio compared to the other systems examined in thesis, as any deficiencies in the deposition are outweighed by the improved adhesive performance. The adhesive strength of the calixarene was also investigated using AFM pull-off forces. The surfaces had a measured work of adhesion similar to the hydrophobic interactions of a surface under the same conditions, and was therefore moderately adhesive, but not as adhesive as some of the stronger physical bonds, such as hydrogen bonding. However, the surface deposition was not uniform, so further work would need to be done to determine the adhesive strength of a calixarene surface.

The values obtained for the work of debonding for these grafted-to brushes were shown to be similar to the values obtained by La Spina et al.²⁷ and Alfheid et al.³⁴ for ‘grafted-from’ brushes. This answers the second research question b), and shows that the data obtained is realistic within the context of these polyelectrolyte brush systems. It also shows that:

the calixarene is anchoring the brush to the surface as sufficiently as a chemical bond.

This work contributes to the literature on ‘grafted-from’ brushes by providing access to the same adhesive system, but via a ‘one-pot’ grafted-to technique, meaning they no longer have to be prepared in situ. This gives the potential for their use in applications previously unavailable due to the limitations of surface preparation, thus moving pH switchable adhesives closer to commercial viability.

7.3. Study Limitations and Final Conclusions

Although the use of Langmuir deposition generated uniform layers of densely packed brushes, the process is not as convenient as spontaneous assembly from solution. It moves the process away from the desirable dip-and-dry self-assembly. However, it is still a relatively simple technique capable of depositing a monolayer of the adhesive in a single coating, and is still simpler than ‘grafting-from’ methodologies.

The brushes deposited are fairly short when compared to those studied in the literature, this is due to the degree of polymerisation of the material prepared in solution compared to that for material prepared on the surface. The literature studies have shown that increased brush length improves adhesion. Investigation of longer brushes deposited by grafting-to would be predicted to show an improved adhesion. However, the brushes used in this study still show a similar adhesion to those in the wider literature, demonstrating the usefulness of this material, with a potential increase in the adhesive performance if longer deposited brushes were to be used.

These experiments provide a first step towards creating a reversible adhesive that would be practicable in real-world environments. To achieve this, a ‘one-pot’ approach was used where by a pre-synthesised polymer was deposited on a surface without the need for more complicated ‘grafting-from’ methods. These experiments showed that this approach has some promise. However, controlled evaluation, as demonstrated here, requires specific physical application techniques; in this case the use of a Langmuir trough. Furthermore, the other (oppositely-charged) surface is a standard polymer gel, which would also not mimic a real-world situation. Nevertheless, it is clear that a one-pot route to reversible and repeatable adhesion is viable, although methodologies would need to be tailored to different kinds of surfaces.

7.4. Future Work

The work presented in this thesis represents a positive first step towards making pH switchable adhesives a functional coating. However, more development is needed to take this proof-of-concept forward. Two areas identified for improvement are the strength of the surface anchor and the strength of deposited adhesive. If the strength of the surface anchor is improved, then the material should deposit better from solution, and the monolayer formed, either through spontaneous assembly or a Langmuir film, should also prevent failure at the substrate-material interface. Improving the strength of the adhesive will create a stronger joint, and move the material closer to a commercially viable product.

Although the maximum adhesion was measured at pH6, the switchability of the adhesive was not investigated. Therefore, the potential switchable behaviour of the deposited material should be investigated in future to determine the switchable capacity of the new material, and how well it compares to the previous 'grafted-from' adhesive.

The first, and most simple, modification to the new material would be to increase the length of the polyelectrolyte chain, which would consist of using a greater monomer to initiator ratio in the polymerisation step. As suggested earlier, this may improve the film thickness when deposited through self-assembly by increasing the radius of gyration of the polymer. It would also increase the film thickness if pre-ordered and deposited using a Langmuir trough, as the polymers become stretched when compressed. Therefore, longer polymer chains will stretch out further, giving a thicker deposited layer.

The other sites of the calixarene could also be utilised to grow additional polymer chains from the same site. This may increase the effective grafting density of the polyelectrolytes, and give more material with which to adhere. This could be achieved by using the tetra-functional instead of mono-functional calixarene, which requires less starting material as there is no wastage through the formation of the tetra-alkane coproduct. It also reduces the wastage of di-*tert*-butyl decarbonate (Boc_2O), as all the material protected is the desired tetra-functional material. This also simplifies the separation and purification stages of the process, as only one major product needs to be separated, instead of two. However, tetra-functionalised material could potentially result in a brush with a local grafting density high enough to cause a reduction in adhesive response through counter-ion condensation, as the chains would be tethered within close proximity.

In addition to improving the quantity of polyelectrolyte, the strength of the calixarene surface adhesion could also be improved. The upper rim of the calixarene could be functionalised to improve its adhesion to the substrate. For example, dopamine, which is the active component in blue mussel adhesive proteins, could be coupled to the upper rim, as it has been shown to give a strong adhesion to various surfaces.²⁴² Synthetic methodology exists in the literature for selectively protecting the catechol functionality,²⁴³ and amines have been shown to couple to calixarenes through use of the Mannich reaction.²⁴⁴ Combination of these techniques could allow the functionalisation of the calixarene with dopamine (Figure 7.1). Initial work has successfully modified the original literature procedure²⁴³ to prepare the bis-protected dopamine, N-(2-(2,2-dimethylbenzo-1,3-dioxol-5-yl)ethyl)phthalimide (Figure 7.1).

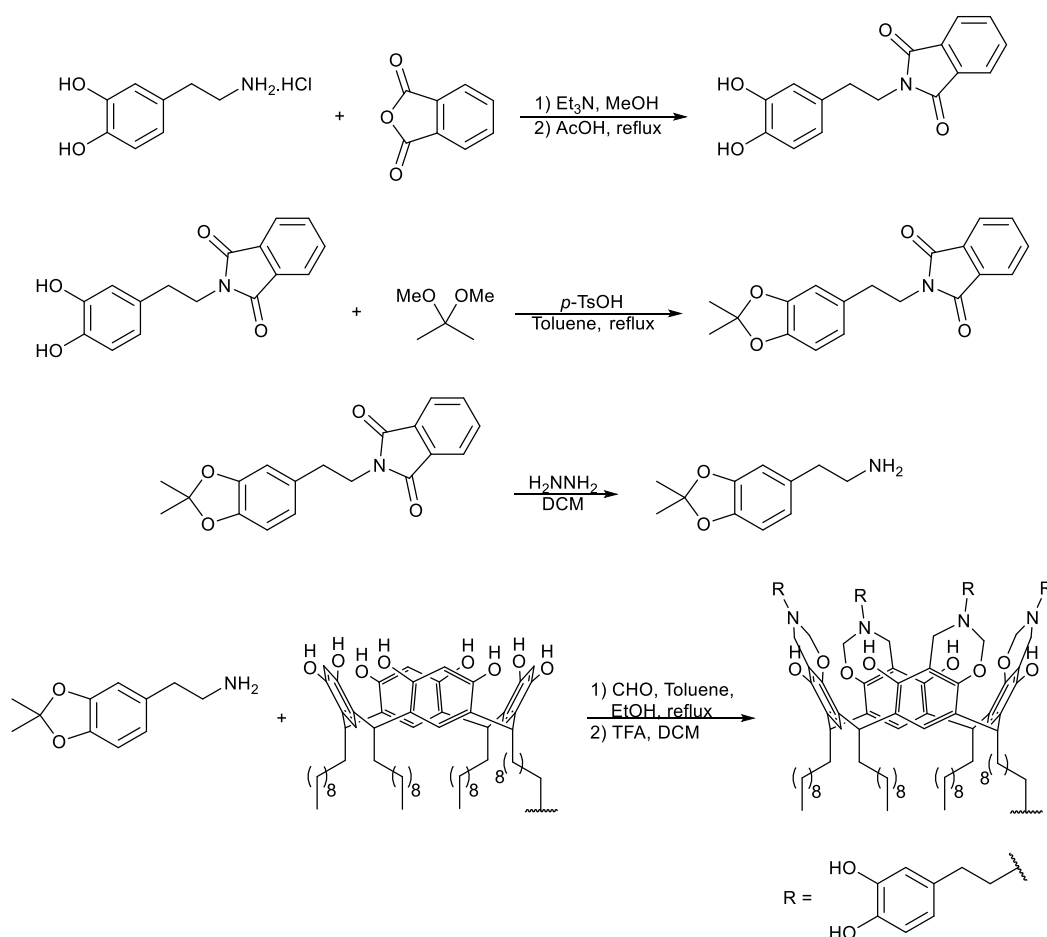


Figure 7.1: Synthetic route for functionalising calixarene with dopamine. AcOH – acetic acid. *p*-TsOH – *p*-toluenesulfonic acid. H₂NNH₂ – hydrazine. CHO – formaldehyde. TFA – trifluoroacetic acid.

The number of calixarenes per polyelectrolyte could also be increased, as this would improve the anchoring ability of the material by multiplying the number of adhesive contacts with the substrate. Preliminary work showed that a methacrylate monomer functionalised with a calixarene could not be polymerised with either ATRP or RAFT. Therefore, post-polymerisation modification should be used to functionalise a block co-polymer. Initial work investigated the use of an azide side group and an alkyne functionalised calixarene (Figure 7.2), based upon previous literature on post-polymerisation modification.²⁴⁵ The alkyne was successfully coupled to calixarene, but further work is required to demonstrate its ability to couple to the azide functionalised polymer. The calixarene functionalised polymer could then be used to grow a second block of polyelectrolyte, or an azide-polyelectrolyte block co-polymer could be formed before functionalisation with calixarene.

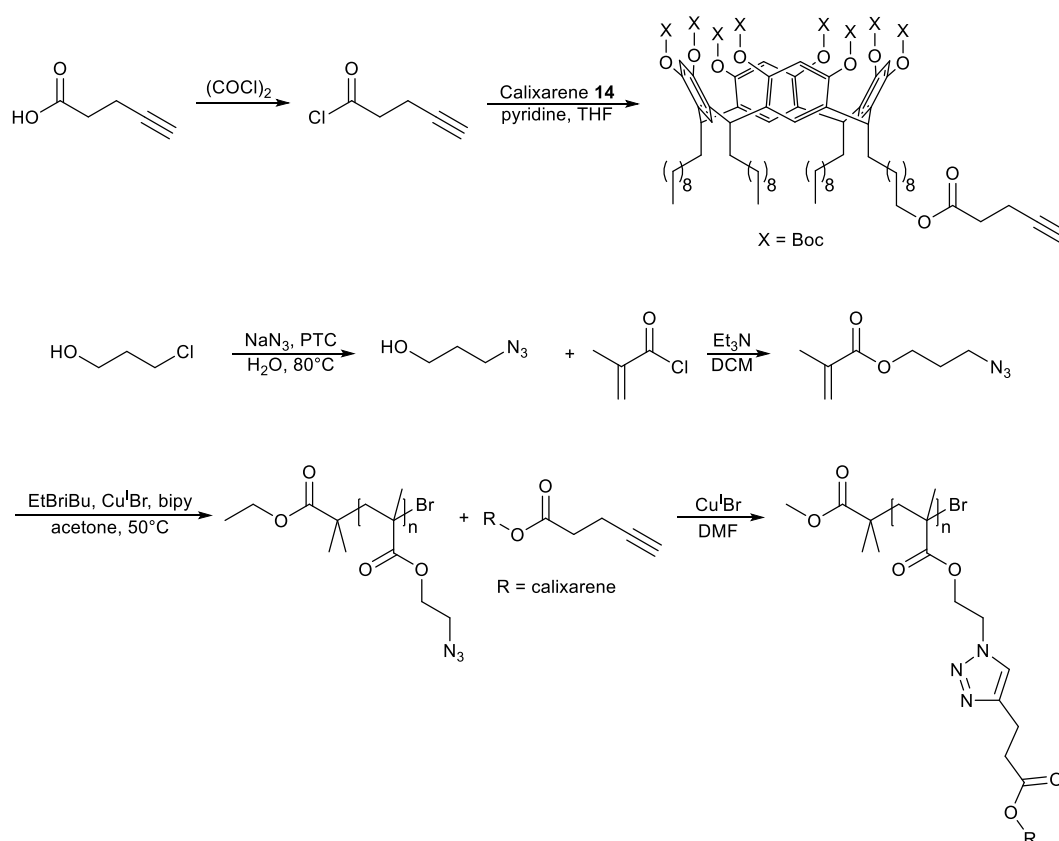


Figure 7.2: Synthetic route for post-polymerisation modification with calixarene. $(\text{COCl})_2$ – oxalyl chloride. NaN_3 – sodium azide. PTC – phase transfer catalyst (tetrabutylammonium hydrogen sulfate). EtBriBu – ethyl 2-bromoisobutyrate. DMF – dimethylformamide.

Overall, the current state of the research into the new material developed in this work is still in its nascent phase. The utilisation of any, or a combination of, the proposals above will further develop this new material towards commercial viability.

8. Experimental

Organic solutions were concentrated using a Büchi rotary evaporator. ^1H and ^{13}C NMR spectra were recorded on a Bruker ARX spectrometer (400 MHz). Data for ^1H NMR are reported as follows: chemical shift (δ ppm), multiplicity (s = singlet, d = doublet, t = triplet, q = quartet, m = multiplet, br = broad), coupling constant (Hz), integration, and assignment. Data for ^{13}C NMR are reported in terms of chemical shift (δ ppm) and assignment. Fourier transform IR spectra were recorded on a Perkin-Elmer Spectrum RX I FT-IR spectrometer and are reported in terms of frequency of absorption (cm^{-1}). Mass spectra were recorded using a Bruker Reflex III MALDI-ToF spectrometer and a Waters LCT ES-ToF spectrometer. All reagents were used as received from commercial suppliers. Anhydrous solvents were obtained from a Grubbs solvent apparatus. Flash chromatography was carried out using BDH silica gel 60 (40-63 mesh). Thin layer chromatography (TLC) utilised precoated Merck aluminium plates coated with silica gel 60 F₂₅₄ (0.2 mm). TLC plates were visualised by means of UV light or stained with permanganate dip.

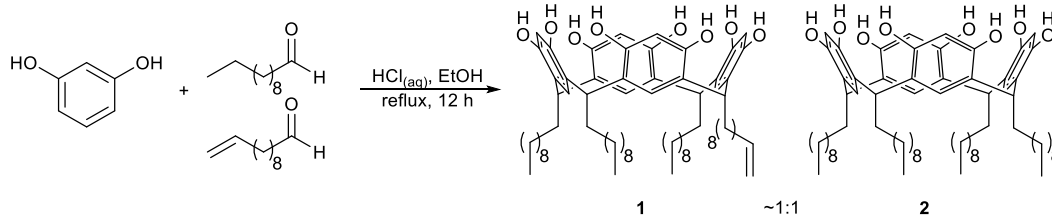
The molecular weights and dispersities of all polymer samples were deduced by chloroform GPC at 40 °C using two Polymer Laboratories (PL) gel 5 μm mixed columns connected to a Varian 390 LC refractive index detector suite and a Varian 290 LC pump injection module. The mobile phase was chloroform with a flow rate of 1 ml min^{-1} . 1% w/v samples were prepared using chloroform as the solvent and toluene as the flow rate marker. Poly(methyl methacrylate) (pMMA) standards ($M_n = 625\text{--}618,000 \text{ g mol}^{-1}$) were used for calibration. Data was analysed using Varian Cirrus GPC software.

Pressure-area isotherms were recorded using a Langmuir Film Balance for Brewster Angle Microscope, Type: 601BAM, NIMA Technology. Langmuir-Schaefer depositions were performed using a Dipper Mechanism, Type: D1L, NIMA Technology, controlled by a Tacho Speed Control, Model TSC7, and Micro-Processor Interface IU4, both NIMA Technology. Thicknesses of deposited materials were determined using a M-2000V Rotating Compensator Ellipsometer (J. A. Woollam Co.). The data were fitted using a B-Spline model for the polymer with a silicon substrate using CompleteEASE software.

Adhesion measurements were performed using a Texture Analyser TA.XT*plus* (Stable Microsystems), which brought a hemispherical hydrogel of the opposite charge into contact with the sample surface using a standard protocol. The gel was brought to the polyelectrolyte film using an approach speed of 50 mm min⁻¹. Upon contact a pressure of 0.1 N, 0.5 N, or 2 N was applied for a period of 2 min, before the gel was withdrawn at a constant speed of 50 mm min⁻¹. The surface and the hydrogel probe were both immersed in Milli-Q water for the duration of the experiment. A double network (DN) poly(methacrylic acid)-poly(oligo(ethylene glycol) methyl ether methacrylate) (pMAA-pOEGMA) hydrogel was used for calix[4]resorcinarene adhesives **11** and **12**, and decyl control **14**. A pDEAEMA hydrogel was used for calix[4]resorcinarene adhesive **22** and decyl control **17**. Results were processed using Exponent software, Stable Microsystems. Side-view images of the interface were taken using a camera, Stable Microsystems, and the images processed using ImageJ to determine contact diameter and height.

Atomic Force Microscope measurements were recorded using an Asylum MFP-3D AFM, the C cantilever of an MLCT probe (Bruker), with a nominal spring constant of 10 pN nm⁻¹, which was calibrated against mica using the method established by Hutter and Bechhoefer²⁴⁶ to identify deflection sensitivity and spring constant. Images were taken in contact mode over a 5 μm square area with a resolution of 256 x 256 points.

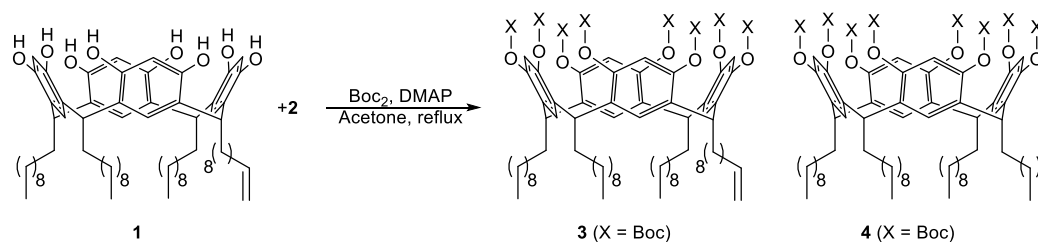
8.1. Synthesis of mono-C-decenyyl, tri-C-decyl calix[4]resorcinarene (**1**)



A solution of resorcinol (10.0 g, 90.8 mmol), undecylenic aldehyde (3.64 ml, 18.16 mmol), and undecyl aldehyde (14.92 ml, 72.64 mmol) was prepared in ethanol (100 ml). The solution was cooled on ice as hydrochloric acid (35%, 25 ml) was added dropwise. The solution was heated at 75 °C overnight. The resulting red solution was cooled and poured into water (500 ml). The precipitate was collected by filtration and recrystallised from methanol to give a mix of both the mono-alkene calix[4]resorcinarene **1** and tetra-alkane calix[4]resorcinarene **2** as a pale red powder (19.11 g, ~18.25 mmol, 80%).

^1H NMR (400 MHz, acetone- d_6) δ_{H} 0.92 (t, $J = 6.15$ Hz, 3H, $-\text{CH}_3$), 1.27-1.46 (m, 14-18H, $-\text{CH}_2-$), 2.31 (q, $J = 7.6$ Hz, 2H, ArCH- CH_2-), 4.32 (t, $J = 7.96$ Hz, 1H, Ar- $\text{CH}-$), 4.94 (ddt, $^3J_{\text{cis}} = 10.3$ Hz, $^2J_{\text{gem}} = 1.53$ Hz, $^4J_{\text{trans}} = 1.15$ Hz, 1H, $-\text{CH}=\text{CH}_{\text{trans}}\text{H}_{\text{cis}}$), 5.01 (dd, $^3J_{\text{trans}} = 17.1$ Hz, $^2J_{\text{gem}} = 1.53$ Hz, 1H, $-\text{CH}=\text{CH}_{\text{trans}}\text{H}_{\text{cis}}$), 5.84 (ddt, $^3J_{\text{trans}} = 17.1$ Hz, $^3J_{\text{cis}} = 10.3$ Hz, $^3J_{\text{gem}} = 6.6$ Hz, 1H, $-\text{CH}=\text{CH}_2$), 6.26 (s, 1H, CH-Ar(**H**)-CH), 7.56 (s, 1H, HO-Ar(**H**)-OH), 8.58 (s, 2H, Ar-OH); ^{13}C NMR (100 MHz, d_6 -acetone) δ_{C} 14.44 ($-\text{CH}_3$), 23.41 ($-\text{CH}_2-\text{CH}_3$), 29.09-30.64 ($-\text{CH}_2-$), 34.35 ($-\text{CH}_2-\text{CH}=\text{}$), 34.56 (Ar- $\text{CH}-$), 103.71 (CH-Ar-CH), 114.72 ($-\text{CH}=\text{CH}_2$), 125.21 (Ar-CH-), 125.38 (HO-Ar-OH), 139.84 ($-\text{CH}=\text{CH}_2$), 152.72 (Ar-OH); IR (neat) $\nu_{\text{max}}/\text{cm}^{-1}$ 3199, 2923, 2852, 1619, 1497, 1449, 1293, 1169, 1086, 907, 837, 720, 609; MS (MALDI-TOF) m/z 1048.7 [monoalkene MH] $^+$, 1070.7 [monoalkene MNa] $^+$.

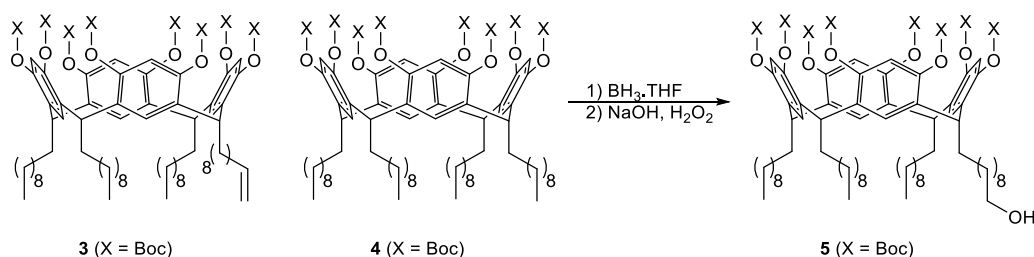
8.2. Synthesis of Boc-mono-C-deceneyl, tri-C-decyl calix[4]resorcinarene (**3**)



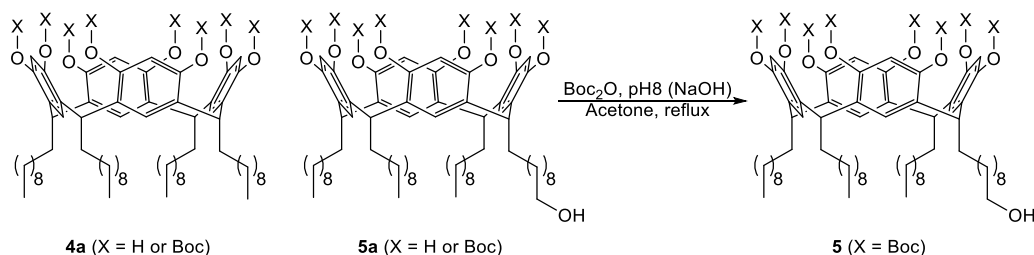
A solution of mono-alkene **1**/tetra-alkane **2** calix[4]resorcinarene mix (4.0 g, ~3.83 mmol), di-*t*-butyl dicarbonate (6.71 g, 30.7 mmol), and 4-dimethylaminopyridine (26.2 mg, 0.2 mmol) in acetone (100 ml) was refluxed for 24 h. The acetone was removed by rotary evaporation and the residue redissolved in diethyl ether, which was then washed with 1M HCl, water, and brine. The solvent was removed by rotary evaporation to give a semi-crystalline solid which was then recrystallised from ethanol to give the Boc protected mono-alkene **3**/tetra-alkane **4** calix[4]resorcinarenes as an orange powder (4.49 g, ~2.43 mmol, 63%).

$^1\text{H NMR}$ (400 MHz, CDCl_3) δ_{H} 0.88 (t, $J = 6.15$ Hz, 3H, $-\text{CH}_3$), 1.18-1.35 (m, 14-18H, $-\text{CH}_2-$), 1.50 (s, 18H, (*t*-Bu) CH_3), 2.02 (q, $J = 7.6$ Hz, 2H, ArCH- CH_2-), 4.34 (t, $J = 7.96$ Hz, 1H, Ar- $\text{CH}-$), 4.92 (ddt, $^3J_{\text{cis}} = 10.3$ Hz, $^2J_{\text{gem}} = 1.53$ Hz, $^4J_{\text{trans}} = 1.15$ Hz, 1H, $-\text{CH}=\text{CH}_{\text{trans}}\text{H}_{\text{cis}}$), 4.98 (dd, $^3J_{\text{trans}} = 17.1$ Hz, $^2J_{\text{gem}} = 1.53$ Hz, 1H, $-\text{CH}=\text{CH}_{\text{trans}}\text{H}_{\text{cis}}$), 5.80 (ddt, $^3J_{\text{trans}} = 17.1$ Hz, $^3J_{\text{cis}} = 10.3$ Hz, $^3J_{\text{gem}} = 6.6$ Hz, 1H, $-\text{CH}=\text{CH}_2$), 6.52 (s, 1H, CH-Ar(**H**)-CH), 6.94 (br s, 1H, BocO-Ar(**H**)-OBoc), 8.58 (s, 2H, Ar-OH); $^{13}\text{C NMR}$ (100 MHz, CDCl_3) δ_{C} 14.09 ($-\text{CH}_3$), 22.67 ($-\text{CH}_2-\text{CH}_3$), 27.66 ((*t*-Bu) CH_3), 29.36-29.84 ($-\text{CH}_2-$), 31.91 ($-\text{CH}_2-\text{CH}=\text{}$), 35.03 (Ar- $\text{CH}-$), 82.64 ((*t*-Bu) $\text{C}-\text{CH}_3$), 103.71 (CH-Ar-CH), 114.04 ($-\text{CH}=\text{CH}_2$), 126.10 (Ar- $\text{CH}-$), 139.15 ($-\text{CH}=\text{CH}_2$), 147.19 ($-\text{OC}(\text{O})\text{OBoc}$), 151.40 (BocO-Ar-OBoc); IR (neat) $\nu_{\text{max}}/\text{cm}^{-1}$ 2926, 2855, 1755, 1495, 1459, 1395, 1370, 1269, 1241, 1140, 1124, 1049, 993, 908, 847, 781, 723, 648, 592; MS (MALDI-TOF) m/z 1871.4 [monoalkene MNa^+], 1887.4 [monoalkene MK^+].

8.3. Synthesis of Boc-mono-C-decanol, tri-C-decyl calix[4]resorcinarene (5)



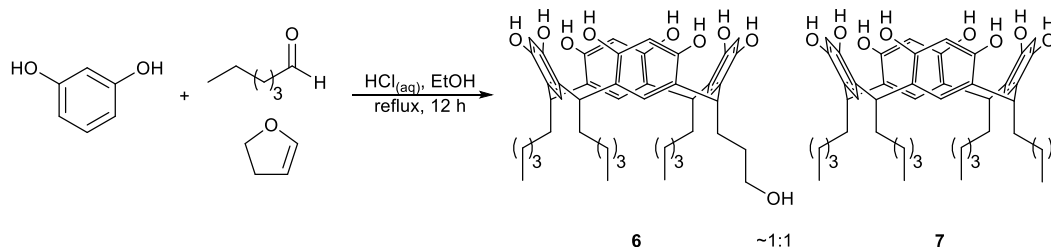
$\text{BH}_3 \cdot \text{THF}$ (1 M, 10 ml, 10 mmol) was added to a solution of Boc protected mono-alkene **3**/tetra-alkane **4** calix[4]resorcinarene mix (10.3 g, ~5.57 mmol) in dry THF (100 ml), and the reaction mixture was stirred at room temperature under nitrogen for five days. The excess of BH_3 was quenched with water, and NaOH (3 M, 10 ml) and H_2O_2 (30%, 10 ml, 98 mmol) were added. The solution was resolubilised with additional THF and was stirred at room temperature for 2 h. The mixture was diluted with brine and extracted with Et_2O . The organic layer was dried with magnesium sulfate and concentrated to give an oil which was purified by column chromatography (10% EtOAc:Hexane, increasing to 40% EtOAc:Hexane) to give the tetra-alkane calix[4]resorcinarene **4**, and the mono-hydroxyl calix[4]resorcinarene **5** (3.84 g, 2.06 mmol, 74%).



Partially Boc protected material can be selectively reprotected using the following method. Partially Boc protected mono-hydroxyl **5a**/tetra-alkane **4a** calix[4]resorcinarene mix (16.4 g) was dissolved in acetone (150 ml) and NaOH (1 N) was added dropwise to produce a pH8 solution. Di-*t*-butyl dicarbonate (15.3 g, 70.2 mmol) was added, and the solution refluxed at 75°C overnight. The solvent was removed and the residue redissolved in diethyl ether and washed with 1M HCl, water, and brine, and dried over magnesium sulfate. The solvent was removed and the residue purified by column chromatography (5% EtOAc:petroleum spirit 40-60, increasing to 20% EtOAc:petroleum spirit 40-60) to give *per*-Boc calix[4]resorcinarene **4** (1.25 g, 0.68 mmol), and *per*-Boc mono-hydroxyl calix[4]resorcinarene **5** (3.17 g, 1.70 mmol).

^1H NMR (400 MHz, CDCl_3) δ_{H} 0.88 (t, $J = 6.15$ Hz, 3H, $-\text{CH}_3$), 1.18-1.35 (m, 14-18H, $-\text{CH}_2-$), 1.50 (s, 18H, (*t*-Bu) CH_3), 2.02 (q, $J = 7.60$ Hz, 2H, ArCH- CH_2-), 3.62 (t, $J = 6.72$ Hz, 2H, $-\text{CH}_2-\text{OH}$), 4.34 (t, $J = 7.96$ Hz, 1H, Ar- $\text{CH}-$), 6.52 (s, 1H, CH-Ar(**H**)-CH), 6.94 (br s, 1H, BocO-Ar(**H**)-OBoc); ^{13}C NMR (100 MHz, CDCl_3) δ_{C} 14.14 ($-\text{CH}_3$), 22.70 ($-\text{CH}_2-\text{CH}_3$), 27.67 ((*t*-Bu) CH_3), 28.00-29.86 ($-\text{CH}_2-$), 35.04 (Ar- $\text{CH}-$), 63.10 ($-\text{CH}_2-\text{OH}$), 82.68 ((*t*-Bu)C- CH_3), 103.71 (CH-Ar-CH), 126.09 (Ar- $\text{CH}-$), 147.19 ($-\text{OC}(\text{O})\text{OBoc}$), 151.39 (BocO-Ar-OBoc); IR (neat) $\nu_{\text{max}}/\text{cm}^{-1}$ 2924, 1751, 1369, 1242, 1141, 886, 779; MS (MALDI-TOF) m/z 1867.1 $[\text{M}]^+$, 1889.1 $[\text{MNa}]^+$, 1906.5 $[\text{MK}]^+$.

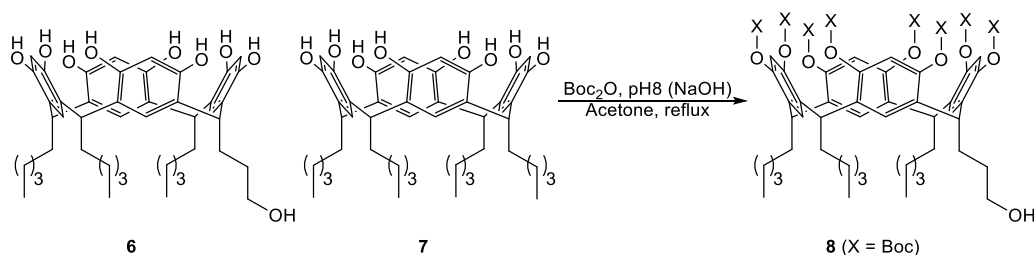
8.4. Synthesis of mono-C-hydroxypropyl, tri-C-pentyl calix[4]resorcinarene (6)



Resorcinol (1 g, 9.08 mmol), 2,3-dihydrofuran (0.14 ml, 1.82 mmol), and hexanal (0.89 ml, 7.28 mmol) were dissolved in ethanol (10 ml). HCl (35%, 2.5 ml) was added and the solution refluxed overnight. The crude mixture was poured into water to precipitate a mix of the mono-hydroxyl calix[4]resorcinarene **6** and the tetra-alkane calix[4]resorcinarene **7** (1.59 g, ~2.1 mmol, 93%).

^1H NMR (400 MHz, acetone- d_6) δ_{H} 0.90 (t, $J = 6.38$ Hz, 3H, $-\text{CH}_3$), 1.33 (m, 6H, $-\text{CH}_2-$), 1.53 (p, 2H, $J = 7.06$ Hz, $-\text{CH}_2-\text{CH}_2\text{OH}$), 2.28 (q, $J = 7.6$ Hz, 2H, ArCH- CH_2-), 3.62 (t, $J = 6.51$ Hz, 2H, $-\text{CH}_2-\text{OH}$), 4.32 (t, $J = 7.6$ Hz, 1H, Ar- $\text{CH}-$), 6.26 (s, 1H, CH-Ar(**H**)-CH), 7.60 (s, 1H, HO-Ar(**H**)-OH), 8.52 (s, 2H, Ar-OH); ^{13}C NMR (100 MHz, acetone- d_6) δ_{C} 14.44 ($-\text{CH}_3$), 22.71 ($-\text{CH}_2-\text{CH}_3$), 27.75-31.93 ($-\text{CH}_2-$), 34.56 (Ar- $\text{CH}-$), 62.07 ($-\text{CH}_2-\text{OH}$), 103.71 (CH-Ar-CH), 125.38 (Ar- $\text{CH}-$), 126.96 (HO-Ar-OH), 152.72 (Ar-OH); IR (neat) $\nu_{\text{max}}/\text{cm}^{-1}$ 3199, 2923, 1619, 1497, 1449, 1293, 1169, 1086, 837, 720, 609.

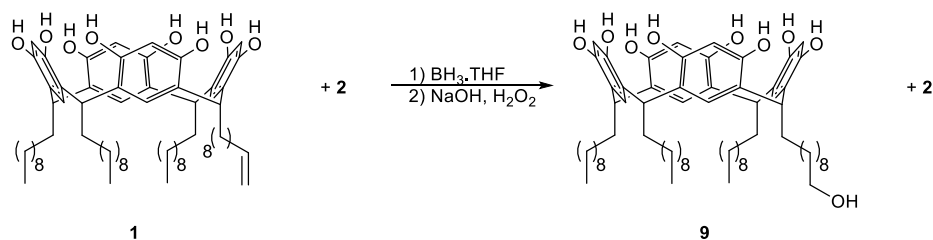
8.5. Synthesis of Boc-mono-C-hydroxypropyl, tri-C-pentyl calix[4]resorcinarene (**8**)



Mono-hydroxyl **6**/tetra-alkane **7** calix[4]resorcinarene mix (0.5 g, ~0.66 mmol) was dissolved in acetone (20 ml) and NaOH (1 N) was added dropwise to produce a pH 8 solution. Di-*t*-butyl dicarbonate (1.44 g, 6.6 mmol) was added, and the solution refluxed at 75 °C overnight. The solvent was removed and the residue redissolved in diethyl ether and washed with 1M HCl, water, and brine, and dried over magnesium sulfate. The solvent was removed and the residue purified by column chromatography (7.5% EtOAc:petroleum spirit 40-60, increasing to 30% EtOAc:petroleum spirit 40-60) to give Boc calix[4]resorcinarene **7** (0.11 g, 0.07 mmol), and Boc mono-hydroxyl calix[4]resorcinarene **8** (0.17 g, 0.11 mmol, 33%).

^1H NMR (400 MHz, CDCl_3) δ_{H} 0.89 (t, $J = 6.38$ Hz, 3H, $-\text{CH}_3$), 1.25 (m, 6H, $-\text{CH}_2-$), 1.50 (s, 18H, (*t*-Bu) CH_3), 1.53 (p, 2H, $J = 7.06$ Hz, $-\text{CH}_2-\text{CH}_2\text{OH}$), 2.28 (q, $J = 7.6$ Hz, 2H, ArCH- CH_2-), 3.60 (t, $J = 6.51$ Hz, 2H, $-\text{CH}_2-\text{OH}$), 4.32 (t, $J = 7.6$ Hz, 1H, Ar- $\text{CH}-$), 6.52 (s, 1H, CH-Ar(**H**)-CH), 6.94 (br s, 1H, BocO-Ar(**H**)-OBoc); ^{13}C NMR (100 MHz, CDCl_3) δ_{C} 14.14 ($-\text{CH}_3$), 22.71 ($-\text{CH}_2-\text{CH}_3$), 27.65 ((*t*-Bu) CH_3), 27.75-31.93 ($-\text{CH}_2-$), 35.04 (Ar- $\text{CH}-$), 62.07 ($-\text{CH}_2-\text{OH}$), 82.72 ((*t*-Bu) $\text{C}-\text{CH}_3$), 103.71 (CH-Ar-CH), 126.96 (Ar- $\text{CH}-$), 146.45 ($-\text{OC}(\text{O})\text{OBoc}$), 151.29 (BocO-Ar-OBoc); IR (neat) $\nu_{\text{max}}/\text{cm}^{-1}$ 2924, 1751, 1369, 1242, 1141, 886, 779.

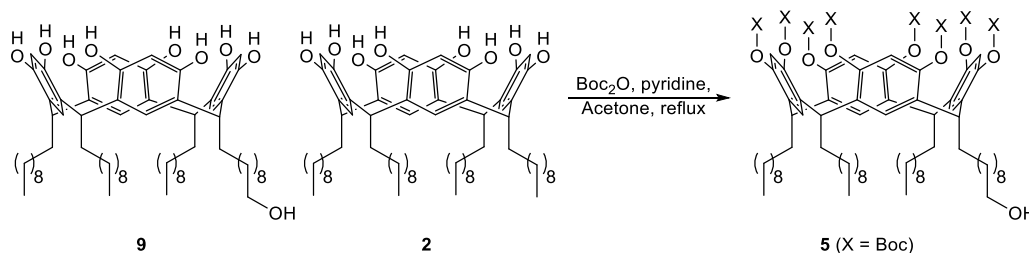
8.6. Synthesis of mono-C-hydroxydecyl, tri-C-decyl calix[4]resorcinarene (**9**)



$\text{BH}_3 \cdot \text{Me}_2\text{S}$ (1.36 ml, 14.3 mmol, 5 eq.) was added to a solution of mono-alkene **1**/tetra-alkane **2** calix[4]resorcinarene mix (3 g, ~2.86 mmol) in dry THF (50 ml), and the reaction mixture was stirred at room temperature under argon overnight. The excess of BH_3 was quenched with water, and NaOH (3M, 10 ml) and H_2O_2 (30%, 10 ml, 98 mmol) were added. The solution was resolubilised with additional THF and was stirred at room temperature for 2 h. The mixture was diluted with brine and extracted with Et_2O . The organic layer was dried with magnesium sulfate and the solvent removed. The crude material was redissolved in hot methanol, and poured into an excess of water to precipitate the tetra-alkane calix[4]resorcinarene **2**, and the mono-hydroxyl calix[4]resorcinarene **9**, which were collected by filtration and dried (2.38 g, 2.23 mmol, 78%).

^1H NMR (400 MHz, acetone- d_6) δ_{H} 0.91 (t, $J = 6.15$ Hz, 3H, $-\text{CH}_3$), 1.21-1.45 (m, 14-18H, $-\text{CH}_2-$), 2.07 (q, $J = 7.60$ Hz, 2H, ArCH- CH_2-), 3.56 (t, $J = 6.72$ Hz, 2H, $-\text{CH}_2-\text{OH}$), 4.32 (t, $J = 7.96$ Hz, 1H, Ar- $\text{CH}-$), 6.25 (s, 1H, CH-Ar(**H**)-CH), 7.57 (s, 1H, HO-Ar(**H**)-OH), 8.49 (s, 2H, Ar-OH); ^{13}C NMR (100 MHz, d_6 -acetone) δ_{C} 13.53 ($-\text{CH}_3$), 22.51 ($-\text{CH}_2-\text{CH}_3$), 29.31-29.75 ($-\text{CH}_2-$), 33.43 (Ar- $\text{CH}-$), 61.61 ($-\text{CH}_2-\text{OH}$), 102.77 (CH-Ar-CH), 124.31 (Ar-CH-), 124.54 (HO-Ar-OH), 151.80 (Ar-OH); IR (neat) $\nu_{\text{max}}/\text{cm}^{-1}$ 3221, 2922, 2852, 1703, 1616, 1500, 1452, 1293, 1212. 1171, 1087, 902, 835; HRMS-ES-TOF m/z calcd for $\text{C}_{68}\text{H}_{104}\text{O}_9$ ($[\text{M}+\text{H}]^+$): 1065.7753, Found 1065.7754.

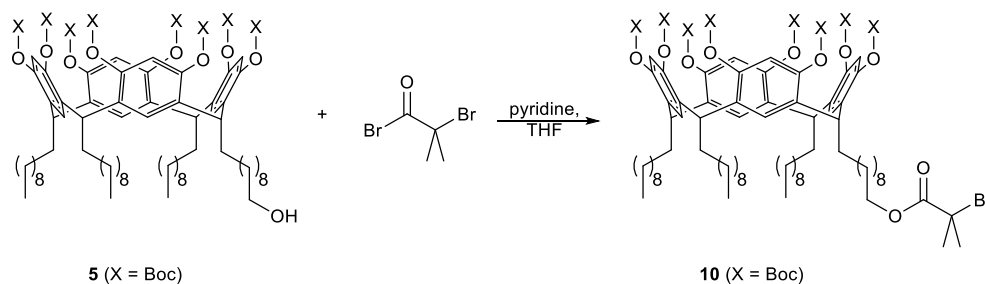
8.7. Synthesis of Boc-mono-C-decanol, tri-C-decyl calix[4]resorcinarene (5)



A solution of mono-hydroxyl **9**/tetra-alkane **2** calix[4]resorcinarene mix (0.66 g, ~0.62 mmol), di-*t*-butyl dicarbonate (1.35 g, 6.2 mmol), and pyridine (50 μ l, 0.62 mmol) in acetone (200 ml) was refluxed overnight. The acetone was removed by rotary evaporation and the residue redissolved in diethyl ether; which was then washed with 1M HCl, water, and brine. The solvent was removed by rotary evaporation and the residue purified by alumina chromatography (10-20% EtOAc:petroleum spirit 40-60) to give the tetra-alkane calix[4]resorcinarene **4**, and the mono-hydroxyl calix[4]resorcinarene **5** (0.52 g, 0.28 mmol, 90%).

^1H NMR (400 MHz, CDCl_3) δ_{H} 0.88 (t, $J = 6.15$ Hz, 3H, $-\text{CH}_3$), 1.18-1.35 (m, 14-18H, $-\text{CH}_2-$), 1.50 (s, 18H, (*t*-Bu) CH_3), 2.02 (q, $J = 7.60$ Hz, 2H, ArCH- CH_2-), 3.62 (t, $J = 6.72$ Hz, 2H, $-\text{CH}_2-\text{OH}$), 4.34 (t, $J = 7.96$ Hz, 1H, Ar- $\text{CH}-$), 6.52 (s, 1H, CH-Ar(**H**)-CH), 6.94 (br s, 1H, BocO-Ar(**H**)-OBoc); ^{13}C NMR (100 MHz, CDCl_3) δ_{C} 14.14 ($-\text{CH}_3$), 22.70 ($-\text{CH}_2-\text{CH}_3$), 27.67 ((*t*-Bu) CH_3), 28.00-29.86 ($-\text{CH}_2-$), 35.04 (Ar- $\text{CH}-$), 63.10 ($-\text{CH}_2-\text{OH}$), 82.68 ((*t*-Bu) $\text{C}-\text{CH}_3$), 103.71 (CH-Ar-CH), 126.09 (Ar- $\text{CH}-$), 147.19 ($-\text{OC}(\text{O})\text{OBoc}$), 151.39 (BocO-Ar-OBoc); IR (neat) $\nu_{\text{max}}/\text{cm}^{-1}$ 2924, 1751, 1369, 1242, 1141, 886, 779; MS (MALDI-TOF) m/z 1867.1 [M] $^+$, 1889.1 [MNa] $^+$, 1906.5 [MK] $^+$.

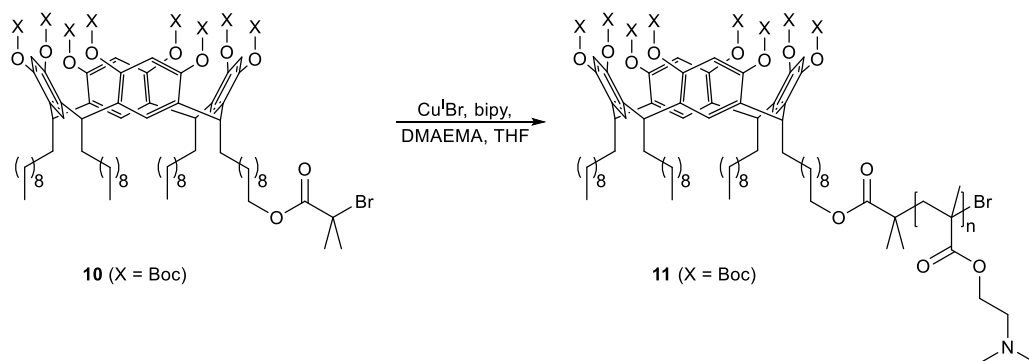
8.8. Synthesis of Boc-mono-C-bromoisobutyloxydecyl, tri-C-decyl calix[4]resorcinarene (**10**)



α -bromoisobutyryl bromide (0.1 ml, 0.81 mmol) was added to a solution of mono-hydroxyl calix[4]resorcinarene **5** (0.5 g, 0.27 mmol) and pyridine (0.1 ml, 1.24 mmol) dissolved in dry THF (10 ml) and stirred under nitrogen overnight. The solvent was removed and the residue redissolved in hexane and washed with saturated sodium hydrogen carbonate, water, and brine, and dried over magnesium sulfate. The solvent was removed and the residue purified by alumina chromatography (10% EtOAc:petroleum spirit 40-60) to give the bromoinitiator product **10** (0.51 g, 0.25 mmol, 93%).

$^1\text{H NMR}$ (400 MHz, CDCl_3) δ_{H} 0.88 (t, $J = 6.15$ Hz, 3H, $-\text{CH}_3$), 1.17-1.38 (m, 14-18H, $-\text{CH}_2-$), 1.50 (s, 18H, (*t*-Bu) CH_3), 1.95 (s, 6H, $-\text{C}(\text{O})\text{C}(\text{CH}_3)_2\text{Br}$), 4.16 (t, $J = 6.65$ Hz, 2H, $-\text{CH}_2\text{-O}$), 4.32 (t, $J = 7.96$ Hz, 1H, Ar- CH-), 6.52 (s, 1H, CH-Ar(**H**)-CH), 6.94 (br s, 1H, BocO-Ar(**H**)-OBoc); $^{13}\text{C NMR}$ (100 MHz, CDCl_3) δ_{C} 14.00 ($-\text{CH}_3$), 22.56 ($-\text{CH}_2\text{-CH}_3$), 27.51 ((*t*-Bu) CH_3), 29.91-29.72 ($-\text{CH}_2-$), 30.70 ($-\text{C}(\text{O})\text{C}(\text{CH}_3)_2\text{Br}$), 36.36 (Ar- CH-), 55.83 ($-\text{C}(\text{O})\text{C}(\text{CH}_3)_2\text{Br}$), 65.93 ($-\text{CH}_2\text{-O}$), 82.57 ((*t*-Bu) C-CH_3), 103.59 (CH-Ar-CH), 126.01 (Ar- CH-), 147.09 ($-\text{OC}(\text{O})\text{OBoc}$), 151.29 (BocO-Ar-OBoc), 171.46 ($>\text{C=O}$); IR (neat) $\nu_{\text{max}}/\text{cm}^{-1}$ 2926, 2855, 1754, 1495, 1459, 1394, 1369, 1269, 1242, 1140, 1124, 1068, 993, 900, 846, 780, 722, 664, 598; MS (MALDI-TOF) m/z 2040.0 [MNa^+], 2055.5 [MK^+]; Anal. Calcd for $\text{C}_{112}\text{H}_{173}\text{O}_{26}\text{Br}$: C, 66.74; H, 8.65; Br, 3.96. Found: C, 66.82; H, 8.58; Br, 3.91.

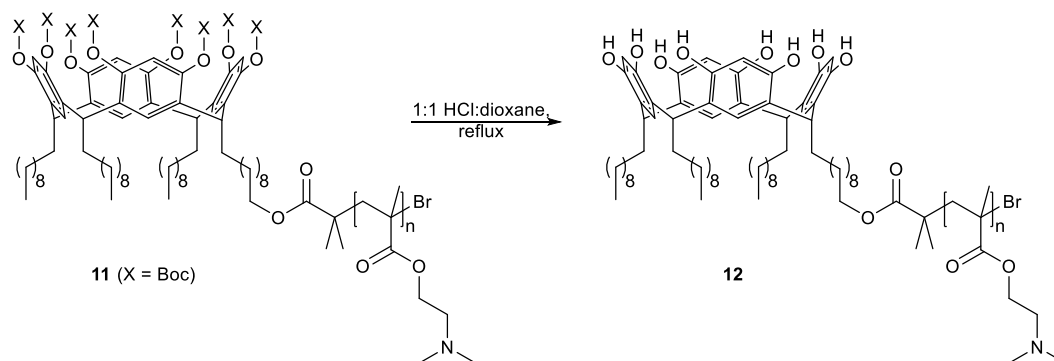
8.9. Synthesis of Boc-mono-C-pDMAEMA-isobutyloxydecyl, tri-C-decyl calix[4]resorcinarene (**11**)



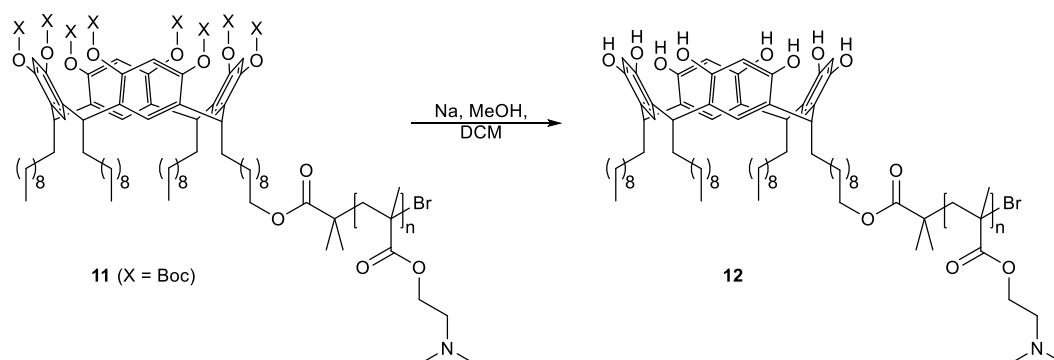
$\text{Cu}^{\text{I}}\text{Br}$ (0.2 g, 1.36 mmol, 1 eq.) and 2,2'-bipyridyl (0.53 g, 3.4 mmol, 2.5 eq.) were placed in a sealed vessel and degassed with nitrogen. Degassed THF (10 ml) was added and the solution stirred until the complex had formed. 2-(dimethylamino)ethyl methacrylate (13.7 ml, 81.6 mmol, 60 eq.) was added and the solution stirred for 5 min. Calixarene bromoinitiator **10** (2.74 g, 1.36 mmol, 1 eq.) in degassed THF (10 ml) was then added and the solution stirred at room temperature overnight. The resulting mixture was diluted with THF and passed through neutral alumina to remove the spent ATRP catalyst. The solution was reduced and added dropwise to an excess of hexane to precipitate the polymer **11** (15.36 g, 99%).

^1H NMR (400 MHz, CDCl_3) δ_{H} 1.50 (s, 18H, (*t*-Bu)**CH**₃), 1.84 (br, polymer-**CH**₃), 1.93 (br, polymer-**CH**₂-), 2.31 (br, polymer-N(**CH**₃)₂), 2.60 (br, polymer-**CH**₂-NMe₂), 4.08 (br, polymer-O-**CH**₂-); ^{13}C NMR (100 MHz, CDCl_3) δ_{C} 29.05 (polymer-**CH**₃), 46.83 (polymer-N(**CH**₃)₂), 49.35-50.63 (polymer-**CH**₂-), 58.97 (polymer-**CH**₂-NMe₂), 64.74 (polymer-O-**CH**₂-); IR (neat) $\nu_{\text{max}}/\text{cm}^{-1}$ 3408, 2961, 2679, 2160, 2034, 1709, 1619, 1469, 1400, 1361, 1269, 1223, 1146, 987, 965, 748, 530, 450, 417, 406; GPC $M_{\text{n}} = 14842 \text{ gmol}^{-1}$, $M_{\text{w}} = 20060 \text{ gmol}^{-1}$, $M_{\text{w}}/M_{\text{n}} = 1.77$.

8.10. Synthesis of mono-C-pDMAEMA-isobutyloxydecyl, tri-C-decyl calix[4]resorcinarene (**12**)



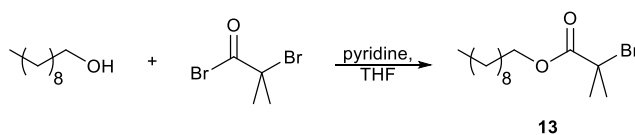
Boc-calix[4]resorcinarene-pDMAEMA **11** (0.5 g) was dissolved in 3M HCl:dioxane (1:1, 20 ml) and refluxed for 3 h. The reaction mixture was partitioned between DCM and sodium hydrogen carbonate. The DCM was separated and dried over sodium sulfate and the solvent removed to give the deprotected polymer **12** (0.27 g, 57%).



Alternatively, Boc-calix[4]resorcinarene-pDMAEMA **11** (0.1 g) was dissolved in DCM (1 ml). Methanol (0.4 ml) followed by sodium metal (0.05 g, 2.17 mmol) were added and the reaction stirred at room temperature overnight. The reaction was diluted with DCM and washed with dil. HCl, water, and brine. The DCM was dried over magnesium sulfate and the solvent removed to give the deprotected polymer **12** (32 mg, 34%).

^1H NMR (400 MHz, CDCl_3) δ_{H} 1.84 (br, polymer- CH_3), 1.93 (br, polymer- CH_2 -), 2.31 (br, polymer- $\text{N}(\text{CH}_3)_2$), 2.60 (br, polymer- $\text{CH}_2\text{-NMe}_2$), 4.08 (br, polymer- O-CH_2 -); ^{13}C NMR (100 MHz, CDCl_3) δ_{C} 29.05 (polymer- CH_3), 46.83 (polymer- $\text{N}(\text{CH}_3)_2$), 49.35-50.63 (polymer- CH_2 -), 58.97 (polymer- $\text{CH}_2\text{-NMe}_2$), 64.74 (polymer- O-CH_2 -); IR (neat) $\nu_{\text{max}}/\text{cm}^{-1}$ 3408, 2961, 2679, 2160, 2034, 1709, 1619, 1469, 1400, 1361, 1269, 1223, 1146, 987, 965, 748, 530, 450, 417, 406.

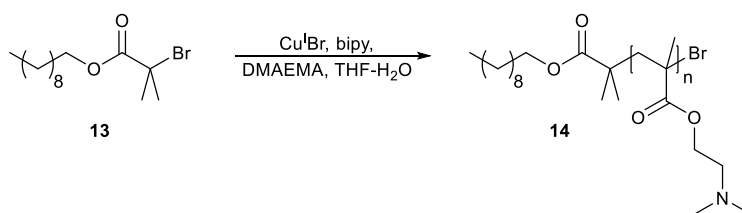
8.11. Synthesis of decyl-2-bromo-2-methylpropanoate (**13**)



A solution of α -bromoisobutyryl bromide (1.21 ml, 9.79 mmol), pyridine (0.79 ml, 9.77 mmol), and decanol (1.88 ml, 9.85 mmol) in dry THF (30 ml) was stirred under nitrogen overnight. The solvent was removed and the residue redissolved in hexane and washed with water, saturated sodium hydrogen carbonate, water, and brine, and dried over magnesium sulfate. The solvent was removed and the residue purified by vacuum distillation (b.p. 191-193 °C, 4 mbar) to give decyl-2-bromo-2-methylpropanoate **13** as a clear liquid (2.48 g, 8.07 mmol, 82%).

$^1\text{H NMR}$ (400 MHz, CDCl_3) δ_{H} 0.90 (t, $J = 7.37$ Hz, 3H, $-\text{CH}_3$), 1.28 (m, 14H, $-\text{CH}_2-$), 1.70 (p, $J = 6.59$ Hz, 2H, $-\text{CH}_2-\text{CH}_2-\text{O}$), 1.95 (s, 6H, $-\text{C}(\text{O})\text{C}(\text{CH}_3)_2\text{Br}$), 4.18 (t, $J = 6.59$ Hz, 2H, $-\text{CH}_2-\text{O}$); $^{13}\text{C NMR}$ (100 MHz, CDCl_3) δ_{C} 14.13 ($-\text{CH}_3$), 22.69 ($-\text{CH}_2-\text{CH}_3$), 28.35-29.51 ($-\text{CH}_2-$), 30.79 ($-\text{C}(\text{O})\text{C}(\text{CH}_3)_2\text{Br}$), 55.97 ($-\text{C}(\text{O})\text{C}(\text{CH}_3)_2\text{Br}$), 66.19 ($-\text{CH}_2-\text{O}$), 171.76 ($>\text{C}=\text{O}$); IR (neat) $\nu_{\text{max}}/\text{cm}^{-1}$ 2924, 2855, 1735, 1464, 1390, 1371, 1274, 1160, 1108, 1011, 978, 925, 763, 722, 645; HRMS-ES-TOF m/z calcd for $\text{C}_{14}\text{H}_{27}\text{O}_2\text{Br}$ ($[\text{M}]^+$): 306.119441, Found 306.118813; Anal. Calcd for $\text{C}_{14}\text{H}_{27}\text{O}_2\text{Br}$: C, 54.72; H, 8.86; Br, 26.00. Found: C, 54.71; H, 8.71; Br, 26.01.

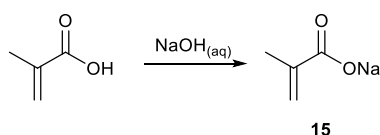
8.12. Synthesis of decyl-pDMAEMA-2-methylpropanoate (**14**)



Decyl-2-bromo-2-methylpropanoate **13** (0.5 g, 1.63 mmol, 1 eq.) and 2-(dimethylamino)ethyl methacrylate (16.43 ml, 48.8 mmol, 30 eq.) were dissolved in THF- H_2O (30 ml, 7% H_2O v/v). After purging with nitrogen for 30 min the $\text{Cu}^{\text{I}}\text{Br}$ catalyst (0.24 g, 1.63 mmol, 1 eq.) and 2,2'-bipyridyl (0.64 g, 4.07 mmol, 2.5 eq.) were added under nitrogen and the solution was allowed to stir under nitrogen overnight. The resulting mixture was diluted with methanol and passed through silica to remove spent ATRP catalyst. The solvent was removed by rotary evaporation. Dissolution of the residue in chloroform and trituration from cold hexane gave the polymer **14** (0.68 g, 43%).

^1H NMR (400 MHz, CDCl_3) δ_{H} 1.84 (br, polymer- CH_3), 1.93 (br, polymer- CH_2 -), 2.31 (br, polymer- $\text{N}(\text{CH}_3)_2$), 2.60 (br, polymer- $\text{CH}_2\text{-NMe}_2$), 4.08 (br, polymer- O-CH_2 -); ^{13}C NMR (100 MHz, CDCl_3) δ_{C} 29.05 (polymer- CH_3), 46.83 (polymer- $\text{N}(\text{CH}_3)_2$), 49.35-50.63 (polymer- CH_2 -), 58.97 (polymer- $\text{CH}_2\text{-NMe}_2$), 64.74 (polymer- O-CH_2 -); IR (neat) $\nu_{\text{max}}/\text{cm}^{-1}$ 2964 ($-\text{CH}_3$), 2714 ($-\text{N}(\text{CH}_3)_2$), 1722 ($>\text{C}=\text{O}$), 1469 ($-\text{CH}_2$ -), 1394 ($-\text{CH}_3$), 1270 ($-\text{CH}_3$), 1149 (C-O/C-N) cm^{-1} ; GPC $M_n = 9608 \text{ gmol}^{-1}$, $M_w = 12850 \text{ gmol}^{-1}$, $M_w/M_n = 1.34$.

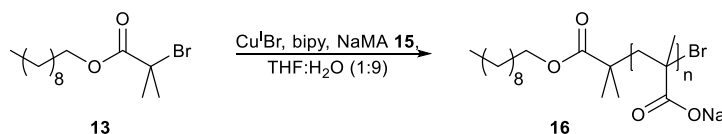
8.13. Synthesis of sodium methacrylate (**15**)



Sodium hydroxide (4 g, 100 mmol) was dissolved in water (10 ml). The sodium hydroxide solution was added to methacrylic acid (10 g, 116.2 mmol) with constant stirring. The mixture was allowed to cool and acetone (50 ml) was added. The resultant precipitate was filtered off to give sodium methacrylate **15** as a white solid (12.2 g, 112.9 mmol, 97%).

^1H NMR (400 MHz, D_2O) δ_{H} 1.72 (s, 3H, $-\text{CH}_3$), 5.19 (s, 1H, $=\text{CH}_2$), 5.45 (s, 1H, $=\text{CH}_2$); ^{13}C NMR (100 MHz, D_2O) δ_{C} 18.64 ($-\text{CH}_3$), 121.38 ($=\text{CH}_2$), 141.25 ($>\text{C}=\text{CH}_2$), 176.53 ($>\text{C}=\text{O}$); IR (neat) $\nu_{\text{max}}/\text{cm}^{-1}$ 3396, 2968, 2929, 2594, 1698, 1643, 1567, 1549, 1455, 1412, 1395, 1365, 1315, 1292, 1234, 1195, 1177, 1004, 934, 919, 854, 836, 820, 803; HRMS-ES-TOF m/z calcd for $\text{C}_4\text{H}_5\text{O}_2\text{Na}_2$ ($[\text{M}]^+$): 131.0085, Found 131.0081.

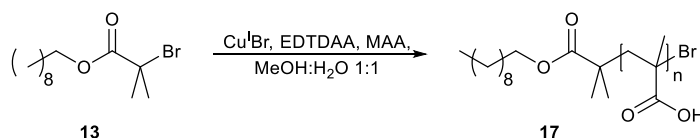
8.14. Synthesis of decyl-pNaMA-2-methylpropanoate (**16**)



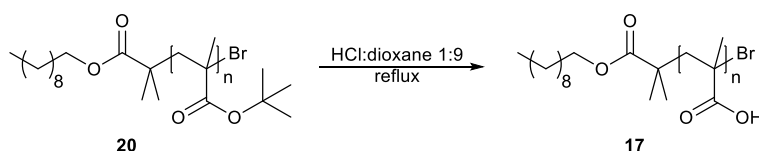
Sodium methacrylate **15** (1.06 g, 9.81 mmol, 30 eq.) was dissolved in water (9 ml) and degassed by three freeze-pump-thaw cycles. Decyl-2-bromo-2-methylpropanoate **13** (0.11 g, 0.36 mmol, 1 eq.) was dissolved in THF (1 ml) and degassed by nitrogen purging before being added to the sodium methacrylate solution. $\text{Cu}^{\text{I}}\text{Br}$ (47 mg, 0.33 mmol, 1 eq.) and 2,2'-bipyridyl (0.13 g, 0.83 mmol, 2.5 eq.) were then added and the reaction allowed to stir under nitrogen overnight. The solution was poured into ethanol to precipitate the crude material (0.68 g), analysis by ^1H NMR and GPC showed a lack of polymeric material.

^1H NMR (400 MHz, D_2O) δ_{H} 0.81 (br, polymer- CH_3), 1.54 (br, polymer- CH_2 -); ^{13}C NMR (100 MHz, D_2O) δ_{C} 18.85 (polymer- CH_2 -), 45.96 (polymer- CH_3), 67.75 ($\text{C}-\text{CO}_2\text{H}$), 177.48 (polymer $>\text{C}=\text{O}$); IR (neat) $\nu_{\text{max}}/\text{cm}^{-1}$ 3328, 2983, 2929, 2857, 1724, 1647, 1537, 1479, 1446, 1395, 1367, 1338, 1204, 1140, 968, 848, 765; GPC $M_{\text{n}} = 406 \text{ gmol}^{-1}$, $M_{\text{w}} = 412 \text{ gmol}^{-1}$, $M_{\text{w}}/M_{\text{n}} = 1.01$.

8.15. Synthesis of decyl-pMAA-2-methylpropanoate (**17**)



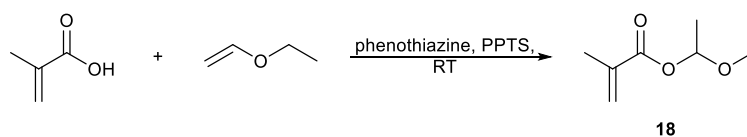
2,2'-(ethylenedithio)diacetic acid (0.135 g, 0.64 mmol, 2 eq.) was dissolved in water (2 ml). The solution was degassed by five freeze-pump-thaw cycles and $\text{Cu}^{\text{I}}\text{Br}$ (46 mg, 0.32 mmol, 1 eq.) was added over the frozen solution. The flask was closed, evacuated, and back-filled with nitrogen five times. The solution was then allowed to thaw. Methacrylic acid (0.93 ml, 10.6 mmol, 33 eq.) and decyl-2-bromo-2-methylpropanoate **13** (0.1 g, 0.33 mmol, 1 eq.) were dissolved in methanol (2 ml). The solution was then degassed by five freeze-pump-thaw cycles. The solution was then added to the water solution and allowed to stir under nitrogen at 75°C for 17 days with monitoring by ^1H NMR. The solution was evaporated to give the reaction product **17** (0.34 g, 32%).



Alternatively, Decyl-p^tBMA **20** (1 g) was dissolved in HCl:dioxane (1:9 v/v, 10 ml) and refluxed overnight. Evaporation of the solvent gave the deprotected polymer **17** (0.6 g, 99%).

^1H NMR (400 MHz, D_2O) δ_{H} 1.06 (br, polymer- CH_3), 1.96 (br, polymer- CH_2 -); ^{13}C NMR (100 MHz, D_2O) δ_{C} 18.85 (polymer- CH_2 -), 45.96 (polymer- CH_3), 67.75 ($\text{C}-\text{CO}_2\text{H}$), 177.48 (polymer $>\text{C}=\text{O}$); IR (neat) $\nu_{\text{max}}/\text{cm}^{-1}$ 3457, 3164, 2990, 2927, 2852, 2584, 1697, 1484, 1451, 1389, 1369, 1263, 1173, 968, 932, 823, 802, 766.

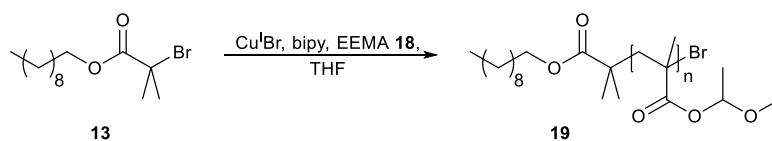
8.16. Synthesis of 1-ethoxyethyl methacrylate (**18**)



Phenothiazine (50 mg, 0.25 mmol) was added to ethyl vinyl ether (19.2 ml, 200 mmol) and methacrylic acid (8.48 ml, 100 mmol) at $<10^{\circ}\text{C}$. The solution was stirred at room temperature for 4 h. Pyridinium *p*-toluene sulfonate (0.5 g, 1.99 mmol) was added and the reaction was stirred at room temperature for 2 h and allowed to stand overnight. Sodium bicarbonate (0.5 g, 5.95 mmol) and sodium sulfate (0.5 g, 3.52 mmol) were added and the mixture was stirred at room temperature for 1 h. The solids were removed by filtration and the solution was concentrated under reduced pressure to give 1-ethoxyethyl methacrylate **18** (12.7 g, 80.3 mmol, 80%).

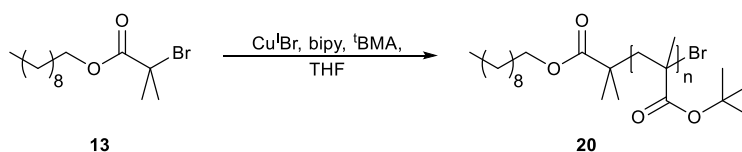
^1H NMR (400 MHz, CDCl_3) δ_{H} 1.21 (t, $J = 7.16$ Hz, 3H, $\text{CH}_2\text{-CH}_3$), 1.43 (d, $J = 5.37$ Hz, 3H, CH-CH_3), 1.94 (s, 3H, $=\text{C-CH}_3$), 3.51-3.76 (m, 2H, O-CH_2 -), 5.59 (t, $J = 1.51$ Hz, 1H, $=\text{CH}_2$), 5.91 (d, $J = 5.37$ Hz, 1H, O-CH-O), 6.15 (t, $J = 1.51$ Hz, 1H, $=\text{CH}_2$); ^{13}C NMR (100 MHz, CDCl_3) δ_{C} 14.92 ($-\text{CH}_3$), 18.08 ($=\text{C-CH}_3$), 20.73 (C-CH_3), 64.54 (O-CH_2 -), 96.59 (O-CH-O), 125.76 ($=\text{CH}_2$), 136.18 ($>\text{C}=\text{CH}_2$), 166.91 ($>\text{C}=\text{O}$); IR (neat) $\nu_{\text{max}}/\text{cm}^{-1}$ 2982, 1715, 1637, 1452, 1384, 1317, 1296, 1170, 1127, 1072, 1035, 1007, 945, 851, 832, 813, 739, 654; HRMS-ES-TOF m/z calcd for $\text{C}_8\text{H}_{14}\text{O}_3\text{Na}$ ($[\text{MNa}]^+$): 181.0841, Found 181.0848.

8.17. Synthesis of decyl-poly(1-ethoxyethyl methacrylate)-2-methylpropanoate (**19**)



Decyl-2-bromo-2-methylpropanoate **13** (0.09 ml, 0.33 mmol), 1-ethoxyethyl methacrylate **18** (1.76 ml, 10.6 mmol), and 2,2'-bipyridyl (0.13 g, 0.82 mmol) were dissolved in THF (30 ml) and degassed with nitrogen. $\text{Cu}^{\text{I}}\text{Br}$ (46 mg, 0.32 mmol) was added under nitrogen. The reaction was stirred at room temperature overnight. Analysis of the crude material by ^1H NMR showed a large proportion of methacrylic acid, which prevented the polymerisation.

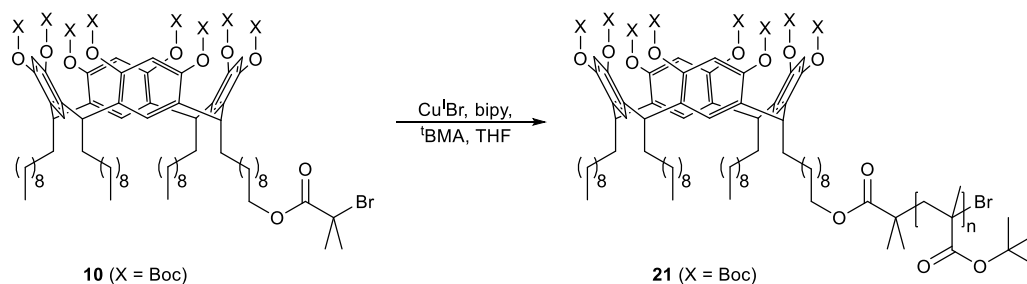
8.18. Synthesis of decyl-p^tBMA-2-methylpropanoate (**20**)



$\text{Cu}^{\text{I}}\text{Br}$ (26 mg, 0.18 mmol), and 2,2'-bipyridyl (71 mg, 0.46 mmol) were placed in a sealed vessel and degassed with three vacuum-nitrogen backfill cycles. A solution of *tert*-butyl methacrylate (1.76 ml, 11 mmol) in THF (2 ml) was degassed with nitrogen purging for 1 h, and the solution was added to the vessel containing the catalyst. The solution was then stirred until the catalyst complex had formed. Decyl-2-bromo-2-methylpropanoate **13** (50 μl , 0.18 mmol) was added and the solution heated to 60 °C under nitrogen overnight. The solution was diluted with THF and passed through alumina to remove the catalyst and the solvent removed. The polymer was purified by dissolution in hot methanol followed by trituration from an excess of water, which was filtered and dried to give the pure polymer **20** (1.26 g, 79%).

^1H NMR (400 MHz, CDCl_3) δ_{H} 1.06 (br, polymer- CH_3), 1.31 (br, polymer- CH_2 -), 1.47 (br, polymer- $\text{C}(\text{CH}_3)_3$); ^{13}C NMR (100 MHz, CDCl_3) δ_{C} 14.05 ($-\text{CH}_2-\text{CH}_3$), 22.58 ($-\text{CO}_2\text{C}(\text{CH}_3)_2$), 27.66 ($\text{C}(\text{CH}_3)_3$), 27.94 ($\text{C}-\text{CH}_3$), 28.24-29.44 ($-\text{CH}_2-$), 30.67 ($\text{C}-\text{CO}_2$), 31.79 ($-\text{CH}_2-\text{C}(\text{CH}_3)$), 46.09 ($-\text{COC}(\text{CH}_3)$), 64.57 ($-\text{CH}_2-\text{O}$), 66.04 ($\text{C}(\text{CH}_3)_3$), 176.60 ($\text{CO}_2\text{C}(\text{CH}_3)_2$), 177.14 (CO_2C); IR (neat) $\nu_{\text{max}}/\text{cm}^{-1}$ 2977, 2933, 1781, 1721, 1476, 1456, 1393, 1366, 1275, 1248, 1134, 1038, 970, 941, 875, 847, 753; GPC $M_n = 15342 \text{ gmol}^{-1}$, $M_w = 22723 \text{ gmol}^{-1}$, $M_w/M_n = 1.48$.

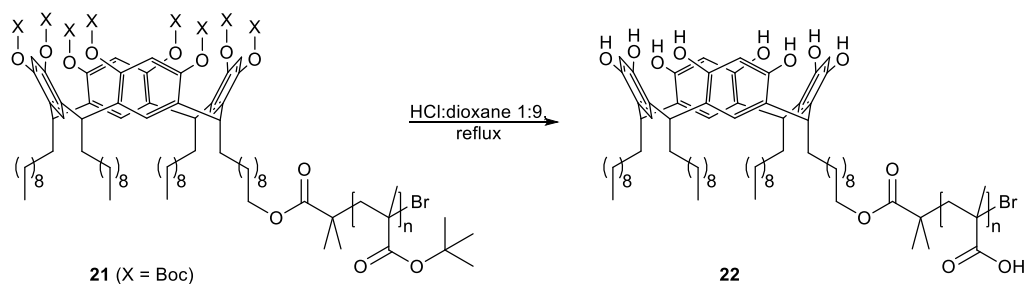
8.19. Synthesis of Boc-mono-C-ptBMA-isobutyloxydecyl, tri-C-decyl calix[4]resorcinarene (**21**)



$\text{Cu}^{\text{I}}\text{Br}$ (0.14 g, 0.95 mmol, 1 eq.) and 2,2'-bipyridyl (0.37 g, 2.38 mmol, 2.5 eq.) were placed in a sealed vessel and degassed with three vacuum-nitrogen backfill cycles. Degassed (nitrogen purged) THF (5 ml) was added to the vessel containing the catalyst and the solution stirred until the catalyst complex had formed (solution turns brown). Degassed *tert*-butyl methacrylate (9.26 ml, 57 mmol, 60 eq.) was added and the solution stirred for 5 min under nitrogen. Calixarene initiator **10** (1.91 g, 0.95 mmol, 1 eq.) in degassed THF (5 ml) was then added and the solution stirred at 60 °C under nitrogen overnight. The reaction mixture was diluted with THF and passed through neutral alumina to remove the ATRP catalyst. The solution was then poured into water to precipitate the pure polymer **21**, which was filtered and dried (9.91 g, 99%).

^1H NMR (400 MHz, CDCl_3) δ_{H} 0.97 (br, polymer- CH_3), 1.06 (br, polymer- CH_2 -), 1.15 (br, polymer- CH_2 -), 1.36 (br, polymer- $\text{C}(\text{CH}_3)_3$), 1.50 (s, 18H, (*t*-Bu) CH_3); ^{13}C NMR (100 MHz, CDCl_3) δ_{C} 14.11 ($-\text{CH}_2-\text{CH}_3$), 22.67 ($-\text{CO}_2\text{C}(\text{CH}_3)_2$), 27.66 ($\text{C}-\text{CH}_3$), 27.75 ($\text{C}(\text{CH}_3)_3$), 29.13-29.65 ($-\text{CH}_2-$), 29.83 ($\text{C}-\text{CO}_2$), 31.91 ($-\text{CH}_2-\text{C}(\text{CH}_3)_3$), 46.20 ($-\text{COC}(\text{CH}_3)$), 67.65 ($-\text{CH}_2-\text{O}$), 67.97 ($\text{C}(\text{CH}_3)_3$), 82.62 ($\text{Ar}-\text{CH}-$), 124.25 ($\text{Ar}-\text{CH}-$), 176.68 ($\text{CO}_2\text{C}(\text{CH}_3)_2$), 177.19 (CO_2C); IR (neat) $\nu_{\text{max}}/\text{cm}^{-1}$ 2977, 2937, 1762, 1717, 1479, 1456, 1392, 1367, 1275, 1247, 1133, 1040, 969, 847, 753; GPC $M_n = 14097 \text{ gmol}^{-1}$, $M_w = 21009 \text{ gmol}^{-1}$, $M_w/M_n = 1.49$.

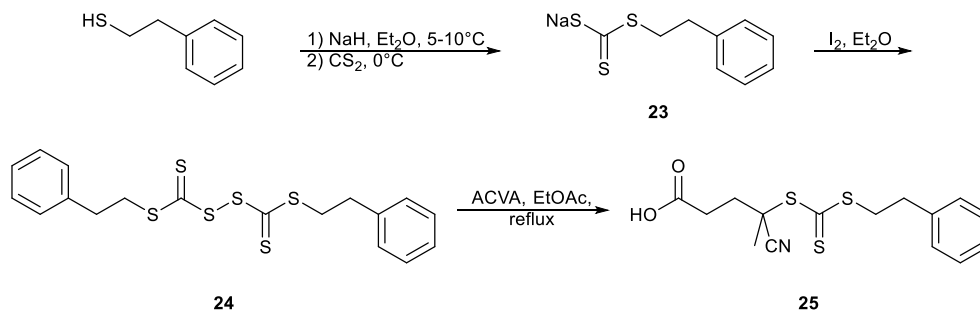
8.20. Synthesis of mono-C-pMAA-isobutyloxydecyl, tri-C-decyl calix[4]resorcinarene (**22**)



Calixarene-p^tBMA **21** (0.5 g) was dissolved in HCl:dioxane (1:9 v/v, 10 ml) and refluxed overnight. Evaporation of the solvent gave the deprotected polymer **22** (0.28 g, 93%).

¹H NMR (400 MHz, MeOD) δ_{H} 1.09 (br, polymer-**CH**₃), 1.19 (br, polymer-**CH**₂-); ¹³C NMR (100 MHz, MeOD) δ_{C} 17.71 (polymer-**CH**₂-), 44.86 (polymer-**CH**₃), 66.73 (C-CO₂H), 181.17 (polymer >C=O); IR (neat) $\nu_{\text{max}}/\text{cm}^{-1}$ 3442, 3182, 2995, 2927, 2852, 2579, 1697, 1486, 1448, 1388, 1369, 1256, 1164, 1116, 1080, 966, 930, 889, 871, 825, 797.

8.21. Synthesis of 4-cyano-4-[(phenethylthio)thiocarbonylthio] valerate (**25**)



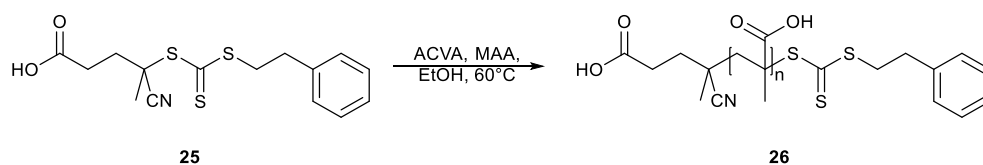
2-phenylethanethiol (5.09 ml, 38 mmol) was added over 10 min to a stirred suspension of sodium hydride (60% in oil, 1.58 g, 39 mmol) in diethyl ether (75 ml) at 5-10°C. The vigorous evolution of hydrogen was observed, and the greyish suspension became a viscous white slurry of sodium phenylethanethiolate over 30 min. The reaction mixture was cooled to 0°C, and carbon disulfide (2.37 ml, 39 mmol) was gradually added to provide a thick yellow precipitate of sodium 2-phenylethanetrithiocarbonate **23**, which was collected by filtration after 30 min and used in the next step without purification (10.6 g).

A suspension of sodium 2-phenylethanetrithiocarbonate **23** (11.1 g, 47 mmol) in diethyl ether (100 ml) was treated by the gradual addition of solid iodine (6.03 g, 24 mmol). The reaction mixture was stirred at room temperature for 1 h, and the insoluble white sodium iodide was removed by filtration. The yellow-brown filtrate was washed with an aqueous solution of sodium thiosulfate to remove excess iodine and dried over sodium sulfate. The solvent was removed to give the bis-(2-phenylethane trithiocarbonyl) disulphide **24** (7.99 g, 18.7 mmol).

A solution of 4,4'-azobis(4-cyanopentanoic acid) (8.1 g, 28.9 mmol) and bis-(2-phenylethane trithiocarbonyl) disulphide **24** (8.22 g, 19.3 mmol) in ethyl acetate (150 ml) was degassed with nitrogen and refluxed under nitrogen for two days. The crude product was washed with water (5 x 100 ml) and dried over magnesium sulfate. The organic phase was concentrated and purified by silica chromatography (7:3 petroleum spirit 40-60:EtOAc, gradually increasing to 4:6) to give PETTC **25** as a yellow oil (9.68 g, 28.5 mmol, 74%).

^1H NMR (400 MHz, CDCl_3) δ_{H} 1.91 (s, 3H, $-\text{CH}_3$), 2.38-2.60 (m, 2H, $-\text{C}(\text{Me})(\text{CN})-\text{CH}_2-$), 2.71 (t, $J = 8.06$ Hz, 2H, $-\text{CH}_2-\text{CO}_2\text{H}$), 3.01 (t, $J = 7.31$ Hz, 2H, Ar- CH_2-), 3.60 (t, $J = 7.31$ Hz, 2H, $-\text{CH}_2-\text{S}$), 7.23-7.37 (m, 5H, Ar-**H**); ^{13}C NMR (100 MHz, CDCl_3) δ_{C} 24.84 ($-\text{CH}_3$), 29.46 ($-\text{CH}_2-\text{CO}_2\text{H}$), 30.01 (Ar- CH_2-), 33.54 ($-\text{C}(\text{Me})(\text{CN})-\text{CH}_2-$), 39.98 ($-\text{CH}_2-\text{S}$), 46.37 (S- $\text{C}(\text{Me})(\text{CN})-$), 118.83 (CN), 126.86, 128.55, 128.69 (Ar), 139.14 (Ar- CH_2), 176.57 (C=O), 216.43 (C=S); IR (neat) $\nu_{\text{max}}/\text{cm}^{-1}$ 3438, 1692, 1637, 1581, 1496, 1447, 1393, 1375, 1321, 1212, 1121, 1057, 961, 920, 806, 761, 718, HRMS-ES-TOF m/z calcd for $\text{C}_{15}\text{H}_{18}\text{NO}_2\text{S}_3$ ($[\text{M}]^+$): 340.0500, Found 340.0514.

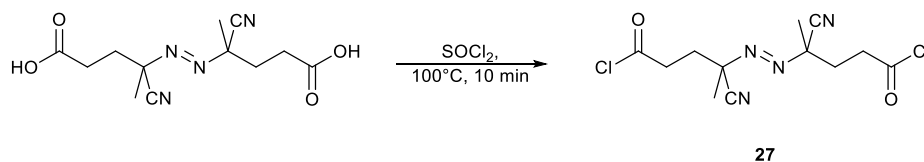
8.22. Synthesis of 4-cyano-4-[pMAA-(phenethylthio)thiocarbonylthio] valerate (**26**)



PETTC **25** (0.1 g, 0.29 mmol, 1 eq.), 4,4'-azobis(4-cyanopentanoic acid) (40 mg, 0.15 mmol, 0.5 eq.), and methacrylic acid (0.74 ml, 8.7 mmol, 30 eq.) were dissolved in ethanol (0.95 ml) to obtain a 50% w/w solution of methacrylic acid. The reaction mixture was degassed with nitrogen for 40 min at 0°C before being placed into a preheated oil bath at 60°C and the reaction was left overnight. The solvent was removed to leave the polymer **26** (0.63 g, 74%).

^1H NMR (400 MHz, MeOD) δ_{H} 1.12 (br, polymer-**CH**₃), 1.90 (br, polymer-**CH**₂-), 7.19-7.32 (m, 5H, Ar-**H**); ^{13}C NMR (100 MHz, MeOD) δ_{C} 16.98 (polymer-**CH**₂-), 44.49 (polymer-**CH**₃), 56.93 (**C**-CO₂H), 180.92 (polymer **>**C=O); IR (neat) $\nu_{\text{max}}/\text{cm}^{-1}$ 3437, 3174, 2977, 2934, 2579, 1694, 1485, 1448, 1388, 1263, 1169, 1083, 1043, 963, 931, 875, 798, 746.

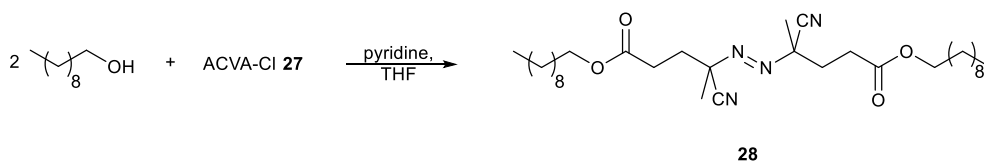
8.23. Synthesis of 4,4'-azobis(4-cyano-valeroyl chloride) (**27**)



4,4'-azobis(4-cyanopentanoic acid) (1 g, 3.57 mmol) was added to thionyl chloride (40 ml) and refluxed for 10 min at 100°C. The hot solution was immersed in an ice bath and cooled to room temperature. Excess thionyl chloride was removed by rotary evaporation to leave the acyl chloride **27** (1.01 g, 3.18 mmol, 89%).

^1H NMR (400 MHz, CDCl₃) δ_{H} 1.71 (s, 3H, -**CH**₃), 1.77 (s, 3H, -**CH**₃), 2.45-2.66 (m, 4H, -**CH**₂-C(CN)), 2.94-3.25 (m, 4H, -**CH**₂-COCl); ^{13}C NMR (100 MHz, CDCl₃) δ_{C} 23.70, 23.86 (-**CH**₃), 32.93 (-**CH**₂-CO₂Cl), 41.75, 41.85 (-C(Me)(CN)-**CH**₂-), 71.37, 71.52 (N-C(Me)(CN)-), 116.84, 116.94 (CN), 171.23, 172.31 (C=O); IR $\nu_{\text{max}}/\text{cm}^{-1}$ 2943 (**CH**), 1790 (>**C=O**(Cl)), 2246 (CN).

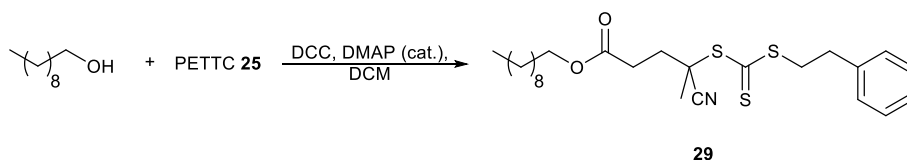
8.24. Synthesis of 4,4'-azobis(decyl 4-cyano-valerate) (**28**)



4,4'-azobis(4-cyano-valeroyl chloride) **27** (1 g, 3.15 mmol, 1 eq.) and decanol (1.08 ml, 5.68 mmol, 1.8 eq.) were dissolved in anhydrous THF (10 ml). Pyridine (0.51 ml, 6.3 mmol, 2 eq.) was added, and the solution stirred overnight. An additional portion of 4,4'-azobis(4-cyano-valeroyl chloride) **27** (0.25 g, 0.79 mmol, 0.25 eq.), pyridine (0.13 ml, 1.58 mmol, 0.5 eq.), and THF (1 ml) were added to remove any unreacted decanol, and the solution stirred for 1 h. The solvent was removed and the residue redissolved in hexane, and washed with water, saturated sodium hydrogen carbonate, water, and brine, and dried over magnesium sulfate. The solvent was removed and the residue purified by column chromatography (20% Et₂O:petroleum spirit 40-60) to give the diester **28** (0.9 g, 1.6 mmol, 57%).

^1H NMR (400 MHz, CDCl_3) δ_{H} 0.89 (t, $J = 7.04$ Hz, 6H, $-\text{CH}_2-\text{CH}_3$), 1.28 (m, 28H, $-\text{CH}_2-$), 1.65 (p, $J = 6.79$ Hz, 4H, $-\text{CH}_2-\text{CH}_2\text{O}$), 1.70 (s, 3H, C- CH_3), 1.75 (s, 3H, C- CH_3), 2.31-2.56 (m, 8H, $-\text{C}(\text{Me})(\text{CN})-\text{CH}_2-\text{CH}_2-$), 4.10 (t, $J = 6.73$ Hz, 2H, $-\text{CH}_2-\text{O}$), 4.11 (t, $J = 6.73$ Hz, 2H, $-\text{CH}_2-\text{O}$); ^{13}C NMR (100 MHz, CDCl_3) δ_{C} 14.15 ($-\text{CH}_2-\text{CH}_3$), 22.70 ($-\text{CH}_2-\text{CH}_3$), 25.88 ($-\text{CH}_3$), 28.52-29.32 ($-\text{CH}_2-$), 29.56 ($-\text{CH}_2-\text{CO}_2\text{C}$), 31.90 ($-\text{CH}_2-$), 33.17 ($-\text{C}(\text{Me})(\text{CN})-\text{CH}_2-$), 65.34 ($-\text{CH}_2-\text{O}$), 71.86 (N-C(Me)(CN)-), 117.50 (CN), 171.42 (C=O); IR (neat) $\nu_{\text{max}}/\text{cm}^{-1}$ 2952, 2917, 2850, 1733, 1469, 1447, 1401, 1380, 1304, 1193, 1173, 1005, 973; HRMS-ES-TOF m/z calcd for $\text{C}_{32}\text{H}_{56}\text{N}_4\text{O}_4\text{Na}$ ($[\text{MNa}]^+$): 583.4199, Found 583.4196.

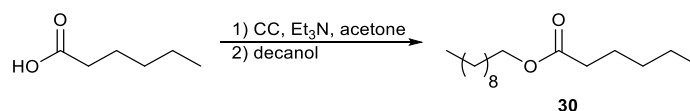
8.25. Synthesis of decyl 4-cyano-4-[(phenethylthio)thiocarbonylthio] valerate (**29**)



PETTC **25** (0.1 g, 0.29 mmol, 1 eq.), decanol (0.11 ml, 0.58 mmol, 2 eq.), and 4-dimethylamino pyridine (3.5 mg, 29 μmol , 10 mol%) were dissolved in anhydrous DCM (1 ml). *N,N'*-Dicyclohexylcarbodiimide (72 mg, 0.35 mmol, 1.2 eq.) was added to the reaction mixture at 0°C . The reaction was stirred at 0°C for 5 min, followed by 3 h at room temperature. Dicyclohexylurea was removed by filtration and the solution diluted with DCM. The solution was washed with dil. HCl, saturated sodium hydrogen carbonate, and dried over magnesium sulfate. The residue was purified by column chromatography (10% EtOAc:petroleum spirit 40-60) to give decyl-PETTC **29** (71.4 mg, 0.15 mmol, 52%).

^1H NMR (400 MHz, CDCl_3) δ_{H} 0.91 (t, $J = 7.03$ Hz, 3H, $-\text{CH}_2-\text{CH}_3$), 1.30 (m, 14H, $-\text{CH}_2-$), 1.65 (p, $J = 6.71$ Hz, 2H, $-\text{CH}_2-\text{CH}_2\text{O}$), 1.91 (s, 3H, C- CH_3), 2.38-2.60 (m, 2H, $-\text{C}(\text{Me})(\text{CN})-\text{CH}_2-$), 2.65 (t, $J = 8.06$ Hz, 2H, $-\text{CH}_2-\text{CO}_2\text{C}$), 3.01 (t, $J = 7.31$ Hz, 2H, Ar- CH_2-), 3.60 (t, $J = 7.31$ Hz, 2H, $-\text{CH}_2-\text{S}$), 4.12 (t, $J = 6.71$ Hz, 2H, $-\text{CH}_2-\text{O}$), 7.23-7.37 (m, 5H, Ar- H); ^{13}C NMR (100 MHz, CDCl_3) δ_{C} 14.18 ($-\text{CH}_2-\text{CH}_3$), 24.85 ($-\text{CH}_3$), 28.55-29.34 ($-\text{CH}_2-$), 29.56 ($-\text{CH}_2-\text{CO}_2\text{C}$), 30.13 (Ar- CH_2-), 33.69 ($-\text{C}(\text{Me})(\text{CN})-\text{CH}_2-$), 39.87 ($-\text{CH}_2-\text{S}$), 46.41 (S-C(Me)(CN)-), 65.32 ($-\text{CH}_2-\text{O}$), 118.98 (CN), 126.86, 128.59, 128.70 (Ar), 139.19 (Ar- CH_2), 171.80 (C=O), 216.56 (C=S); IR (neat) $\nu_{\text{max}}/\text{cm}^{-1}$ 3028, 2956, 2924, 2854, 1733 (C=O), 1497, 1454, 1394, 1378, 1289, 1259, 1182, 1075, 1066, 1030, 867, 799; HRMS-ES-TOF m/z calcd for $\text{C}_{25}\text{H}_{37}\text{NO}_2\text{S}_3$ ($[\text{M}+\text{H}]^+$): 480.2059, Found 480.2065.

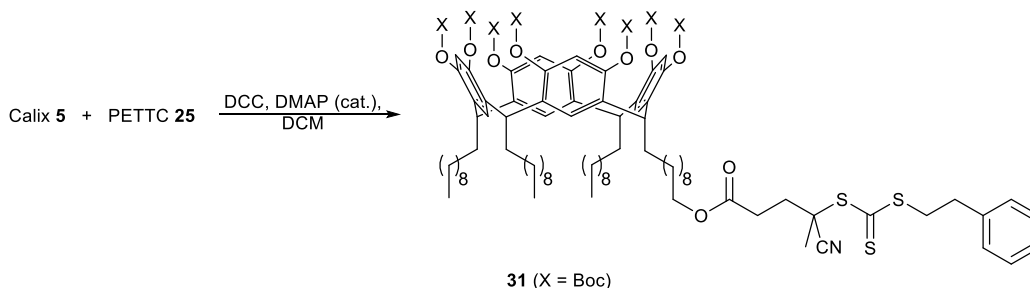
8.26. Synthesis of decyl hexanoate (30)



Cyanuric chloride (0.53 g, 2.9 mmol) was dissolved in dry acetone (8 ml) to produce a clear solution. Hexanoic acid (0.36 ml, 2.9 ml) and triethylamine (0.4 ml, 2.9 mmol) were added to the solution, which was stirred at room temperature for 3 h. Decanol (0.6 ml, 2.9 mmol) was then added and the solution stirred for a further 2 h. The precipitated triazine was removed by filtration and the volatiles removed by rotary evaporation to give decyl hexanoate **30** (0.57 g, 2.23 mmol, 77%).

$^1\text{H NMR}$ (400 MHz, CDCl_3) δ_{H} 0.85 (t, $J = 6.90$ Hz, 3H, $-\text{CH}_3$), 0.87 (t, $J = 6.80$ Hz, 3H, $-\text{CH}_3$), 1.24-1.30 (m, 18H, $-\text{CH}_2-$), 1.60 (tt, $J = 7.60$ Hz, $J = 2.71$ Hz, 2H, $-\text{CH}_2-\text{CH}_2\text{CO}$), 1.74 (p, $J = 7.62$ Hz, 2H, $-\text{CH}_2-\text{CH}_2\text{O}$), 2.26 (t, $J = 7.60$ Hz, 2H, $-\text{CH}_2-\text{CO}$), 4.03 (t, $J = 6.71$ Hz, 2H, $-\text{CH}_2-\text{O}$).

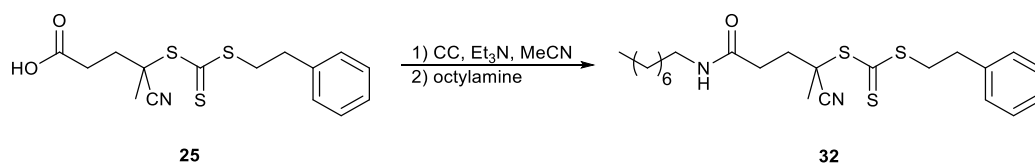
8.27. Synthesis of Boc-mono-C-4-cyano-4-[(phenethylthio)thiocarbonylthio] valerate, tri-C-decyl calix[4]resorcinarene (31)



PETTC **25** (0.12 g, 0.34 mmol, 1 eq.), mono-hydroxyl calix[4]resorcinarene **5** (0.64 g, 0.34 mmol, 1 eq.), and 4-dimethylamino pyridine (4.2 mg, 34 μmol , 10 mol%) were dissolved in anhydrous DCM (1.5 ml). *N,N'*-Dicyclohexylcarbodiimide (84.6 mg, 0.41 mmol, 1.2 eq.) was added to the reaction mixture at 0°C. The reaction was stirred at 0°C for 5 min, then overnight at room temperature. Dicyclohexylurea was removed by filtration and the solution diluted with DCM. The solution was washed with dil. HCl, saturated sodium hydrogen carbonate, and dried over magnesium sulfate. The residue was purified by column chromatography (10% EtOAc:petroleum spirit 40-60) to give Boc-calix[4]resorcinarene-PETTC **31** (0.28 g, 0.13 mmol, 38%).

^1H NMR (400 MHz, CDCl_3) δ_{H} 0.88 (t, $J = 6.15$ Hz, 3H, $-\text{CH}_3$), 1.18-1.35 (m, 14-18H, $-\text{CH}_2-$), 1.50 (s, 18H, (*t*-Bu) CH_3), 1.89 (s, 3H, C- CH_3), 2.37-2.56 (m, 2H, $-\text{C}(\text{Me})(\text{CN})-\text{CH}_2-$), 2.61 (t, $J = 5.51$ Hz, 2H, $-\text{CH}_2-\text{CO}_2\text{C}$), 3.00 (t, $J = 7.31$ Hz, 2H, Ar- CH_2-), 3.59 (t, $J = 7.31$ Hz, 2H, $-\text{CH}_2-\text{S}$), 4.09 (t, $J = 6.35$ Hz, 2H, $-\text{CH}_2-\text{O}$), 4.34 (t, $J = 7.96$ Hz, 1H, Ar- CH -), 6.52 (s, 1H, CH-Ar(H)-CH), 6.94 (br s, 1H, BocO-Ar(H)-OBoc), 7.22-7.36 (m, 5H, Ar-H); ^{13}C NMR (100 MHz, CDCl_3) δ_{C} 14.15 ($-\text{CH}_3$), 24.83 ($-\text{CH}_3$), 22.70 ($-\text{CH}_2-\text{CH}_3$), 27.67 ((*t*-Bu) CH_3), 28.00-29.86 ($-\text{CH}_2-$), 29.68 ($-\text{CH}_2-\text{CO}_2\text{C}$), 31.93 (Ar- CH_2-), 33.87 ($-\text{C}(\text{Me})(\text{CN})-\text{CH}_2-$), 34.07 (Ar- CH -), 37.91 ($-\text{CH}_2-\text{S}$), 46.49 (S-C(Me)(CN)-), 65.33 ($-\text{CH}_2-\text{O}$), 82.65 ((*t*-Bu)C- CH_3), 103.71 (CH-Ar-CH), 118.96 (CN), 126.07 (Ar- CH -), 126.84, 128.57, 128.69 (Ar), 139.18 (Ar- CH_2), 147.19 ($-\text{OC}(\text{O})\text{OBoc}$), 151.37 (BocO-Ar-OBoc), 171.54 (C=O), 216.55 (C=S); IR $\nu_{\text{max}}/\text{cm}^{-1}$ 2981, 2925, 2854, 1755, 1591, 1495, 1458, 1394, 1369, 1269, 1241, 1139, 1123, 1049; HRMS-ES-TOF m/z calcd for $\text{C}_{123}\text{H}_{183}\text{NO}_{26}\text{S}_3\text{Na}$ ($[\text{MNa}]^+$): 2209.2083, Found 2209.2128.

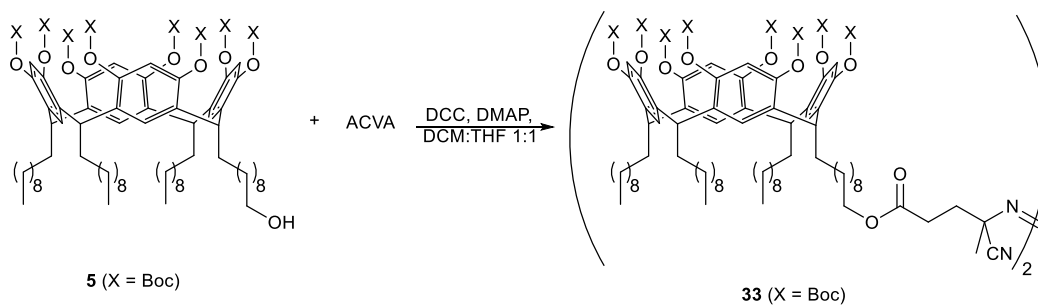
8.28. Synthesis of N-octyl 4-cyano-4-[(phenethylthio)thiocarbonylthio] valeramide (32)



Cyanuric chloride (0.1 g, 0.54 mmol) and PETTC **25** (0.1 g, 0.29 mmol) were dissolved in acetonitrile (1 ml). Triethylamine (0.1 ml, 0.72 mmol) was added and the reaction stirred at room temperature overnight. Octylamine (0.05 ml, 0.3 mmol) was added and the reaction stirred at room temperature overnight. The precipitates were removed and the product purified by column chromatography (30% EtOAc:petroleum spirit 40-60) to give the amide **32** (13 mg, 0.03 mmol, 10%).

^1H NMR (400 MHz, CDCl_3) δ_{H} 0.93 (t, $J = 7.24$ Hz, 3H, $-\text{CH}_2-\text{CH}_3$), 1.28 (m, 10H, $-\text{CH}_2-$), 1.58 (p, $J = 6.56$ Hz, 2H, $-\text{CH}_2-\text{CH}_2\text{N}$), 1.89 (s, 3H, C- CH_3), 2.38-2.60 (m, 2H, $-\text{C}(\text{Me})(\text{CN})-\text{CH}_2-$), 2.65 (t, $J = 8.06$ Hz, 2H, $-\text{CH}_2-\text{CO}_2\text{C}$), 2.98 (t, $J = 7.48$ Hz, 2H, Ar- CH_2-), 3.30 (t, $J = 6.56$ Hz, 2H, $-\text{CH}_2-\text{N}$), 3.54 (t, $J = 7.48$ Hz, 2H, $-\text{CH}_2-\text{S}$), 7.23-7.35 (m, 5H, Ar-H), 7.99 (br s, 1H, $-\text{NH}_2$); ^{13}C NMR (100 MHz, CDCl_3) δ_{C} 14.15 ($-\text{CH}_2-\text{CH}_3$), 24.85 ($-\text{CH}_3$), 29.09-29.31 ($-\text{CH}_2-$), 29.56 ($-\text{CH}_2-\text{CO}_2\text{N}$), 30.13 (Ar- CH_2-), 33.67 ($-\text{C}(\text{Me})(\text{CN})-\text{CH}_2-$), 39.18 ($-\text{CH}_2-\text{N}$), 39.87 ($-\text{CH}_2-\text{S}$), 46.41 (S-C(Me)(CN)-), 118.98 (CN), 126.81, 128.60, 128.64 (Ar), 138.98 (Ar- CH_2), 171.40 ($>\text{C}=\text{O}$), 221.00 ($>\text{C}=\text{S}$); IR (neat) $\nu_{\text{max}}/\text{cm}^{-1}$ 3944, 3660, 3362, 3054, 2986, 2685, 2572, 2412, 2306, 1711, 1684, 1625, 1585, 1495, 1474, 1442, 1421, 1390, 1364, 1266, 1187, 1162, 1063, 1039, 910, 836, 737.

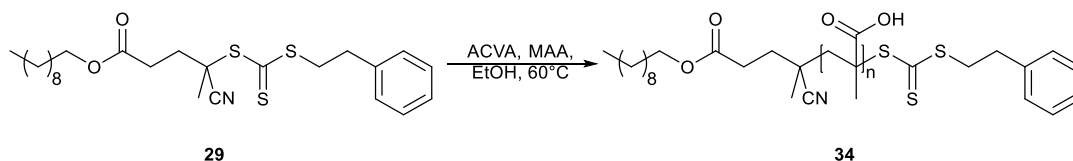
8.29. Synthesis of 4,4'-azobis(Boc-mono-C-decyl-4-cyano-valerate, tri-C-decyl calix[4]resorcinarene) (**33**)



4,4'-azobis(4-cyanopentanoic acid) (50 mg, 0.18 mmol), mono-hydroxyl calixarene **5** (0.92 g, 0.49 mmol), and 4-dimethylaminopyridine (20 mg, 0.14 mmol) were dissolved in DCM/THF (1:1 v/v, 0.7 ml). *N,N*-dicyclohexylcarbodiimide (80 mg, 0.4 mmol) in DCM (0.3 ml) was added dropwise. The reaction was stirred at room temperature overnight. After completion of the reaction, two drops of acetic acid were added to the reaction mixture, and stirring continued for 30 min. Dicyclohexylurea was removed by filtration and the solvent removed by rotary evaporation. The residue was purified by column chromatography (25% EtOAc:petroleum spirit 40-60) to give the calixarene diester **33** (30 mg, 0.76 μ mol, 4%).

^1H NMR (400 MHz, CDCl_3) δ_{H} 0.88 (t, $J = 6.15$ Hz, 3H, $-\text{CH}_3$), 0.89 (t, $J = 7.04$ Hz, 3H, $-\text{CH}_2-\text{CH}_3$), 1.18-1.35 (m, 14-18H, $-\text{CH}_2-$), 1.50 (s, 18H, (*t*-Bu) CH_3), 1.68 (s, 3H, $-\text{CH}_3$), 2.31-2.56 (m, 4H, $-\text{C}(\text{Me})(\text{CN})-\text{CH}_2-\text{CH}_2-$), 4.08 (t, $J = 6.79$ Hz, 2H, $-\text{CH}_2-\text{O}$), 4.34 (t, $J = 7.96$ Hz, 1H, Ar- $\text{CH}-$), 6.52 (s, 1H, CH-Ar(**H**)-CH), 6.94 (br s, 1H, BocO-Ar(**H**)-OBoc); ^{13}C NMR (100 MHz, CDCl_3) δ_{C} 14.12 ($-\text{CH}_3$), 22.69 ($-\text{CH}_2-\text{CH}_3$), 27.67 ((*t*-Bu) CH_3), 28.00-29.85 ($-\text{CH}_2-$), 29.74 ($-\text{CH}_3$), 33.17 ($-\text{CH}_2-\text{CO}_2$), 35.03 ($-\text{C}(\text{Me})(\text{CN})-\text{CH}_2-$), 36.46 (Ar- $\text{CH}-$), 71.86 (N- $\text{C}(\text{Me})(\text{CN})-$), 65.34 ($-\text{CH}_2-\text{O}$), 82.67 ((*t*-Bu) $\text{C}-\text{CH}_3$), 103.71 (CH-Ar-CH), 126.10 (Ar- $\text{CH}-$), 126.78 (CN), 147.22 ($-\text{OC}(\text{O})\text{OBoc}$), 151.39 (BocO-Ar-OBoc), 171.37 ($>\text{C}=\text{O}$).

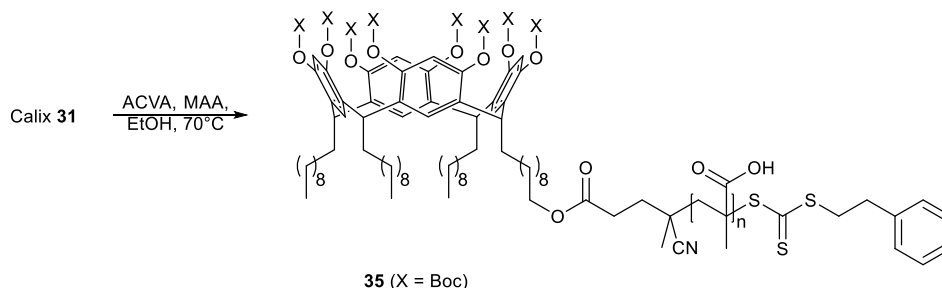
8.30. Synthesis of decyl 4-cyano-4-[pMAA-(phenethylthio)thiocarbonylthio] valerate (**34**)



decyl-PETTC **29** (40 mg, 30 μmol , 1 eq.), 4,4'-azobis(4-cyanopentanoic acid) (20 mg, 70 μmol , 2 eq.), and methacrylic acid (0.3 ml, 3.54 mmol, 89 eq.) were dissolved in ethanol (5 ml). The reaction mixture was degassed with nitrogen for 30 min at 0 °C before being placed into a preheated oil bath at 60 °C and the reaction was left overnight. The solvent was removed to leave the polymer **34** (0.25 g, 72%).

^1H NMR (400 MHz, MeOD) δ_{H} 0.92 (br, $-\text{CH}_2-\text{CH}_3$), 1.12 (br, polymer- CH_3), 1.55 (br, $-\text{CH}_2-\text{CH}_2\text{O}$), 1.91 (br, C- CH_3), 1.90 (br, polymer- CH_2-), 2.40 (br, $-\text{C}(\text{Me})(\text{CN})-\text{CH}_2-$), 2.55 (br, $-\text{CH}_2-\text{CO}$), 3.02 (br, Ar- CH_2-), 3.46 (br, $-\text{CH}_2-\text{S}$), 4.10 (br, $-\text{CH}_2-\text{O}$), 7.19-7.32 (m, 5H, Ar-**H**); ^{13}C NMR (100 MHz, MeOD) δ_{C} 15.90 ($-\text{CH}_2-\text{CH}_3$), 17.07 (polymer- CH_2-), 44.49 (polymer- CH_3), 46.41 (S-C(Me)(CN)-), 118.98 (CN), 128.16, 128.34 (Ar), 136.71 (Ar- CH_2), 169.46 ($>\text{C}=\text{O}$), 180.95 (polymer $>\text{C}=\text{O}$); IR (neat) $\nu_{\text{max}}/\text{cm}^{-1}$ 3182, 2995, 2932, 2587, 1694, 1634, 1486, 1454, 1420, 1375, 1263, 1177, 1009, 941, 798.

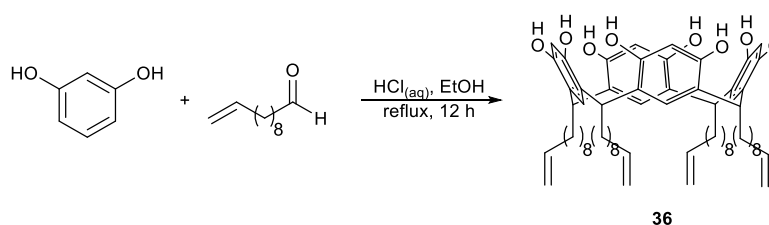
8.31. Synthesis of Boc-mono-C-4-cyano-4-[pMAA-(phenethylthio)thiocarbonylthio] valerate, tri-C-decyl calix[4]resorcinarene (**35**)



Boc-calix[4]resorcinarene-PETTC **31** (0.23 g, 0.11 mmol, 1 eq.), 4,4'-azobis(4-cyanopentanoic acid) (6 mg, 21 μmol , 20 mol%), and methacrylic acid (0.54 ml, 6.39 mmol, 60 eq.) were dissolved in ethanol (0.7 ml) to obtain a 50% w/w solution of methacrylic acid. The reaction mixture was degassed with argon being placed into a preheated oil bath at 70 °C for 15 min. The polymer was diluted with ethanol (1.1 ml), and precipitated into a ten-fold excess of diethyl ether to remove any unreacted methacrylic acid monomer. The purified polymer was filtered and dried to give the polymer **35** as a yellow solid (0.54 g, 69%).

^1H NMR (400 MHz, MeOD) δ_{H} 0.91 (br, $-\text{CH}_2-\text{CH}_3$), 1.11 (br, polymer- CH_3), 1.25-1.40 (br, $-\text{CH}_2-$), 1.54 (br s, (*t*-Bu) CH_3), 1.90, 2.02 (br, polymer- CH_2-), 2.51 (br, $-\text{C}(\text{Me})(\text{CN})-\text{CH}_2-$), 2.59 (br, $-\text{CH}_2-\text{CO}$), 2.95 (br, Ar- CH_2-), 3.46 (br, $-\text{CH}_2-\text{S}$), 4.09 (br, $-\text{CH}_2-\text{O}$), 4.34 (t, $J = 7.52$ Hz, Ar- $\text{CH}-$), 6.84 (br s, 1H, BocO-Ar(**H**)-OBoc), 7.21-7.35 (m, Ar-**H**); ^{13}C NMR (100 MHz, MeOD) δ_{C} 14.05 ($-\text{CH}_2-\text{CH}_3$), 16.97 (polymer- CH_3), 22.39 ($-\text{CH}_2-\text{CH}_3$), 23.51 ($-\text{CH}_3$), 26.66 ((*t*-Bu) CH_3), 29.09-29.49 ($-\text{CH}_2-$), 29.59 ($-\text{CH}_2-\text{CO}_2\text{C}$), 31.71 (Ar- CH_2-), 33.45 ($-\text{C}(\text{Me})(\text{CN})-\text{CH}_2-$), 34.42 (Ar- $\text{CH}-$), 37.21 ($-\text{CH}_2-\text{S}$), 44.48, 44.85 (polymer- CH_2-), 45.85 (*S*- $\text{C}(\text{Me})(\text{CN})-$), 65.52 ($-\text{CH}_2-\text{O}$), 83.03 ((*t*-Bu) $\text{C}-\text{CH}_3$), 104.05 ($\text{CH}-\text{Ar}-\text{CH}$), 118.65 (**CN**), 124.65 (Ar- $\text{CH}-$), 128.20, 128.25 (**Ar**), 135.28 (Ar- CH_2), 147.10 ($-\text{OC}(\text{O})\text{OBoc}$), 151.53 (BocO-Ar-OBoc), 169.29 ($>\text{C}=\text{O}$), 180.00, 180.87, 181.17 (polymer $>\text{C}=\text{O}$), 216.39 (**C=S**); GPC $M_n = 10776$ g mol^{-1} , $M_w = 14943$ g mol^{-1} , $M_w/M_n = 1.39$.

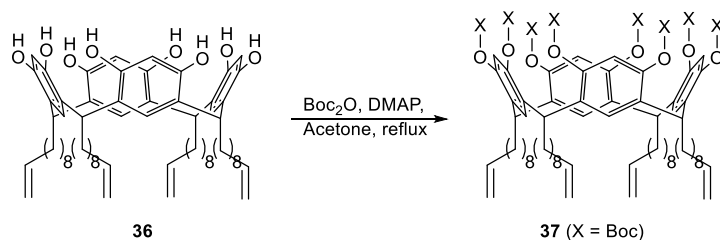
8.32. Synthesis of C-decenyyl calix[4]resorcinarene (**36**)



A solution of resorcinol (10.0 g, 90.82 mmol) and undecylenic aldehyde (18.87 ml, 90.82 mmol) was prepared in ethanol (175 ml). The solution was cooled on ice as hydrochloric acid (35%, 25 ml) was added dropwise. The solution was then heated to 75°C for 48 hrs. The resulting solution was cooled and poured into water (500 ml). The precipitate was collected by filtration and recrystallised twice from acetonitrile to yield the tetra-alkene calix[4]resorcinarene **36** as an orange powder (14.6 g, 14.0 mmol, 62%).

^1H NMR (400 MHz, d_6 -acetone) δ_{H} 1.21-1.46 (m, 14H, $-\text{CH}_2-$), 2.30 (q, $J = 7.6$ Hz, 2H, ArCH- CH_2-), 4.30 (t, $J = 7.96$ Hz, 1H, Ar- $\text{CH}-$), 4.93 (ddt, $^3J_{\text{cis}} = 10.3$ Hz, $^2J_{\text{gem}} = 1.53$ Hz, $^4J_{\text{trans}} = 1.15$ Hz, 1H, $-\text{CH}=\text{CH}_{\text{trans}}\text{H}_{\text{cis}}$), 5.01 (dd, $^3J_{\text{trans}} = 17.1$ Hz, $^2J_{\text{gem}} = 1.53$ Hz, 1H, $-\text{CH}=\text{CH}_{\text{trans}}\text{H}_{\text{cis}}$), 5.83 (ddt, $^3J_{\text{trans}} = 17.1$ Hz, $^3J_{\text{cis}} = 10.3$ Hz, $^3J_{\text{gem}} = 6.6$ Hz, 1H, $-\text{CH}=\text{CH}_2$), 6.28 (s, 1H, CH-Ar(**H**)-CH), 7.52 (s, 1H, HO-Ar(**H**)-OH); ^{13}C NMR (100 MHz, d_6 -acetone) δ_{C} 29.06-30.59 ($-\text{CH}_2-$), 34.36 ($-\text{CH}_2-\text{CH}=\text{}$), 34.56 (Ar- $\text{CH}-$), 103.60 (CH-Ar-CH), 114.75 ($-\text{CH}=\text{CH}_2$), 125.17 (Ar- $\text{CH}-$), 125.43 (HO-Ar-OH), 139.85 ($-\text{CH}=\text{CH}_2$), 152.61 (Ar-OH); IR (neat) 3209, 2923, 2853, 1619, 1497, 1445, 1291, 1166, 1085, 907, 835, 606 cm^{-1} ; MS (MALDI-TOF) m/z 1040.6 $[\text{M}]^+$, 1063.8 $[\text{MNa}]^+$. HRMS-ES-TOF m/z calcd for $\text{C}_{68}\text{H}_{97}\text{O}_8$ ($[\text{M}+\text{H}]^+$): 1041.7183, Found 1041.7202.

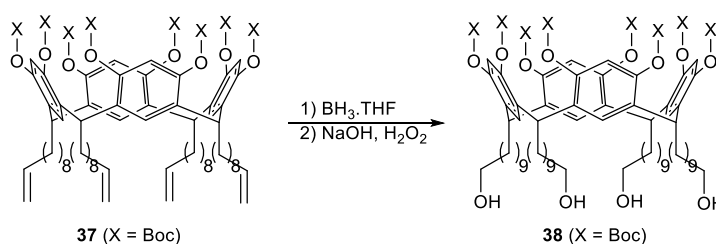
8.33. Synthesis of Boc-C-decenylyl calix[4]resorcinarene (**37**)



A solution of tetra-alkene calix[4]resorcinarene **36** (4.0 g, 3.84 mmol), di-*t*-butyl dicarbonate (6.87 g, 31.48 mmol), and 4-dimethylaminopyridine (25.1 mg, 0.21 mmol) in dry acetone (100 ml) was refluxed for 24 hrs. The acetone was removed and the residue redissolved in diethyl ether, which was then washed with 1M HCl, water, and brine. The solvent was removed by rotary evaporation to give a semi-crystalline orange solid which was recrystallised from ethanol to give the Boc protected tetra-alkene calix[4]resorcinarene **37** as an off-white solid (4.24 g, 2.30 mmol, 60%).

^1H NMR (400 MHz, CDCl_3) δ_{H} 1.19-1.38 (m, 14H, $-\text{CH}_2-$), 1.50 (s, 18H, (*t*-Bu) CH_3), 2.03 (q, $J = 7.6$ Hz, 2H, ArCH- CH_2-), 4.34 (t, $J = 7.96$ Hz, 1H, Ar- $\text{CH}-$), 4.93 (ddt, $^3J_{\text{cis}} = 10.3$ Hz, $^2J_{\text{gem}} = 1.53$ Hz, $^4J_{\text{trans}} = 1.15$ Hz, 1H, $-\text{CH}=\text{CH}_{\text{trans}}\text{H}_{\text{cis}}$), 4.99 (dd, $^3J_{\text{trans}} = 17.1$ Hz, $^2J_{\text{gem}} = 1.53$ Hz, 1H, $-\text{CH}=\text{CH}_{\text{trans}}\text{H}_{\text{cis}}$), 5.81 (ddt, $^3J_{\text{trans}} = 17.1$ Hz, $^3J_{\text{cis}} = 10.3$ Hz, $^3J_{\text{gem}} = 6.6$ Hz, 1H, $-\text{CH}=\text{CH}_2$), 6.52 (s, 1H, CH-Ar(**H**)-CH), 6.94 (br s, 1H, BocO-Ar(**H**)-OBoc); ^{13}C NMR (100 MHz, CDCl_3) δ_{C} 27.65 ((*t*-Bu) CH_3), 29.06-30.59 ($-\text{CH}_2-$), 33.80 ($-\text{CH}_2-\text{CH}=\text{}$), 34.56 (Ar- $\text{CH}-$), 82.65 ((*t*-Bu) $\text{C}-\text{CH}_3$), 103.60 (CH-Ar-CH), 114.05 ($-\text{CH}=\text{CH}_2$), 126.07 (Ar- $\text{CH}-$), 139.17 ($-\text{CH}=\text{CH}_2$), 146.45 ($-\text{OC}(\text{O})\text{OBoc}$), 151.36 (BocO-Ar-OBoc), 206.91 (Ar-OBoc); MS (MALDI-TOF) m/z 1866.4 [MNa] $^+$, 1881.6 [MK] $^+$.

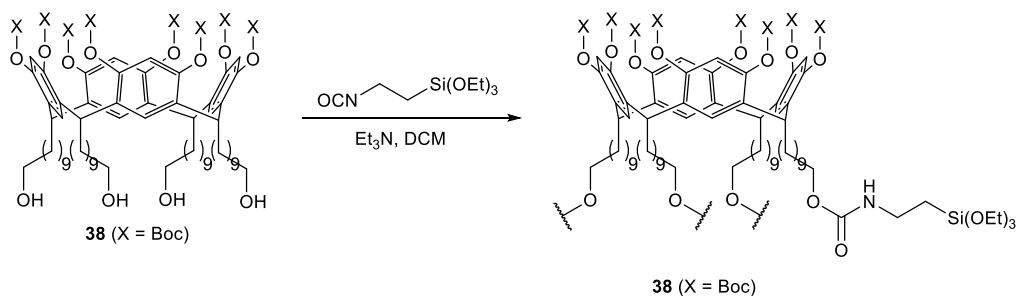
8.34. Synthesis of Boc-C-hydroxydecyl calix[4]resorcinarene (**38**)



$\text{BH}_3 \cdot \text{THF}$ (1M, 12 ml, 12 mmol) was added to a solution of Boc protected tetra-alkene calix[4]resorcinarene **37** (3.95 g, 2.14 mmol) in dry THF (30 ml), and the reaction mixture was stirred at room temperature for 5 days. The excess of BH_3 was quenched with water, and NaOH (1N, 8 ml) and H_2O_2 (30%, 24 ml) were added. After stirring at room temperature for 1 hr then at 50°C for 4 hrs, the mixture was poured into water and extracted twice with CH_2Cl_2 . The organic layer was dried with MgSO_4 and concentrated to give a viscous orange oil which was purified by gradient column chromatography (30% EtOAc:Petrol 40-60, followed by EtOAc and MeOH) to give the tetra-hydroxylate product **38** (3.56 g, 1.86 mmol, 87%).

^1H NMR (400 MHz, CDCl_3) δ_{H} 1.19-1.38 (m, 14H, $-\text{CH}_2-$), 1.50 (s, 18H, (*t*-Bu) CH_3), 2.03 (q, $J = 7.6$ Hz, 2H, ArCH- CH_2-), 3.63 (t, $J = 6.72$ Hz, 2H, $-\text{CH}_2-\text{OH}$), 4.34 (t, $J = 7.96$ Hz, 1H, Ar- $\text{CH}-$), 6.52 (s, 1H, CH-Ar(**H**)-CH), 6.94 (br s, 1H, BocO-Ar(**H**)-OBoc); ^{13}C NMR (100 MHz, CDCl_3) δ_{C} 27.67 ((*t*-Bu) CH_3), 28.96-29.82 ($-\text{CH}_2-$), 33.82 (Ar- $\text{CH}-$), 63.07 ($-\text{CH}_2-\text{OH}$), 82.64 ((*t*-Bu) $\text{C}-\text{CH}_3$), 103.71 (CH-Ar-CH), 126.09 (Ar- $\text{CH}-$), 147.19 ($-\text{OC}(\text{O})\text{OBoc}$), 151.31 (BocO-Ar-OBoc); IR (neat) 3348, 2980, 2926, 2854, 1755, 1495, 1459, 1395, 1340, 1270, 1241, 1138, 1116, 1049, 886, 846, 780, 722, 592 cm^{-1} ; MS (MALDI-TOF) m/z 1939.9 $[\text{MNa}]^+$, 1959.2 $[\text{MK}]^+$.

8.35. Synthesis of Boc- C-decyl-3-triethoxysilylpropylcarbonamate calix[4]resorcinarene (**39**)



Boc protected hydroxyl calix[4]resorcinarene **38** (1 g, 0.52 mmol) and triethylamine (1.92 ml, 13.7 mmol) were dissolved in dry DCM (10 ml). 3-(triethoxysilyl)propyl isocyanate (1.14 ml, 4.58 mmol) was added dropwise and the solution stirred at room temperature overnight. The solvent was removed and the crude material purified by column chromatography (30% EtOAc:Petrol 40-60 increasing to 50% EtOAc:Petrol 40-60) to give the APTES functionalised calix[4]resorcinarene **39** (1.18 g, 0.42 mmol, 81%).

^1H NMR (400 MHz, CDCl_3) δ_{H} 1.19-1.38 (m, 14H, $-\text{CH}_2-$), 1.50 (s, 18H, $(t\text{-Bu})\text{CH}_3$), 2.03 (q, $J = 7.6$ Hz, 2H, ArCH-CH_2-), 3.25 (t, $J = 7.28$ Hz, 2H, $-\text{CH}_2\text{-N}$), 3.64 (q, $J = 7.12$ Hz, 6H, $\text{CH}_3\text{-CH}_2\text{-O}$), 4.09 (t, $J = 7.10$ Hz, 2H, $-\text{CH}_2\text{-O}$), 4.34 (t, $J = 7.96$ Hz, 1H, Ar-CH-), 6.52 (s, 1H, CH-Ar(H)-CH), 6.94 (br s, 1H, BocO-Ar(H)-OBoc); ^{13}C NMR (100 MHz, CDCl_3) δ_{C} 13.72 ($-\text{CH}_2\text{-Si}$), 18.32 ($\text{CH}_3\text{-CH}_2\text{-O}$), 27.67 ($(t\text{-Bu})\text{CH}_3$), 28.96-29.82 ($-\text{CH}_2-$), 33.82 (Ar-CH-), 50.01 ($-\text{CH}_2\text{-N}$), 61.05 ($\text{CH}_3\text{-CH}_2\text{-O}$), 65.53 ($-\text{CH}_2\text{-O}$), 82.64 ($(t\text{-Bu})\text{C-CH}_3$), 103.71 (CH-Ar-CH), 126.09 (Ar-CH-), 147.19 ($-\text{OC(O)OBoc}$), 151.31 (BocO-Ar-OBoc), 155.8 (O(C=O)N); MS (MALDI-TOF) m/z 2830.8 [MNa] $^+$, 2846.8 [MK] $^+$.

8.36. Synthesis of poly(methacrylic acid) hydrogels

A solution of methacrylic acid (20 ml, 0.23 mol), 2,2'-Azobis(2-methyl propionamide) dihydrochloride (30 mg, 0.11 mmol), and *N,N'*-methylenebisacrylamide (60 mg, 0.39 mmol) in deionised water (100 ml, 5.56 mol) was stirred to effect dissolution. The resulting solution was poured into a mould, which was sealed and placed in a pre-heated oven at 80°C for 2 h. The mould was removed and the gel cut into individual hemispherical pieces of 4 mm diameter and stored in deionised water for a minimum of three days before use. The deionised water was changed at least twice during this period.

8.37. Synthesis of poly(diethylaminoethyl methacrylate) hydrogels

A solution of 2-(diethylamino)ethyl methacrylate (30 ml, 0.15 mol), 2,2'-Azobis(2-methyl propionamide) dihydrochloride (0.59 g, 2.18 mmol), and ethylene glycol dimethacrylate (0.57 ml, 3.02 mmol) in a mixture of deionised water (35 ml, 1.94 mol) and methanol (38 ml, 0.94 mol) was stirred to effect dissolution. The resulting solution was poured into a mould, which was sealed and placed in a pre-heated oven at 80°C for 2 h. The mould was removed and the gel cut into individual hemispherical pieces of 4 mm diameter and stored in deionised water for a least three days before use. The deionised water was changed at least twice during this period.

8.38. Synthesis of poly(methacrylic acid)-poly(oligo(ethylene glycol) methyl ether methacrylate) double network hydrogels

A solution of methacrylic acid (10 ml, 0.12 mol), potassium persulfate (0.13 g, 0.48 mmol), and *N,N'*-methylenebisacrylamide (0.94 g, 6.10 mmol) in deionised water (50 ml, 2.8 mol) was stirred to effect dissolution. The resulting solution was poured into a mould, which was sealed and placed in a pre-heated oven at 60°C for 6 h. The mould was removed and the gel cut into individual hemispherical pieces of 4 mm diameter and stored in deionised water for a least three days before use. The deionised water was changed at least twice during this period.

The poly(methacrylic acid) hydrogels were then immersed in a solution of oligo(ethylene glycol) methyl ether methacrylate (average $M_n = 950 \text{ g mol}^{-1}$, 12 g, 12.6 mmol), potassium persulfate (40 mg, 0.15 mmol), and *N,N'*-methylenebisacrylamide (20 mg, 0.13 mmol) in deionised water (60 ml, 3.3 mol) for 5 days. The hydrogels were then rinsed in fresh deionised water and placed in a sealed container which was put in a pre-heated oven at 80 °C for 2 hrs. The hydrogels were removed and stored in deionised water for a least three days before use. The deionised water was changed at least twice during this period.

8.39. Preparation of silicon wafers

Silicon wafers were purchased from Prolog Semicor Ltd with the following characteristics: diameter 50.8 mm (2"), dopant p-type boron, orientation (100) $\pm 1^\circ$, resistivity 0-0.3 Ωm , thickness $275 \pm 25 \mu\text{m}$.

Wafers were either used whole, or cut to size (~12 x 15 mm). Wafers were cleaned and rendered hydrophilic using piranha solution (3:1 sulfuric acid:hydrogen peroxide). Once the solution had cooled, the wafer samples were washed repeatedly with deionised water and oven dried.

Hydrophobic wafers were prepared by treating piranha solution cleaned wafers with hexamethyldisilazane (HMDS). Clean wafers were placed in a sealed sample tube with three drops of HMDS and heated to 80 °C for 15 min. Once the wafers had cooled, they were rinsed in toluene and then dried under a stream of compressed air.

(3-aminopropyl)triethoxysilane functionalised wafers were prepared by immersing piranha solution cleaned wafers in a 2% (v/v) solution of (3-aminopropyl)triethoxysilane in ethanol for 30 min. The wafers were rinsed with ethanol, dried under a stream of compressed air, and then annealed for 30 min at 120 °C.

8.40. Spin-coating of PVAc

The surface of a piranha cleaned wafer was flooded with poly(vinyl acetate) ($M_w = 50,000$) dissolved in toluene (87 μM), and the sample spun at either 1750 or 4500 rpm for 60 seconds.

8.41. Preparation of layer-by-layer functionalised surfaces

For samples starting with a silicon substrate: piranha cleaned wafers were immersed in alternating solutions of decyl-pDMAEMA **14** dissolved in dichloromethane (10 mM based upon repeat unit), and decyl-pMAA **17** dissolved in 0.5 M NaCl_(aq) (10 mM based upon repeat unit). Between each deposition the samples were rinsed in clean solvent and dried under a stream of compressed air.

For samples starting with an APTES functionalised surface: APTES coated wafers were immersed in alternating solutions of decyl-pMAA **17** dissolved in 0.5 M NaCl_(aq) (10 mM based upon repeat unit), and decyl-pDMAEMA **14** dissolved in dichloromethane (10 mM based upon repeat unit). Between each deposition the samples were rinsed in clean solvent and dried under a stream of compressed air.

8.42. Preparation of APTES-calix[4]resorcinarene functionalised surfaces

APTES-calix[4]resorcinarene functionalised wafers were prepared by immersing piranha solution cleaned wafers in a 2% (v/v) solution of APTES functionalised calix[4]resorcinarene **39** in ethanol for 30 min. The wafers were rinsed with ethanol, dried under a stream of compressed air, and then annealed for 30 min at 120°C.

9. References

- 1 P. P. A. Mazza, F. Martini, B. Sala, M. Magi, M. P. Colombini, G. Giachi, F. Landucci, C. Lemorini, F. Modugno and E. Ribechini, *J. Archaeol. Sci.*, 2006, **33**, 1310–1318.
- 2 D. V. Thompson, *The Materials and Techniques of Medieval Painting*, Dover Publications, 1st edn., 1956.
- 3 Permabond, Industrial Uses of Adhesives, <http://www.permabond.co.uk/industries>, (accessed 29 August 2017).
- 4 O. Kutsch, *Market Study: Adhesives - World*, Ceresana, 2nd edn., 2015.
- 5 J. Comyn, in *Adhesion Science*, ed. J. Comyn, The Royal Society of Chemistry, 1997, pp. 1–17.
- 6 CIBA-GEIGY, in *User's Guide to Adhesives*, pp. 194–212.
- 7 M. P. Weir and A. J. Parnell, *Polymers (Basel)*, 2011, **3**, 2107–2132.
- 8 R. La Spina, A. Chiche, M. R. Tomlinson and M. Geoghegan, *Eur. Coatings J.*, 2011, 22–28.
- 9 G. L. Schneberger, in *Handbook of Adhesives*, ed. I. Skeist, Chapman & Hall, New York, 3rd edn., 1990, pp. 729–735.
- 10 *DIRECTIVE 2000/53/EC OF THE EUROPEAN PARLIAMENT AND OF THE COUNCIL of 18 September 2000 on end-of life vehicles*, 2000.
- 11 R. Dawson, *Automot. World*, 2013, 61–62.
- 12 W. Wei and M. Hansen, *J. Transp. Econ. Policy*, 2003, **37**, 279–296.
- 13 Boeing, About Boeing Commercial Airplanes, <http://www.boeing.com/company/about-bca/index.page%23/prices>, (accessed 29 September 2017).
- 14 Business Insider, Some Unbelievable Statistics About The GE Engine On The Boeing 777, <http://www.businessinsider.com/some-unbelievable-statistics-about-the-ge-engine-on-the-boeing-777-2011-12?IR=T>, (accessed 29 September 2017).
- 15 R. E. Politi, in *Handbook of Adhesives*, ed. I. Skeist, Chapman & Hall, New York, 3rd edn., 1990, pp. 713–728.
- 16 M. Richardson and S. Lichtle, *Aerosp. Manuf.*, 2011.
- 17 D. Wang, How Are Planes Decommissioned, and How Much Value Can Be Salvaged From Their Parts?, <https://www.flexport.com/blog/decommissioned-planes-salvage-value/>, (accessed 29 September 2017).
- 18 M. Sabaghi, Y. Cai, C. Mascle and P. Baptiste, *Procedia CIRP*, 2016, **40**, 156–161.
- 19 I. Towle, C. Johnston, R. Lingwood and P. S. Grant, *The aircraft at the End of Life Sector: A Preliminary Study*, 2004.
- 20 M. J. Vogel and P. H. Steen, *Proc. Natl. Acad. Sci. U. S. A.*, 2010, **107**, 3377–3381.
- 21 S. Reddy, E. Arzt and A. del Campo, *Adv. Mater.*, 2007, **19**, 3833–3837.

- 22 H. E. Jeong, M. K. Kwak and K. Y. Suh, *Langmuir*, 2010, **26**, 2223–2226.
- 23 S. Minko, M. Müller, M. Motornov, M. Nitschke, K. Grundke and M. Stamm, *J. Am. Chem. Soc.*, 2003, **125**, 3896–3900.
- 24 S. Kim, M. Sitti, T. Xie and X. Xiao, *Soft Matter*, 2009, **5**, 3689–3693.
- 25 M. T. Northen, C. Greiner, E. Arzt and K. L. Turner, *Adv. Mater.*, 2008, **20**, 3905–3909.
- 26 S. Khongtong and G. S. Ferguson, *J. Am. Chem. Soc.*, 2002, **124**, 7254–7255.
- 27 R. La Spina, M. R. Tomlinson, L. Ruiz-Pérez, A. Chiche, S. Langridge and M. Geoghegan, *Angew. Chemie - Int. Ed.*, 2007, **46**, 6460–6463.
- 28 M. Kobayashi, M. Terada and A. Takahara, *Soft Matter*, 2011, **7**, 5717–5722.
- 29 A. Synytska, E. Svetushkina, N. Pureskiy, G. Stoychev, S. Berger, L. Ionov, C. Bellmann, K.-J. Eichhorn and M. Stamm, *Soft Matter*, 2010, **6**, 5907–5914.
- 30 US 2013/0017246 A1, 2013.
- 31 P. S. Shuttleworth, J. H. Clark, R. Mantle and N. Stansfield, *Green Chem.*, 2010, **12**, 798–803.
- 32 E. Kizilkan, J. Strueben, A. Staubitz and S. N. Gorb, *Sci. Robot.*, 2017, **2**, eaak9454.
- 33 L. Alfhaid, W. D. Seddon, N. H. Williams and M. Geoghegan, *Soft Matter*, 2016, **12**, 5022–5028.
- 34 L. Alfhaid, R. La Spina, M. R. Tomlinson, A. R. Hall, W. D. Seddon, N. H. Williams, F. Cousin, S. Gorb and M. Geoghegan, *J. Adhes.*, 2018, **94**, 58–76.
- 35 G. Fourche, *Polym. Eng. Sci.*, 1995, **35**, 957–967.
- 36 J. Liu and T. Sawa, *J. Adhes. Sci. Technol.*, 2001, **15**, 43–61.
- 37 A. Baldan, *Int. J. Adhes. Adhes.*, 2012, **38**, 95–116.
- 38 J. W. McBain and D. G. Hopkins, *J. Phys. Chem.*, 1925, **29**, 188–204.
- 39 S. Yang, L. Gu and R. F. Gibson, *Compos. Struct.*, 2001, **51**, 63–71.
- 40 F. Awaja, M. Gilbert, G. Kelly, B. Fox and P. J. Pigram, *Prog. Polym. Sci.*, 2009, **34**, 948–968.
- 41 A. J. Kinloch, *J. Mater. Sci.*, 1980, **15**, 2141–2166.
- 42 S. S. Voyutskii, *Autohesion and adhesion of high polymers*, Wiley-Interscience, New York, 1963.
- 43 G. Grundmeier and M. Stratmann, *Annu. Rev. Mater. Res.*, 2005, **35**, 571–615.
- 44 L. H. Sharpe and H. Schonhorn, in *Contact Angle, Wettability, and Adhesion*, ed. F. M. Fowkes, American Chemical Society, 1964, vol. 43, pp. 189–201.
- 45 J. J. Bikerman, *The Science of Adhesive Joints*, Academic Press Inc., New York, 2nd edn., 1968.
- 46 J. J. Licari and D. W. Swanson, in *Adhesives Technology for Electronic Applications*, Elsevier, 2011, pp. 75–141.
- 47 H. Lee and K. Neville, *Handbook of epoxy resins*, McGraw-Hill, Inc., New York, 1967.
- 48 I. Skeist and J. Miron, in *Handbook of Adhesives*, ed. I. Skeist, Chapman & Hall, New York, 3rd edn., 1990, pp. 3–20.

- 49 B. Ellis, *Chemistry and Technology of Epoxy Resins*, Blackie Academic and Professional, London, 1993.
- 50 B. Arkles, *REACTIVE SILICONES: Forging new polymer links*, Gelest, Inc., 2013.
- 51 J. Bauer, L. Höper and M. Bauer, *Macromol. Chem. Phys.*, 1998, **199**, 2417–2423.
- 52 L. P. Bré, Y. Zheng, A. P. Pêgo and W. Wang, *Biomater. Sci.*, 2013, **1**, 239–253.
- 53 W. A. Lees, *Br. Polym. J.*, 1979, **11**, 64–71.
- 54 Y. Okamoto, *J. Adhes.*, 1990, **32**, 227–235.
- 55 Dymax, *Removal of Cured UV Adhesives and Resins*, 2011.
- 56 A. Biswas, I. S. Bayer, A. S. Biris, T. Wang, E. Dervishi and F. Faupel, *Adv. Colloid Interface Sci.*, 2012, **170**, 2–27.
- 57 J. V. Barth, G. Costantini and K. Kern, *Nature*, 2005, **437**, 671–679.
- 58 R. Bawa, S. R. Bawa, S. B. Maebius, T. Flynn and C. Wei, *Nanomedicine Nanotechnology, Biol. Med.*, 2005, **1**, 150–158.
- 59 M. A. Kastner, *Phys. Today*, 1993, **46**, 24–31.
- 60 C. Dekker, *Phys. Today*, 1999, **52**, 22–28.
- 61 K. C. Schwab and M. L. Roukes, *Phys. Today*, 2005, **58**, 36–42.
- 62 W. Chen, L. F. Register and S. K. Banerjee, *IEEE Trans. Electron Devices*, 2002, **49**, 652–657.
- 63 C. Genet, F. Intravaia, A. Lambrecht and S. Reynaud, *Ann. la Fond. Louis Broglie*, 2004, **29**, 331–348.
- 64 B. D. Hamilton, J. M. Ha, M. A. Hillmyer and M. D. Ward, *Acc. Chem. Res.*, 2012, **45**, 414–423.
- 65 A. V. Biradar and T. Asefa, *Appl. Catal. A Gen.*, 2012, **435–436**, 19–26.
- 66 T. Xie and X. Xiao, *Chem. Mater.*, 2008, **20**, 2866–2868.
- 67 E. P. Chan, E. J. Smith, R. C. Hayward and A. J. Crosby, *Adv. Mater.*, 2008, **20**, 711–716.
- 68 N. Nadermann, J. Ning, A. Jagota and C.-Y. Hui, *Langmuir*, 2010, **26**, 15464–15471.
- 69 S. R. Deka, A. Quarta, R. Di-Corato, A. Falqui, L. Manna, R. Cingolani and T. Pellegrino, *Langmuir*, 2010, **26**, 10315–10324.
- 70 B. D. Gates, Q. Xu, M. Stewart, D. Ryan, C. G. Willson and G. M. Whitesides, *Chem. Rev.*, 2005, **105**, 1171–1196.
- 71 D. Maily, *Eur. Phys. J. Spec. Top.*, 2009, **172**, 333–342.
- 72 K. Ariga, J. P. Hill, M. V. Lee, A. Vinu, R. Charvet and S. Acharya, *Sci. Technol. Adv. Mater.*, 2008, **9**, 014109.
- 73 I. M. Atkinson and L. F. Lindoy, in *Self Assembly in Supramolecular Systems*, eds. J. F. Stoddart, L. F. Lindoy and I. M. Atkinson, Royal Society of Chemistry, Cambridge, 2000, pp. 1–6.
- 74 A. Ulman, *Chem. Rev.*, 1996, **96**, 1533–1554.
- 75 N. Ishida and M. Kobayashi, *J. Colloid Interface Sci.*, 2006, **297**, 513–519.
- 76 J. Lehn, *Angew. Chemie Int. Ed. English*, 1990, **29**, 1304–1319.

- 77 L. C. Palmer and S. I. Stupp, *Acc. Chem. Res.*, 2008, **41**, 1674–1684.
- 78 L. H. Dubois and R. G. Nuzzo, *Annu. Rev. Phys. Chem.*, 1992, **43**, 437–463.
- 79 C. D. Bain and G. M. Whitesides, *Adv. Mater.*, 1989, **1**, 110–116.
- 80 T. R. Lee, P. E. Laibinis, J. P. Folkers and G. M. Whitesides, *Pure Appl. Chem.*, 1991, **63**, 821–8.
- 81 H. Sellers, A. Ulman, Y. Shnidman and J. E. Eilers, *J. Am. Chem. Soc.*, 1993, **115**, 9389–9401.
- 82 C. D. Bain, E. B. Troughton, Y.-T. Tao, J. Evall, G. M. Whitesides and R. G. Nuzzo, *J. Am. Chem. Soc.*, 1989, **111**, 321–335.
- 83 J. Sagiv, *J. Am. Chem. Soc.*, 1980, **102**, 92–98.
- 84 P. Silberzan, L. Léger, D. Ausserré and J. J. Benattar, *Langmuir*, 1991, **7**, 1647–1651.
- 85 J. D. Le Grange, J. L. Markham and C. R. Kurkjian, *Langmuir*, 1993, **9**, 1749–1753.
- 86 J. Gun and J. Sagiv, *J. Colloid Interface Sci.*, 1986, **112**, 457–472.
- 87 J. Gun, R. Iscovici and J. Sagiv, *J. Colloid Interface Sci.*, 1984, **101**, 201–213.
- 88 N. Tillman, A. Ulman, J. S. Schildkraut and T. L. Penner, *J. Am. Chem. Soc.*, 1988, **110**, 6136–6144.
- 89 S. Brandriss and S. Margel, *Langmuir*, 1993, **9**, 1232–1240.
- 90 K. Mathauer and C. W. Frank, *Langmuir*, 1993, **9**, 3002–3008.
- 91 S. Argentiere, L. Blasi, G. Ciccarella, A. Cazzato, G. Barbarella, R. Cingolani and G. Gigli, *Soft Matter*, 2009, **5**, 4101–4103.
- 92 G. Cortese, F. Martina, G. Vasapollo, R. Cingolani, G. Gigli and G. Ciccarella, *J. Fluor. Chem.*, 2010, **131**, 357–363.
- 93 K. V. Holmberg, M. Abdolhosseini, Y. Li, X. Chen, S.-U. Gorr and C. Aparicio, *Acta Biomater.*, 2013, **9**, 8224–8231.
- 94 G. de Crevoisier, P. Fabre, J.-M. Corpart and L. Leibler, *Science*, 1999, **285**, 1246–1249.
- 95 R. A. Chivers, *Int. J. Adhes. Adhes.*, 2001, **21**, 381–388.
- 96 C. de las H. Alarcón, S. Pennadam and C. Alexander, *Chem. Soc. Rev.*, 2005, **34**, 276–285.
- 97 S. Kessel, S. Schmidt, R. Müller, E. Wischerhoff, A. Laschewsky, J.-F. Lutz, K. Uhlig, A. Lankenau, C. Duschl and A. Fery, *Langmuir*, 2010, **26**, 3462–3467.
- 98 I. Webster, *Int. J. Adhes. Adhes.*, 1999, **19**, 29–34.
- 99 J. M. Boyne, E. J. Millan and I. Webster, *Int. J. Adhes. Adhes.*, 2001, **21**, 49–53.
- 100 R. Sheparovych, M. Motornov and S. Minko, *Langmuir*, 2008, **24**, 13828–13832.
- 101 H. Retsos, A. Kiriy, V. Senkovskyy, M. Stamm, M. M. Feldstein and C. Creton, *Adv. Mater.*, 2006, **18**, 2624–2628.
- 102 T. Wang, E. Canetta, T. G. Weerakkody, J. L. Keddie and U. Rivas, *ACS Appl. Mater. Interfaces*, 2009, **1**, 631–639.
- 103 A. J. Nolte, J. Y. Chung, M. L. Walker and C. M. Stafford, *ACS Appl. Mater. Interfaces*, 2009, **1**, 373–380.
- 104 H. Gao, X. Wang, H. Yao, S. Gorb and E. Arzt, *Mech. Mater.*, 2005, **37**, 275–285.

- 105 J. M. G. Cowie and V. Arrighi, *Polymers: Chemistry and Physics of Modern Materials*, CRC Press, Taylor and Francis Group, 3rd edn., 2008.
- 106 I. Teraoka, *Polymer Solutions: An introduction to physical properties*, 2002, vol. 3.
- 107 Agilent Technologies, *An Introduction to Gel Permeation Chromatography and Size Exclusion Chromatography*, 2011.
- 108 K. Matyjaszewski and J. Xia, *Chem. Rev.*, 2001, **101**, 2921–2990.
- 109 D. J. Keddie, G. Moad, E. Rizzardo and S. H. Thang, *Macromolecules*, 2012, **45**, 5321–5342.
- 110 D. J. Keddie, *Chem. Soc. Rev.*, 2014, **43**, 496–505.
- 111 D. Hinderberger, H. W. Spiess and G. Jeschke, *Appl. Magn. Reson.*, 2010, **37**, 657–683.
- 112 V. Vlachy, *Pure Appl. Chem.*, 2008, **80**, 1253–1266.
- 113 A. Yethiraj, *J. Phys. Chem. B*, 2009, **113**, 1539–1551.
- 114 N. Ahmad, A. Saeed, K. Ahad and M. S. Khan, *J. Chem. Soc. Pakistan*, 1994, **16**, 235–239.
- 115 R. H. Colby, *Rheol. Acta*, 2010, **49**, 425–442.
- 116 N. Ayres, S. G. Boyes and W. J. Brittain, *Langmuir*, 2007, **23**, 182–189.
- 117 M. Ballauff and O. Borisov, *Curr. Opin. Colloid Interface Sci.*, 2006, **11**, 316–323.
- 118 R. R. Bhat, M. R. Tomlinson, T. Wu and J. Genzer, *Adv. Polym. Sci.*, 2006, **198**, 51–124.
- 119 L. Ruiz-Pérez, A. Pryke, M. Sommer, G. Battaglia, I. Soutar, L. Swanson and M. Geoghegan, *Macromolecules*, 2008, **41**, 2203–2211.
- 120 C. D. Gutsche and R. Muthukrishnan, *J. Org. Chem.*, 1978, **43**, 4905–4906.
- 121 Y. Aoyama, Y. Tanaka and S. Sugahara, *J. Am. Chem. Soc.*, 1989, **111**, 5397–5404.
- 122 A. Ikeda and S. Shinkai, *Chem. Rev.*, 1997, **97**, 1713–1734.
- 123 S. León, D. A. Leigh and F. Zerbetto, *Chem. - A Eur. J.*, 2002, **8**, 4854–4866.
- 124 K. Kobayashi, K. Ishii, S. Sakamoto, T. Shirasaka and K. Yamaguchi, *J. Am. Chem. Soc.*, 2003, **125**, 10615–10624.
- 125 A. Shivanyuk, M. Saadioui, F. Broda, I. Thondorf, M. O. Vysotsky, K. Rissanen, E. Kolehmainen and V. Böhmer, *Chem. - A Eur. J.*, 2004, **10**, 2138–2148.
- 126 A. Dubes, K. A. Udachin, P. Shahgaldian, A. N. Lazar, A. W. Coleman and J. A. Ripmeester, *New J. Chem.*, 2005, **29**, 1141–1146.
- 127 H. M. Chawla, S. P. Singh, S. N. Sahu and S. Upreti, *Tetrahedron*, 2006, **62**, 7854–7865.
- 128 J. R. Fransen and P. J. Dutton, *Can. J. Chem.*, 1995, **73**, 2217–2223.
- 129 L. Pirondini, D. Bonifazi, E. Menozzi, E. Wegelius, K. Rissanen, C. Massera and E. Dalcanale, *European J. Org. Chem.*, 2001, 2311–2320.
- 130 S. Sayin and M. Yilmaz, *J. Chem. Eng. Data*, 2011, **56**, 2020–2029.
- 131 A. Casnati, A. Pochini, R. Ungaro, F. Ugozzoli, F. Arnaud, S. Fanni, M.-J. Schwing, R. J. M. Egberink, F. de Jong and D. N. Reinhoudt, *J. Am. Chem. Soc.*, 1995, **117**, 2767–2777.

- 132 J. S. Kim, O. J. Shon, J. W. Ko, M. H. Cho, I. Y. Yu and J. Vicens, *J. Org. Chem.*, 2000, **65**, 2386–2392.
- 133 P. M. Marcos and J. R. Ascenso, *Tetrahedron*, 2006, **62**, 3081–3088.
- 134 F. Kivlehan, W. J. Mace, H. A. Moynihan and D. W. M. Arrigan, *Anal. Chim. Acta*, 2007, **585**, 154–160.
- 135 H. Sakly, R. Mlika, I. Bonnamour, F. Aouni, H. Ben Ouada and N. J. Renault, *Electrochim. Acta*, 2007, **52**, 3697–3703.
- 136 J. M. Notestein, E. Iglesia and A. Katz, *J. Am. Chem. Soc.*, 2004, **126**, 16478–16486.
- 137 R. Cacciapaglia, A. Casnati, L. Mandolini, D. N. Reinhoudt, R. Salvio, A. Sartori and R. Ungaro, *J. Org. Chem.*, 2005, **70**, 624–630.
- 138 N. R. Cha, M. Y. Kim, Y. H. Kim, J.-I. Choe and S.-K. Chang, *J. Chem. Soc. Perkin Trans. 2*, 2002, 1193–1196.
- 139 J. S. Kim, O. J. Shon, J. A. Rim, S. K. Kim and J. Yoon, *J. Org. Chem.*, 2002, **67**, 2348–2351.
- 140 J. Y. Lee, S. K. Kim, J. H. Jung and J. S. Kim, *J. Org. Chem.*, 2005, **70**, 1463–1466.
- 141 S. K. Kim, J. H. Bok, R. A. Bartsch, J. Y. Lee and J. S. Kim, *Org. Lett.*, 2005, **7**, 4839–4842.
- 142 S. K. Kim, S. H. Kim, H. J. Kim, S. H. Lee, S. W. Lee, J. Ko, R. A. Bartsch and J. S. Kim, *Inorg. Chem.*, 2005, **44**, 7866–7875.
- 143 E. U. T. van Velzen, J. F. J. Engbersen and D. N. Reinhoudt, *J. Am. Chem. Soc.*, 1994, **116**, 3597–3598.
- 144 E. U. T. van Velzen, J. F. J. Engbersen and D. N. Reinhoudt, *Synthesis (Stuttg.)*, 1995, 1995, 989–997.
- 145 F. Davis and C. J. M. Stirling, *Langmuir*, 1996, **12**, 5365–5374.
- 146 E. Wirtheim, L. Avram and Y. Cohen, *Tetrahedron*, 2009, **65**, 7268–7276.
- 147 H. Adams, F. Davis and C. J. M. Stirling, *J. Chem. Soc. Chem. Commun.*, 1994, 2527–2529.
- 148 J. D. Faull and V. K. Gupta, *Langmuir*, 2001, 1470–1476.
- 149 S. D. Collyer, F. Davis, A. Lucke, C. J. M. Stirling and S. P. J. Higson, *J. Electroanal. Chem.*, 2003, **549**, 119–127.
- 150 S. Akin, M. Gülen, S. Sayin, H. Azak, H. B. Yildiz and S. Sönmezoğlu, *J. Power Sources*, 2016, **307**, 796–805.
- 151 E. van Dienst, W. I. Iwema Bakker, J. F. J. Engbersen, W. Verboom and D. N. Reinhoudt, *Pure Appl. Chem.*, 1993, **65**, 387–392.
- 152 C. D. Gutsche, B. Dhawan, J. A. Levine, K. Hyun No and L. J. Bauer, *Tetrahedron*, 1983, **39**, 409–426.
- 153 M. Ueda, N. Fukushima, K. Kudo and K. Ichimura, *J. Mater. Chem.*, 1997, **7**, 641–645.
- 154 A. G. S. Högberg, *J. Am. Chem. Soc.*, 1980, **102**, 6046–6050.
- 155 E. Kurita, N. Fukushima, M. Fujimaki, Y. Matsuzawa, K. Kudo and K. Ichimura, *J. Mater. Chem.*, 1998, **8**, 397–403.

- 156 K. V. Kostyukevych, R. V. Khristosenko, A. S. Pavluchenko, A. A. Vakhula, Z. I. Kazantseva, I. A. Koshets and Y. M. Shirshov, *Sensors Actuators B Chem.*, 2016, **223**, 470–480.
- 157 A. Wei, B. Kim, S. V. Puszta, S. L. Tripp and R. Balasubramanian, *J. Incl. Phenom.*, 2001, **41**, 83–86.
- 158 A. K. Hassan, A. K. Ray, A. V. Nabok and T. Wilkop, *Appl. Surf. Sci.*, 2001, **182**, 49–54.
- 159 A. K. Hassan, A. K. Ray, A. V. Nabok and F. Davis, *Sensors Actuators, B Chem.*, 2001, **77**, 638–641.
- 160 F. Davis, E. Frary and C. J. M. Stirling, *Langmuir*, 2004, **20**, 9075–9079.
- 161 M. Charnley, K. Fairfull-Smith, S. Haldar, R. Elliott, S. L. McArthur, N. H. Williams and J. W. Haycock, *Adv. Mater.*, 2009, **21**, 2909–2915.
- 162 S.-Keun Oh, M. Nakagawa and K. Ichimura, *J. Mater. Chem.*, 2001, **11**, 1563–1569.
- 163 Y. Hayashi, S. Suzuki and K. Ichimura, *J. Mater. Chem.*, 2001, **11**, 1805–1811.
- 164 C. D. Gutsche, *Calixarenes: An Introduction*, Royal Society of Chemistry, Cambridge, 2008.
- 165 P. Martin and M. Szablewski, *Langmuir-Blodgett Troughs - Operating Manual*, Nima Technology Ltd, Coventry, 6th edn., 2001.
- 166 M. Evyapan and A. D. F. Dunbar, *Sensors Actuators, B Chem.*, 2015, **206**, 74–83.
- 167 M. Bass, E. W. Van Stryland, D. R. Williams and W. L. Wolfe, *Handbook of Optics, Volume II*, McGraw-Hill, Inc., 2nd edn., 1995.
- 168 M. Bass, E. W. Van Stryland, D. R. Williams and W. L. Wolfe, *Handbook of Optics, Volume I*, McGraw-Hill, Inc., 2nd edn., 1995.
- 169 G. Binnig, C. F. Quate and C. Gerber, *Phys. Rev. Lett.*, 1986, **56**, 930–933.
- 170 R. W. Carpick and M. Salmeron, *Chem. Rev.*, 1997, **97**, 1163–1194.
- 171 O. Noel, H. Awada, G. Castelein, M. Brogly and J. Schultz, *J. Adhes.*, 2006, **82**, 649–669.
- 172 C. Creton and M. Ciccotti, *Reports Prog. Phys.*, 2016, **79**, 046601.
- 173 K. L. Johnson, K. Kendall and A. D. Roberts, *Proc. R. Soc. A Math. Phys. Eng. Sci.*, 1971, **324**, 301–313.
- 174 M. Deruelle, H. Hervet, G. Jandeau and L. Léger, *J. Adhes. Sci. Technol.*, 1998, **12**, 225–247.
- 175 R. Villey, C. Creton, P.-P. Cortet, M.-J. Dalbe, T. Jet, B. Saintyves, S. Santucci, L. Vanel, D. J. Yarusso and M. Ciccotti, *Soft Matter*, 2015, **11**, 3480–3491.
- 176 K. Fairfull-Smith, P. M. J. Redon, J. W. Haycock and N. H. Williams, *Tetrahedron Lett.*, 2007, **48**, 1317–1319.
- 177 H. Ito, T. Nakayama, M. Sherwood, D. Miller and M. Ueda, *Chem. Mater.*, 2008, **20**, 341–356.
- 178 V. Srivastava, A. Tandon and S. Ray, *Synth. Commun.*, 1992, **22**, 2703–2710.
- 179 O. Gawron, M. Duggan and C. J. Grelecki, *Anal. Chem.*, 1952, **24**, 969–970.
- 180 D. R. Edwards, D. C. Lohman and R. Wolfenden, *J. Am. Chem. Soc.*, 2012, **134**, 525–531.

- 181 F. Hauke, A. J. Myles and J. Rebek Jr., *Chem. Commun.*, 2005, 4164–4166.
- 182 Q. Zhang and K. Tiefenbacher, *J. Am. Chem. Soc.*, 2013, **135**, 16213–16219.
- 183 K. Takeshi, R. Nakayama and M. Ueda, *Chem. Lett.*, 1998, **27**, 865–866.
- 184 K. Young-Gil, B. Kim, T. Fujigaya and M. Ueda, *J. Mater. Chem.*, 2002, **12**, 53–57.
- 185 M. M. Hansen and J. R. Riggs, *Tetrahedron Lett.*, 1998, **39**, 2705–2706.
- 186 T. Nakayama, K. Haga, O. Haba and M. Ueda, *Chem. Lett.*, 1997, 26, 265–266.
- 187 Y. Li, S. P. Armes, X. Jin and S. Zhu, *Macromolecules*, 2003, **36**, 8268–8275.
- 188 A. Katchalsky and G. Blauer, *Trans. Faraday Soc.*, 1951, **47**, 1360–1370.
- 189 D. D. Perrin, *Aust. J. Chem.*, 1964, **17**, 484–488.
- 190 I. Balti, a. Barrère, V. Gueguen, L. Poussard, G. Pavon-Djavid, a. Meddahi-Pellé, P. Rabu, L. S. Smiri, N. Jouini and F. Chaubet, *J. Nanoparticle Res.*, 2012, **14**, 1266.
- 191 E. J. Ashford, V. Naldi, R. O'Dell, N. C. Billingham and S. P. Armes, *Chem. Commun.*, 1999, 1285–1286.
- 192 S. Tugulu, R. Barbey, M. Harms, M. Fricke, D. Volkmer, A. Rossi and H. Klok, *Macromolecules*, 2007, **40**, 168–177.
- 193 N. Schüwer and H.-A. Klok, *Langmuir*, 2011, **27**, 4789–4796.
- 194 7,332,550, *U.S. Pat. Appl. Publ.*, 2008, 41 pp., Cont.-in-part of U.S. Pat. Appl. 2004 44,1.
- 195 V. A. Kabanov, D. A. Topchiev, T. M. Karaputadze and L. A. Mkrtchian, *Eur. Polym. J.*, 1975, **11**, 153–159.
- 196 G. Blauer, *Trans. Faraday Soc.*, 1960, **606**, 111–112.
- 197 S. Beuermann, M. Buback, P. Hesse, S. Kukučková and I. Lacík, *Macromol. Symp.*, 2007, **248**, 23–32.
- 198 S. Beuermann, M. Buback, P. Hesse and I. Lacík, *Macromolecules*, 2006, **39**, 184–193.
- 199 J. P. A. Heuts, R. G. Gilbert and L. Radom, *Macromolecules*, 1995, **28**, 8771–8781.
- 200 J. P. A. Heuts, in *Handbook of Radical Polymerization*, eds. K. Matyjaszewski and T. P. Davis, 2002, pp. 1–76.
- 201 A. J. Parnell, S. J. Martin, C. C. Dang, M. Geoghegan, R. a. L. Jones, C. J. Crook, J. R. Howse and A. J. Ryan, *Polymer (Guildf.)*, 2009, **50**, 1005–1014.
- 202 W. Van Camp, F. E. Du Prez and S. A. F. Bon, *Macromolecules*, 2004, **22**, 6673–6675.
- 203 EP0794199A2, 1997.
- 204 M. Ye, D. Zhang, L. Han, J. Tejada and C. Ortiz, *Soft Matter*, 2006, **2**, 243–256.
- 205 P. Yang, L. P. D. Ratcliffe and S. P. Armes, *Macromolecules*, 2013, **46**, 8545–8556.
- 206 M. Semsarilar, V. Ladmiraal, A. Blanazs and S. P. Armes, *Polym. Chem.*, 2014, **5**, 3466–3475.
- 207 M. Semsarilar, V. Ladmiraal, A. Blanazs and S. P. Armes, *Langmuir*, 2012, **28**, 914–922.
- 208 S. Zuffanti, *J. Chem. Educ.*, 1948, **25**, 481.
- 209 Z. Cui, S. Zhang, J. Yang and L. Tang, *Front. Chem. China*, 2008, **3**, 425–431.

- 210 S. Haseloh, P. van der Schoot and R. Zentel, *Soft Matter*, 2010, **6**, 4112–4119.
- 211 B. Li, University of Toronto, 2008.
- 212 S. R. Gondi, A. P. Vogt and B. S. Sumerlin, *Macromolecules*, 2007, **40**, 474–481.
- 213 R. Schmidt, T. Zhao, J.-B. Green and D. J. Dyer, *Langmuir*, 2002, **18**, 1281–1287.
- 214 G. Bouhadir, N. Legrand, B. Quiclet-Sire and S. Z. Zard, *Tetrahedron Lett.*, 1999, **40**, 277–280.
- 215 K. Venkataraman and D. R. Wagle, *Tetrahedron Lett.*, 1979, **20**, 3037–3040.
- 216 H. L. Rayle and L. Fellmeth, *Org. Process Res. Dev.*, 1999, **3**, 172–176.
- 217 C. A. G. N. Montalbetti, V. Falque, M. Park and A. Ox, *Tetrahedron*, 2005, **61**, 10827–10852.
- 218 Z. J. Kamiński, B. Kolesińska, J. Kolesińska, G. Sabatino, M. Chelli, P. Rovero, M. Błaszczuk, M. L. Głowska and A. M. Papini, *J. Am. Chem. Soc.*, 2005, **127**, 16912–16920.
- 219 R. Pöttsch, S. Fleischmann, C. Tock, H. Komber and B. I. Voit, *Macromolecules*, 2011, **44**, 3260–3269.
- 220 M. Mitsuya, K. Kobayashi, K. Kawakami, A. Satoh, Y. Ogino, T. Kakikawa, N. Ohtake, T. Kimura, H. Hirose, A. Sato, T. Numazawa, T. Hasegawa, K. Noguchi and T. Mase, *J. Med. Chem.*, 2000, **43**, 5017–5029.
- 221 A. V. Fuchs and K. J. Thurecht, *ACS Macro Lett.*, 2017, **6**, 287–291.
- 222 B. Neises and W. Steglich, *Angew. Chemie Int. Ed. English*, 1978, **17**, 522–524.
- 223 X. Wei, X. Gong and T. Ngai, *Polym. Chem.*, 2013, **4**, 4356–4365.
- 224 R. Heeb, R. M. Bielecki, S. Lee and N. D. Spencer, *Macromolecules*, 2009, **42**, 9124–9132.
- 225 E. Spruijt, F. A. M. Leermakers, R. Fokkink, R. Schweins, A. A. Van Well, M. A. Cohen Stuart and J. Van Der Gucht, *Macromolecules*, 2013, **46**, 4596–4605.
- 226 T. Bickel, C. Jeppesen and C. M. Marques, *Eur. Phys. J. E*, 2001, **4**, 33–43.
- 227 A. Zengin, G. Karakose and T. Caykara, *Eur. Polym. J.*, 2013, **49**, 3350–3358.
- 228 A. Oth and P. Doty, *J. Phys. Chem.*, 1952, **56**, 43–50.
- 229 S. Sanjuan, P. Perrin, N. Pantoustier and Y. Tran, *Langmuir*, 2007, **23**, 5769–5778.
- 230 W. J. Brittain and S. Minko, *J. Polym. Sci. Part A Polym. Chem.*, 2007, **45**, 3505–3512.
- 231 J. B. Peng and G. T. Barnes, *Langmuir*, 1990, **6**, 578–582.
- 232 J. B. Peng and G. T. Barnes, *Langmuir*, 1991, **7**, 1749–1754.
- 233 D. B. Hall, P. Underhill and J. M. Torkelson, *Polym. Eng. Sci.*, 1998, **38**, 2039–2045.
- 234 D. E. Bornside, C. W. Macosko and L. E. Scriven, *J. Electrochem. Soc.*, 1991, **138**, 317.
- 235 L. M. Besley and G. A. Bottomley, *J. Chem. Thermodyn.*, 1974, **6**, 577–580.
- 236 H. Modarress and M. Mohsen-Nia, *J. Appl. Polym. Sci.*, 2005, **96**, 1244–1249.
- 237 H. Modarress, M. Mohsen-Nia and M. A. Mahdavi, *J. Appl. Polym. Sci.*, 2004, **91**, 1724–1729.

-
- 238 Y. Ma, J. Dong, S. Bhattacharjee, S. Wijeratne, M. L. Bruening and G. L. Baker, *Langmuir*, 2013, **29**, 2946–2954.
- 239 G. Decher, J. D. Hong and J. Schmitt, *Thin Solid Films*, 1992, **210–211**, 831–835.
- 240 S. Gourianova, N. Willenbacher and M. Kutschera, *Langmuir*, 2005, **21**, 5429–5438.
- 241 Bruker AFM Probes, MLCT Product Description, <https://www.brukerafmprobes.com/p-3444-mlct.aspx>, (accessed 5 March 2019).
- 242 H. Lee, N. F. Scherer and P. B. Messersmith, *Proc. Natl. Acad. Sci.*, 2006, **103**, 12999–13003.
- 243 United States Patent Office, US 2013/0030192, 2013, 115.
- 244 R. Arnecke, V. Böhmer, E. F. Paulus and W. Vogt, *J. Am. Chem. Soc.*, 1995, **117**, 3286–3287.
- 245 B. S. Sumerlin, N. V. Tsarevsky, G. Louche, R. Y. Lee and K. Matyjaszewski, *Macromolecules*, 2005, **38**, 7540–7545.
- 246 J. L. Hutter and J. Bechhoefer, *Rev. Sci. Instrum.*, 1993, **64**, 1868–1873.